Cloud Publications
International Journal of Advanced Earth Science and Engineering
2017, Volume 6, Issue 1, pp. 538-547
ISSN: 2320 – 3609, Crossref: 10.23953/cloud.ijaese.276

Case Study

Stress Field Delineation using Well Log Data – A Case Study

Rakhi Arvind Pandey

Western offshore basin ONGC, Mumbai, Maharashtra, India

Publication Date: 10 June 2017

DOI: https://doi.org/10.23953/cloud.ijaese.276

Abstract The essentiality of stress field delineation in the subsurface arises in several contexts like well planning and monitoring to ensure safe drilling of a borehole. Work reported here concerns with methodology developed for delineating stress fields in rock strata using log data which includes crossed dipole and monopole acoustic data acquired in boreholes. Orientation of the principal stresses in the horizontal plane has been arrived at by computing relative azimuth of maximum and minimum stress directions with respect to a designated dipole transmitter's axial orientation. Static Poisson Ratio and Static Young's modulus have been computed using customized relationships with due care has been taken to factor-in fluid effects where compressible fluids are known to present within pore space of the rock. Stresses magnitudes and UCS model have been subjected to a validity check through prediction versus actual of presence / absence of breakouts (the latter from image data evidence) and the match is very good.
Keywords *LOT; maximum horizontal stress; minimum horizontal stress; XLOT*

1. Introduction

Delineation of local stress field and its relationship between regional stress fields, gives the all-important depth-wise behavior of magnitude as well as orientation of the principal stresses. The distinguishing features of the work flows are modeling azimuthally anisotropic principal stresses in horizontal plane using fast shear and slow shear slowness and a realistic model of residual strains (due to residual tectonic stresses). LOT/XLOT data used as calibration, and a robust validation scheme wherein borehole failure or absence thereof is predicted from model and cross checking for validity with electric images data. Borehole images and drilling observations have been noted as fully corroborating model based predictions and Static Young's Modulus, PR,UCS and Friction angle are validated by laboratory estimation based on cores cut in stratigraphic and lithological rock in a well currently under drilling and not necessarily a part of the case study reported.

2. Area of Study

The work flows have been developed for exploration areas off Kutch-Saurashtra coast India [1].The case study presented involves 2 wells and well sections pertaining to tertiary as well as pre-tertiary have been made a part of the case study. Two wells have been analyzed; general information of the same is given below

Table 1: *General information of studied wells* [2][3]

	Well 1	Well 2
Target depth	4250m	2030m
Drilled Depth	4250m	2030m
Water Depth	12.80m	27.11m

3. Methodology Adopted

Input data sets include resistivity, nuclear, gamma ray logs and formation tester pressures, electrical Images and complemented by LOT and XLOT data acquired during the drilling. Monopole excitation derived acoustic wave forms inclusive of Stoneley mode, multiplexed crossed dipole excitation (from crossed dipole transmitters) derived flexural wave trains. From the advanced acoustic data sets mentioned above compressional slowness, fast and slow shear slowness and Stoneley mode slowness of the formation is derived.

In the current study it has been assumed that reservoir rock has isotropic elastic properties in unstressed state, which is also supported by image data. Thus it is assumed that anisotropy in rock mechanical properties arises only due to stress anisotropy. Vp/Vs have been computed as ratio of shear wave slowness to compressional wave slowness. Dynamic elastic moduli has been computed as

$PR_{Dyn} = (Vp/Vs)^2 – 0.5)/ (Vp/Vs)^2 – 1.0)$
$G = \rho_b * Vs^2$
$E_{Dyn} = 2G (1+ PR_{Dyn})$

Where, PR_{Dyn}-Dynamic Poisson's ratio, G-Shear Modulus, E_{Dyn}- Dynamic Young's modulus. Vp-Compressional velocity of formation (computed as reciprocal of compressional slowness). Vs -Shear velocity of formation (computed as reciprocal of shear slowness), and ρ_b-formation bulk density. Stress Field delineation relies on static moduli and therefore it is necessary to compute static moduli of elasticity starting from the dynamic moduli data. The computation is discussed below.

A) Computation of PR_{Static} (The symbol 'v' will henceforth denote PR_{Static} in this paper)

From a theoretical standpoint the relationship between static and dynamic Poisson Ratio values has to depend on two factors firstly the ratio of population of high aspect ratio pores to that of low aspect ratio pores, abundance of open cracks and confining pressure (more the confining pressure less the open cracks left). These are difficult to model into an effective medium theory when the data sets comprise well log data. Therefore a different approach has been followed in the current case study. Survey of literature brings home the fact that the most productive form of relation between Dynamic and static PR is of the linear form

$PR_{Static} (v) = k^* PR_{Dyn}$

B) Computation of Static Young's Modulus (E_{Static})

For our present study we have adopted a linear relationship between Static Young's Modulus (E_{Static}) and Dynamic Young's Modulus (E_{Dyn}). The relationship we have used is

$E_{Static} = 0.809^* E_{Dyn}$.

This form of the relationship and the subsequent UCS models based on E_{Static} have been seen to be well validated by match between behavior of formation face exposed in the different well sections from the perspective of predicted presence / absence of mechanical failure of formation at and near borehole and actual condition as confirmed from borehole images.

C) Modeling of UCS and Tensile strength of Rocks

For modeling UCS we have used a power law type of relationship between UCS and E_{Static} of the form

$$UCS = A^* (E_{Static})^B$$

Value of modeled UCS is constrained by presence or absence of shear failure of formation at and near borehole wall. We have arrived at the following values for A and B where we have seen a consistency lithology wise and whether the rock is an outcome of a tertiary or pre-tertiary deposition. The sections studied in our current work comprise tertiary as well as younger depositions. The values of A B used lithology which we have used to model UCS have been found to be consistent lithology and age wise. These values are given in Table 2.

Table 2: *Constant used in UCS calculation*

Age	Lithology	A	B
Tertiary	Shale	3.3-3.7	0.33-0.37
	Siltstone	3.5	0.35
	Sandstone	2.5	0.25
	Limestone	3.5	0.35
Pre-Tertiary	Shale	4.5	0.45
	Siltstone	4.1	0.35
	Sandstone	4.1	0.35
	*Limestone	-	-
*Not encountered in studied wells			

In conformance with the relationship assumed between UCS and Tensile strength of rocks a linear relation has been assumed as relating Tensile Strength of rock to UCS. The relation used in the current work is

$$T = UCS/11.1$$

Where, T-Tensile Strength of rock and UCS its Unconfined Compressive strength.

D) Computation of shear moduli of elasticity relevant to shear stresses and shear strains in the respective principal planes

Considering, a co-ordinate system with X axis along the maximum horizontal stress direction. Y axis along the minimum horizontal stress direction and z axis along the vertical direction. C44 C55 C66 respectively corresponds to shear moduli applicable for shear stresses and strains in the principal planes yz xz and xy respectively. If ρb is the formation density C44 C55 and C66 are computed as

$$C44 = \rho b \, Vsslow^2$$
$$C55 = \rho b \, Vsfast^2$$
$$C66 = \rho mud / [(DTmud)^2 - (DTstoneley)^2]$$

E) Modeling of Friction Angle (φ)

Friction angle φ for grain supported rock facies has been computed using the Weingarten and Perkins (1999) correlation [6]

φ = 57.5-105ψ where φ is expressed in Degrees and ψ sands for porosity in units of volume fraction.
Friction angle φ for mud supported rock facies has been computed using the correlation given by Lal (1992) [4]

φ = sin-1((Vp-1000)/ (VP+1000))
where φ is in radians and Vp is compressional velocity for the rock in units of m/sec.

F) Analysis of LOT / XLOT data

Out of the well sections studied, LOT data exists for all sections. Additionally XLOT data exists for two sections one in well NAA-1. XLOT data available for well NAA-1 comprises pump pressure volume pumped and time elapsed data The objective of this analysis had been estimation of magnitude of minimum horizontal stress, and also to confirm that only a single fracture was initiated.

G) Analysis of XLOT data for estimating minimum horizontal stress magnitude at XLOT depth

Pump pressure has been plotted on y axis against volume of mud pumped on x axis. The value of pump pressure PLOP at which first deviation from linear relation between pump pressure and volume pumped, occurs has been considered as surface pressure corresponding to leak off pressure in the subsurface. Leak off pressure has been considered as an estimate of minimum horizontal stress magnitude where only LOT data is available. Leak-Off Pressure has been computed as PLOP + pressure due to hydrostatic column in the borehole from surface down to the LOT depth.

H) Estimation of pore pressure (Pp)

Wells studied have a rich data set of formation tester pressures. The data density is enough to have reliable trends of pore pressure vs depth. Formation pressure vs depth trends indicate normal pressure regime with maximum increase not exceeding hydrostatic plus 10%. Hence no regular pore pressure prediction work flow was necessitated and none attempted.

I) Computation of magnitudes of principal vertical stress

Vertical stress σv has been computed by adding the stress due to water column and stress due to sediment weight. Density logs are not available up to the mud line. Mud line sediment density has been assumed from area knowledge and where soil coring penetration data is available, from an estimate of likely mud line sediment density therefrom. A linear increase of sediment density from mud line to the shallowest depth of available density log data has been assumed. Such an assumption is not unreasonable since shallowest density log depth would involve around 150m of sediment column above this depth level, which column would correspond to the upper half of a hypothetical column from mud line to a depth where the sediment porosity would go below the critical porosity value for the shallow sediments encountered. After bringing the available density log depth thus up to mud line level this sediment density versus depth function has been integrated with respect to depth to obtain sediment load derived vertical stress for any depth level. The stress due to the weight of water column above mud line has been added to get the vertical stress.

J) Computation of magnitudes of principal stresses in the horizontal plane

If σv, σH, σh stand for the vertical maximum horizontal and minimum horizontal principal stress magnitudes respectively then these are related to C44 C55 C66 as

(C44 - C66) / (C55 - C66) = (σv - σH)/(σv - σh) [5]

Therefore by evaluating the LHS we evaluate the RHS which we denote as 'ξ'

Then σH = ξ* σh + 1- ξ* σv

At LOT / XLOT depth level the value of σh is estimated as discussed in the foregoing and σH computed as from above. The value of σH / σh is computed at LOT / XLOT depth level and denoted as 'λ'

Next, horizontal stress magnitude in absence of residual tectonic stresses is computed as

σ0 = (v/(1- v))*(σv – Pp) + Pp where Pp is pore pressure and v is static Poisson Ratio.

It is assumed that deviation of magnitude of actual principal stresses in horizontal plane is expression of residual tectonic stresses. Residual tectonic stresses would result in anisotropic strain field in horizontal plane. If εH and εh respectively stand for magnitude of additional strain along maximum horizontal stress direction and minimum horizontal stress direction respectively then the following relations apply

$\sigma h = \sigma 0 + (Estatic/(1- v^2))* \varepsilon h + (Estatic* v /(1- v^2))* \varepsilon H$
$\sigma H = \sigma 0 + (Estatic* v /(1- v^2))* \varepsilon h + (Estatic /(1- v^2))* \varepsilon H$

From LOT/ XLOT data analysis described in the foregoing magnitude of σh at LOT / XLOT depth is computed. Subsequently σH magnitude at LOT / XLOT depth level is also computed as described in the foregoing.

The ratio (σH / σh) is designated here as 'λ' and its value is computed for LOT / XLOT depth level as described above. We have, in light of equations for σh and σH above and equation

σH = ξ* σh + 1- ξ* σv
εh/ εH = {(σh – v* σH) – (1- v)* σ0} / {(σH – v* σh) – (1- v)* σ0}

The ratio (εh/ εH) is designated here as 'μ' and its value is computed for LOT / XLOT depth level as described above.

In the course of our work we have noted integrating area knowledge that LOT / XLOT depths are shallow level depths of respective well sections (within which they occur) that share common tectonic history. Hence it is reasonable to assume that these sections respectively share their λ and μ values with the depth levels where LOT /XLOT had been conducted. Therefore it has been assumed that λ and μ values computed for LOT / XLOT depths are applicable for each level of the respective sections which the LOT / XLOT depth levels form part of. And therefore level by level evaluation of σh, σH as

σh = {σ0*(1- μ)*(1- λ)}/{1 - v*(λ - μ)- λ*μ}
σH = σh* λ

In some of the well sections studied it was noted by us that usable fast shear and slow shear data could not be derived. However we have noted that this data is available against correlated section in nearby wells. We have used the ξ parameter value for those sections to compute σH at LOT / XLOT depths in accordance with the relation

σH = ξ* σh + 1- ξ* σv and computed λ and μ in accordance with the computation above and thereby computed σh and σH level by level in accordance with the method shown above.

K) Computation of Orientation of the principal stresses in space

One of the principal stresses is oriented vertically. We set up a coordinate system in which z axis is taken as vertical, x axis taken along maximum horizontal stress direction and y axis is taken along minimum horizontal stress direction. Another coordinate system is also considered which has its z axis along the tool axis and hence the borehole axis, its x axis along the axis of the designated dipole transmitter, and which is also called the tool face and its y axis orthogonal to the above two axes. We denote this coordinates system as the x1y1z1 coordinates system. With the acoustic tool a directional triaxial package is also run which enables us to know the inclination of the tool axis with respect to the vertical and thus the angle between z and z1 axes, and the azimuth of x1 with respect to true north. Through a workflow called as four component rotation the azimuth of x1 with respect to x is computed using the in line and cross line dipole array receivers responses to crossed dipole transmitters excitation. Since azimuth of x1 with respect to true north is known the azimuth of x and therefore of y axes with respect to true north is now known. And thus the orientation of the principal horizontal stresses is known. Since the other principal axis is vertical the stress field is spatially delineated.

Since the magnitude of principal stresses is also by now computed as discussed in detail in the foregoing, the stress field stands completely delineated in magnitude as well as directionally.

4. Validation of Results

Using model data of the rock mechanical properties, minimum mud weight predicted as necessary to be exceeded in order to avoid bore hole breakout (denoted as Pmbrout) and the maximum mud weight threshold (Pmfrac) which when exceeded by effective circulation density (ECD) would result in tensile failure of the formation at the bore hole wall, have been computed for all levels applying Mohr-Coulomb Failure Criteria.

Pmbrout and Pmfrac have been computed using the following relations

Pmbrout = [1/(Kp+1)]*{3*σH – σh – UCS + (Kp-1)*Pp} / {(D*1.422)/8.33)}
Where D is depth in meters, of the level for which Pmbrout is being computed, and Kp the Passive

Mohr-Coulomb Coefficient is given by
Kp = (1+sinφ)/ (1-sinφ), φ being friction angle.

All other variables and parameters on RHS are in units of psi. Pmbrout is computed in units of ppg).
Pmfrac = {3*σh–σH–Pp + T} / {(D*1.422)/8.33)}
Where D is depth in meters, of the level for which Pmfrac is being computed, and T is Tensile Strength of formation.

All variables other than D on RHS are in units of psi. Pmfrac is computed in units of ppg).

Pmbrout and Pmfrac are thus respectively the end points within which ECD has to be managed in order to ensure that neither shear failure nor tensile failure of formation would occur during drilling of the well (Figure 1). The accuracy and hence usefulness of the computed values of Pmbrout and Pmfrac against different depth levels has been checked, using FMI image data, FMI recorded in reservoir interval shows breakout from 2300- 2600m (Figure 2) and from the Figure 1, it is very much clear that mud weight is less than required mud weight (threshold mud weight) to overcome breakout. FMI images also show the direction of breakout i.e. minimum horizontal stress (as breakout always occur in this direction) and rose diagram of fast shear azimuth (Figure 3) shows the direction of maximum horizontal stress as NE which is orthogonal to minimum horizontal stress. Figure 2 (FMI Images) shows the azimuth of breakout NW-SE which is orthogonal to what Figure 3 shows (rose diagram) as fast shear azimuth which is direction of maximum horizontal stress. Since breakouts occur along direction of minimum horizontal stress, clearly images validate the fast shear azimuth obtained from advanced acoustic data processing. Thus model predictions on principal stress orientations are also validated. Similar validation is presented for well 2 where model does not predict formation mechanical failure at bore hole wall (Figure 5) which prediction is validated by images against the relevant interval (Figure 6).

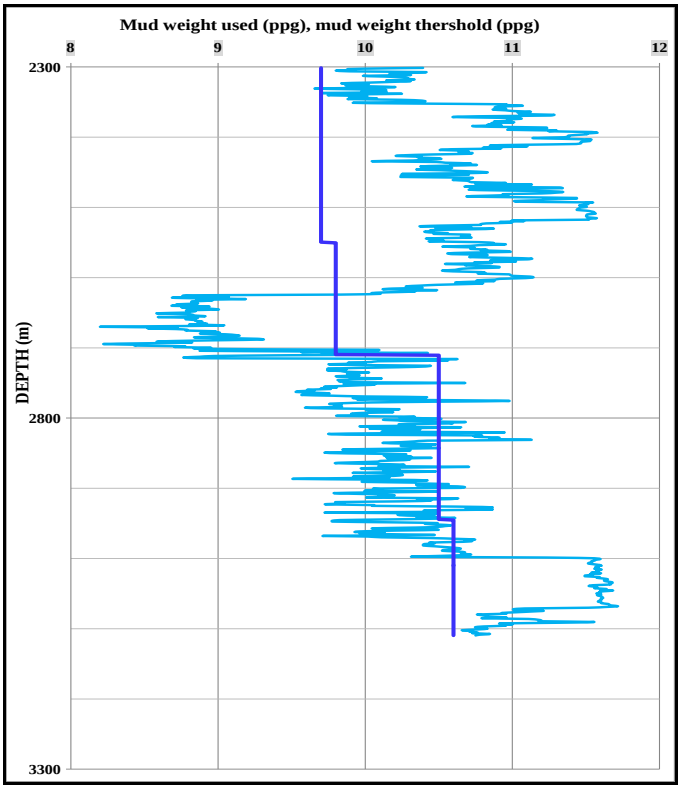

Figure 1: *Calculation of Pm brout vs mud weight used in well 1*

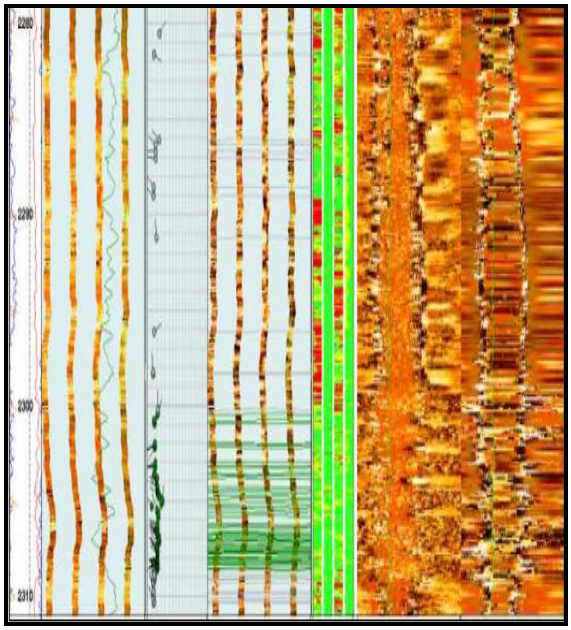

Figure 2: *FMI image encountered against the reservoir interval showing breakout in well 1*

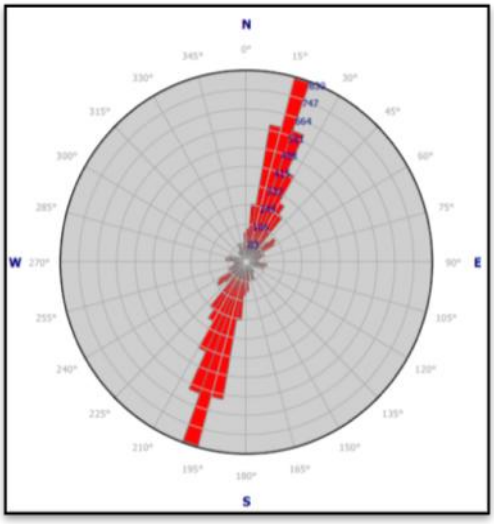

Figure 3: *Rose diagram of fast shear azimuth*

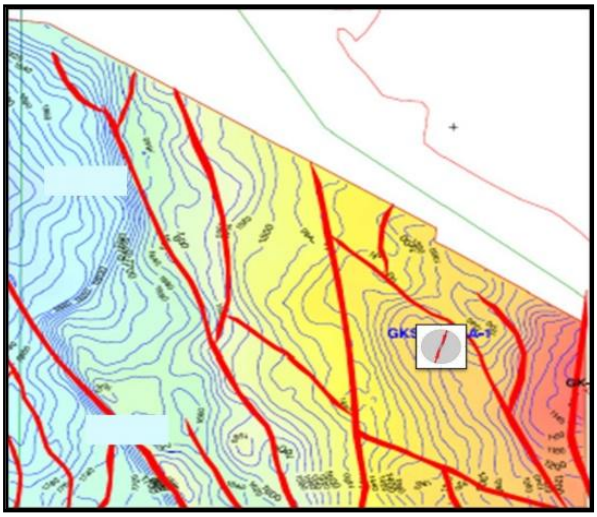

Figure 4: *Rose diagram of fast shear azimuth against the studied well plotted over Time Structure Map at the top of Bhuj formation (Age-Cretaceous)*

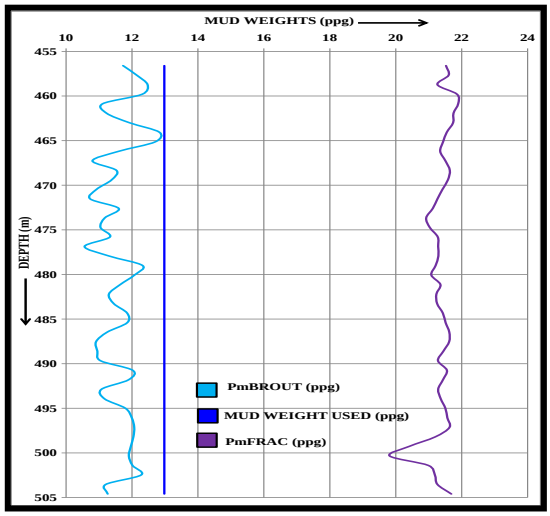

Figure 5: *Calculation of Pm brout vs mud weight used in well 2*

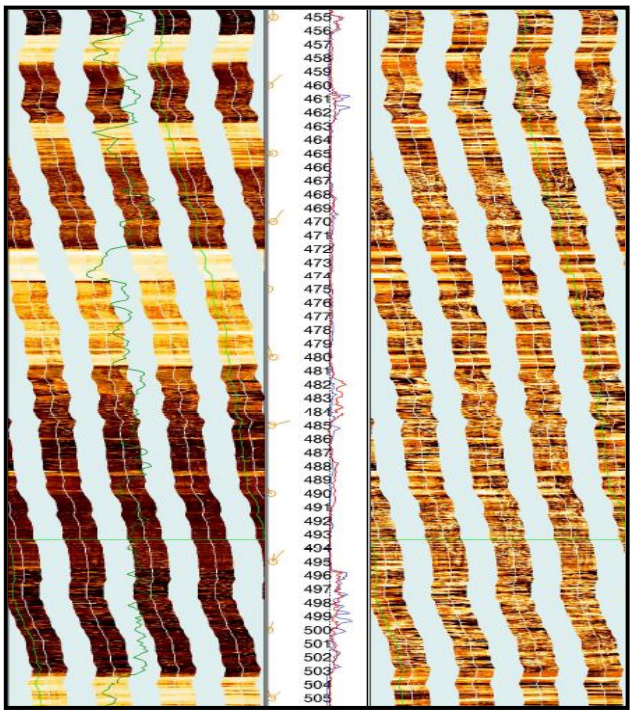

Figure 6: *FMI image encountered against the reservoir interval showing breakout in well 2*

5. Results and Discussion

σH, σh, σv and σ0 have been presented as plots against depth for different sections studied. The results bring out that the stress regime as today is normal stress regime. This indicates that even for the cases of inversion the deformability of the sediment layers coupled with subsequent tectonic history has led to normal stress regime to be the stress signature for the study area. Individual well wise maximum horizontal stress directions have been presented as rose plots which show that direction of maximum horizontal stress is NE SW dominantly in the area. Examination of the ratio (σH/σh) brings out that across different wells and different stratigraphic sections horizontal stress anisotropy is of a low degree. This is in line with the general geological understanding of the areas of studied. Regional Stress Distribution has been superimposed on the same maps in order to show the degree of conformity or otherwise between the locally delineated stress field's spatial orientation vis-a-vis that of the regional field. It is noted that the degree of conformance is good.

6. Conclusions

A viable methodology for stress field delineation has been demonstrated which is based on robust modeling with in-built means of constraining model parameters and validation by images, drilling observations, well history and laboratory results. Strong LOT/XLOT data support crossed dipole acoustic data and low frequency monopole data for stoneley mode properties in addition to compressional slowness determination, formation tester data of sufficient data density and good quality images and conventional resistivity nuclear gamma suites are a necessary requirement for implementing the workflows demonstrated in this work.

References

[1] Zutshi, P.L., Sood, A., Mahapatra, P., Ramani, K.K.V., Dwivedi, A.K. and Srivastva, H.C.: Lithostratigraphy of Indian Petroleum Basins. Document V: Bombay offshore Basin. KDMIPE Dehradun. (1993)

[2] Well completion report of well-1 (actual name modified). Geological operation group ONGC, Mumbai. Unpublished report. (2014).

[3] Well completion report of well-2 (actual name modified). Geological operation group ONGC, Mumbai. Unpublished report. (2015).

[4] Lal, M.: Shale stability: drilling fluid interaction and shale strength. SPE Latin American and Caribbean Petroleum Engineering Conference held in Caracus, Venezuela. (1999)

[5] Sinha, K.B.: Recent advances in Borehole Sonic Technology. 7th International Conference & Exposition on Petroleum geophysics. 163 (2008)

[6] Weingarten, J.S., Perkins, T.K.: Prediction of sand production in gas wells: method and Gulf of Mexico case studies. Paper SPE 24797 Washington DC, 4/7 October. (1992)

Cloud Publications
International Journal of Advanced Earth Science and Engineering
2017, Volume 6, Issue 1, pp. 548-556
ISSN: 2320 – 3609, Crossref: 10.23953/cloud.ijaese.277

Case Study

Analysis of Pore Pressure - Predrill Tool in Operation Geology

Rakhi Arvind Pandey

Western offshore basin ONGC, Mumbai, Maharashtra, India

Publication Date: 10 June 2017

DOI: https://doi.org/10.23953/cloud.ijaese.277

Abstract Formation pressure plays an important parameter in the health of a borehole. In the oil field, pressure is commonly measured in pounds per square inch (psi). At the wellsite, we are typically concerned with the pressures throughout the circulating system. Study of Pore pressure or formation pressure makes a very important subject for the wellsite Geologists.

Keywords *Hydrostatic Pressure; Subnormal Pressure; Overburden Pressure; Pore Pressure*

1. Introduction

Pressure is defined as the force acting on a unit area. In the oil field, pressure is commonly measured in pounds per square inch (psi). At the wellsite, we are typically concerned with the pressures throughout the circulating system. We may need to know the pressure at a particular point in the wellbore (such as the casing shoe or a lost circulation zone) or we may want to know the total pressure required to pump a certain mud volume at a given rate. The different kinds of reservoir pressures which are usually encountered during the course of drilling are broadly divided into three main components (Figure 1):

- Hydrostatic or normal pressure,
- Overburden or load pressure and
- Formation or pore pressure.

1.1. Hydrostatic Pressure

The normal, predicted pressure for a given depth or the pressure exerted per unit area by a column of freshwater from sea level to a given depth.

1.2. Overburden Pressure

The overburden pressure at any point in the formation is that pressure exerted by the total weight of the overlying formations. In other words the overburden pressure is the result of the combined weight of the formation matrix plus the fluids in the pore spaces, overlying the formation of interest. The calculation and establishing of overburden pressure is the first step in analysis of wellbore pressures because all other pressures quantities are consequent upon the overburden.

The overburden pressure can be expressed as the hydrostatic head of all materials overlying a certain point or depth of interest. So,

$$Sp = g\ \rho_b\ H$$

Where- Sp = Overburden Pressure, G = Gravity value, ρ_b = Average Density, H = Height of the column

1.3. Formation Fluid Pressure

Clastic rocks are composed of matrix, cementing material and pore spaces. These spaces are occupied by fluids that will constitute hydrostatic columns depending on the effectiveness of vertical communication. This vertical communication may be to the surface, the water table, or to permeability barrier of some kind, such as closure fault or salt bed. This pore fluids pressures constitutes the pore pressures. The overburden load is suppurated at a particular depth of interest by the pore pressure at that depth and the vertical component of matrix stress.

2. Types of Formation Pressure

The formation pore pressure is defined as the pressure acting upon fluids in the pore space of the formation; fluid can be oil or water and also gas in the pore space. Pressure expressed either in pound/inch^2, atmosphere or kg/cm^2 or psi/ft. there are three types of formation/pore pressures which are present in the sediments.

2.1. Normal Pressure

The pressure exerted by the column of water extending from any given level to the surface. Normal formation pressure gradient ranges from 0.433 psi/ft to 0.465 psi/ft or 1.0 gm/cc - 1.08 gm/ cc.

Overall pressure detection and prediction are very helpful while preparing mud, lowering casing, to prevent mud losses and lost circulation and also guiding for prevent kick or major blowout. Pressure can be defined by following equations;

$$P_H = g \times p \times h$$

Where, P_H = hydrostatic pressure, g = gravity value, p = avg. fluid density, h = height of the column.

2.2. Subnormal Pressure

Subnormal pressures are those pressures, which are less than the hydrostatic pressure. Hydrostatic gradient is less than 0.433 psi/ft or 1 gm/cc. In the Indian sub-continent, subnormal pressure occur in various places, both offshore and onshore, in carbonate as well as clastic reservoirs. It may occur due to following situations.

- Erosion,
- Depletion of reservoir,
- Artesian condition,
- Tectonic set up,
- Precipitation,
- Temperature change etc.

2.3. Overpressure (abnormal pressure)

Abnormal pressures are those pressures which are greater than the hydrostatic pressure. Pressure gradient is more than 0.465 psi/ft than the formation is said to have abnormal high pressure or overpressure. Overpressure is common in areas with rapid deposition, especially of younger sediments or in tectonically stressed areas or folded belts areas.

2.3.1. *Origin of Abnormal High Pressure Zones*

The causes for development of overpressure have been discussed by Hubert and Rubey (1959) [1]. The various phenomena for occurrence of overpressure are described below; these all phenomena can be divided into three major heads which are (Figure 2)

1) Sedimentological overpressure,
2) Structural overpressure and
3) Overpressure due to chemical or physical phenomena etc.

3. Why do we need to know pore pressure

Prediction of Pore pressure and Fracture pressure prior to drilling minimizes cost and risks associated with drillings. “Half the cost of high value wells comes from uncertainty; a large percentage of the uncertainty comes from pore-pressure and geo mechanics related issues”. In case of economic viability the prediction is very helpful and it minimizes cost of the wells to be drilled. Hence basic understandings of the Formation pore pressures parameters are very much needed. There is no control over Pore Pressure Gradients, or Fracture gradients, and these are often largely unknown before drilling. It occurs nearly in all sedimentary basins; correct prediction not only reduces drilling costs substantially but also prevents many hazards which may result in well kicks, blow outs and other potential well complications, which may otherwise lead to the loss or abandonment of the well. Figure 3 shows a yearly NPT (non-productive time) of Western offshore Basin (shallow) rig during the period of (01-04-2007 to 31-3-2008). The Pie diagram shows nearly 77% Productive Time and 23% Non-Productive Time. Out of 23% NPT more than 60% rig time loss are due to complications. Such complications could be related to Pore Pressure or well bore stability i.e. Geo-dynamic and are considered to be avoidable, and 40% are non-avoidable including repair job, waiting on weather and man & materials.

3.1. Well site overpressure indicators

In the wellsite from the following change one can identify the overpressure zones. During drilling if the Rate of Penetration / Gas / “Splintery” Shale cuttings / Volume of Shale cuttings / Flowline temperature / Chlorides / Shale travel time increases or d-exponent / Shale Density / Resistivity decreases then it shows that any overpressure zone is present beneath the surface which is drilling now [2]. The standpipe pressure and pump rate exhibit changes in down hole conditions and may consequently be utilized to determine loss of overbalance. It should be observable that any of the following parameters indirectly related to the kick situation are also indicators. The various wellsite pressure indicators are used during drilling are listed in the Table 1:

Table 1: *Shows Wellsite (During Drilling) pressure indicator*

Pressure Indicator	Change In Value	Reason For Change
Drill rate	Increases	Formation is under compacted, differential pressure at the bit approaches zero.
D – Exponent	Decreases	Reflecting overall increased formation drill ability.
Total gas	Increases	Reflects greater volumes of in situ gas.
Background gas	Increases	Greater volumes of in situ gas, loss of overbalance.
Fill	Increases	Hole instability.
Flowline density	Decreases	As overbalance is lost, formation fluid contaminates drilling fluid.
Flowline viscosity	Increases	Formation fluid is often hotter, containing mineral hardness, causing mud flocculation.
Flowline salinity	Increases	The more highly saline formation fluid enters wellbore as overbalance is diminished.
Shale density	Decreases	Reflects under compaction in an Overpressured environment.
Cuttings shape, size	Increases	Reflects hole instability less gouging of formation presence of cavings.
Flowline temperature	Increases	Overpressured zones, possessing greater than normal pore fluid, act as thermal insulators.

4. Prediction of pore pressure at depth

Pore pressure prediction can be done by direct as well as indirect methods. Mud weight used during drilling against a permeable zone gives a clue about the pore pressure. Direct measurement of pore pressure of permeable zone is also possible by using variety of commercially available technologies. Geophysical data are also use for measurement of pore pressure. Seismic reflection data are used for the prediction of pore pressure before drilling the well. This is very important for the areas where high pore pressure is recorded and proper planning of drilling is required.

4.1. Pore Pressure Indicator

All pore pressure estimation methods are based on the premise that pore pressure influences compaction - dependent shale properties such as porosity, density, sonic velocity, and resistivity [2]. Any wireline or geophysical measurement that is sensitive to Pore pressure will be referred to as a Pore Pressure Indicator. The main Pore pressure indicators are summarized in Table 2.

Table 2: *Pore pressure indicators*

Before Drilling	Seismic Velocities
During Drilling	ROP(Normalized Rate Of Penetration), MWD, Pit Levels, Mud Gas (Drill gas, Connection gas, Trip gas, Pumps-off gas, C2/C3 ratio etc.), Mud Density, Cutting's Shape & size, LWD Resistivity, DT, Density, Formation Temperature (Formation temperature is usually inferred from circulating temperature or flowline temperature) Drilling Events Such as kick, influx, loss. Mud Chlorides (Background Chlorides, Trip Chlorides)
Post Drilling	a)Resistivity b)Sonic c)Density / Neutron, Measure direct pressure information i.e. Wireline formation tests. Drill stem tests, Well Seismic Checks (VSP, Checkshots etc.)

5. Case Study

Tapti Daman block in Bombay Offshore basin of India is a Tertiary clastic sub basin formed at junction of the Cambay and Narmada rifts and contains a sedimentary thickness in excess of 5000m. This block comprises of homoclinal area (Saurastra homocline and Eastern homocline) and number of ENE-WSW trending lows (Daman low, Purna low and Navsari low). The basin is divided into two areas Tapti in the north and Daman in the South The deeper Panna Formation in Tapti-Daman block consist of syn-rift and post rift sediments is predominantly argillaceous and represents the major source rock. Extensive Exploration in this area has revealed the structural and combination type entrapment of hydrocarbon in the clastic reservoirs of Daman (Late Oligocene) and Mahuva (Early Oligocene) Formation. Daman Formation consists of sandstone-shale alterations with a few coal lenticles and Mahuva Formation consists of dominantly shale with thin limestone bands and occasional sandstone stringers. The north south vertical pressure profile constructed from sonic trends reveals that the top of overpressure cuts across stratigraphic boundaries and is seen to rising towards the southern part of the block. The top of maturation is seen to be generally above the high pressured compartment. The pressure mechanism appears to be dominantly compaction disequilibrium [3].

The candidate well is drilled with objective of exploring hydrocarbon potential of carbonates within Panna formation and sands within Mahuva and Daman formation. The target depth of well was 4550m and water depth was 23m [4].

5.1. Methodology for prediction of predrill pore pressure and fracture gradient

From the well log data, Pore Pressure Gradient and Fracture Gradient have been calculated as described in the flow chart. (Figure 4)

The Predrill prediction of Pore pressure and fracture gradient for this well is carried out with the help of nearby well data and seismic survey study. In WOB, ONGC this study is estimated using **"Drillworks Software**" [5] [6]. The Figure 5 shows the study for this well.

1) The overpressure zone starts from Mahuva formation.
2) Pore pressure gradient is higher than the overburden gradient.
3) Observed gain at 3300, 3400 & 3800 m while drilling with near balance mud weight.
4) The maximum allowable mud weight between PP and FG is very narrow thus in such condition very challenging for safe drilling.
5) The well was drilled with hydrostatic + more than 100% mud hydrostatic and maximum BHT recorded 356°F (Log Header).

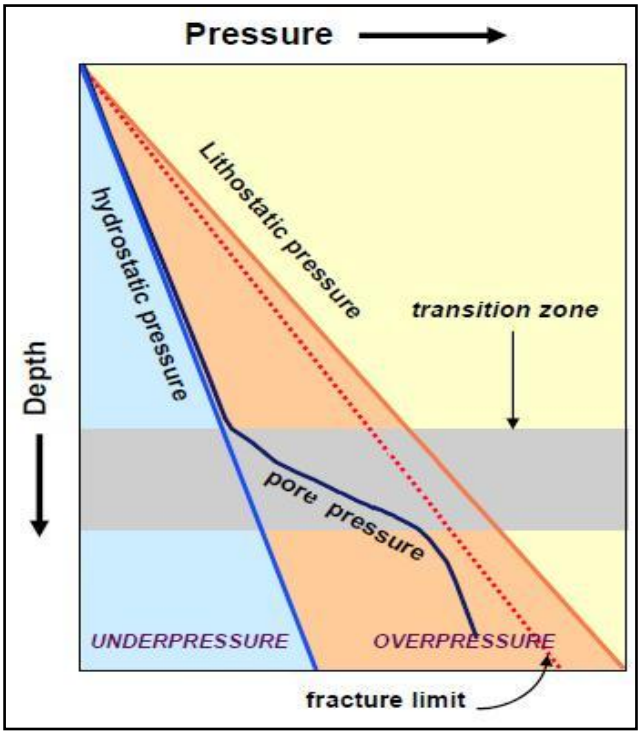

Figure 1: *Shows Pressure v/s Depth relationship, Hydrostatic, Pore pressure curve, Overburden curve (Lithostatic) pressure etc. (Source - Presentation by Nader C. Dutta, May-2005, Mumbai)*

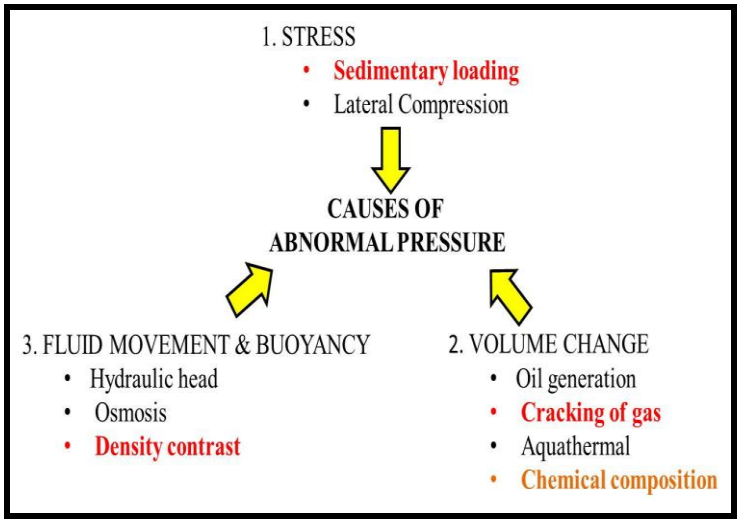

Figure 2: *Shows the causes of Abnormal Pressures*

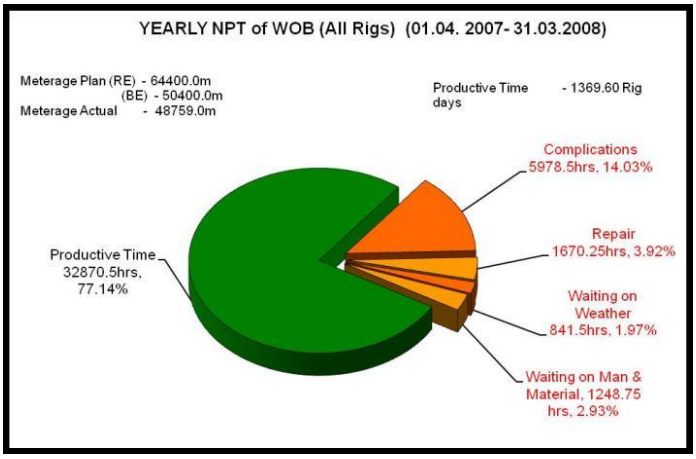

Figure 3: *Yearly NPT of WOB (Source ONGC reports, 2007-2008)*

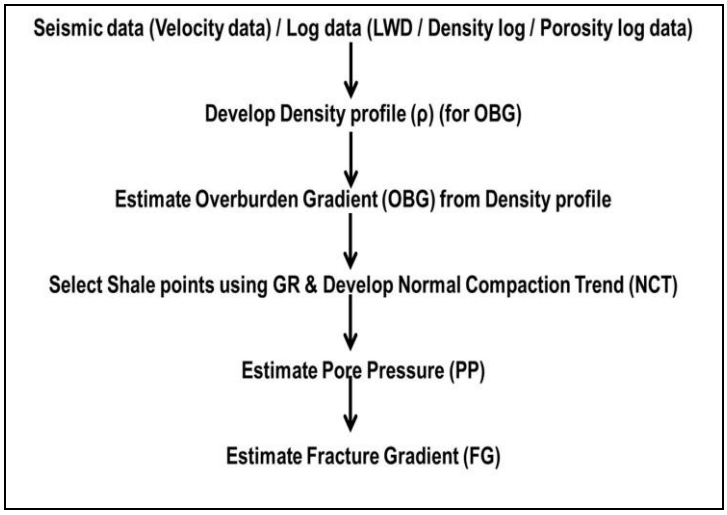

Figure 4: *Pore Pressure and Fracture Gradient Estimation [4]*

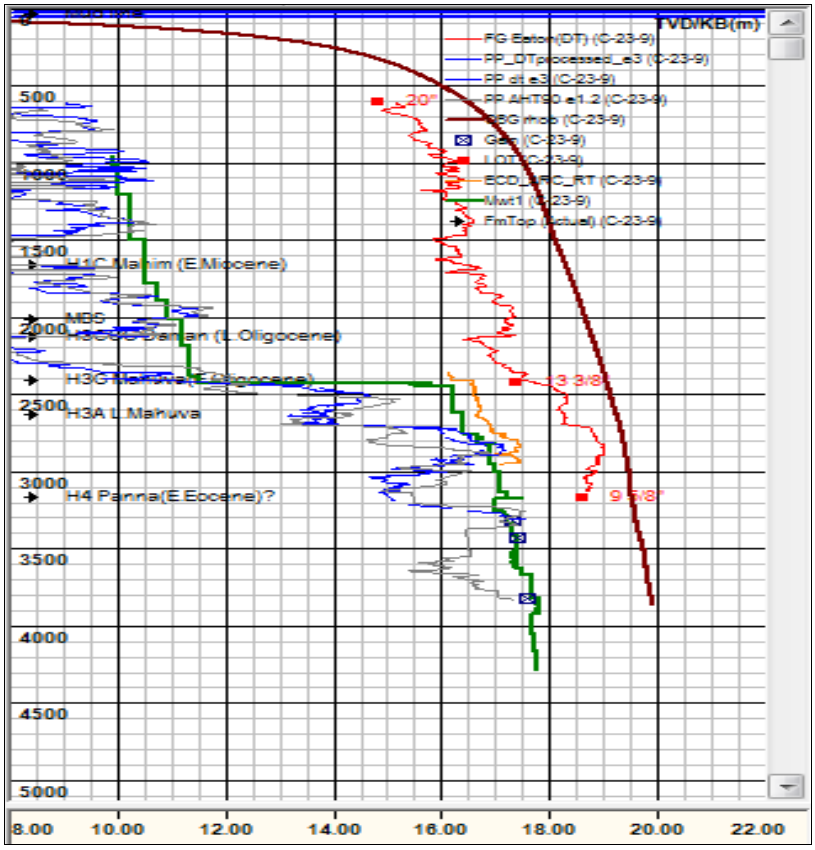

Figure 5: *Shows the final summary of Pore Pressure estimation*

6. Conclusion

Formation pressure, rock stress and sediment compaction is caused by the overburden load and tectonic stresses. Before drilling, during drilling and after drilling of the wellbore, proper evaluation of pore pressure is very important as every stage of the well drilling provide the useful insight about the formation pressure. Theoretical pore pressure model is fundamental approach for determination of formation fluid pressure of the formation. Compaction disequilibrium is the primary mechanism for generation of overpressure. By using the calibrated well log from the drilled wellbore Pore pressure can be accurately obtained.

References

[1] Hubbert, M.K., Rubey, W.W.: Role of fluid pressures in mechanics of overthrust faulting. I. Geol. Soc. Am. Bull. 70, 115-166 (1959)

[2] Applied Drilling Technology – Wellsite Manual, ONGC – India.

[3] Manas K. Chakrabarti, Ashesh R. Desai: Tapti-Daman block of Bombay Offshore, India – A possible site for Tight Gas Reservoir, ONGC, WOB, Mumbai, India.

[4] Well completion report of well-2 (actual name modified). Geological operation group ONGC, Mumbai. Unpublished report. (2015)

[5] Knowledge System Part I, Drillworks Predict. – Linda Mudrock.

[6] Paul, S., Chhatterjee, R., Kundan, A.: Estimation of Pore Pressure and Fracture Gradient from Well Logs: A theoretical analysis of techniques in use: 16th Annual India Oil & Gas Review Summit & International Exhibition, September 10-11, Mumbai, India. (2009)

Cloud Publications
International Journal of Advanced Earth Science and Engineering
2017, Volume 6, Issue 1, pp. 492–499
ISSN: 2320–3609, Crossref: 10.23953/cloud.ijaese.236

Case Study | Open Access

A Case Study: Morphometric Characteristics of Sub-Watershed (P-17) in Paras Region, Akola District, Maharashtra, India – using Remote Sensing & GIS

Shah, K.C., Pranay, R. Pali

Department of Geology and Geoinformatics, Shri Shivaji College, Akola, Maharashtra, India

Publication Date: 21 April 2017

DOI: https://doi.org/10.23953/cloud.ijaese.236

Abstract In this study, an attempt has been made to understand the morphometric characteristics of surrounding of Paras thermal power plant, using remote sensing and GIS techniques. The main objective of this study is to give priority for river sub-watershed (P-17) development by determining the morphometric parameters. This study involves drainage network delineation and morphometric parameters determination, using onscreen digitization on 1:50,000 topographic maps through GIS environs.

Keywords *Geographical Information System & Remote Sensing; Stream Order Map; GPS; Morphometric Analysis*

1. Introduction

Land is not easy to get resource in the earth planet and hence it requires intensive conservation, preservation and management actions. The prioritization of sub-watershed (P-17) is practical application for conservation and management of soil. The channel receives supply from the drainage basin. The two purposes are fulfilling by morphometric analysis of drainage basins. It provides a classic description of the landscape. It also helps in comparing the form and process of drainage basins that may be widely apart in space and time (Easthernbrook, 1993). A great step forward was made by Horton (1932), moved further, previous works and added new measures and proposed general methods for the description of drainage basins characteristic. The drainage basin has shown temporal and spatial variation in morphometric characteristics. Therefore, it seems necessary to investigate in detail of basin characteristics, form area to area and time to time. The reason is, the shape of a basin depending upon morphometric characteristics determine the processes operating in such a basin. The elevation varies from 270m to 290m above mean sea level. There are mainly two types of soil found in the study area, namely-Medium Black and Deep Black soil. The crops grown are Cotton, Pulses, Jowar, Oil seeds. Due to heavy rainfall, the eroded parts and also the grit act as erosive tool. These scrape the gullies in its course downstream. In the upstream, the management practices like grassing, plantation and a forestation are largely followed. Water management, both in its conservation and control aspects, has significantly benefited from satellite remote sensing inputs

that has become an effective tool for a number of applications related to water resources development and management. Remotely sensed data enable us to inventorying of surface water resources through mapping of water bodies and study various hydrological processes and there by water balance with reasonable accuracy. Sub-watershed (P-17) assessment needs an approach that can handle complex problems but is easy, that is flexible consistent, can be applied at different spatial scales, and that can readily be translated into easily communicated descriptions related to management decisions (Khadrri, 2013).

2. Study Area

The area of study surrounds Paras Thermal Power Plant. It is bounded by latitudes $20^0$47`N and longitudes $76^0$45`E. It forms part of Survey of India Toposheet 55 D/13 and 55 D/14 with scale 1:50,000. It covers an area of 1283 sq/km. It falls in Akola district of Maharashtra State (Figure 1). According to the 2001 Census, there was 546 Gram Panchayat for the purpose of Management. The main crops grown in the district are Jowar, Wheat, Cotton, Tur, and Mung. The two main rivers of the district are the Purna and the Penganga, the other less important rivers being the tributaries of these two rivers. Purna River is the main river passing through the study area. Others are tributary to this river, such as Mun River, Man River and Bhikund River. The Bhikund is closest river to the study area. The Bhikund river confluence to the Man River. It is flowing SE zone. The NH-6 national highway is closest to the study area. After its confluence with the Bhuikund, the Man is crossed by the Bombay-Nagpur railway line over a bridge which is south-east of Nagjhari railway station.

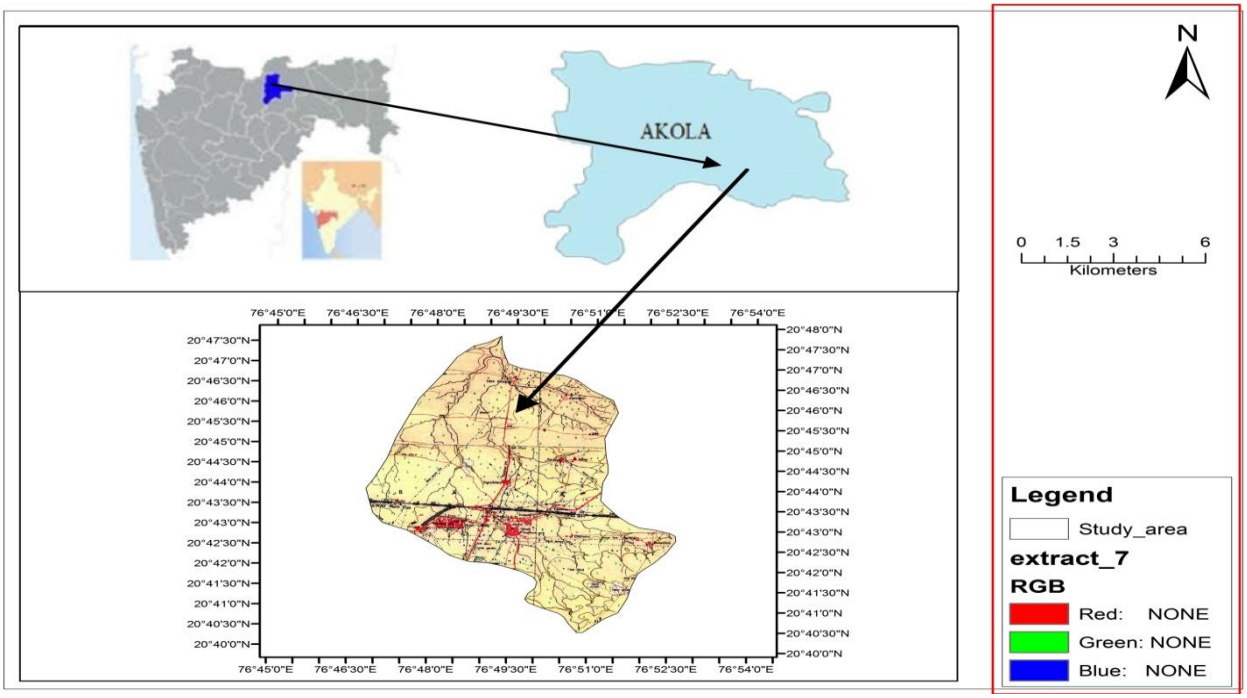

Figure 1: *Location map of the study area*

2.1. Climate

The climate of the district is characterized by a hot summer. General dryness prevail throughout the year except during the south-west monsoon season. The period from about the middle of November to the end of February constitutes the winter season. The summer season extends from March to June. This is followed by the south-west monsoon season which extends up to the end of October. (Khadrri, 2013).

2.2. Rainfall

The average annual rainfall of the district is 846.5 mm (33.33"). The rainfall during the monsoon months constitutes about 85 per cent of the annual rainfall.

2.3. Temperature

Temperature rises rapidly after half of January till May which is the hottest month of the year. In May, the mean daily maximum temperature at Akola is 42°C and the mean daily minimum temperature is 27°C. Days are hot in the summer season and the nights are comparatively tolerable. During the period from April to June the maximum temperature, may be about 46°C or 47°C. The weather becomes pleasant with the arrival of the south-west monsoon in the district by about mid-June. The day temperature increases gradually after the withdrawal of the monsoon. On the other hand, night temperature decreases progressively after September. From October till December, day and night temperature decreases rapidly.

2.4. Humidity

The air is generally dry over the district, except during the southwest monsoon season. During this season the humidity is between 60 to 80 percent. The relative humidity is even less than 20 percent in the afternoons on summer days.

3. Research Method

This work is based on map analysis carried out by onscreen digitization. Toposheet number 55 D/13 and 55 D/14 with the scale of 1:50,000. (Survey of India) were mosaic to subset the study region. The subset image is geometrically corrected through the process of georeferencing.

4. Results and Analysis

The result of the work has been presented in the following section and discussion of each item of result has been done simultaneously. Morphometric analysis of Paras region sub-watershed (P-17) tributary has been carried out quantitatively including linear, aerial and relief aspects. In the linear aspects are calculated in various morphometric parameters, such as stream order (μ), stream number (Nμ), stream length (Lμ), and bifurcation ratio (Rb); presented in Table 1. Figure 2 shows the drainage network as well as stream numbers. The areal aspects of the drainage basin are perimeter, geometric shape of basin, drainage density (Dd), Stream Frequency (Fs) and drainage texture (Dt). The relief aspect is altitude determine by TIN networks creation and ground slope as presented in (Figure 4 & 5). Strahler's, Horton's and Schumm's methods have been employed to assess the fluvial characteristics of the study region (Horton, 1945; Strahler, 1964). The maps were georeferenced and digitized using the Arc GIS 9.3 and ERDAS Imagine 9.1 GIS software's and attributes were assigned to create the digital database.

4.1. Drainage density (Dd)

According to Deju A., Raul (1971) Drainage density is the ratio of total length of all the streams in the sub-watershed (P-17) to the area of sub-watershed. It helps in determining the permeability and porosity of the sub-watershed and an indicator of landform elements in stream eroded topography. Thus, it concludes that the drainage density increase with the decrease in areal coverage and the soil moisture in the region remains more. Similarly, as the drainage density decrease the area of the intra basin increase and soil moisture decreases.

The drainage density of the Paras sub-watershed basin is 3.37. High drainage density is the result of weak or impermeable surface materials, sparse vegetation, and mountainous relief. Low drainage density leads to coarse drainage texture (Strahler, 1964). As per Drainage map the area shows low drainage density and drainage texture is coarse. The simplest way to calculate drainage density on a regional scale is to divide the basin into grid squares of one square mile or one square kilometer each and to measure the total stream lengths in each grid square.

4.2. Stream Frequency (Fs)

Stream frequency or drainage frequency (Fs) is the total number of stream segments of all orders per unit area (Horton, 1932). The stream frequency value of the basin is 0.40.

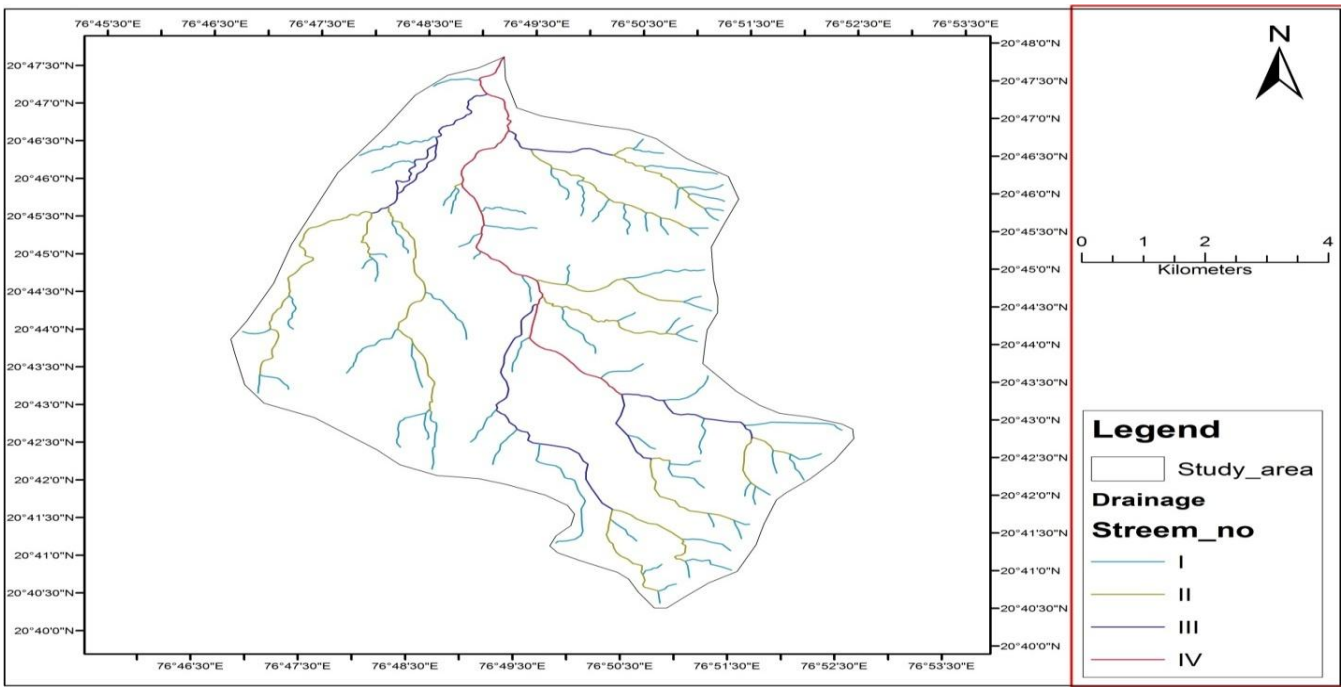

Figure 2: *Drainage Map of the study area*

4.3. Drainage texture (Dt)

Drainage texture is defined as the total number of stream segments of all orders per perimeter of that area (Horton, 1945). Drainage texture in the area is coarse.

4.4. Bifurcation Ratio (Rb)

The bifurcation ratio is the ratio of the number of the stream segments of given order 'Nu' to the number of streams in the next higher order (Nu+1), Table 1. Horton (1945) considered the "bifurcation ratio as index of relief and dissections and demonstrated that bifurcation shows a small range of variation for different regions or for different environment except where the powerful geological control dominates". It is observed that the Rb is not same for one order to its next order (Schumm, 1956). These irregularities dependent upon the geological as well as lithological development of the drainage basin (Strahler, 1964). The bifurcation ratio is dimension less property and generally ranges from 3.0 to 5.0. The lower values of Rb are characteristics of the sub-watershed, which have suffered less structural disturbances (Strahler, 1964) and the drainage pattern has not been distorted because of the structural disturbances (Nag, 1998). In the present study, the higher values of Rb indicate

strong structural control on the drainage pattern.

4.5. Stream Length (Lu)

A stream length supports the theory that geometrical similarity is preserved generally in sub-watershed of increasing order (Horton, 1945). Author has computed the stream length based on the law proposed by (Horton, R.E. 1945), Table 1. It is observed that stream length is maximum that is

Stream Order	Number of Stream	Bifurcation Ratio	Length of Stream (km)
1	76	5.07	54.07
2	15	03	163.12
3	05	05	12.89
4	01		10.45
Total	97	13.07	240.53

163.12 for second order streams.

Table 1: *Stream order and number of streams*

4.6. Generation of contour map

Contours are imagery lines of joining points of equal elevation. The elevation points were prepared from SRTM data. All individual projected values in maps were finally merged as a single layer. The contours were with an interval of 10m. The contour attribute table contains an elevation attribute for each contour line (Table 2). The contour map was prepared using Arc Map of ArcGIS 9.3. Contour map is a useful surface representation to enable, simultaneously visualize flat and steep areas, ridges, valleys in study area (Anji Reddy, M 2001).

4.7. Contour Map

A contour map is a map illustrated with contour lines. Area shows three contours with 10 meter interval having value 270 meter, 280 meter, 290 meter. The gradient between 280 and 290 contour is steep while that between 270 and 280 is gentle (Figure 3*).*

4.8. Slope Map

In Figure 4 shows, a shaded relief map of the study region prepared using 3D analyst extension of Arc GIS 9.3 software. It works as a model and simulates how the terrain looks with the interaction between sunlight and surface features. A mountain slope directly facing towards sunlight will be very bright as well as a slope opposite to the light will be changed. The analysis reveals that the south eastern part of the study region is hilly and undulating as compare to north part.

4.9. Triangular Irregular Network (TIN)

A Triangular Irregular Network (TIN) is a raster representation of a continuous surface, usually referring to the surface of the earth. The TIN map is used to refer specifically to a regular grid of spot heights (Anji Reddy, 2001). It is the simplest and most common form of digital representation of topography (Figure 5).

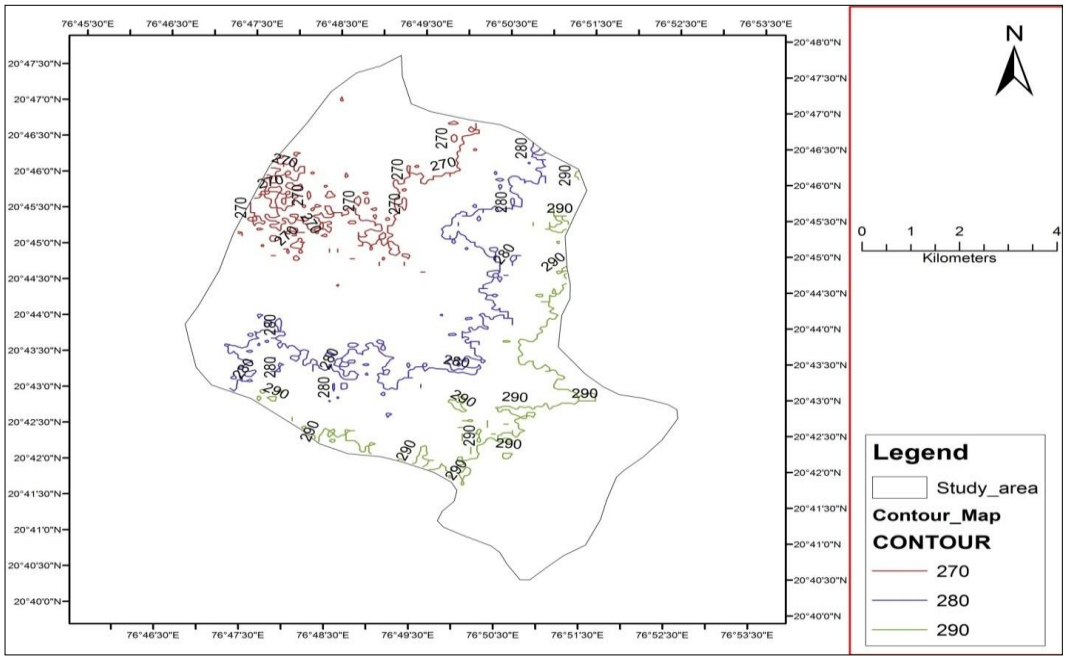

Figure 3: *Contour map of the study area*

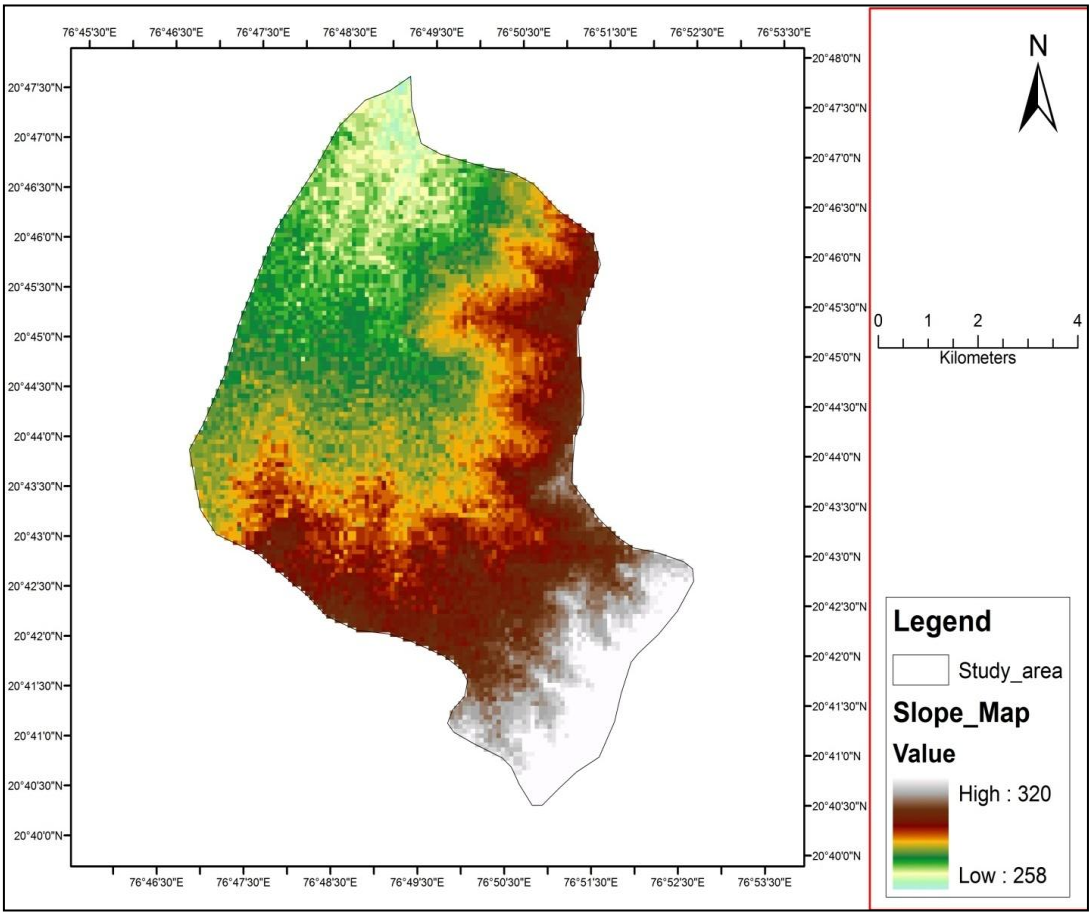

Figure 4: *Slope map of the study area*

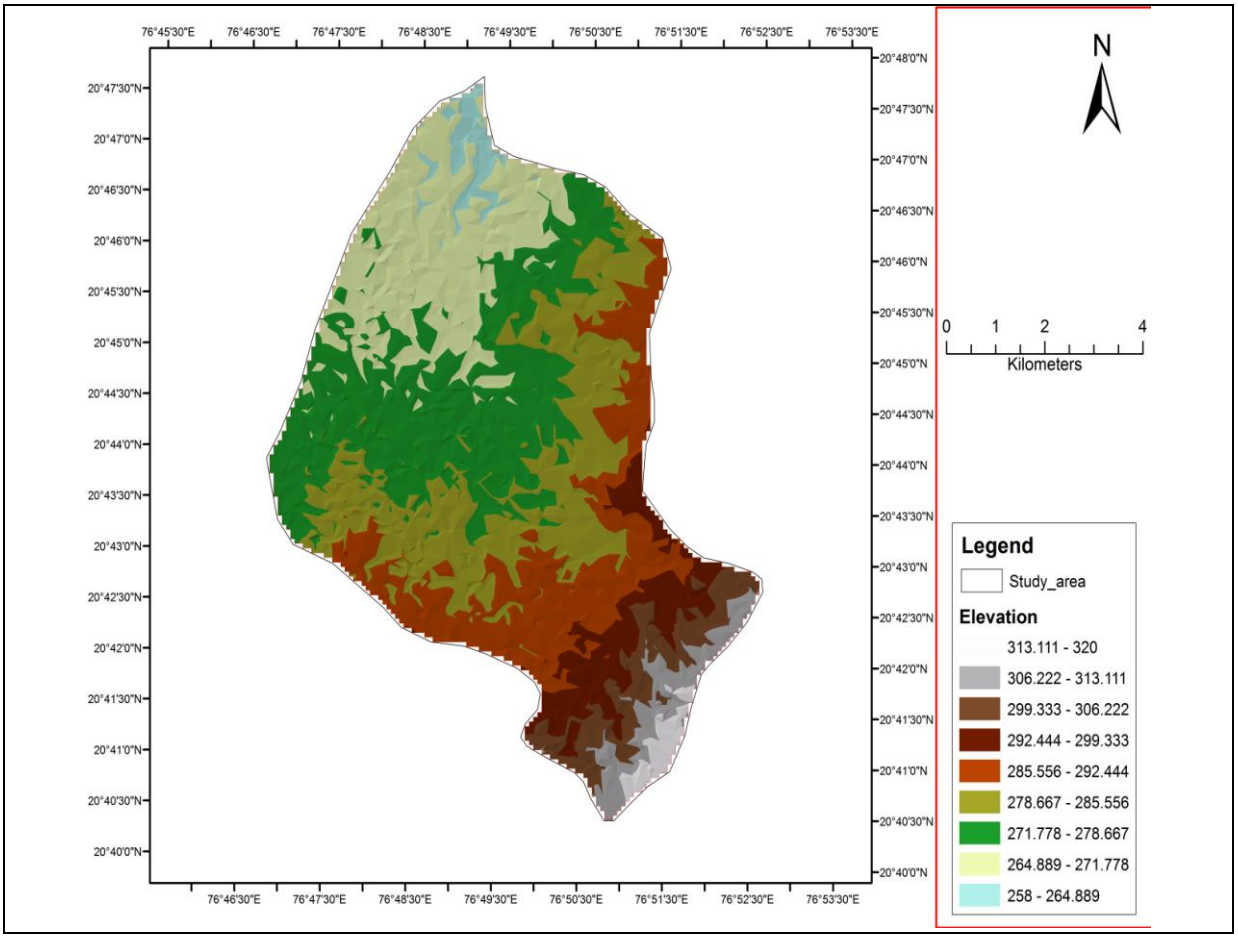

Figure 5: *TIN map of the study area*

5. Conclusion

This study, attempts to understand morphometric characteristics of area surrounding Paras thermal power plant, using remote sensing and GIS techniques. The drainage network delineation and morphometric study were done using on screen digitization on 1:50,000 topographic map through GIS environment such as ArcGIS 9.3 software. Stream frequency value of the basin is 0.40 in the present study. The higher value of Rb indicates strong structural control on the drainage pattern. It is observed that stream Length is maximum i.e. 163.12 km for second order streams. Area shows three contours with 10 meter interval having value 270 meter, 280 meter, 290 meter. The gradient between 280 and 290 contour is steep while that between 270 and 280 is gentle. The underlying exposed rock is predominantly basaltic. A little hilly structure is seen in the South-East Region. As per Drainage map the area shows low drainage density and drainage texture is coarse this indicate permeable surface material dense vegetation and gentle relief. The drainage is flowing from SW to North. Drainage density is slightly higher on NE side of the basin while it is low on NW side. TIN Map is the 3-D presentation of the surface derived by the interpolation of contour map. It represents x, y and z-axes in pixel size of the order 23.5 meters. The altitude or z axis ranges from 258 meters to 320 meters above sea level. Most of these criteria suggest good ground water resource.

Acknowledgment

We are very grateful to Principal of Shri Shivaji College of Arts, Commerce and Science, Akola (MS) for constant motivation and support. We are thankful to Dr. N.R. Kokate, Shri. G.L. Taker and Ms. Sonal Thorat for their time to time help and suggestions. We are also thankful to Shri J.R. Thokal, for his help in typing work.

References

Anji Reddy, M. (2001). *A Text Book of Remote Sensing & GIS*. 2nd edition. Hyderabad: B.S. Publications.

Deju A., Raul (1971). *Regional Hydrology Fundamentals Hardcover*. United Kingdom: Harwood Academic

Easthernbrook, D.J. (1993). *Surface Processes and Landforms.* New York: Macmillan Publishing Co.

Horton, R.E. (1932). Drainage Basins Characteristics. *Trans. America Geophys. Union, 13,* 350-361.

Horton, R.E. (1945). Erosional Development of Streams and their Drainage Basins: Hydro Physical Approach to Quantitative Morphology. *Geol. Soc. Am. Bull., 56*, 275-370.

Karuppannan, S., Venkateswaran, S., & Vijaya Prabhu M. (2015). Morphometric Analysis using GIS in Pambar Sub Basin, Krishnagiri and Vellore District, Tamilnadu, India. *International Journal of Advanced Earth Science and Engineering, 4*, 293-307.

Khadrri, S.F.R. (2013). Delineation of Groundwater Potential Zones around Paras Thermal Power Plant using Remote Sensing and GIS Techniques. *IJPRET, 2*(2), 30-53.

Nag, S.K. (1998). Morphometric analysis using remote sensing techniques in the Chaka subbas in Purulia district, West Bengal. *J. Indian Soc. Remote Sensing, 26*, 6976.

Schumm, S.A. (1956). The Evolution of Drainage Systems and Slopes in Badlands at Perth Amboy, New Jersey. *Geol. Soc. Amer. Bull., 67*, 597-646.

Strahler, A.H. (1964). *Quantitative Geomorphology of Drainage Basins and Channel Networks*. In Handbook of Applied Hydrology. New York: McGraw Hill Book Company.

Cloud Publications
International Journal of Advanced Earth Science and Engineering
2017, Volume 6, Issue 1, pp. 500–515
ISSN: 2320–3609, Crossref: 10.23953/cloud.ijaese.269

Research Article

Studies on the Effect of Natural Treatment on Sewage Water, El-Salhiya - Qena City, Egypt

Mohammed M. Askalany[1], M. Diab[2], Fathy A. Abdalla[3] and Abdelmonsef M. Hassan[4]

[1]Geology Department, Faculty of Science, South Valley University, Qena, Egypt
[2]Geology Department, Faculty of Science, Monifya University, Egypt
[3]Academic Publishing and Press, King Saud University, Riyadh, Saudi Arabia
[4]Environmental Researcher, Egyptian Environmental Affairs Agency, Egypt

Publication Date: 31 May 2017

DOI: https://doi.org/10.23953/cloud.ijaese.269

Abstract Natural treatment of sewage wastewater has an environmental and economic means. It is applied by infiltrating wastewater through the vadose zone (unsaturated zone) of an aquifer. This method of treatment proved its effectiveness in removing or reducing most of harmful substances through physic-chemical and biological analysis. The obtained results validated that most of toxic substances were removed by percent of 99.1%, 97.6%, 94.7%, 98.6%, 100%, 99.9% and 100% for TSS, BOD, COD, NH_3, PO_4, total coliform and fecal coliform bacteria, respectively. The study suggests that, the possible removal mechanisms in the vadose zone were primarily filtrations, adsorption and biodegradation, which are the most commonly referenced. These processes are low cost, low or no energy consumption, and low mechanical technology as well as helps in environmental cleanup.

Keywords *Natural treatment; groundwater; sewage wastewater; hydro chemistry*

1. Introduction

1.1. Background

Due to increasing development in desert areas outside the densely populated Nile Valley and Delta has led to the need for exploring alternative renewable water resources (Abdalla, 2012; Abdelkareem et al., 2012; Abdelkareem and El-Baz, 2015). Renewable water resources available in Egypt represent a total of approximately 57 billion cubic meters (BCM)/year. Approximately 97 percent comes from the Nile, with the remainder from precipitation; which is mainly confined to the northern coast. On the other hand, Water demand increasing by 72 BCM/year, over 80 percent of which is used for agriculture. The present per capita water share is below 1,000 m^3/year and it might reach 600 m^3/year in the year 2025, which would indicate water scarcity (water scarcity level starts at 1,000 m^3/year) (Abdel Kader and Abdel Rassoul, 2010). Sewage effluent comprises 99.9% water and 0.1 % organic and inorganic solids in suspended and soluble forms. Raw sewage water contains many microorganisms (bacteria, viruses, and parasitic protozoa), which may be pathogenic, and parasitic worms (Lim et al., 2010).

Sanitation and wastewater treatment services in Egypt are less developed than water supply services. In 2012, Egypt had 372 municipal wastewater treatment plants treating an average of 10.1 million cubic meters per day. The capacity of Egypt's wastewater treatment plants was more than 11 million cubic meters per day, serving more than 18 million people (Abdallah, 2014). Egypt produces 5.5–6.5 BCM per year as sewage water. Of that amount, about 2.97 BCM per year is treated, but only 0.7 BCM per year is used for agriculture (0.26 BCM is undergoing secondary treatment and 0.44 BCM undergoing primary treatment), mainly in direct reuse in desert areas or indirect reuse through mixing with agricultural drainage water (Abdel-Shafy and Abdel-Sabour, 2006). The main wastewater treatment technologies used in Egypt are trickling filter, conventional activated sludge, oxidation ditches, stabilization ponds, constructed wetlands, rotating biological contactor (RBC), sequencing batch reactors (SBR), up-flow anaerobic sludge blanket, and modified septic tank (Abdallah, 2014).

1.2. Previous Work

Natural treatment of contaminated water were studied by many authors such as Shamrukh and Abdalla (2010, 2011 and 2016) studied the effects of riverbank filtration RBF as a natural treatment process to improve water supply quality along Nile towns in Upper Egypt. The study showed that the effectiveness of RBF for removing the pathogens and suspended solids in the abstracted water. Akber et al., (2008) examined the feasibility of long-term irrigation with municipal tertiary treated wastewater using pilot-scale soil aquifer treatment system SAT in Kuwait. The removal efficiencies of biological oxygen demand (BOD), organic carbon (OC) and ammonia were about 100, 90 and 90% respectively. In addition, bacteria were also removed with 50-100% efficiency depending on its type. Gungor and Unlu (2005) studied the nitrite and nitrate removal efficiencies of soil aquifer treatment columns, bench-scale soil column experiments were performed to examine the effects of soil type and infiltration conditions on the removal efficiencies of wastewater nitrites and nitrates during the biological ripening phase of soil aquifer treatment (SAT) columns. The study showed that infiltration rate and the length of wetting period were important parameters affecting nitrogen removal efficiency of SAT columns. Cherif et al., (2013) studied the aquifer recharge by treated wastewaters Korba case study, Tunisia. The study describes the evolution of groundwater quality after recharge with treated wastewaters, three significant parameters controlled throughout the studied area: salinity, nitrates concentrations and total coliforms. The study showed that an improvement of the salinity groundwater levels but no net change in the distribution of nitrate and bacteria else than displacement of the polluted area.

1.3. Objective of the Current Study

The main purpose of this study is to assess and quantify the effects of natural treatment processes on groundwater quality in surface aquifer using the possible aquifer physical, chemical and microbiological indicators in El-Saliya area (Qena), Egypt, where the Quaternary aquifer is recharging mainly from vertical infiltration of sewage wastewater.

2. Study Area

The study area located in the southern part of Upper Egypt between Latitude: 26°13´54´´N and longitudes 32°51´17´´E east of the River Nile (Figure 1). The major source of fresh water in the study area is the River Nile which diverted through Asfun and El-Kalabia irrigation canals and the Quaternary groundwater aquifer. The study area was selected for the present study because of the following: It includes El-Salhiya sewage water plant which was constructed in Qena city (25°9′24″N 32°46′34″E), Egypt in 1985. The capacity of this plant is 25000 m^3/day. Usually, it receives a huge amount of sewage water more than 45000 m^3/day. There is a farm belongs to this plant that has an area of 500 acres with wooden trees. Also, the Quaternary aquifer in the study area exhibits the best conditions in favor of surface recharge where it is unconfined under the reclaimed new areas. As well

as most of groundwater wells in the study area are used to irrigate the reclaimed land. In many parts of the study area, the aquifer is recharged by effluent treated or untreated sewage water from sewage bonds, some of this wastewater used to irrigate wooden forests in the area (Figure 2). All of the above mentioned reasons help to study the effect of natural treatment on wastewater in the study area.

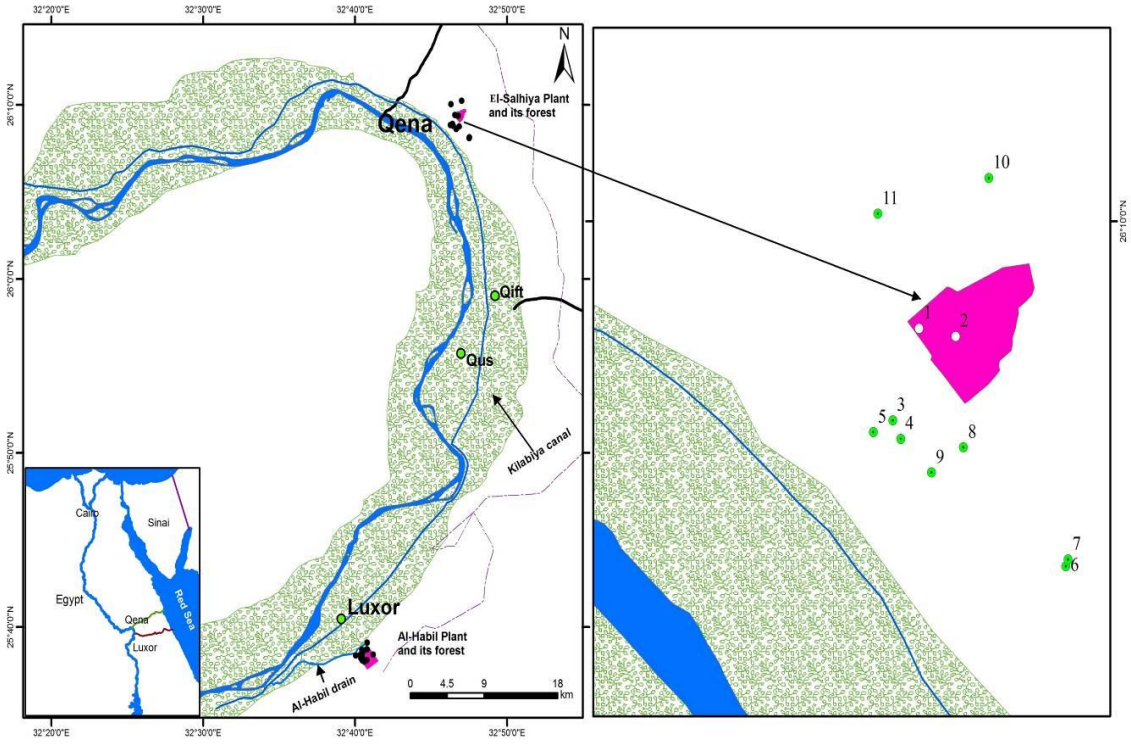

Figure 1: *Location map of the study area showing sampling points location in El-Salhyia area*

(A) (B)

Figure 2: *Field photograph shows sewage water ponds and irrigation of wooden forests at El-Salhyia sewage plant*

2.1. Topography and Climate

The study area is characterized by variation in elevation; in Qena area, the highest elevation is in the east, and decreases toward the west (cultivated area). The elevation is ranging between 45 and 116 m above sea level. Qena is located on the alluvial plains which are represented by the cultivated younger plain occupying the central part of the Nile Valley and the older reclaimed plain at the valley fringes. The study area is located in the arid zone characterized by very dry and hot weather condition. The annual rainfall is very rare and precipitation scarcely occurs as flash floods during winter. The average temperature ranges from 23°C in winter to 44°C in summer. The relative humidity ranges between 53% in winter and 29% in summer.

2.2. Geological Setting

The area has been studied by a variety of authors such as Said (1962, 1981, 1983, 1990), Ahmed (1983), Askalany (1988), Issawi and McCauley (1992), El Balasy (1994), Abadi (1995). The sedimentary sequence in the Qena area (from top to base) as shown in the geologic map (Figure 3) could be summarized as follows:

The Quaternary deposits in the study area are comprised the following deposits:

The Holocene unit: It is represented by the silty clay layer of the Nile floodplain as well as the wadi deposits. The silty clay layer has a thickness ranging from 1 to 14 m and forms the fertile soil of the cultivated lands.
Late Pleistocene: This unit is represented by the Pre-Nile deposits composed of sand and gravel with a thickness of 30 m and extends below the silty clay layer and forms the main Quaternary aquifer in the study area.
Plio-Pleistocene: This unit is represented by the Proto-Nile and Pre Nile deposits composed of clay, sands and gravels locally capped by travertine beds. The exposed thickness of this unit is about 60 m.
Pliocene: This unit is represented by the Paleo-Nile deposits dominated by clay facies represented by clay with sand interbeds. This unit overlies the eroded surface of the Eocene carbonate.
Eocene: The Eocene unit in the study area is composed of the karstified chalky and dolomitic limestone and marl with flint bands and nodules. The exposed thickness of this unit is more than 200 m and acts as a fissured carbonate aquifer.
Paleocene-Late Cretaceous: It is dominated by shale facies with thin interbeds of chalk and phosphate which acts as an aquiclude separating the Eocene fissured carbonate aquifer from the Nubian aquifer underneath.
Upper Cretaceous-paleozoic: This unit is represented by sandstone with shale intercalations. This unit unconformably overlies the basement complex and forms the most common and extended water bearing formation of the Nubian aquifer.

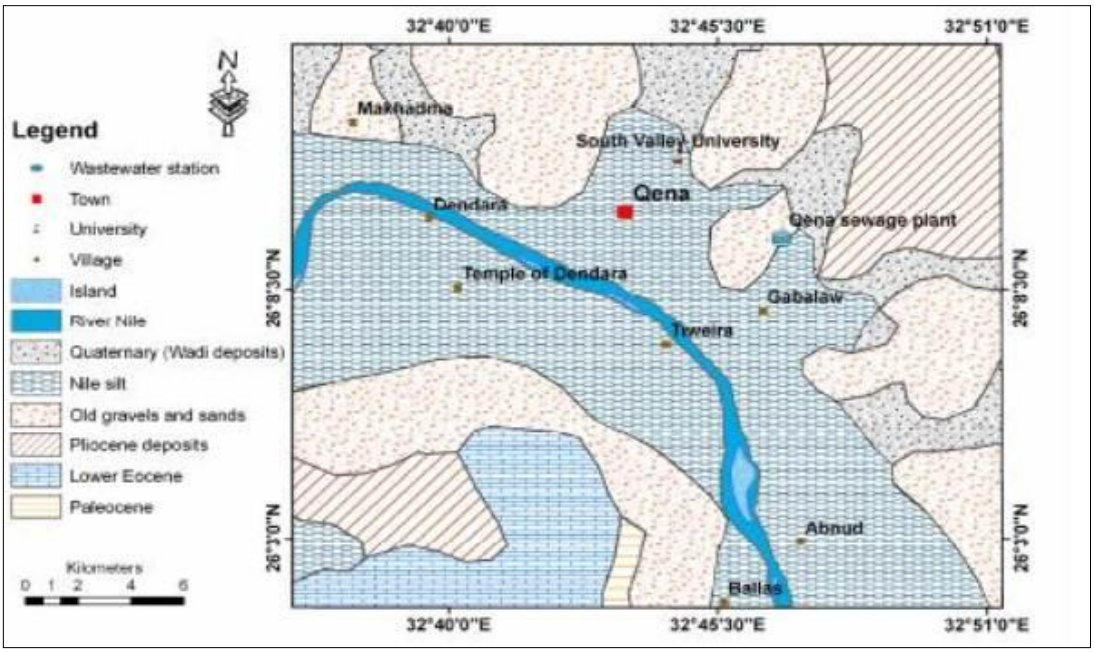

Figure 3: *Geologic map of the study area showing the exposed stratigraphic units (TEGPC and CONOCO 1987)*

2.3. Hydrogeology

The groundwater system in the study area belongs to the regional Quaternary aquifer that extends along the Nile Valley.

2.3.1. *The Quaternary aquifer*

This aquifer can be categorized into two hydrogeological units: the upper Holocene aquitard and the lower Pleistocene aquifer. The Holocene aquitard which composed of clay, silty-clay and clayey-silt deposits and graded sand and gravel intercalated with clayey lenses (Figure 4). The Holocene aquitard is including the phreatic groundwater that constitutes the base of the cultivated lands with thickness varies from 12.5 m to 26 m in the western bank of the River Nile (Kamel, 2004). This unit receives the surface water seepage from irrigation activities. The horizontal and vertical permeability ranges from 0.40 to 1.00 m/day while the vertical hydraulic conductivity is low and increases with depth (Abd El-Moneim, 1988). The Pleistocene aquifer is formed from graded sand and gravel intercalated with clayey lenses. The aquifer in the Nile Valley is extensive and highly productive and distinguished into semi-confined conditions under the cultivated areas and unconfined conditions under the new reclaimed areas at the desert fringes on both sides of the Nile Valley. The aquifer thickness decreases from 300 m at the northern boundary to a few meters in the south western boundary of the study area (Sayed, 2004). The hydraulic conductivity (K) ranges from 60 to 100 m/day and transmissivity ranges from 2000 to 6000 m^2/day (Attia, 1985; Abd El Bassier, 1997). The infiltration tests, according to (Barber and Carr, 1981; Abdel Moneim, 1988) were applied to estimate the infiltration rate of the top layer, the results indicated that the average infiltration rate is 2.5 m/day, this indicating that there is a good hydraulic connection between the upper and lower layer.

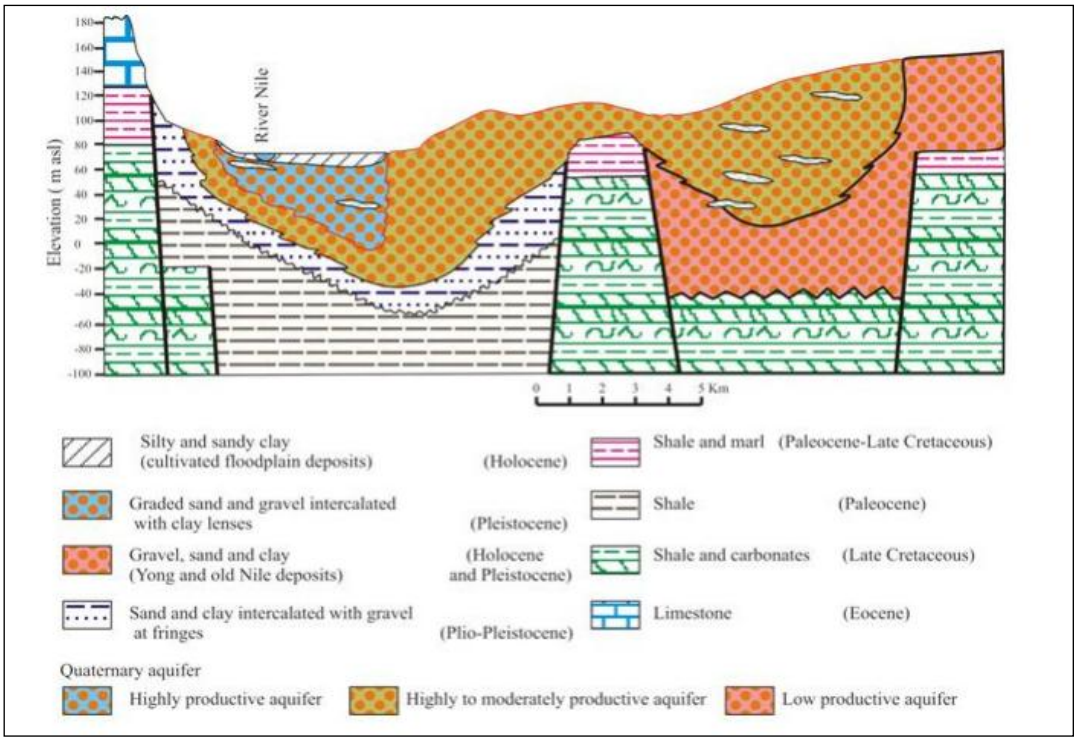

Figure 4: *Hydrogeologic cross section at Qena area (RIGW, 1994)*

In the study area the Quaternary aquifer is mainly recharged by the irrigation water and seepage from irrigation canal through the Holocene aquitard, secondary source of groundwater recharge is the under flow from rainfall during winter months each few years (Brikowski and Faid, 2006; Ahmed, 2003). In addition, seepage from irrigation of the new reclaimed areas at the desert fringes in the study area (Figure 5). The sewage wastewater in the study area of the El-Salhyia sewage water plant, are considered as another recharge source, where raw and treated sewage water are discharged directly on the ground forming some ponds that are used in irrigating woody forests in El-Salhyia areas. Discharge component from the aquifer is through groundwater pumping for irrigation and drinking purposes and natural discharge towards the River Nile (Ahmed, 2003). The depth to groundwater in the Quaternary aquifer as measured from some available wells varies from 30 m to about 120 m. The Plio-Pleistocene aquifer this aquifer represents the secondary aquifer in the study area and exposed at the outer fringes of the Nile aquifer system adjacent to the floodplain. It is composed of clay sand, and gravel (Kamel, 2004; Ismail et al., 2005). The Plio-Pleistocene aquifer has more thickness near the Quaternary aquifer and decreases towards the Eocene limestone boundary on both sides of the Nile valley. At the valley fringes, the groundwater in this aquifer is under phreatic conditions. This aquifer is of low productivity.

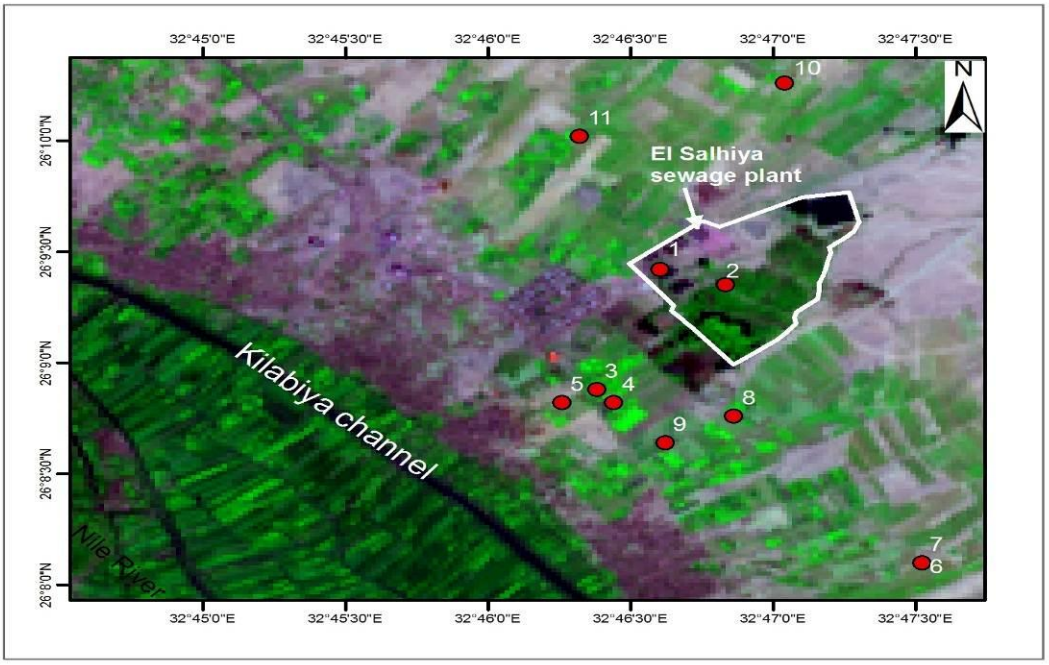

Figure 5: *Land sat image of Qena study area showing the new reclaimed areas at El-Salhyia sewage plant*

3. Methodology

Eleven samples were collected from El-Salhyia sewage water treatment plant and surrounding groundwater in the study area. Physico-chemical water quality measurements and microbial parameters were analyzed. pH and electrical conductivity (EC) of the water samples were measured immediately at the sampling sites. The samples were analyzed for Total Suspended Solid (TSS), Total Dissolved Solids (TDS), nitrates, ammonia, phosphates, Biochemical Oxygen Demand (BOD), Chemical Oxygen Demand (COD) and total, fecal coliform bacteria according to Egyptian standards and the procedures of the American Public Health Association (APHA, 1998). pH and Electrical Conductivity (EC): of the water samples were measured by using checker meter (Model Horiba water checker U-10). Soluble anions: of the water samples were determined by using High Performance Liquid Chromatography HPLC (Model Shimadzu -SCL- 10ASB) and (TDS) of the water, samples were determined by gravimetry method (A-9) according to standard methods for examination of water and wastewater. Microbial measurements for pathogens were carried out at the laboratories of Ministry of Health in Egypt. The results of groundwater samples were compared with those of the outflow sewage water sample for El-Salhyia sewage water treatment plant, and the usefulness of the natural treatment processes are evaluated based on this comparison.

4. Results and Discussion

4.1. Physico-chemical characteristics of El-Salhiya sewage water treatment plant

The various physico-chemical characteristics of El-Salhiya sewage water treatment plant in Qena are listed in Table 1. The result showed that, pH values of sewage water samples range from 6.8 to 7.3 for inflow and outflow wastewater respectively, the TSS concentrations range from 124 mg/l for inflow wastewater to 97 mg/l in effluent sewage water which might be due to gravity settling of suspended particulates in settling tank during the secondary treatment process (WSP, 2008).

Table 1: *Physico-chemical characteristics of El-Salhiya sewage water treatment plant*

Location	Sample number	pH	TSS	TDS	BOD	COD	NO_3^-	NH_3	PO_4^{3-}	SO_4^{2-}
		(-)	(mg/L)							
Inflow wastewater	1	6.8	124	437	130	152	21.5	16.5	2.3	41.0
Outflow wastewater	2	7.3	97	453	99	123	22.0	16.3	2.9	22.8

The TDS values range from 437 mg/l for inflow wastewater to 453 mg/l in effluent sewage water. BOD concentration was reduced from 130 mg/l in inflow wastewater to 99 mg/l in effluent sewage water; COD was reduced from 152 mg/l in inflow wastewater to 123 mg/l in effluent sewage water which are treated by biological treatment (activated sludge), aerobic sludge consisting of active bacteria, which consume and remove aerobically biodegradable organic substances**,** this natural treatment is represented by the following equation (Fujii, 2009); Organic pollutants → mCO_2 + nH_2O + Bacteria cell. Nitrate concentration is slightly increased from 21.5 mg/l in inflow wastewater to 22.0 mg/l in effluent sewage water, reflecting the nitrification process. The transformation of ammonia to nitrate via an intermediate step of nitrite is called nitrification. The transformation of nitrate to gaseous nitrogen is referred as denitrification (Tilley et al., 2014), while ammonia is slightly reduced from 16.5 mg/l in inflow wastewater to 16.3 mg/l in effluent sewage water. Phosphates concentration increased from 2.3 mg/l in inflow wastewater to 2.9 mg/l in effluent sewage water. Biological elimination of phosphorus in conventional wastewater treatment system occurs through the uptake of phosphorus by some bacterial cells. However, only little phosphorus can be removed through this way, as the phosphorus mass fraction in volatile sludge is only about 2.5% (Haandel and Lubbe, 2007). For sulfate, the results showed that the concentration in inflow sewage water sample is 41 mg/L but it decreased to 22.8 mg/L in outflow sample, this may be due to sulfur oxidation bacteria (Thiobacillus Thiooxidans) in secondary treatment process (Biological treatment) oxidize reducing sulfur compounds such as thiosulfuric ($S_2O_3^{2-}$) and sulfide (S^{2-}), sulfite (SO_3^{2-}) into sulfuric acid ion (SO_4^{2-}) by utilizing oxygen in air (Fujii, 2009).

4.2. Microbiological analysis of El-Salhiya sewage water plant

The results of total and fecal indicator organisms for El-Salhiya sewage plant are shown in (Table 2). The results showed that the count of total coliform bacteria in inflow sewage water sample in El-Salhiya sewage plant is >1.810.000 cell/100 ml, while in outflow sample was less than 1.810.000 cell/100 ml. The results showed that the count of fecal coliform bacteria in inflow sewage water sample in El-Salhiya sewage plant is 100.000 cell/100ml while it decreased to 80.000 cell/100 ml in outflow sample, the decrease in fecal count in outflow wastewater may be due to sedimentation processes which eliminate large numbers of pathogens, while aeration promotes antagonistic reactions between different microorganisms, causing their elimination (Leong, 1983). The station is unable to filter the impurities because it receives a huge amount of sewage water.

4.3. Groundwater characteristics around El-Salhiya sewage water

The main physico-chemical characteristics of groundwater samples around El-Salhiya sewage water plant were determined. Discussion on some of the important water quality parameters follows.

Hydrogen ion concentration (pH) Interpolation of pH values using GIS (Figure 6) shows the distribution of pH values for groundwater samples around El-Salhiya sewage plant. The map showed that the groundwater, in most wells have slightly alkaline conditions (7.4 to 8.2), this alkaline condition might be due to the high concentration of base compounds such as bicarbonates.

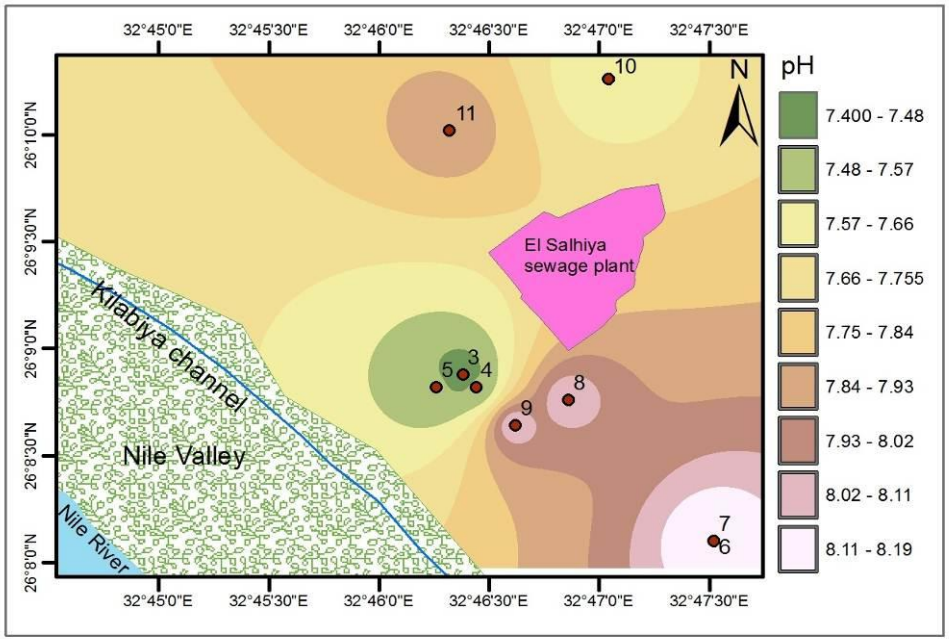

Figure 6: *GIS map shows pH distributions in groundwater samples around El-Salhiya plant*

Total Dissolved Solids (TDS) TDS values for groundwater samples around El-Salhiya sewage plant ranged from 715 mg/L to 3160 mg/L. Interpolation of TDS values (Figure 7) shows that TDS values increase towards desert and reclaimed lands, this might be due to the leaching processes of fertilizer and natural minerals already present in the desert soil (as gypsum $CaSO_4$, $2H_2O$ and halite NaCl). No significant change in the TDS was observed between the outflow sewage water of El-Salhiya plant and the groundwater around it.

Total Suspended Solid (TSS) The results showed that the TSS values of groundwater samples around El-Salhiya sewage plant are less than the values of outflow water sample in El-Salhiya sewage plant. Figure 8 shows the comparison of TSS values between effluent sewage water of El-Salhiya plant and groundwater samples around it. The Figure indicates that infiltrating effluent sewage water, which recharges the groundwater has been filtrated during their passage through the top soil layer. Therefore the TSS are removed by physical mechanism (filtration) at or near the soil surface (in first few meters), where the TSS has been reduced by about 99.1%. These results proof the natural filtration effectiveness, these are in agreement with the previous work carried out at other sites (Idelovitch et al., 2003; Akber et al., 2003).

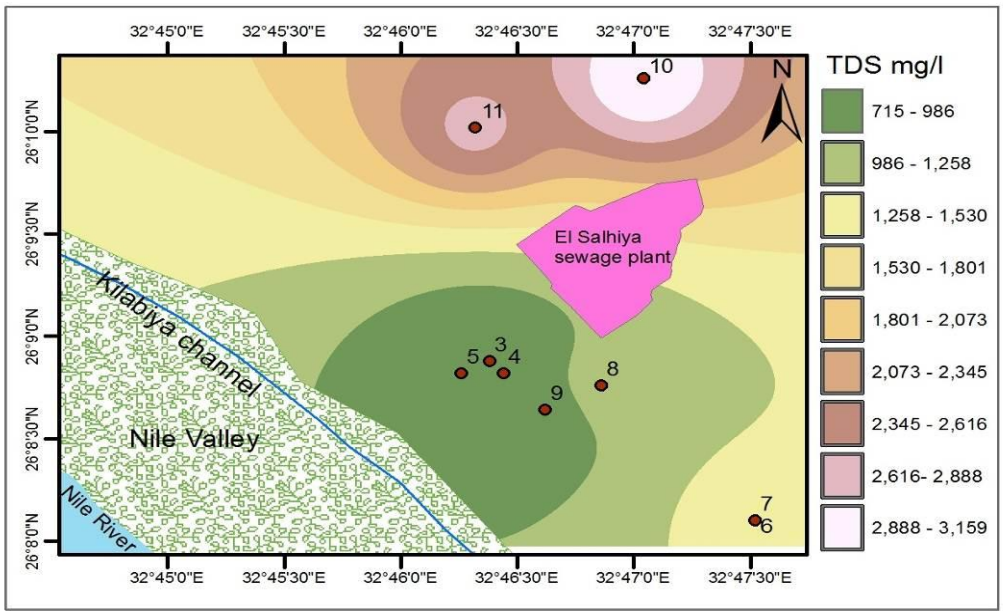

Figure 7: *GIS map shows TDS distributions in groundwater samples around El-Salhiya plant*

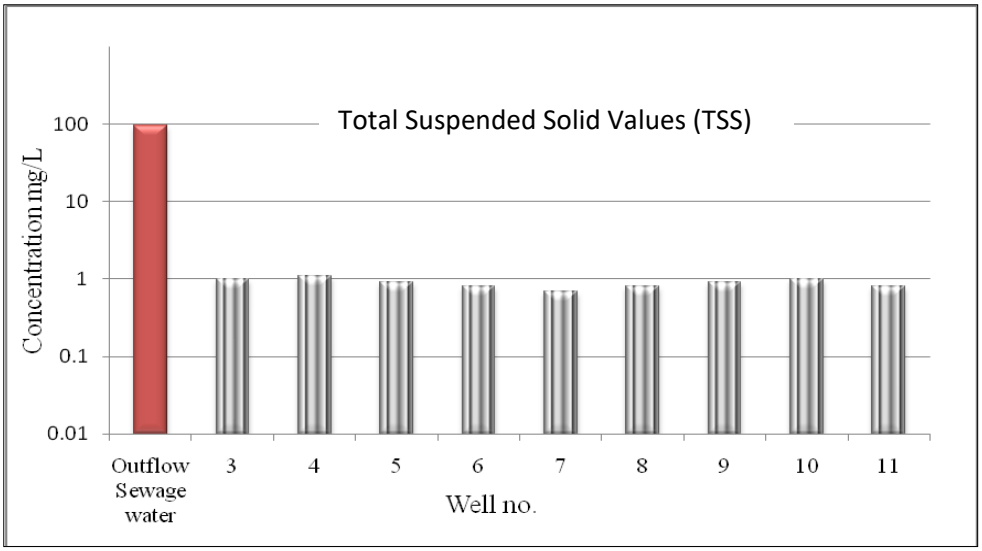

Figure 8: *Comparison of TSS values between outflow sewage water and groundwater around El-Salhiya plant*

Biochemical Oxygen Demand (BOD) The results showed that the BOD values of groundwater samples around El-Salhiya sewage plant are less than the values of outflow water sample in El-Salhiya sewage plant. Figure 9 shows the comparison of BOD values between effluent sewage water samples of El-Salhiya plant and groundwater samples around it. The figure indicates that infiltrating of sewage water effluent into the groundwater, has been naturally treated by soil aquifer. BOD content is removed by two major processes: biodegradation by aerobic and anaerobic bacteria, and adsorption by the soil particles through the vadose (unsaturated) zone. Generally microbial metabolism and degradation processes require electron donators and acceptors, organic matter of unfiltered sewage water and of solid phase working as electron donors (Shamrukh and Abdalla, 2010). BOD has been reduced by about 97.6%, reflecting the major role of natural treatment and its effectiveness, these are in agreement with the previous work carried out at other sites (Idelovitch et al., 2003; Akber et al., 2008).

Chemical Oxygen Demand (COD) Figure 9 shows the comparison of COD values between effluent sewage water samples of El-Salhiya plant and groundwater samples around it. The figure indicates that infiltrating the sewage water into the groundwater reduces the values of COD, this proof that sewage water has been naturally treated by soil aquifer. As in BOD the COD is removed by two major processes: biodegradation by aerobic and anaerobic bacteria, and adsorption by the soil particles through the vadose (unsaturated) zone. COD has been reduced by about 94.7%, reflecting the role of the natural treatment processes. These are in agreement with the previous work carried out at other sites (Sato et al., 2005; Akber et al., 2008).

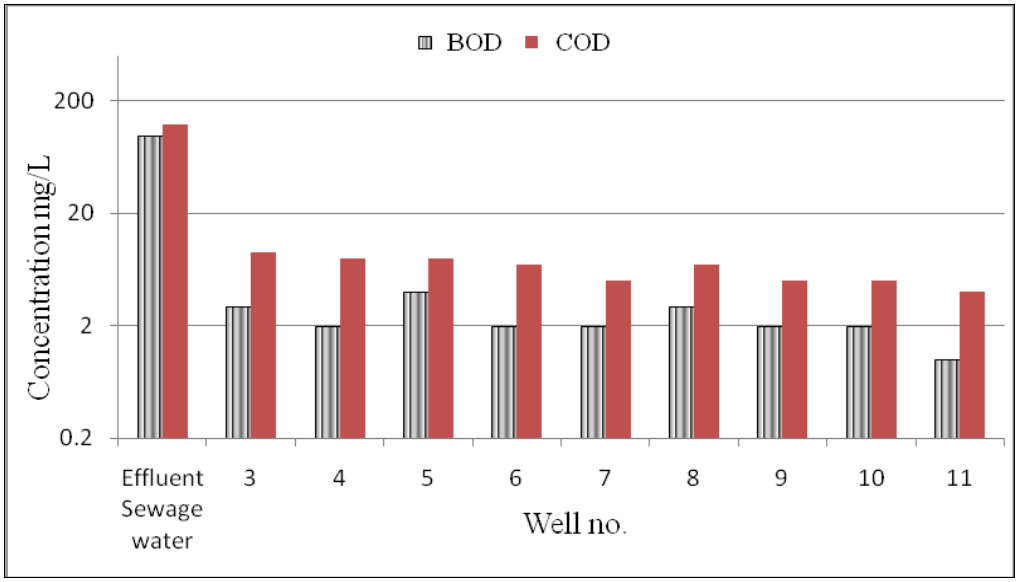

Figure 9: *Comparison of BOD and COD values between effluent sewage water and groundwater around El-Salhiya plant*

Nitrate (NO_3^-) The comparison of nitrate values between effluent sewage water samples of El-Salhiya plant and groundwater samples around it (Figure 10) shows that infiltrating sewage water, which recharges the groundwater, has been naturally treated by soil aquifer. About 44 % of the groundwater samples have lower levels of NO_3 than effluent sewage water due to denitrification process by aerobic and anaerobic bacteria (Idelovitch et al., 2003; Akber et al., 2008). While 56 % of the groundwater samples have NO_3 higher than effluent sewage water due to attributable to nitrification of NH_3, and use of nitrogen fertilizers in new cultivated area around the sewage treatment station (Divya and Belagali, 2012).

Ammonia (NH_3) The results showed that the NH_3 values of groundwater samples around (El-Salhiya) sewage plant decreased more than the values of outflow water sample in El-Salhiya sewage plant. Figure 10 shows the comparison of NH_3 values between effluent sewage water samples of El-Salhiya plant and groundwater samples around it. It indicates that infiltrating sewage water has been naturally treated by soil aquifer. Ammonia is removed with nitrification processes in a soil aquifer system. During infiltration, most of the ammonia is oxidized into nitrate due to aerobic bioprocesses (nitrification) (Foppen, 2002; Yun-zheng and Jian-long, 2006). NH_3 has been reduced by about 98.6%; these results of natural treatment effectiveness are in agreement with the previous work carried out at other sites (Idelovitch et al., 2003; Akber et al., 2008).

Phosphates (PO_4^{3-}) Phosphate not detected in groundwater samples around El-Salhiya sewage water plant. This might be due to the natural treatment effect of the soil aquifer, where phosphate is completely removed (100%) by physical and chemical mechanisms. Chemical precipitation and adsorption on clay and silt lenses are mainly effective on the removal of PO_4^{3-} and the reduction of

phosphate could also be a result of bacterial uptake (Reemtsma et al., 2000; Viswanathan et al., 1999). These results of natural treatment effectiveness are in agreement with the previous work carried out at other sites (Cha et al., 2006; Idelovitch et al., 2003; Akber et al., 2003).

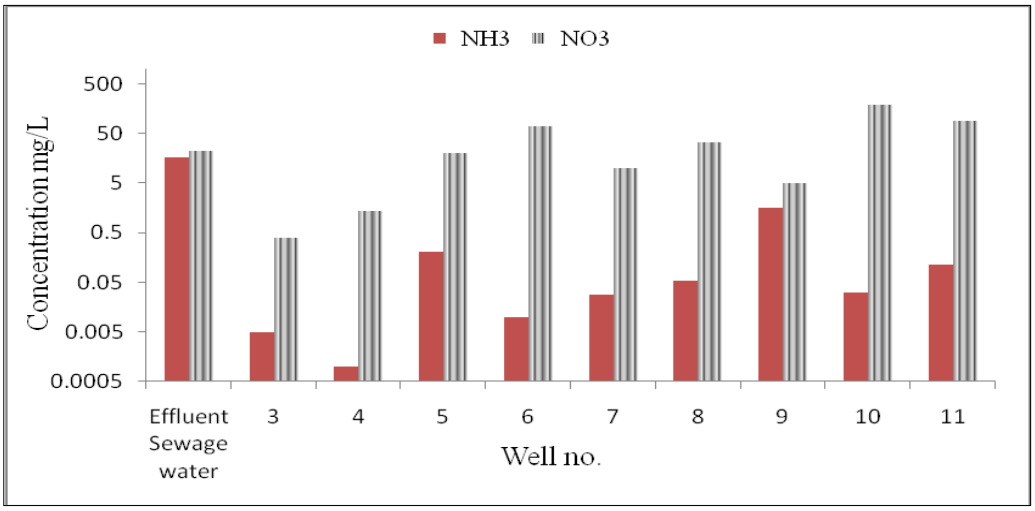

Figure 10: *Comparison of NH_3 and NO_3 concentrations between effluent sewage water and groundwater around El-Salhiya plant*

Total coliform bacteria Total coliform bacteria is not detected in wells (6, 7, 10 and 11) reflecting the removal efficiency of the soil particles (Table 2). Table 2 indicates that infiltered effluent sewage water, which recharges the groundwater, has been naturally treated by soil aquifer, where total coliform bacteria are removed by about 99.9% due to filtration processes and impact of travel time during percolation through soil matrix. This finding is in agreement with other results of Akber et al., (2008); Shamrukh and Abdalla, (2010); Viswanathan et al., (1999).

Fecal coliform bacteria The results of microbiological analysis showed that fecal coliform bacteria in groundwater samples around El-Salhiya sewage water plant was not detected (Table 2). This might indicate that infiltrating effluent sewage water has been naturally treated during wastewater effluent infiltration and percolation through the vadose zone, where fecal coliform bacteria are removed by about 100% may due to filtration processes and impact of travel time during percolation into the aquifer.

Table 2: *Comparison of total and fecal coliform bacteria between influent, effluent sewage water and groundwater around El-Salhiya plant*

Sample NO.	Total coliform (cell/100ml)	Fecal coliform (cell/100ml)
Influent sewage water (1)	>1.810.000	100.000
Effluent sewage water (2)	1.810.000	80.000
Well 3	2	Negative
Well 4	3	Negative
Well 5	2	Negative
Well 6	Negative	Negative
Well 7	Negative	Negative
Well 8	1	Negative
Well 9	1	Negative
Well 10	Negative	Negative
Well 11	Negative	Negative

5. Conclusion

The natural treatment process of sewage wastewater during infiltration and percolation into the soil aquifer through the unsaturated zones improved of sewage water in the study area. The significant observations are as follows:

1) Phosphate removal was generally very high in all groundwater samples in the study area.
2) There was a drop in the bacterial content for the groundwater samples in the study area.
3) TSS is removed by physical mechanism (filtration) at or near the soil surface.
4) Organic substances, BOD and COD were removed by biodegradation and adsorption processes.
5) Leaching from the unsaturated zone tends to increase the TDS of the infiltrated water and the nitrification process increases the nitrate content in the groundwater samples.
6) The low content of clay minerals and organics in the unsaturated zone may prevent the 100% removal of some of the bacteria and other pollutants.

References

Abadi, S.A. 1995. *Geological and hydrogeological studies in the area between longitude 3218' - 32 20' E and Latitude 25 28' - 26 00' N, Nag Hammadi - Egypt*. M.Sc. Thesis, Geol. Dept., Faculty of Science, Assiut University.

Abd El Bassier, M. 1997. *Hydrogeological and hydrochemical studies of the Quaternary aquifer in Qena Governorate*. MSc. Thesis, Fac. of Sci., Assuit Uni., p.164.

Abd El-Moneim, A.A. 1988. *Hydrogeology of the Nile Basin in Sohage Province*. MSc. Thesis. Sohag Fac. of Sci., Assuit Uni., p.165.

Abdalla, F. and Shamrukh, M. 2011. *Riverbank Filtration as an Alternative Treatment Technology: AbuTieg Case Study, Egypt.* In: C. Ray and M. Shamrukh (eds.), *Riverbank Filtration for Water Security in Desert Countries*. Dordrecht, Netherlands: Springer Science+Business Media BV.

Abdalla, F. 2012. Mapping of groundwater prospective zones using remote sensing and GIS techniques: A case study from the Central Eastern Desert, Egypt. *Journal of African Earth Sciences,* 70, pp.8-17.

Abdalla, F. and Shamrukh, M. 2016. Quantification of River Nile/Quaternary Aquifer Exchanges via Riverbank Filtration by Hydrochemical and Biological Indicators, Assiut, Egypt. *Journal of Earth System Science*, 125(8), pp.1697-1711.

Abdallah, N., 2014. Wastewater Operation and Maintenance in Egypt (Specific Challenges and Current Responses). *International Journal of Sciences: Basic and Applied Research*, 18(2), pp.125-142.

Abdelkareem, M., El-Baz, F., Askalany, M., Akawy, A. and Ghoneim. E. 2012. Groundwater Prospect Map of Egypt's Qena Valley using Data Fusion. *International Journal of Images and Data Fusion*, 3(2), pp.169-189.

Abdelkareem, M. and El-Baz, F. 2015. Analyses of optical images and radar data reveal structural features and predict groundwater accumulations in the central Eastern Desert of Egypt. *Arabian Journal of Geosciences*, 8, pp.2653-2666.

Abdel Kader, A. and Abdel Rassoul, S., 2010. Prospects of Water Conservation in Egypt-Special Reference to Wastewater Reuse. In: *Fourteenth International Water Technology Conference-IWTC 14*, Cairo, Egypt.

Abdel-Shafy, H.I. and Abdel-Sabour, M.F. 2006. Wastewater Reuse for Irrigation on the Desert Sandy Soil of Egypt: Long-Term Effect. In: P. Hlavinek et al. (Eds): Integrated Urban Water Resources Management, Springer Publishers, Netherland, pp.301-312.

Ahmed, A.A. 2003. *The impact of hydrogeological conditions on the archaeological sites at some localities between Qena and Aswan, Egypt.* PhD. Thesis, South Valley Uni., Sohag, Egypt, p.449.

Ahmed, E. 1983. *Sediment logy and tectonic evolution of Wadi Qena area.* Ph.D. Thesis, Geology Dept., Assiut Univ., p.250.

Akber, A., Al-Awadi, E. and Rashid, T. 2003. Assessment of the use of Soil Aquifer Treatment (Sat) Technology in Improving the Quality of Tertiary Treated Wastewater in Kuwait. *Emirates Journal for Engineering Research*, 8(2), pp.25-31.

Akber, A., Mukhopadhyay, A., Al-Senafy, M., Al-Haddad, A., Al-Awadi, E. and AlQallaf, H. 2008. Feasibility of long-term irrigation as a treatment method for municipal wastewater using natural soil in Kuwait. *Agricultural Water Management*, 95, pp.233-242.

APHA AWWA, WEF. 1998. *Standard Methods for the Examination of Water and Wastewater 20th edn.* American Public Health Association, American Water Work Association, Water Environment Federation, Washington, DC.

Askalany, M.M.S., 1988. *Geological studies on the Neogene and Quaternary sediments of the Nile Basin, Upper Egypt.* Ph. D. Thesis, Fac. Sci., Assiut Univ., Egypt.

Attia, F.R. 1985. *Management of Water systems in Upper Egypt.* Ph.D. Thesis, Fac., Eng. Cairo Univ., Egypt, p.245.

Barber, W. and Carr, D.P. 1981. *Water Management Capabilities of the Alluvial Aquifer System of the Nile Valley, Upper Egypt*. Technical Report No. 11, Water Master Plan, Ministry of Irrigation, Cairo.

Brikowski, T.H. and Faid, A. 2006. Pathline-calibrated groundwater flow models of Nile Valley aquifers, Esna, Upper Egypt. *Journal of Hydrology*, 324, pp.195-209.

Cha, W., Kim, J. and Choi, H. 2006. Evaluation of steel slag for organic and inorganic removals in soil aquifer treatment. *Water Research*, 40, pp.1034-1042.

Cherif, S., Jrad, A. and Trabelsi-Ayadi, M. 2013. Aquifer Recharge by Treated Wastewaters: Korba case study, (Tunisia). *1st Water Biotech Conference*, 9-11 October 2012, Cairo, Egypt.

Divya, J. and Belagali, S.L. 2012. Impact of chemical fertilizers on water quality in selected agricultural areas of Mysore district, Karnataka, India. *International Journal of Environmental Sciences*, 2(3), pp.1449-1458.

El-Balasy, I.M. 1994. *Quaternary geology of some selected drainage basins in Upper Egypt (Qena Edfu area).* Ph. D. Thesis, Geology Dept., Cairo Univ., p.300.

Foppen, J.W.A. 2002. *Impact of high-strength wastewater infiltration on groundwater quality and drinking water supply: The case of Sana a, Yemen*. Journal of hydrology, 263, pp.198-216.

Fujii, M. 2009. *Treatment technology of industrial wastewater and sewage*, the text book of Jica – Kita. Chapter 4, pp. 31-70.

Gungor, K. and Unlu, K. 2005. Nitrite and Nitrate Removal Efficiencies of Soil Aquifer Treatment Columns. *Turkish Journal of Engineering and Environmental Sciences*, 29, pp.159-170.

Haandel, A.C. van and Lubbe, J.G.M. van der. 2007. Mechanisms involved in Biological Phosphorus removal. In: Haandel, A.C. van, Lubbe, J.G.M. van der (eds.), *Handbook Biological Wastewater Treatment, Design and Optimisation of Activated Sludge Systems*. Webshop Wastewater Handbook, pp.188-191.

Idelovitch, E., Icekson-Tal, N., Avraham, O. and Michail, M. 2003. The long-term performance of Soil Aquifer Treatment (SAT) for effluent reuse. *Water Science and Technology: Water Supply*, 3(4), pp.239-246.

Ismail, A., Anderson, N.L and Rogers, J.D. 2005. Hydrogeophysical Investigation at Luxor, Southern Egypt. *Journal of Environmental & Engineering Geophysics*, 10(1), pp.35-49.

Issawi, B. and McCauley, J.F. 1992. The Cenozoic Rivers of Egypt: The Nile Problem. In: Freidman, R., Adams, B. (eds.), the Followers of Hours: Studies Assoc. Public., No. 2, Oxbow Mong. 20, Park End Place, Oxford, 121–138.

Kamel, R. 2004. *Geology of Luxor area and its relationship to groundwater uprising under the Pharaohs temples.* MSc. Thesis, Aswan Fac. of Sci., South Valley Uni, 178pp.

Leong, L. 1983. Removal and inactivation of viruses by treatment processes for potable water and wastewater - a review. *Water Science and Technology*, 15, pp.91-114.

Lim, S., Chu, W. and Phang, S. 2010. Use of Chlorella vulgaris for bioremediation of textile wastewater. *Bioresource Technology*, 101, pp.7314-7322.

Reemtsma, T., Gnir, R. and Jekel, M. 2000. Infiltration of combined sewer overflow and tertiary municipal wastewater: an integrated laboratory and field study on nutrients and dissolved organics. *Water Research*, 34(4), pp.1179-1186.

RIGW (Research Institute of Groundwater), 1994. Hydrogeological maps of Egypt, scale 1:100,000. Water Research Center, Ministry of Public Works and Water Resources, Egypt.

Said, R. 1962. *The Geology of Egypt.* New York, Amsterdam: Elsevier, p.337.

Said, R. 1981. *The Geological evaluation of the River Nile*. New York: Springer-Verlag Publications, p.151.

Said, R. 1983. Proposed classification of the Quaternary of Egypt. *Journal of African Earth Sciences*, 1, p.41-45.

Said, R. 1990. *The Geology of Egypt*. Rotterdam, Brookfield: Egyptian General Hurghada Inc. and Rep. of Exploration, S.A., Balkema, p.751.

Sato, K., Masunaga, T. and Wakatsuki, T. 2005. Characterization of Treatment Processes and Mechanisms of COD, Phosphorus and Nitrogen Removal in a Multi-Soil-Layering System. *Soil Science Plant Nutrition*, 51(2), pp.213-221.

Sayed, S. 2004. Effect of the construction of Aswan High Dam on the groundwater in the area between Qena and Sohage, Nile Valley, Egypt. Ph. D. Thesis, Fac. of Sci., Assuit University, p.220.

Shamrukh, M. and Abdalla, F.A. 2010. Riverbank Filtration to Improve Water Supply Quality along Nile Towns in Upper Egypt. In: *1st International Conference and exhibition sustainable water supply and Sanitation*, 25-27 July, Cairo, Egypt.

TEGPC and CONOCO. 1987. Geological Map of Egypt (Scale 1: 500000 – 1987), sheet: NG 36 NW Assiut.

Tilley, E., Ulrich, L., LuethI, C., Reymond, P. and Zurbruegg, C. 2014. *Compendium of Sanitation Systems and Technologies*. 2nd Revised Edition. Duebendorf, Switzerland: Swiss Federal Institute of Aquatic Science and Technology (Eawag).

Viswanathan, M.N., Al Senafy, M.N., Rashid, T., Al-Awadi, E. and Al-Fahad, K. 1999. Improvement of tertiary wastewater quality by soil aquifer treatment. *Water Science and Technology*, 40(7), pp.159-163.

WSP. 2008. Technology Options for Urban Sanitation in India. A Guide to Decision - Making. Pdf presentation. New Delhi: Water and Sanitation Program (WSP).

Yun-zheng, P.I. and Jian-long, W. 2006. A field study of advanced municipal wastewater treatment technology for artificial groundwater recharge. *Journal of Environmental Sciences*, 18(6), pp.1056-1060.

Cloud Publications
International Journal of Advanced Earth Science and Engineering
2017, Volume 6, Issue 1, pp. 516–537
ISSN: 2320–3609, Crossref: 10.23953/cloud.ijaese.270

Case Study

Petrogenesis and Tectonic Environment of Granites, Eastern Ghats, South India- A Case Study

Brahmaiah, T. [1], Karunakar, Y. [1], Sai Krishna, K.[2], Sai Prasad, K.S.[1]

[1]Department of Geology, S.V. University, Tirupati, Andhra Pradesh, India
[2]Department of Geology, Kakatiya University, Warangal, Telangana, India

Publication Date: 31 May 2017

DOI: https://doi.org/10.23953/cloud.ijaese.270

Abstract This study presents the geochemical characteristics of granitic rocks located a part of the Eastern Ghats which lies to the east of Cuddapah basin (Obachettapalem in Prakasam district, A.P). These granites are typically uniform as is evident from the chemical and modal classification. The field, petrographic and petrochemical studies explain the magmatic nature of the granites. The magma of these granites is peraluminous and calc-alkaline nature and emplaced as syn-collision environment and crystallised at 650^{o}C to 700^{o}C at 5 to 7 kb of PH_2O.
Keywords *Petrogenesis; Peraluminous; Calc-alkaline; Syn-collision*

1. Introduction

The study area (Obachettapalem, Prakasam district, South India) forms that part of the Eastern Ghats which lies to the east of Cuddapah basin (between 15°35' - 15°41' N latitude and 79°43' – 79°51' E longitude). The area forms an igneous and metamorphic complex having a variety of rocks viz., charnockite series (pyroxene granulites and charnockites), khondalites series (paragneisses and quartzites), granites, dyke rocks and pegmatites in the order of their abundance. The chronological sequence of the various rock units has been worked out purely on the contact studies in the field.

In the field, the granites are massive and even some exhibit banded appearance. The banding which is due to the alteration of the bands consisting of felsic and mafic constituents is very clearly displayed particularly when it is close to the pelitic gneisses. The foliation strikes N 10^{0}W to N 20^{0} W and dips at higher angles towards the east; with an angle of 50^{0} to 55^{0} East to vertical. At few places, the trend of foliation changes towards N 20^{0} E retaining the dip in the same direction.

The granites come into contact with the pelitic gneisses and with the charnockites. The contact between the granites and gneisses is considered to be gradational. In the western portion of the area the pelitic gneisses and granites are in contact (Figure 1).

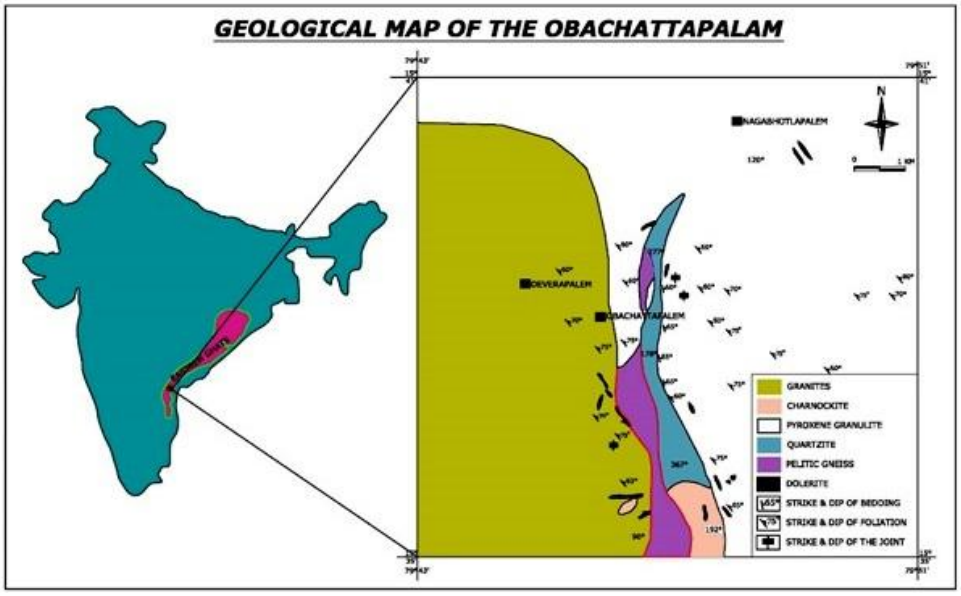

Figure 1: *Location and Geological Map of the Study Area*

Granite is seen in association with charnockites in southern portions of the area. This association has significance in the evolution of the charnockites. Charnockite is seen as a lenticular patch in granite in the southern portion of the area; and also occurs with gradational contact with granites. In some places granite is intruded into the charnockite, which in turn is intruded by dolerite. The coarse fractions of the granites are considered to be pegmatites, while fine portions of leucocratic gneisses are considered to be aplites. In the plains of the southwestern portion of the area, pegmatites and aplites cut across the granites indicating both pegmatites and aplites are the later phases in the evolution of the granites.

The major sets of joints are noted, one paralleling the foliation (N 20^{o} W) and another cutting across it (about E-W), and the third paralleling the topographical surface. These are called L, Q and horizontal joints of sheeting (Cloos, 1937). Both Q and L joints are localized with the dolerite dykes.

2. Method of Study

Our researches in this study consist of two parts: field and laboratory studies. Field studies include identifying the different phases of intrusion, relationship between them and host rock and finally sampling of different phases for laboratory studies. Laboratory investigations include preparing of 40 thin section and petrographic studies, analyzing of 9 samples by ICP-AES and ICP-MS for major, trace and rare earth elements at the PURSE Centre, S.V. University, Tirupati, and National Geophysical Research Institute (NGRI), Hyderabad. Finally, these analyses were processed by using Excel, GCD Kit and IGPET programs.

Petrography

For description and classification purpose, modal compositions are best suited. Johansen (1938); Chayes (1952, 1957); Bateman (1961) and some of the earlier workers who proposed classification of granitic rocks based on modes. The quartz, potash feldspar and plagioclase values, when reduced to 100 and plotted in the trilinear diagram (Figure 2), the rocks have a place in granites. Though all the points lie in the granite field, they occupy different positions within the field reflecting the compositional variations. Streikensen (1973) classification has incorporated the views of the earlier workers and the same is followed in the present work.

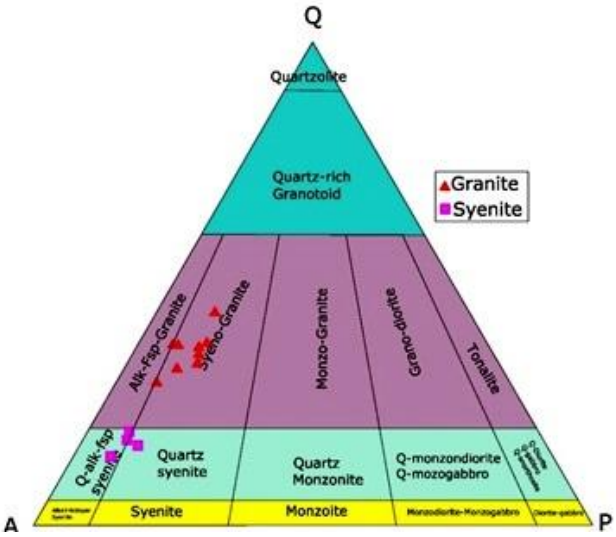

Figure 2: *Quartz (Q) - K-Feldspar (A) - Plagioclase diagram (after Streckeisen, 1973)*

Granites

Granite is a hard compact, coarse – to medium – grained rock with grey colour. The rock exhibits allotriomorphic texture with anhedral grains of perthite, quartz and plagioclase as felsics, and hornblende, biotite and iron ore as mafics. Perthite is noted in large quantities. Wherever perthite intergrowth is noticed, potash feldspar exhibits turbidity, and quartz inclusions are present in perthite. Plagioclase of vein type is present in potash feldspar giving perthitic intergrowth. Sometimes plagioclase is also seen as inclusions in perthite. Hornblende occurs in considerable quantities and only at one or two places it is seen developing after the orthopyroxene. The hornblende grains are riddled with iron ore inclusions. A few small biotite flakes and irregular grains of iron ore noted all over the section. Apatite inclusions are present in almost all the minerals. The modal compositions of the granites are given in Table 1.

Syenite

This is a coarse – grained rock which is hard and compact. The coarse crystals of feldspar and hornblende are seen very clearly. In thin sections, the rock is found to be made up of mostly perthite with smaller portion of quartz and plagioclase. Plagioclase blebs are uniform in potash feldspar host and in most cases confined to the core portions of host, not extending to the marginal portions. The hornblende grains are irregular in distribution and exhibit two sets of cleavages. It shows pleochroism from yellowish-green to green. The coarse nature of the perthite grains indicate that they are crystallized when the magma had considerable amount of volatiles. The modal composition of these rocks is given in Table 1.

Table 1: *Modal Composition of Granites (In volume percentage)*

Sample No	1/70	2/74	3/78	4/103	5/7	6/72	7/73
Quartz	36.58	27.35	30.53	30.10	26.04	32.18	29.07
K-Feldspar	49.08	44.56	45.74	54.52	56.22	48.53	43.33
Plagioclase	11.92	10.23	5.95	8.78	6.52	5.65	9.54
Orthopyroxene	-	-	-	-	0.39	0.48	-
Hornblende	-	6.65	7.63	2.74	3.32	4.19	8.32
Biotite	4.42	9.25	8.92	2.00	3.44	7.89	6.11
Apatite	-	0.57	-	-	1.17	-	0.96

Iron ore	1.00	1.39	1.24	1.86	2.90	1.08	2.67

Sample No	**8/18**	**9/135**	**10/142**	**11/13**	**12/77**	**13/108**	**14/3**
Quartz	31.90	36.51	29.76	16.21	15.15	11.21	14.25
K-Feldspar	48.34	38.07	43.20	61.21	63.96	62.12	62.30
Plagioclase	5.86	8.70	9.30	6.20	6.70	5.20	8.80
Orthopyroxene	0.86	-	-	-	-	-	-
Hornblende	6.78	6.30	7.16	8.82	6.26	9.17	6.16
Biotite	2.74	7.11	7.90	5.90	5.20	9.14	5.81
Apatite	-	-	-	-	0.64	-	0.84
Iron ore	4.23	3.31	2.68	1.68	2.01	3.16	1.84

1-10: Granites 11-14: Syenites

Pegmatite and Aplite

These are quite similar to that of granites. Pegmatite is considered to be only as a textural variant of granite. Aplite is similar in composition to granite, but it does not contain mafics, the difference between them is in granularity. The pegmatite is very coarse-grained, rich in potash feldspar and quartz, whereas aplites are fine-grained and contain quartz, perthite and plagioclase, and both exhibit graphic intergrowth. But for the difference in texture, the aplite and pegmatite are same in composition.

Petrochemistry and Petrogenesis

The results of chemical analysis of the granitic rocks together with CIPW norm, Niggli values are given in Table 2.

Major elements

SiO_2 varies from 63 to 69%, Al_2O_3 from 13.5 to 16.6%, FeO (total) from 3.5 to 6.5%, MgO from 1.4 to 2.6%, CaO from 0.4 to 1.8%, Na_2O from 2.2 to 3.06%, K_2O from 4.2 to 6.8%, TiO_2 from 1.0 to 2.5%, P_2O_5 from 0.13 to 0.20% and MnO from 0.13 to 0.25%. The plots on normative albite (Ab)-anorthite (An)-Orthoclase diagram (O'Conner, 1965); SiO_2 vs Na_2O+K_2O of Cox et al., (1979) and Middlemost, (1994), (Figure 3) indicate the rocks of the present area as granites. Also, when the major Oxides data were plotted in the R_1-R_2 diagram of De La Roche et al. (1980), the R_2 is plotted along the Y –axis and is defined as R_2=(Al+2Mg+6Ca), and R_1 on X – axis as R_1= 4Si-11(Na+K)-2(Fe+Ti). All the plots fall in the granite and granodiorite fields only (Figure 3).

Table 2: *Major element concentrations of granites C.I.P.W. Norm values*

	1/70	2/74	3/78	4/103	5/7	6/72	7/73	8/18	9/135	10/142
SiO_2	69.09	69.94	67.9	71.51	68.83	70.93	70.5	71.9	71.6	70.03
Al_2O_3	16.6	17.71	16.28	16.61	14.27	15.1	16.19	15.02	14.39	16.01
Fe_2O_3	1.53	1.14	1.16	0.3	1.26	1.57	1.75	0.27	1.76	2.04
FeO	1.63	0.92	1.95	0.71	1.31	1.48	1.06	1.2	1.72	1.4
MgO	0.48	0.41	0.73	0.48	0.49	0.76	0.48	0.69	0.46	1.46
CaO	1.24	2.06	2.04	1.08	2.44	2.52	1.21	1.35	1.68	0.36
Na_2O	3.2	4.32	3.65	4.35	4.75	3.65	2.21	3.8	2.2	2.4
K_2O	4.93	2.84	4.58	4.25	3.48	2.47	3.29	4.03	4.26	4.1
TiO_2	1.02	0.17	1.06	0.14	0.49	0.37	1.02	0.26	0.37	1.03

P_2O_5	0.14	0.06	0.16	0.05	0.22	0.19	0.13	0.14	0.16	0.15
MnO	0.06	0.04	0.13	0.02	0.15	0.05	0.16	0.03	0.15	0.15
H_2O	0.19	0.42	0.4	0.82	0.4	0.53	0.11	0.91	0.35	0.52
Total	**100.11**	**100.03**	**100.04**	**100.32**	**98.09**	**99.62**	**98.11**	**99.6**	**99.1**	**99.65**
Quartz	28.567	28.848	23.633	26.668	22.891	33.846	42.12	30.123	38.048	37.861
Corundum	4.08	3.927	1.992	3.01	0	2.295	7.104	2.287	3.488	7.328
Orthoclase	29.135	16.784	27.066	25.116	20.566	14.597	19.443	23.816	25.175	24.23
Albite	27.078	36.555	30.885	36.808	40.193	30.885	18.7	32.155	18.616	20.308
Anorthite	5.237	9.828	9.076	5.031	7.337	11.261	5.154	5.783	7.29	0.806
Diapside	---	---	---	---	2.722	---	---	---	---	---
Hypersthene	1.352	1.563	2.932	2.058	0.724	2.796	1.196	3.326	2.518	3.637
Magnetite	2.219	1.653	1.682	0.435	1.827	2.277	0.982	0.392	2.552	2.016
Ilmenite	1.938	0.323	2.014	0.266	0.931	0.703	1.938	0.494	0.703	1.957
Hematite	0	0	0	0	0	0	1.073	0	0	0.65
Apatite	0.332	0.142	0.379	0.118	0.521	0.45	0.308	0.332	0.379	0.355
Total	**99.937**	**99.622**	**99.659**	**99.511**	**97.712**	**99.109**	**98.018**	**98.706**	**98.769**	**99.149**

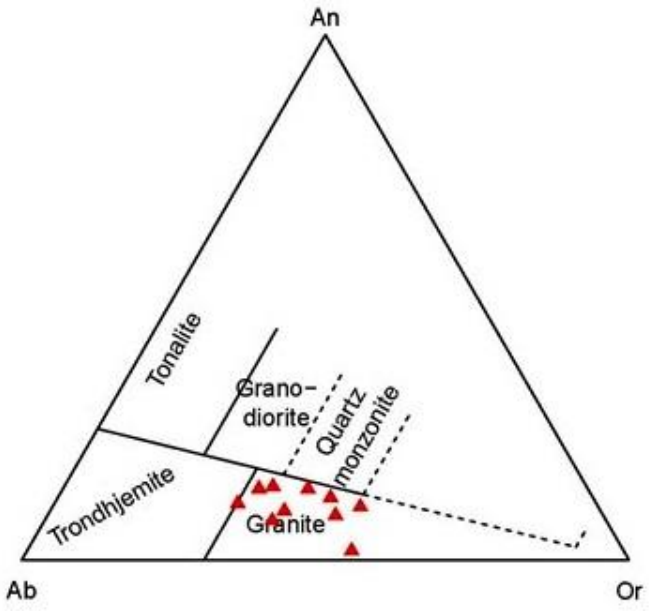

Figure 3A: *Normative Ab-An-Or diagram (O'Conner, 1980)*

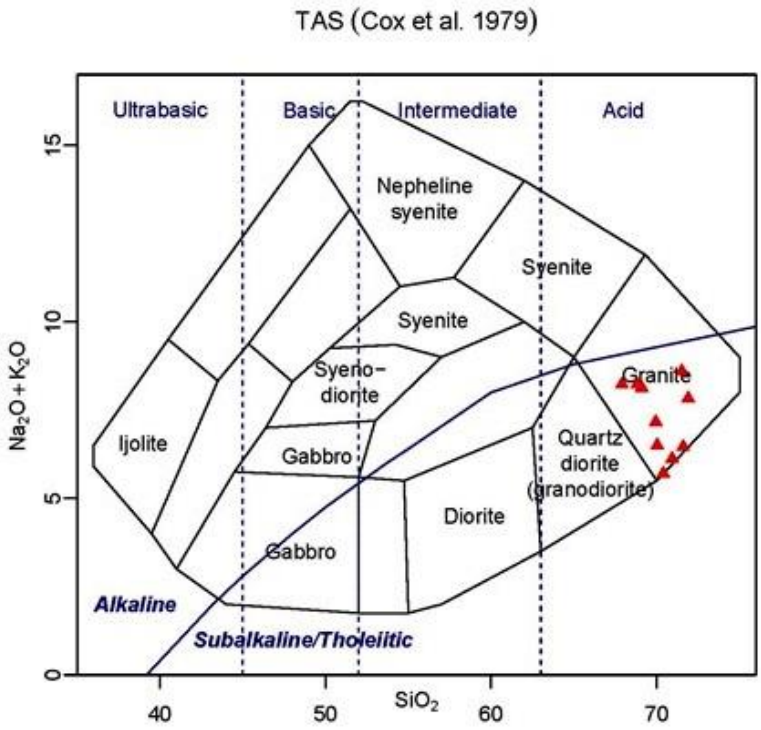

Figure 3B: *SiO_2 vs. $Na_2O + K_2O$(TAS) diagram after Cox et al. (1979)*

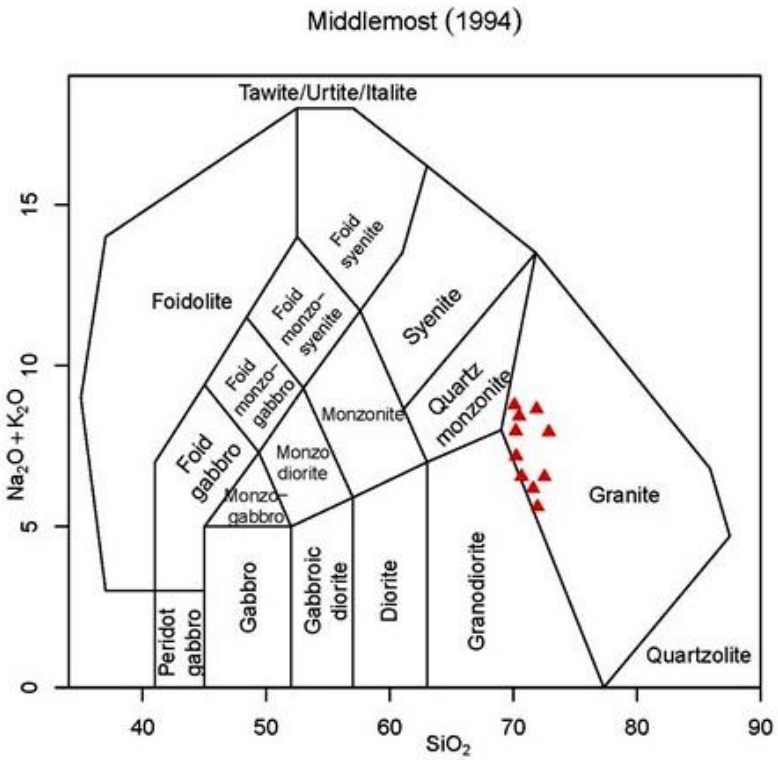

Figure 3C: *TAS diagram classification of rocks in the total alkali-silica diagram (Middlemost, 1994)*

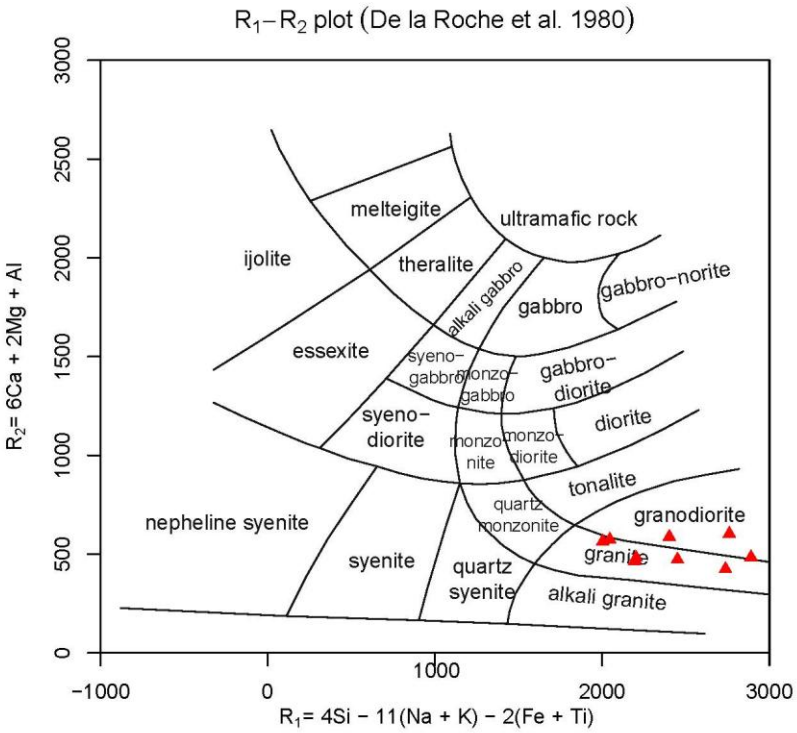

Figure 3D: *R1-R2 diagram of De La Roche et al. (1980)*

The figure (Shand, 1943) shows that the alumina saturation index indicates that these granites are of strong peraluminous with corundum and anorthilte normative; with both Agpatic Index and Alumina saturation Index are >1 (Figure 4a). The characteristic mineral diagram (Figure 4b) which is a measure of Dark minerals [B= Fe +Mg +Ti] and aluminous character [A= Al-(K+Na+2Ca)] also indicates a peraluminous nature of the rocks (Debon and Le Fort, 1983). The peralumious character demonstrated by the A-B diagram reflects the presence of boitite. Generally, granitiods plotting in the peraluminous domain have been derived from anatexis of granitiods magma by first- cycle assimilated intermediate to acid volcaniclastic basin sediments (Leube et al., 1990; and Liaozhongli et al., 2007, Al-Qadhi Abdul-Aleam Ahmed et al., 2016). A–B diagram after Villaseca et al. (1998), showing overall major element variation for the different suites. Two compositional domains are shown: with metaluminous area A < 0 and peraluminous area A > 0. The study area granitoids are of moderate to high Peraluminous type (Figure 5).

Variation in major elements suggesting their chemistry has been modified by interactions with the magma. The study granatoids (SiO2 >60% have also having moderate FeO^t/(FeO+MgO) ratios (,0.8) being classified as Magnessian plutons (Figure 6). The plots of granites on A – F – M diagram (Figure 7) of Irvine and Barger (1971), and the SiO_2-K_2O diagram (Figure 8) of Paccerillo and Taylor (1976) shows that most of the samples fall wilthin high potash clac-alkaline and calc-alkaline series and only one sample in shoshonitic series. The alkaline affinity of these granites is demonistrated on the diagram of Sylvester (1989), which discriminates btweeen alkaline, clac-alkalline and highly fractionated calc-alkaline granites with SiO_2 >68 wt% (Figure 9). Negative trends presented by granites in CaO, P_2O_5, K_2O, TiO_2 and Al_2O_3 versus SiO_2 diagram of Harker (Figure 10), suggests that fractionation of apatite, alkali feldspar took place during the evolution of these granites.

Chappel and White (1974) stated that the rocks of igneous type have atomic ratios of Al/(Na + K + 2 Ca)= up to 1. The granites of the present area have a value of 0.9, indicating that these are igneous in nature.

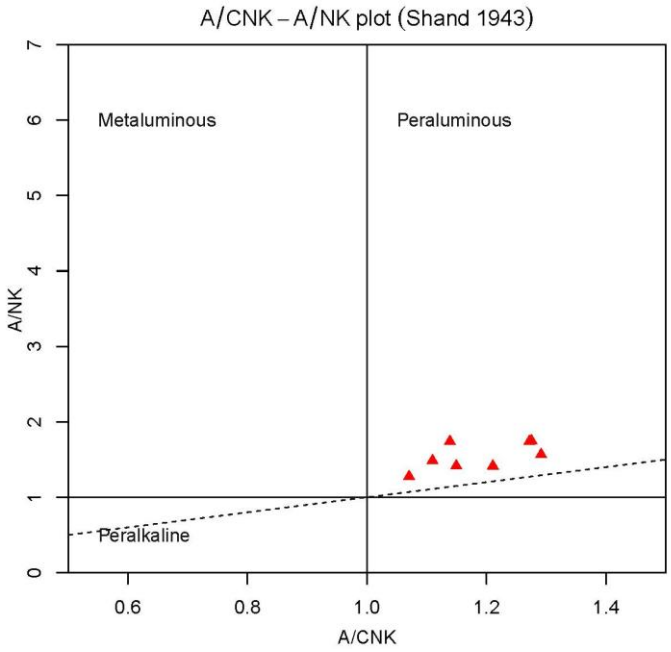

Figure 4a): *The figure shows that the alumina saturation index indicates that these granites are of strong peraluminous in nature (Shand, 1943)*

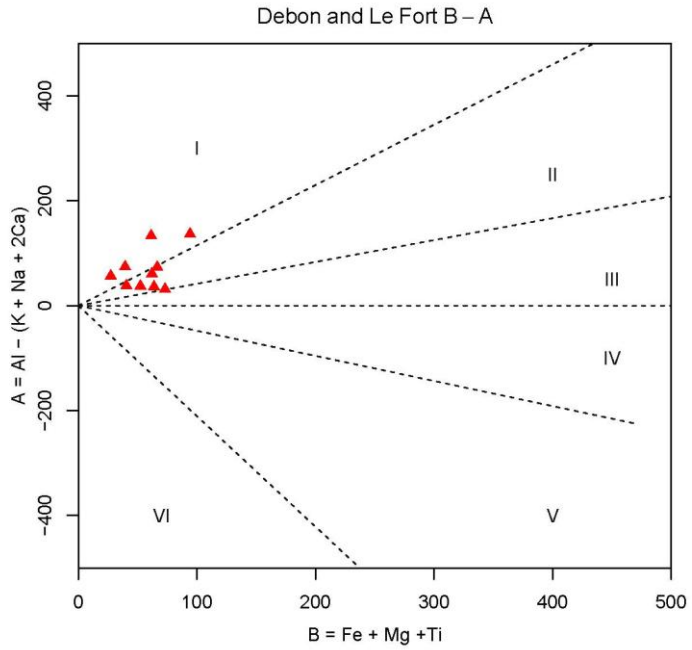

Figure 4b): *Distribution of granitic facies of (A versus B) of Debon & Le Fort (1983)*

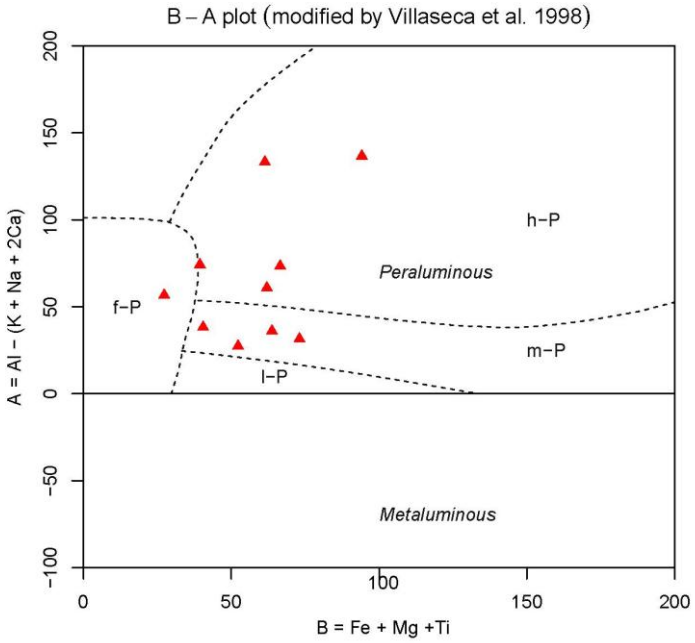

Figure 5: *B-A diagram after Villaseca et al. (1998)*

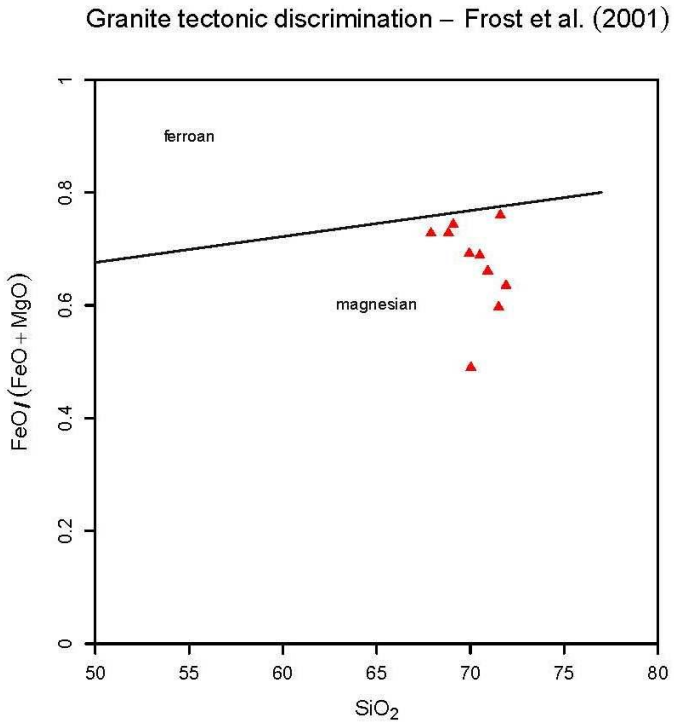

Figure 6: *Chemical classification of granites using FeO*/(FeO+MgO) vs SiO_2*

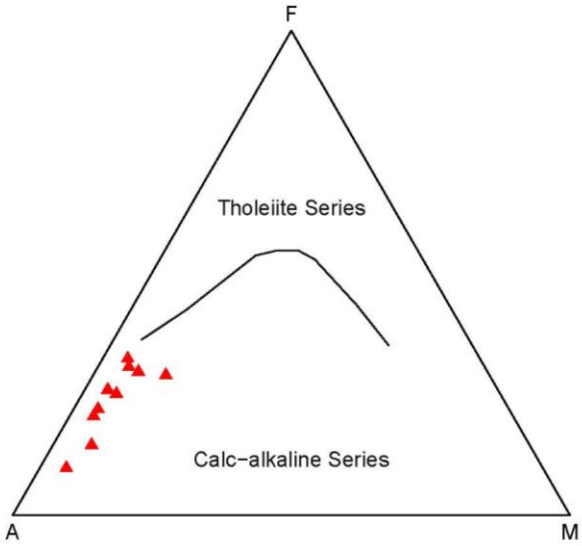

Figure 7: *AFM diagram of Irvine and Baragar (1971) indicating its cale-alkaline nature*

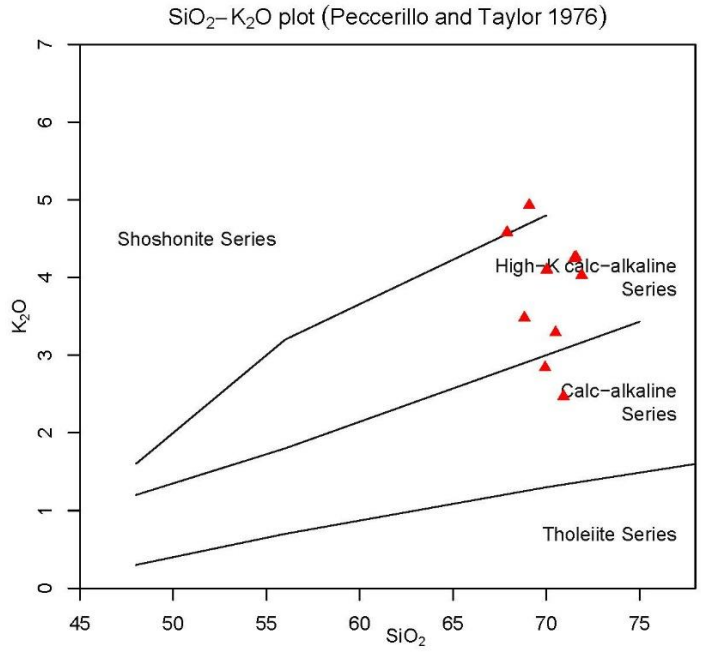

Figure 8: *SiO_2-K_2O diagram pf Paccerillo and Taylor (1976)*

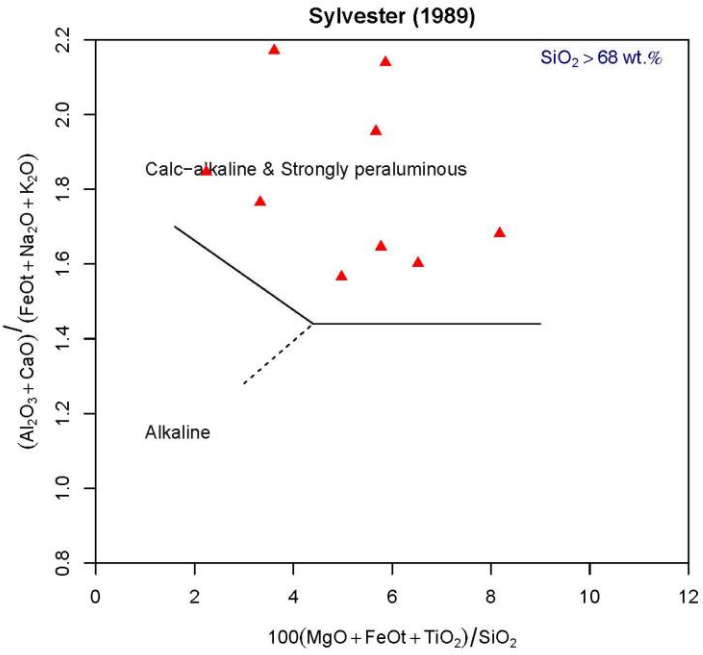

Figure 9: *Demonstrated on the diagram of Sylvester (1989)*

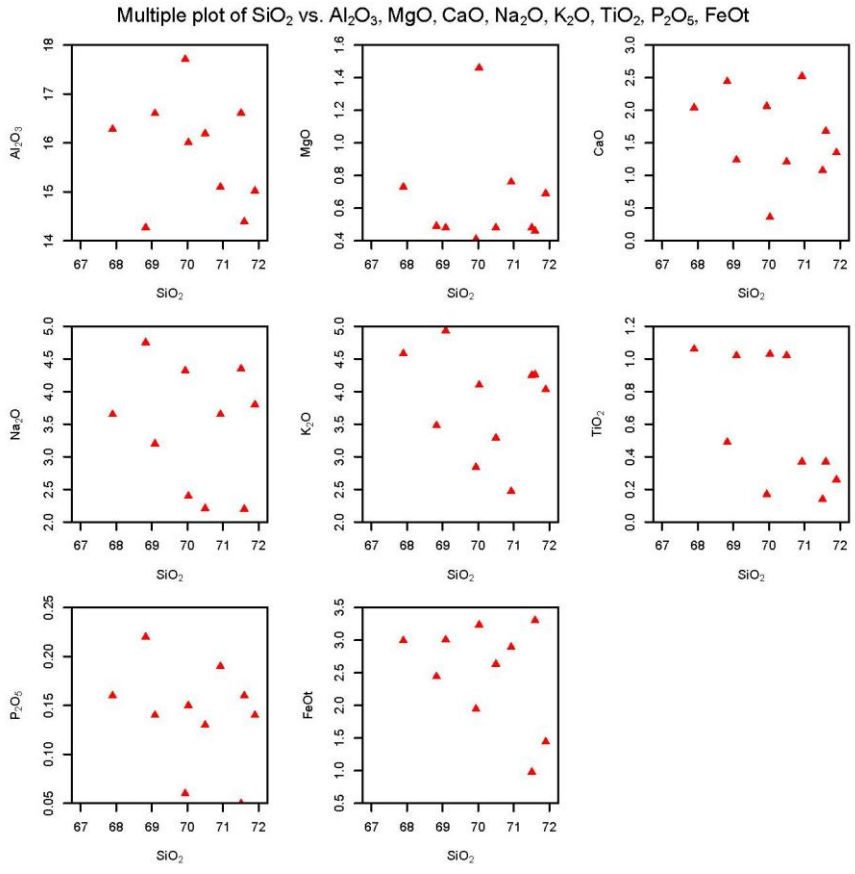

Figure 10: *Harker variation diagram for granites of the study area*

Trace and Rare Earth Elements

The trace element concentrations in a few representative samples are estimated and are given in Table 3.

Table 3: *Trace and Rare Earth Elements Concentrations in Granites*

Sample No	1/70	2/74	3/7	4/72	5/77	6/73
Trace Elements (ppm)						
Sc	9.30	9.90	6.40	6.40	7.90	8.60
Co	3.80	1.30	0.60	2.10	1.50	9.90
Ta	14.10	6.90	3.80	7.20	8.30	6.50
Ba	1550.00	1020.00	560.00	770.00	1610.00	1730.00
Rb	161.00	191.00	228.00	204.00	154.00	131.00
Th	42.00	49.00	53.00	22.50	44.00	24.00
Ce	-	1.38	-	2.10	-	1.20
Zr	530.00	570.00	320.00	450.00	1680.00	780.00
Hf	10.30	10.80	9.60	6.80	32.90	15.10
K/Rb	272.00	243.00	180.00	175.00	270.00	114.00
K/Ba	27.00	46.00	73.00	46.40	25.80	28.70
Ba/Rb	9.60	5.30	2.50	3.80	10.50	13.20
Zr/Hf	51.00	53.00	33.00	66.00	51.00	52.00
Ta/Hf	1.37	0.64	0.40	1.06	0.25	0.43
Rare Earth Elements (ppm)						
La	173.00	74.00	52.00	107.00	411.00	156.00
Ce	350.00	163.00	105.00	187.00	743.00	270.00
Nd	120.00	72.00	-	60.00	212.00	78.00
Sm	19.40	14.20	9.70	10.20	33.80	12.00
Eu	2.30	2.00	0.42	1.59	2.42	2.55
Tb	3.17	2.27	2.04	1.31	3.58	1.09
Yb	6.30	5.90	7.00	4.90	9.00	4.00
Lu	0.74	0.74	0.77	0.64	0.79	0.58
$(La/Yb)_N$	16.60	7.60	4.50	13.20	27.70	23.60
$(Ce/Yb)_N$	11.30	5.50	3.00	7.70	16.70	13.40
(Eu/Eu*)	0.39	0.47	0.14	0.33	0.28	0.90

In Figure 11 decreasing trends of Ba and Ba/Rb ratios and increasing trend of K/Ba ratio with increase in values of differentiation Index (D.I) are observed for the granites. Such trends are typical to the rocks originating through magmatic crystallization.

The REE contents of the selected samples of granites are presented in Table 3. The chondrite normalized patterns are shown in Figure 12. It can be observed from the graph that all the samples show marked negative Eu anomalies. Total REE and $(La/Yb)_N$ of these rocks vary significantly.

Zhonggang et al., (1982) divided the granites into three major categories in terms of Eu/Eu* values as Eu/Eu* values greater than 0.5; 0.3 to 0.4; and less than 0.2. From these values it can be stated that granites belonging to first category are older and closely connected to the process of granitization in origin, those of the second category are of magmatic origin while those of the third category are especially distinguishable for their characteristic features of magmatic differentiation and replacement. The granites of present area is mostly of the second category with Eu/Eu* of 0.28 to 0.47 indicating their magmatic affinity.

Fractional crystallization models focus on the production of higher silica in granitic rocks by crystallization of feldspar to increase the negative Eu anomaly during differentiation (Taylor, 1968; Emmerman et al., 1975; Condie et al., 1981; Cullers and Grof, 1984). Fractional crystallization of amphibole increases the REE content and negative Eu anomaly with increasing SiO_2 content (Rogers et al., 1980). These granites are similar to that of Gabro suite (Eu/Eu*= 0.5) and Mimbulla suite (Eu/Eu* = 0.3) of South Australia (Collins et al., 1982).

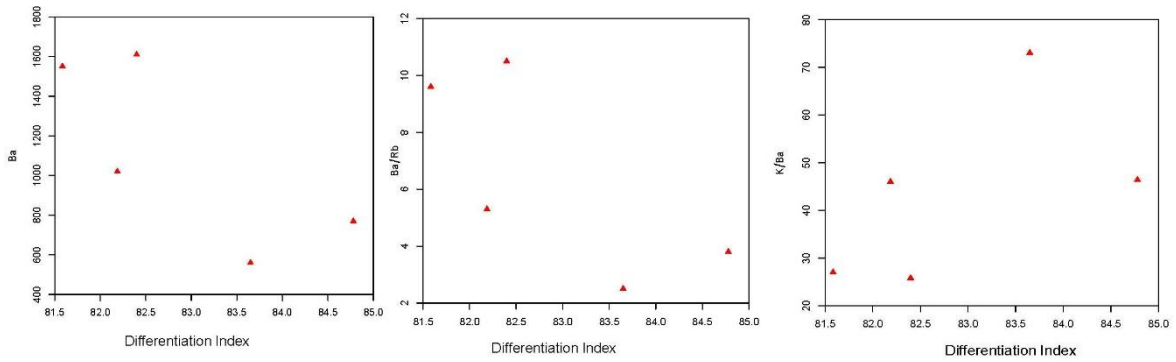

Figure 11: *Variation diagram of Ba, Ba/Rb and K/Ba vs Differentiation Index (D.I.)*

Tectonic evolution

The generation of granitic liquid is directly and indirectly related to tectonic activity, whether associated with extensional or compressional movement. Strong correlation between the types of granites and tectonic settings have been pointed out by Streckeisen (1974); Pearce et al. (1984); Pitcher, (1983); Patchet and Ruiz (1987); Lameyre (1988); Pupin (1988); Maniar and Piccoli (1989); Barbarin (1990); Bonin (1990); and Eby (1990). Fyfe (1988) believes that collision mechanisms or collision thickening provide a suitable mechanism in crustal melting for large granite masses with continental crust chemistry and isotope systematics. Thus, it seems there exit a direct link between the tectonic setting and granite generation.

Harris et al. (1986) have presented a comprehensive picture of geochemical characteristics of collision zone magmatism and proposed four groups of granite intrusion, each associated with a particular stage in the tectonic evolution of a collision zone. They are: (i) Pre-collision calc alkaline (volcanic-arc) intrusions that are mostly derived from mental modified by a subduction component and are enriched in LIL element. (ii) Syn-collision peraluminous intrusions which may be derived from the hydrated bases of continental thrust sheets. (iii) Late or Post-collision calc-alkaline intrusions which may be derived from mantle source but undergo extensive crustal contamination and contain higher ratios of Ta/Hf and Ta/Zr than volcanic-arc intrusions (iv) Post-collision alkaline intrusions which may be derived from mantle lithosphere beneath the collision zone which has high concentration of both LIL and HFS element.

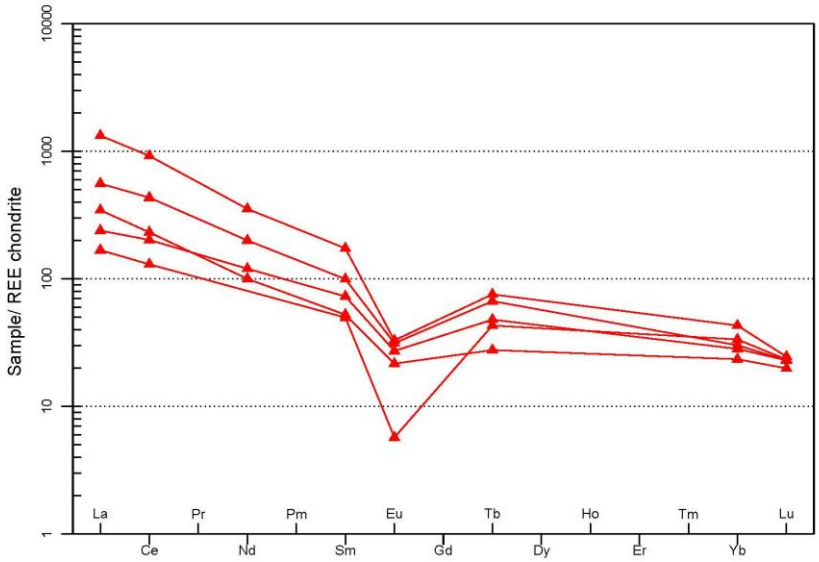

Figure 12: *Condrite normalized REE patterns for granites*

Aluminum Saturation Index

The chemical compositions of the study area granites are reported in Table 2. The SiO_2 content of the representative samples vary from 66 to72 wt.%. The high alumina content (Al_2O_3: 14-17 wt. %) relative to alkalies (Na_2O:22-47 wt. % and K_2O:2.8-4.9 wt. %) and calcium (CaO: 0.36-2.52 wt. %) is reflected in a high percentage of normative corundum and a high molecular ratio Al2O3 (A/CNK). These samples with low FeO display broadly magnesian character. The study area granite samples plot in the Orogenic belt field on the MgO-$Fe_2O_{3\ (t)}$-Al_2O_3 ternary plot after Pearce et al. (1977) (Figure 13). The Figure 14 shows that the aluminium saturation index indicates that these are strongly peraluminious and syn-collision type. Same was also observed by Darvishi et al., (2015) in Maggiyan granites of N-W Iran.

R2-R2 Parameter

Batchelor and Bowden (1985) distinguished granite into different tectonic setting using a main granite rock assemblage diagram (Figure 15). R1 and R2 values can be recalculated according to the main oxide content of granites. Most of the samples are located in the syn-collision granite area. This indicate the granites of this area is located in the upper crust, separation and crystallization of mineral occur only in part of the rock, and melting occurs in most of the rock. So, the granites tectonic setting is syn-collision setting.

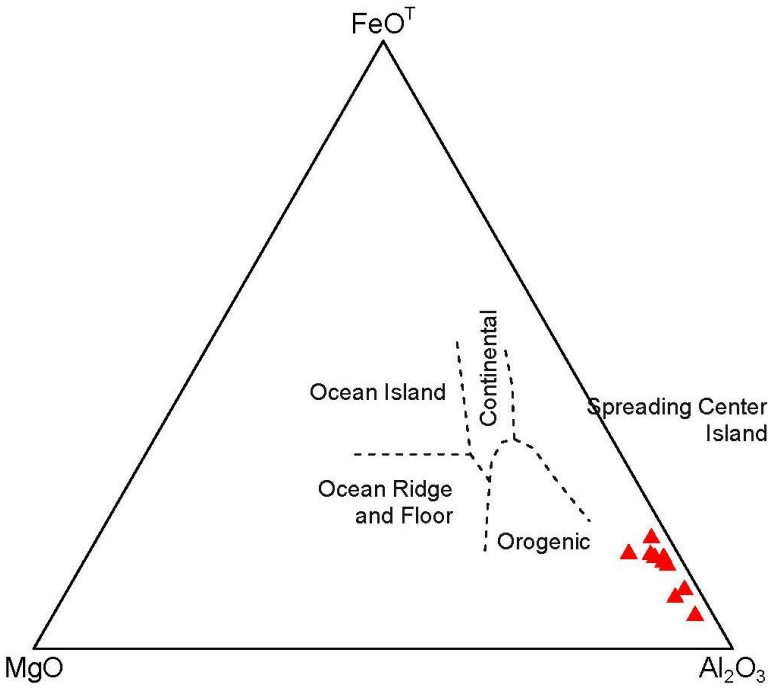

Figure 13: *MgO-Fe2O3 (t) - Al2O3 ternary plot after Pearce et al. (1977)*

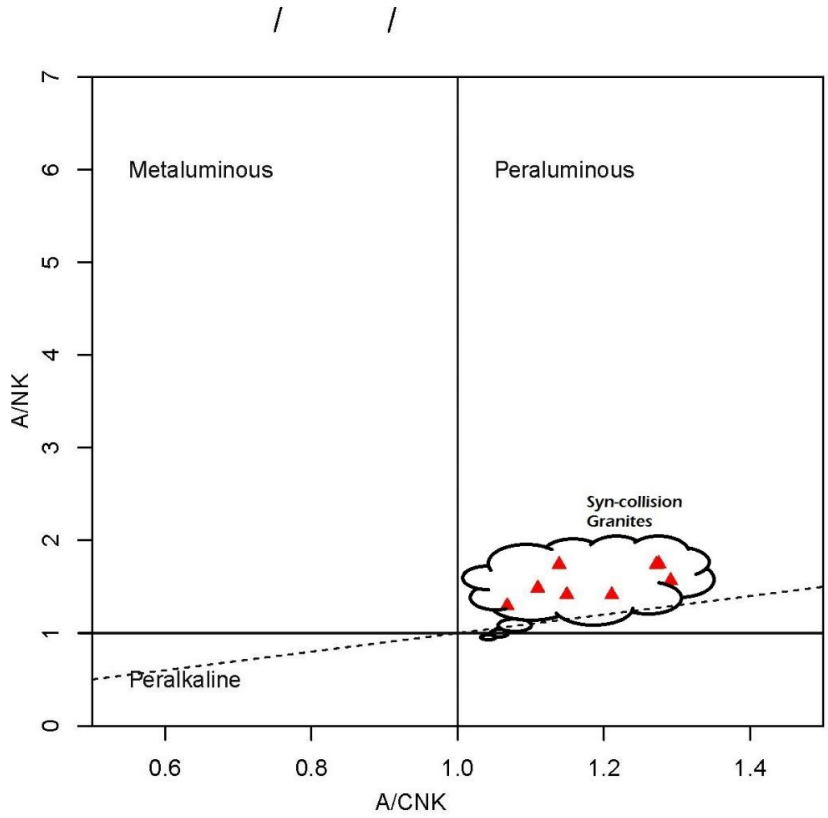

Figure 14: *Sand's Index for the studied granites, field after Maniar and Piccollo (1989)*

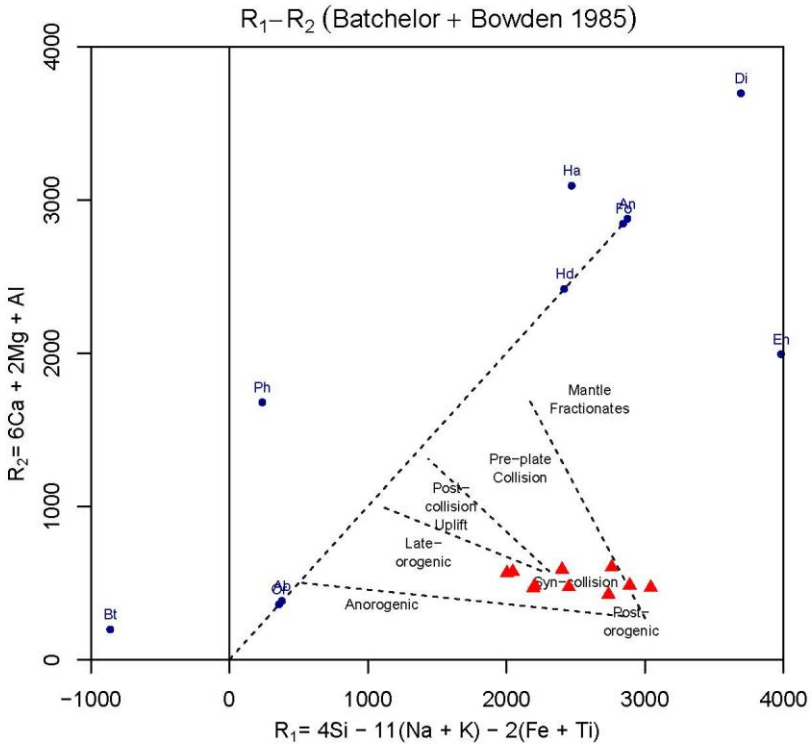

Figure 15: *Discriminant diagram of tectonic setting of R1-R2 (after Batchelor and Bowden, 1985)*

QAP diagram

Granitoids have different contents of quartz, alkali feldspar and plagioclase in different tectonic settings, which determine their particular positions in the QAP diagram. So, we can use QAP diagram to judge a granitoid's tectonic setting (Figure 16). In different tectonic settings, the corresponding rock type can be divided into different rock types. Here all the samples are of CEUG type is of A/P <2.0; alkali granite, alkali felds and quartz syenite. Figure shows that all plots fall into the CEUG area in the QAP diagram indicating that these granites are of Continental Epeiogenic Uplift Granites.

Pearce et al., (1984) emphasized that the fields on the discriminants diagrams strictly reflect source regions and melting (and crystallization histories) rather than tectonic regimes. It may be postulated the Bomdila granites were emplaced during period of crustal thickening. It is generally envisaged that during crustal thickening because of crustal overthrusting the volatiles, driven off the wet sedimentary wedges, may penetrate the hot overlying thrust sheet causing anatexis. This process is widely accepted for the generation of granites magmas at crustal levels (Harris et al., 1986; Fyfe, 1988; and Gopeshwar singh and Villinyagam, 2012).

Temperature and Pressure conditions

Bowen (1954) and Tuttle and Bowen (1958) concluded that there is a composition towards, which the liquids should migrate in the fractional crystallization of any material containing all the rock forming oxides; and they further concluded that the final liquid should have composition of almost equal proportion of quartz – albite – orthoclase. The normative albite, orthoclase and quartz of granites are plotted in the ternary diagram (Figure 17); fall in the minimum temperature trough in the system.

The normative values of Or, Ab and Qz of granites are plotted on Or – Ab – An and Qz – Ab – Or diagrams (Figure 18) (Yoder et al., 1967). An overall range of 650°C to 700° C and an average of 685°C temperature for these granites are inferred.

In the ternary diagram of normative Qz – Or – Ab (Arth et al., 1978) all plots fall in between 5 to 7 kb of pressure (Figure 19). It is inferred that these granitic rocks are formed at 5 to 7 kb PH_2O and at 650°C to 700°C temperature.

The observed P –T ranges and the placement of the granites in the low temperature trough can be taken to indicate that the granites are of magmatic (whether juvenile or anatectic) origin. The older rocks had experienced granulite facies of metamorphism (Prasad et al., 1990), and the production of granite melt of expected in that environment. The low melting components of pelitic gneisses and other rocks of suitable composition may have led to the formation of granites.

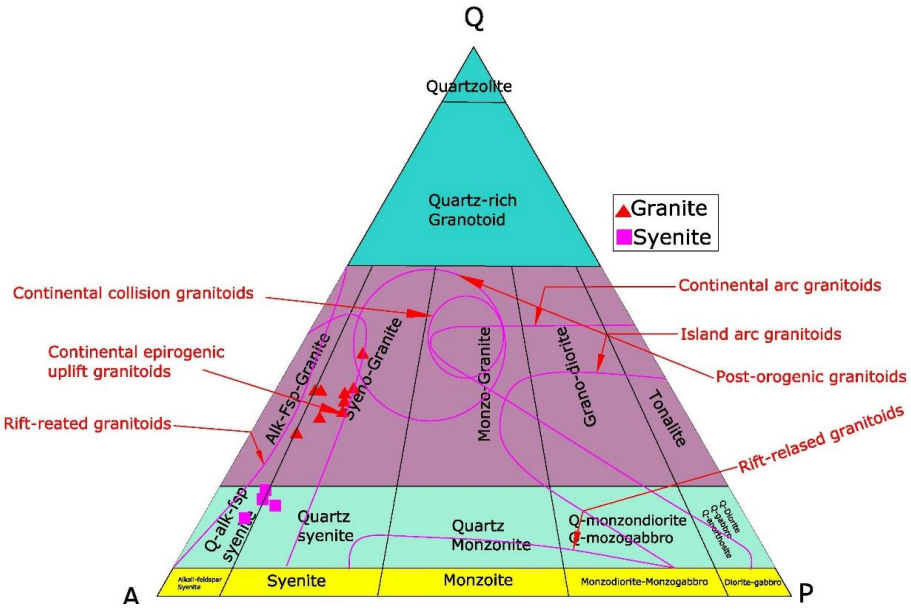

Figure 16: *Diagram for QAP (After Maniar and Piccoli, 1989)*

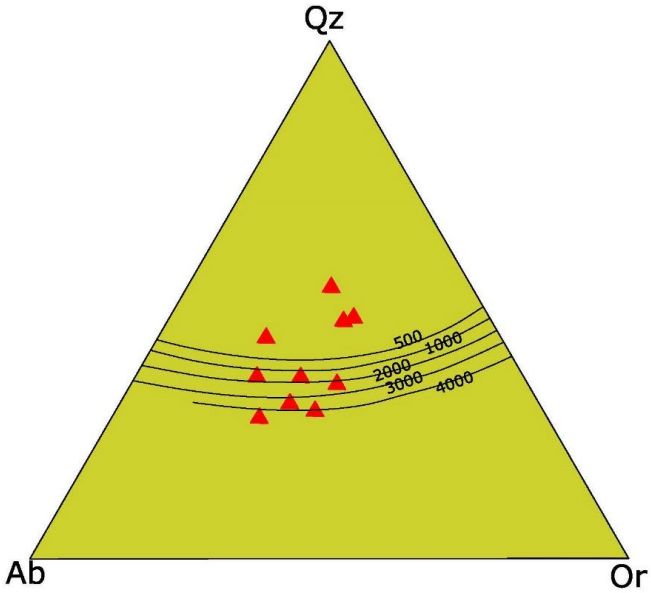

Figure 17: *Normative Quartz-Albite-Orthoclase diagram (after Bowen, 1958)*

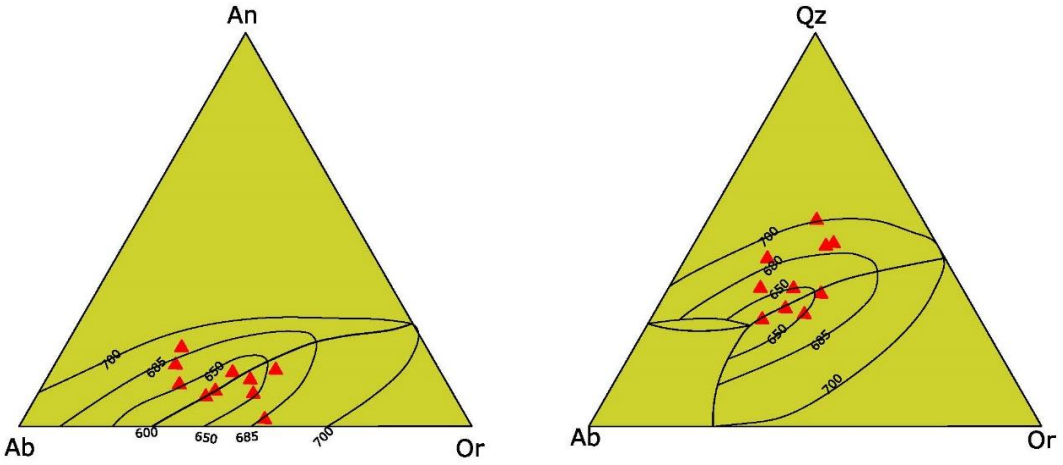

Figure 18: *a) Ab-An-Or; b) Qz-Ab-Or ternary diagrams (after Yoder et al., 1967)*

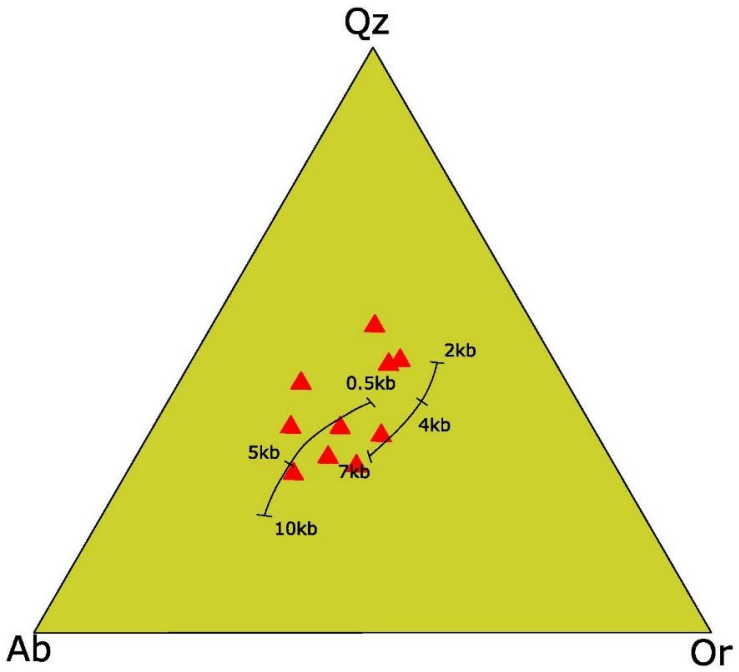

Figure 19: *Qz-Ab-Or ternary diagrams (after Arth et al., 1978)*

3. Conclusion

This study presents the geochemical characteristics of granites located in Obachettapalem in Prakasam district, A.P, forms that part of the Eastern Ghats which lies to the east of Cuddapah basin. Here in this work we discusses the possible petrogenetic process, source characteristics and its tectonic emplacement. These granites are associated with peletic gneisses and pyroxene granulates and charnackites. These granites are made up wholly of peraluminious alkali feldspar granites and are composed of quartz, K-feldspar, amphibole (hornblende), plagioclase, biotite and accessory minerals are ironoxieds, monazite, zircon, and apatite. Petrographically, they show cloudy, perthlitic texture and graphic texture. They are highly evolved magnessian, peraluminious and calc-alkaline type. These granites displaying typical geochemical characteristics with high SiO_2, Na_2O+K_2O, FeO*/MgO, REE (except Eu), Rb, Ba, Zr, depleted in MgO, CaO, Ta and Ce. Their trace and REE characteristics along with the use of various discrimination schemes revealed their

correspondence to magmas derived from crustal origin. On the basis of geochemical data, we conclude that the granites are probably derived from a predominant crustal source with variable mantle involvement in a syn-collision setting, and crystallised at 650^{o}C to 700^{o}C at 5 to 7 kb of PH_2O.

References

Al-Qadhi Abdul-Aleam Ahmed, A.D., Janardhana, M.R. and Prakash Narasimha, K.N. 2016. Field Occurrence and Petrographic Characteristics of Tertiary Volcanic Rocks and Associated Intrusions in and around Taiz City, Yemen. *International Journal of Advanced Earth Science and Engineering*, 5, pp.390-429.

Arth, J.G., Barker, F., Peterman, Z.E. and Friedman, I. 1978. Geochemistry of the Gabbro-Diorite-Tonalite-Trondhjemite Suite of southwest Finland and its Implications for the Origin of Tonalitic and Trondhjemitic Magmas. *Journal of Petrology*, 19, pp.289-316.

Barbarin, B. 1990. Granitoids: Main petrogenetic classifications in relation to origin and tectonic setting. *Geological Journal*, 25, pp.227-238.

Batchelor, R.A. and Bowden, P. 1985. Petrogenetic interpretation of granitoid rock series using multicationic parameters. *Chemical Geology*, 48, pp.43-55.

Bateman, P.C. 1961. Granite formations in the east central sierra Nevada near Bishop, California, *Geological Society of America Bulletin*, 72, pp.1521-1538.

Bonin, B. 1990. From orogenic to anorogenic settings: evolution of granitoid suites after a major orogenesis. Geological Journal, 25, pp.261-270. (W.S. Pitcher Special Issue).

Bowen, N.L. 1954. Experiment as an aid to the understanding of the Natural World. *Proceedings of the Academy of Natural Sciences of Philadelphia*, 160, pp.1-12.

Chappell, B.W. and White, A.J.R. 1974. Two contrasting granite types. *Pacific Geol*, 8, pp.173-174.

Chayes, F. 1952. The fine-grained calc-alkaline granites of granites of New England. *Journal of Geology*, 60, pp.207-254.

Chayes, F. 1957. A provisional reclassification of Granites. *Geological Magazine*, 96, pp.58-68.

Cloos, E. 1937. The application of recent structural methods in the interpretation of the crystalline rocks of Maryland. *Maryland Geological Survey,* 13, pp.36-49.

Collins, W.J., Beams, S.D., White, A.J.R. and Chappell, B.W. 1982. Nature and origin of A-type granites with particular reference to southeastern Australia. *Contributions to Mineralogy and Petrology*, 80, pp.189-200.

Condie, K.C. 1981. *Archean Greenstone Belts*. Amsterdam: Elsevier Science, pp.288-297.

Cox, K.G., Bell, J.D. and Pankhurst, R.J. 1979. *The interpretation of igneous rocks*. Boston: George Allen and Unwin London.

Cullers, R.L. and Graf, J.L., 1984. Rare earth elements in igneous rocks of the continental crust: Intermediate and silicic rocks-ore Petrogenesis. In: Henderson, P. (ed.), *Rare Earth Element Geochemistry*. Elsevier, pp.275-316.

Darviehi, E., Khalili, M., Bevers, R. and Sayar, M. 2015. Petrology and mineral chemistry of Peraluminous Marziyan granites, Sanandaj–Sitjsn metamorphic belt (NW Iran). *Geologica Carpathica*, 66, pp.361-374.

De La Roche, H., Leterrier, J., Grandclaude, P. and Marchal, M. 1980. A classification of volcanic and plutonic rocks using R1R2-diagram and major element analyses – its relationships with current nomenclature. *Chemical Geology,* 29, pp.183-210.

Debon, F. and Le Fort, P. 1983. A chemical–mineralogical classification of common plutonic rocks and associations. *Transactions of the Royal Society of Edinburgh, Earth Sciences,* 73, pp.135-149.

Eby, G.N. 1990. The A-type granitoids: A review of their occurrence and chemical characteristics and speculations on their petrogenesis. *Lithos*, 26, pp.115-134.

Emmerman, R., Daieva, L. and Schneider, J. 1975. Petrologic significance of rare earth distribution in granites. *Contributions to Mineralogy and Petrology*, 52, pp.267-283.

Fyfe, W.S. 1988. Granites and a wet convecting ultramafic planet. *Transactions of the Royal Society of Edinburgh: Earth Sciences*, 79, pp.339-346.

Gopeshwor Singh, L. and Vallinayagam, G. 2012. Petrological and Geochemical Constraints in the Origin and Associated Mineralization of A-Type Granite Suite of the Dhiran Area, Northwestern Peninsular India. Geosciences, 2, pp.66-80.

Harris, N.B.W., Pearce, J.A., Tindle, A.G. 1986. Geochemical characteristics of collision- zone magmatism. In: Coward, M.P., Ries, A.C. (eds.), *Collision Tectonics*. Geological Society London Special Publication, 19, pp.67-81.

Irvine, T.M. and Baragar, W.R. 1971. A guide to the chemical classification of common volcanic rocks. *Canadian Journal of Earth Sciences*, 8, pp.523-548.

Johansen, A. 1938. *A descriptive petrography of the igneous rocks*, vol. 2, The University of Chicago Press.

Lameyre. 1988. Granite settings and tectonics. *Rendiconti della Società Italiana di Mineralogia e Petrologia*, 43, pp.215-236.

Leube, A., Hirdes, W., Mauer, R. and Kesse, G.O. 1990. The early Proterozoic Birimian Supergroup of Ghana and some aspects of its associated gold mineralisation. *Precambrian Research*, 46, 139-165.

Liao Zhongli, Mo Xuanxue, Pan Guitang, Zhu Dicheng, Wang Liquan, Zhao Zhidan, Geng Quanru, Xiong Xingguo and Dong Guochen. 2007. The petrochemistry characteristics and petrogenesis of peraluminous granite in Tibet. *Frontiers of Earth Science in China*, 1, pp.194-205.

Maniar, P.D. and Piccoli, P.M. 1989. Tectonic discrimination of granitoids. *Geological Society of America Bulletin*, 101, pp.635-643.

Middlemost, E.A.K. 1994. Naming materials in the magma/igneous rock system. *Earth-Science Reviews*, 37, pp.215-224.

O'Connor, J.T. 1965. A classification for quartz-rich igneous rocks based on feldspar ratios. In: US Geological Survey Professional Paper B525. USGS, pp.79-84.

Patchet, P.J. and Rjiz, J. 1987. Nd isotopic ages of crustal formation and metamprhism in the Precambrians of eastern and southern Mexico. *Contributions to Mineralogy and Petrology*, 96, pp.523-528.

Pearce J.A, Harris N.B.W, Tindle A.G. 1984. Trace element discrimination diagrams for the tectonic interpretation of granitic rocks. *Journal of Petrology*, 25, pp.959-983.

Pearce, J.A., Harris, N.W. and Tindle, A.G. 1984. Trace element discrimination diagrams for the tectonic interpretation of granitic rocks. *Journal of Petrology,* 25, pp.956-983.

Pearce, T.H., Gorman, B.E. and Birkett, T.C. 1977. The relationship between major element geochemistry and tectonic environment of basic and intermediate volcanic rocks. *Earth and Planetary Science Letters,* 36, pp.121-132.

Peccerillo, A. and Taylor, S.R. 1976. Geochemistry of Eocene calc-alkaline volcanic rocks from the Kastamonu area, Northern Turkey. *Contributions to Mineralogy and Petrology,* 58, pp.63-81.

Pitcher, W.S. 1983. Granite type and tectonic environment. In: Hsu, K. (ed.), *Mountain building process*. London: Academic Press, pp.19-40.

Prasad, K.S.S, Rao, K.L.N. and Murty, M.S. 1900. Charnockites of Obachettapalem, Prakasam District, South India**:** High Grade Metamorphics (Book Print), Theophrastus Publications SA, Greece, pp.237- 261.

Pupin. 1988. Granites as indicators in paleo geodynamics. *Rendiconti della Societa Italian di Mineralogia e Petrogia*, 43, pp.237-262.

Rogers, J.J.W., Hodges, K.V. and Ghuma, M.A. 1980. Trace elements in continental margin magmatism, II: Trace elements in Ben Ghanema Batholith and nature of the Precambrian crust in central North Africa. *Geological Society of America Bulletin*, 91, pp.1742-1788.

Shand, S.J. 1943. *Eruptive Rocks: Their Genesis, Composition, Classification, and Their Relation to Ore-Deposits with a Chapter on Meteorite.* New York: John Wiley & Sons.

Streckeisen, A.L. 1973. Plutonic rocks Classification and nomenclature recommended by IUGS sub commission of systematic of igneous rocks. *Geotimes*, 18, pp.26-30.

Streckeisen, A. 1974. Classification and nomenclature of plutonic rocks recommendations of the IUGS sub commission on the systematics of Igneous Rocks. *Geologische Rundschau*, 63(2), pp.773-786.

Sylvester, P.J. 1998. Post-collisional strongly peraluminous granites. *Lithos*, 45, pp.29-44.

Taylor, S.R. 1968. Geochemistry of andesites. In: Ahrens, L.H. (ed.), *Origin and distribution of elements*. Pergamon: Oxford, pp.559-583.

Tuttle, O.F. and Bowen, N.L. 1958. Origin of Experimental Studies in the System-NaAlSi3O8-KAlSi3O8-SiO2-H2O. *Geological Society of America Memoirs*, 74, pp.65-75.

Villaseca, C., Barbero, L. and Herreros, V. 1998. A re-examination of the typology of peraluminous granite types in intracontinental orogenic belts. *Transactions of the Royal Society of Edinburgh, Earth Sciences,* 89, pp.113-119.

Wang Zhonggang, Zhao Zhenhua and Zhao Huilan, 1982. REE distribution pattern of Granits of South China. *Geochemistry,* 1, pp.39-50.

Yoder, H.S., Stewart, D. and Smith, J.R. 1967. Ternary feldspars: Annual Report of Director of Geophysical Lab, Carnegie Institution of Washington, pp.50, 206.

Cloud Publications
International Journal of Advanced Earth Science and Engineering
2017, Volume 6, Issue 1, pp. 557–566
ISSN: 2320–3609, Crossref: 10.23953/cloud.ijaese.297

Case Study

Analysis of The Industrial Combination Structure based on Doi's Method: Case Study of Tamil Nadu Cauvery Basin (India)

Dayalan N.

Department of Geography, Periyar E. V. R College (A), Trichirappalli-620 023, Tamil Nadu, India

Publication Date: 12 August 2017

DOI: https://doi.org/10.23953/cloud.ijaese.297

Abstract The Cauvery River is the biggest river in south India. The Cauvery river basin flows through districts such as Nilgiris, Coimbatore, Tirupur, Erode, Dharmapuri, Krishnagiri, Salem, Namakkal, Karur, Dindigul, Pudukottai, Trichirappalli, Perambalur, Ariyalur Thanjavur, Tiruvarur, Cuddalore and Nagapattinam in the state Tamil Nadu. The study area is between latitudes 76" 2'E, 79"8' E and 12"7' N, 10"14 N longitudes. The secondary data collected from the Ministry of Micro, Small and Medium enterprises (MSME) and statistical hand book of Cauvery basin districts. The data which collected are Food based, Textile based, Readymade garment and Embroidery, Forest based, Leather based, Chemical based, Plastic & Rubber based, Mineral based, Engineering based, Electrical & Electronics based and others industries. In this article, the industrial combination in the Tamil Nadu Cauvery Basin is outlined, followed by the discussion on the area using Doi's method industrial combination analysis. The study of industrial combination is very significant for any particular region because it provides an idea about the relative position of industries which is necessary for future development of industries in Tamil Nadu Cauvery basin.
Keywords *Cauvery River; Micro, Small and Medium enterprises; Tamil Nadu*

1. Introduction

Manufacturing industry is the processing of primary products into more refined and usable products. Many of the natural resources cannot be utilized directly without processing. Because of this reason, we manufacture cloth from cotton, sugar from sugarcane, paper from wood pulp, and petro chemicals from mineral oil. By doing so, we make the primary products more valuable and usable. In other words, manufacturing industries mean transformation of natural material endowments into commodities of utility by processing, assembling and repairing. The industrial combination closely related to geo-climatic, socio-economic, historical and political factors. Manufacturing is vital for our very existence. It is an activity that works as an engine of economic growth, helps in removing poverty and employment and transform a traditional society into a modern society. The economic strength of a country is judged by the development of its industries. All the developed countries of the world are highly industrialized.

History of industry in India dates back to the history of mankind. Among all the industries of early times, the textiles, especially the cotton textiles industry, had the place of pride both in India and in the outside world. There is enough evidence to show that the Indians knew weaving some 1500

years before Christ, when the Europeans were still covering themselves with animal skins. Pyrard, the 17th century Portuguese writer has record that everyone from the Cape of Good Hope to China was clothed from head to foot in Indian made garments. Iron and steel industries was also advanced stage at that time. Industrial revolution in Europe resulted in modern factories. With this the scale of manufacturing goods increased tremendously leading to mechanization. As a result migration of workers occurred from village to cities. The better system of goods with goods came to an end, exchange of goods with money started. It is correct that a revolution occurred in the manufacturing sphere but the traditional village handicrafts and cottage industries witnessed their death toll (Khullar, 2012). Inter war period: Indian industries made rapid strides during the 1st world war (1914-18) due to rise in demand for industrial goods by the Armed Forces. However, the real spurt was provided by Indian Fiscal commission set up in 1921-22. This gave the much needed protection to industries like iron, steel, textile, cement, sugar, paper and metals.

World War II: while Indian industry proposed during World War I, the Second World War created problems for Indian industry. Indian became an active participant in war and the entry Japan in the hostilities brought war to India's doorstep. However, the impact of war was short lived and the industry was quick to recover from the initial shock and exploited the opportunities offered by the war.

After independence, need to take solid steps for improving Industrial scene was badly felt. It was realized that industrialization was the only vehicle which could lead the shattered economy of the country on the path of process and prosperity. Consequently, industry attached special attention of plans and planners.

Now Indian government follows the 12th five year plan. For sustaining pace of growth and investment, several initiatives have been launched for modernizing, technology, up gradation, reducing transaction costs, increasing export thrust, so as to enhance its global competitiveness and achieve balanced regional development. Further, in order to give export thrust, department of commerce launched major initiatives such as assistances to State Infrastructure Development for Exports

1.1. Significant Factors

The major geographical factor is raw materials, power, labour, transport, market, site and climate. The non-geographical factor is capital, government policies, industrial inertia, efficient organization, banking facilities and insurance.

1.2. Classification of Industrial (Micro, Small and Medium Class)

Food based: Rice, Floor Milling, Mango pulp Oil, Seeds, Tea, and plantation crops etc. *Chemical based:* Safety matches, Polythene bags, chalk crayon, chemical dye, Fertilizer, petroleum filtering etc. *Plastic & Rubber based:* P.V.C. pipes, Rubber, etc. *Electrical & Electronics based:* Battery charging Lamps Starters, T.V. Antenna, computer parts, etc. *Forest based:* Wood, Furniture, Timber, Paper, etc. *Engineering based:* Machining, Metals, Iron and Steel manufactory, Motor Vehicles spare parts etc. *Textile based:* Cotton, Power loom, Silk reeling, etc., *Others (Specify):* Beauty parlor, Paper, printing, gas stove, water filtering, watches, optical, clocks etc., *Leather based:* Leather bags, belt, shoes and winter dress etc. and *Mineral based:* mineral, sand, coal, granite, marble, basalt industries etc.

2. Database and Methodology

Industrial combination is made with help of secondary data obtained from the Ministry of Micro, Small and Medium enterprises (MSME) and Statistical hand book of Nilgiris, Coimbatore, Salem, Namakkal, Erode, Dharmapuri, Karur, Trichirappalli, Thanjavur, Tiruvarur and Nagapattinam districts. In order determine Cauvery basin districts wise combination of Doi's Method is used for the calculation of the location quotient. The following formula used to work out the concentration of industrial combination in Cauvery basin. The Doi's method 1st (1957) used in industrial combination in Tokyo, Japan. After 1959 modified used in crop combination. The present study adopted in Doi's industrial combination in Tamil Nadu Cauvery basin. The aim is present studies have been adapted to show the regional industrial combination in the basin.

2.1. Geographical Back Round of the Study

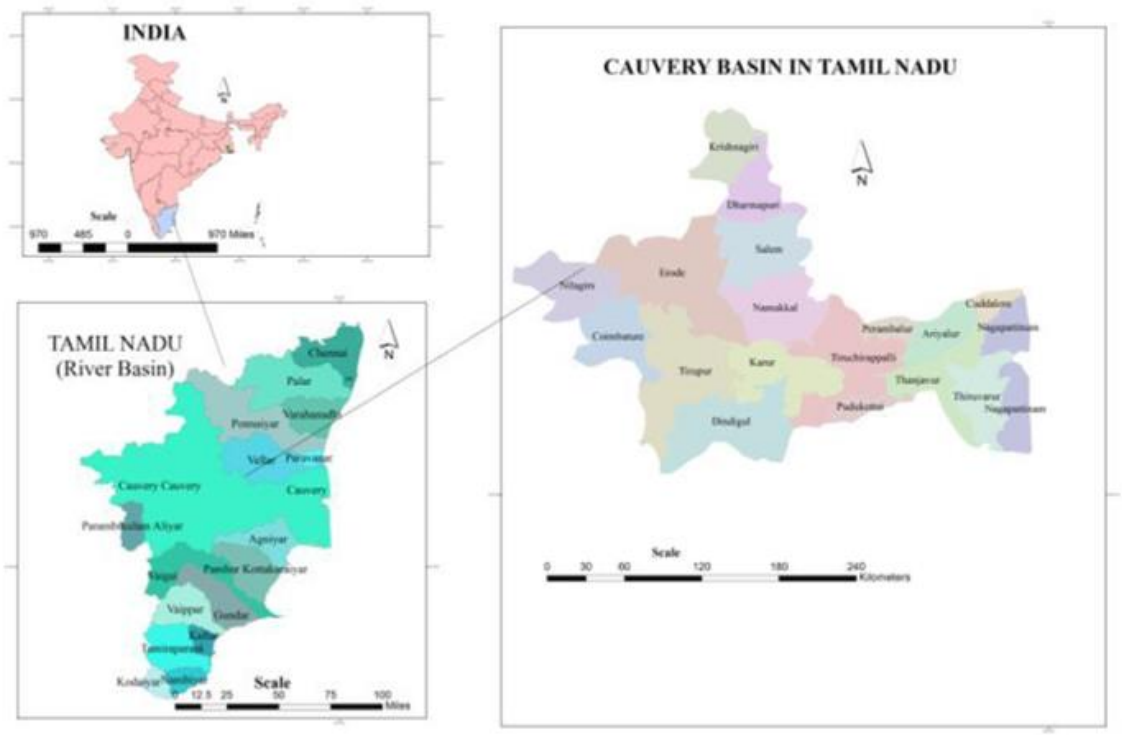

Figure 1: *Study area*

The Cauvery river basin lies between districts is Nilgiris, Coimbatore, Tirupur, Erode, Dharmapuri, Krishnagiri, Salem, Namakkal, Karur, Dindigul, Pudukottai, Trichirappalli, Perambalur, Ariyalur Thanjavur, Tiruvarur, Cuddalore and Nagapattinam of Tamil Nadu state (Figure 1). It is located between latitudes 76" 2'E, 79"8' E and 12"7' N, 10"14 N longitudes. The Cauvery River is biggest river in south India. It originated in the Tala-Cauvery on the Brahmagiri range in the Western Ghats in Karnataka at an elevation of about 1341 m above mean sea level and flows for about 800 km, before it reaches into the Bay of Bengal. The basin drains a total area of 81,155 Sq.Kms (Tamil Nadu, Kerala and Karanataka). It enters Tamil Nadu in the region of Mannar and moves from West to East for 234 kms and joins the Cauvery near Bhavani Town. Due to this, Cauvery basin has tropical climate and our study area has monsoon rain. Here, the recorded maximum and minimum temperatures are 44°C and 18°C respectively. The Physiographic divisions has controlled by Structural hills, Denudational and Pediplain and Fluvial process. The major tributaries are Amravati, Hemavathi, Kabini, Noyil and Bhavani. All the distributaries in this region are non-perennial and river

flow is mainly due to Cauvery water release during June to January. The length of the river Cauvery from the head to its outfall into the sea comprises a length of 43,867 km^2 in Tamil Nadu. The principal soil types found in the basin are Black soils, Red soils, Laterites, Alluvial soils, Forest soils, and mixed soils. Red soils and Back soil occupy large areas in the basin (Coimbatore, Erode, Salem, Tirupur and Karur). Alluvial soils are found in the delta areas (Trichirappalli, Thanjavur, Tiruvarur, Cuddalore, Perambalur, Ariylur and Nagapattinam). This region is major manufacture Industrial economic zone in Tamil Nadu. The Nilgiris district covered the mountains region, developed the forest and food based industries (Vegetables, Fruits and Tea). The Coimbatore, Tirupur and Erode regions found the black and red soil, this soil suitable for cotton production. So, this region located the Textiles based industries. The Cauvery end part of the delta regions such as Trichirappalli, Thanjavur, Cuddalore, Perambalur, Ariyalur, Tiruvarur and Nagapattinam regions where food based industries are located.

3. Discussion

The present study has mainly examined the industrial combination using the Doi's Method on Tamil Nadu Cauvery basin, would be the tools for future planning in case of industrial development in the region. The study of industrial combinational regions constitutes an important aspect of industrial geography or regional geography. The industries are generally in combination and rarely that particular Industry occupies a position of total isolation other industries in a given area, at the point and time.

The Doi's represents critical value for various elements at different ranks against cumulative percentage of elements at higher ranks and industrial element are food based, textile based, chemical based, forest based, plastic and Rubber based enterprises. The critical value table (Annexure-I) requires only the summing up of actual percentages under different industries instead of finding the differences between actual percentages and theoretical distributions. Annexure-I is an abridged format of critical value table prepared by Doi's in 1957 (Husain, 2007).

Table 1: *The percentage of micro, small and medium class's industries in Tamil Nadu Cauvery basin regions*

District	Food based	Textile based	Ready Made Garment and Embroidery	Forest based	Leather based	Chemical based	Plastic & Rubber based	mineral based	Engineering based	Electrical & Electronics based	Others (Specify)
Nilgiris	10	26	0	29	10	0	0	0	14	0	11
Coimbatore	10	32	0	5	0	2	3	3	32	8	5
Erode	23	52	6	1	6	0	1	0	3	1	6
Dharmapuri	28	43	3	0	0	0	3	10	5	0	7
Salem	14	21	1	4	0	0	6	9	16	2	26
Namakkal	23	63	6	1	0	0	0	0	2	3	2
Karur	7	40	7	4	1	4	5	6	8	2	17
Trichy	12	2	44	7	1	2	2	3	24	1	3

Source: Ministry of Micro, Small and Medium Enterprises, Chennai.

The Doi's an Abrided of Deviation Analysis Table can be seen by making use of actual percentages under different industries in the Tamil Nadu Cauvery basin for 2015-16. The ranking industrial per cent and cumulative percentage are as shown the Table 2.

The Doi's techniques have three combinational elements. This technique shows that higher ranking industries have high percentage (above 10 per cent), the lower ranking element with less than 5 per cent which are usually excluded from the combination. This technique is most profitably applied to such a situation as is found in the industrial combination in which interrelationship exists between the component combinations. Using this technique, industries which has cumulative percentage is less than 50 are included in combination; or the critical value for all the industries at different ranks against 50 in Zero. Therefore, the scale of cumulative percentage starts from above 50 percentages which contributed as higher rank may be 1st three industries (Husain, 2007). In the present study Nilgiris District first food based industry occupies 29 per cent, the next automatically included so as to make cumulative percentage above the 50 per cent. The next industry per cent Forest Based, Textile based industry included in the combination which makes the sum of the first two industry 56 per cent (Table 2) from the critical value table (Annex - I). The Cumulative Percentage of 56 (Forest and Textile based) lies between 55 and 60, which is closer to 55 as the sum of percentage of the higher ranking elements is called Mono combination industry and Double combination industry region. The industry contributing is to over 50 per cent of total number of industries. Actual percentage of third industry in larger than critical value, it is to be included in the combination. Same thing fourth and fifth industry cumulative per cent higher than critical value fourth and fifth rank of element, the region developed combination fourth and fifth industrial included combination (Table 3).

Table 2: *Ranking and cumulative percentage (Doi's Method) in industries 2015-16*

Rank/ Districts	R1	R2	R3	R4	R5	R6	R7	R8	R9	R10	R11
Nilgiris	FB	TB	Engg.	Others	LB	Food					
PNI	29	26	14	11	10	10					
CF		55	69	80	90	100					
Coimbatore	TB	Engg.	Food	EE	Others	FB	PR	MB	CB		
PNI	32	32	10	8	5	5	3	3	2		
CF		64	74	82	87	91	94	98	100		
Erode	TB	Food	RGE	LB	Others	Engg.	EE	FB	PR	MB	
PNI	52	52	52	52	52	52	52	52	52	52	
CF		75	81	87	93	95	97	98	99	100	
Dharmapuri	TB	Food	MB	Others	Engg.	RGE	PR	CB	FB		
PNI	43	28	10	7	5	3	3	0	0		
CF		71	81	88	93	96	99	99	100		
Salem	Others	TB	Food	Engg.	MB	PR	FB	EE	RGE		
PNI	26	21	14	16	9	6	4	2	1		
CF		48	61	78	87	92	96	98	100		
Namakkal	TB	Food	EE	RGE	Engg.	Others	FB	MB	PR		
PNI	63	23	3	6	2	2	1	0	0		
CF		86	89	95	97	98	99	99	100		
Karur	TB	Others	RGE	Engg.	Food	MB	PR	FB	CB	EE	LB
PNI	40	17	7	8	7	6	5	4	4	2	1
CF		56	64	72	79	85	89	94	97	99	100
Tiruchirappalli	RGE	Engg.	FB	Food	Others	MB	CB	PR	TB	EE	LB
PNI	44	24	7	12	3	3	2	2	2	1	1
CF		68	75	87	90	92	94	96	98	99	100

Thanjavur	Others	RGE	Food	Engg.	FB	LB	PR	TB	CB	MB	
PNI	25	20	14	13	9	5	5	3	3	3	
CF		45	59	72	81	86	91	94	97	100	
Tiruvarur	RGE	Engg.	Food	Others	FB	MB	EE	CB	TB		
PNI	45	29	8	9	4	2	1	1	1		
CF		74	82	91	95	96	98	98	99	100	
Nagapattinam	TB	RGE	Food	LB	CB	PR	MB	Engg.	EE	Others	
PNI	28	18	17	12	10	4	3	3	3	2	
CF		45	62	74	84	88	91	94	97	99	100
Krishnagiri	RGE	Engg.	Food	Others	MB	TB	PR	EE	CB	FB	LB
PNI	31	24	15	11	5	3	3	3	2	2	1
CF		55	70	81	86	89	91	94	96	99	100
Dindigul	Others	RGE	Engg.	FB	EE	Food	TB	MB	CB	PR	LB
PNI	57	57	57	57	57	57	57	57	57	57	57
CF		72	79	84	89	93	96	97	98	99	100
Perambalur	RGE	Food	Others	LB	Engg.	FB	PR	CB	MB		
PNI	42	18	13	8	7	5	2	2	2		
CF		61	74	82	89	94	97	98	100		
Ariyalur	MB	Engg.	Food	Others							
PNI	50	28	17	6							
CF		77	94	100							
Cuddalore	Others	MB	FB	RGE	Food	Engg.	LB	PR	CB	EE	
PNI	29	29	29	29	29	29	29	29	29	29	
CF		54	74	87	92	95	97	98	99	100	
Pudukottai	Others	Engg.	Food	TB	FB	MB	PR	RGE	CB	EE	
PNI	30	21	13	8	7	6	5	5	4	2	
CF		51	64	71	78	84	89	93	98	100	

Source: Author. Doi's Method.

Legend: Food - Food Based, TB - Textile Based, RGE - Readymade Garment and Embroidery, FB - Forest Based, LB - Leather Based, CB - Chemical Based, PR - Plastic & Rubber Based, MB - Mineral Based, Engg.- Engineering Based, EE - Electrical & Electronics Based, Others - Others (Specify), CF - Cumulative Percentage, PNI - percentage of Number of Industry, R - Rank.

Table 3: *Doi's method industrial combination in Tamil Nadu Cauvery River Basin 2015 – 16*

Type of combination	Number of regions	Industries combination	Region name
Mono combination industrial region	17	Food Based(1)	Nagapattinam
		Textile Based (5)	Coimbatore, Erode, Dharmapuri, Nammakal, Karur,
		Forest based (1)	Nilgiris
		Readymade Garment and Embroidery (4)	Trichirappalli Tiruvarur, Perambalur and Kirshnagiri
		Others (5)	Salem, Dindigul Cuddalore, Pudukottai and Tiruvarur
First two combination industrial region	17	Forest based + Textile based (1)	Nilgiris
		Textile based + Engineering based (1)	Coimbatore
		Textile based + Food based (4)	Erode, Dharmapuri, Namakkal

			and Karur
		Others (Specify) +Textile based (1)	Salem
		Readymade Garment and embroidery + Engineering based (2)	Trichirappalli and Kirshnagiri
		Mineral + Engineering Based (1)	Ariyalur
		Others (Specify) + Mineral (1)	Cuddalore
		Readymade Garment and Embroidery +Food based (2)	Tiruvarur and Perambalur
		Others (Specify) + Engineering Based (1)	Pudukottai
		Food based +Textile based (1)	Nagapattinam
		Others (Specify) + Readymade Garment and	Thanjavur and Dindugul
First three combination industrial region	12	Forest based + Textile based + Engineering based (1)	Nilgiris
		Textile based + Engineering based + Food based (1)	Coimbatore
		Others (Specify) + Textile based + Food based (1)	Salem
		Textile based + Others (Specify)+ Readymade Garment and Embroidery (1)	Karur
		Readymade garment and Embroidery + Engineering based + Food based (2)	Trichirappalli and Kirshnagiri
		Others (Specify) + Readymade Garment and Embroidery+ Food based (1)	Thanjavur
		Others (Specify) + Engineering based + Food based (1)	Pudukottai
		Readymade garment and embroidery + Food based + Engineering based (1)	Tiruvarur
		Food based + Textile based + Readymade Garment and Embroidery (1)	Nagapattinam
		Readymade Garment and Embroidery + Food Based + others (specify) (1)	Perambalur
		Others (Specify) + Mineral Based + Forest Based (1)	Cuddalore
First four combination industrial region	4	Others (Specify) + Textile based + Food based + Engineering based (1)	Salem
		Others (Specify) + Readymade Garment and Embroidery + Food based + Engineering based (1)	Thanjavur
		Food based + Textile based + Readymade Garment and Embroidery + Forest based (1)	Nagapattinam
		Others (Specify) + Engineering based + Food based + Textile based	Pudukottai
First five combination industrial region	1	Others (Specify) + Textile based + Food based + Engineering based + Mineral based (1)	Salem

In this method, the first ranking industry occupied the highest percentage of the total industrial in district wise. It may be noticed from Table 3 that Textile based, Readymade Garment and Embroidery, food and forest based industries ranking first in 17 districts respectively, are the leading

industry in Tamil Nadu Cauvery river basin. The monoculture is not prevalent. So, this method helps in ascertaining the areas of dominance of the first rank industrial region in the study area (Figure 2).

The Tamil Nadu Cauvery basin region has mono industrial combination where Food Based industries are mostly present in lower part of Cauvery basin districts due to favorable physical factors (Climate, Alluvial soil, Delta, Irrigation). The upper part of Cauvery Basin Coimbatore, Erode, Dharmapuri, Nammakal and Karur district has high percentage of textile industries because of the presence of Red Soil and other physical factors. Nilgiris district are surrounded by mountain region due to which presence of forest based industries are more in that region. The Readymade Garment and Embroidery Industries are developed in the centre and lower part of Cauvery River basin (delta region).

On the basis of first and second ranking industry, 11 industrial combinations may be recognized in the Tamil Nadu Cauvery river basin. The resulting industrial combinations present have been shown in the Table 3. It reveals that 17 out of the 11 industrial units reporting districts of Tamil Nadu Cauvery river basin. The relative strength of the first two industries is textile and food based one in 4 districts.

When the first three industries were taken in consideration, the number of industrial combinational region becomes as large as eleven. The districts occupied these type of industries are given in Table 3 which shows that Readymade Garment and Embroidery, Engineering based and Food based industries are dominated constituents in the first three rank combinations, which cover 17 out of 12 reporting districts.

The first four industrial combinations are seen in our study area (4 out of 17 districts) which has been mentioned in the Table 3 and Figure 2.

From the Table 3, we observe that 1 out of 17 districts have five industrial combinational regions on Tamil Nadu Cauvery basin.

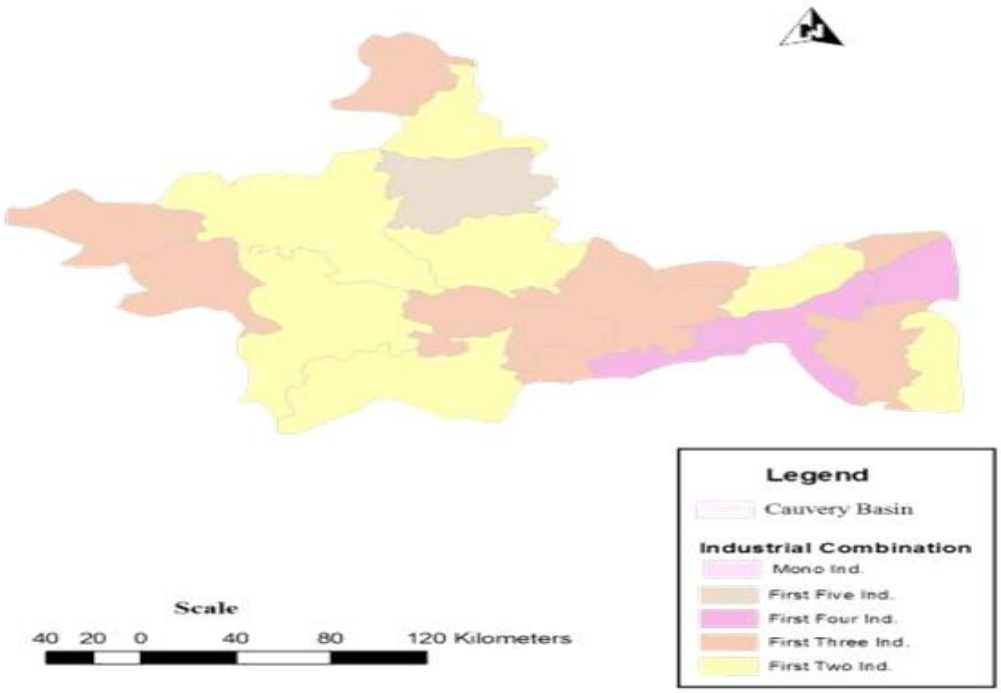

Figure 2: *Cauvery Basin Industrial combination Doi's method*

4. Conclusion

In recent year the concept of industrial combination has engaged the attention of Geographer and Regional Planers. The study of industrial combination is very significant for any particular region because it provide an idea about the relative position industries on region wise. Thus information on industrial combination is the basic requirement for the planning the future orientation of industrial in Tamil Nadu Cauvery Basin. To analyze the industrial combination of Tamil Nadu Cauvery Basin, Doi's method was applied. For simplification and generalization of industries, region which show less than 5 per cent were omitted from the calculation. Then, cumulative percentage is determined and compared with the critical value which gives the district which are included or excluded in the industrial combination. Using Doi's method, we conclude that our study area Tamil Nadu Cauvery basin region has micro, small and medium class industrial combinations. They are mono industries (17 districts), First Two industrial combination 17 industries, First Three Industrial combination 12 districts, First Four industrial combination 4 districts, First Five industrial combination 1 districts.

References

Districts Industrial Profiles, Development Commissioner Micro, Small and Medium Enterprises. Government of India. Available at: dcmsme.gov.in>dips/dipr.html

Husain, M. 2007. Systematic agriculture geography. New Delhi, India: Rawat Publications.

Khullar, D. R. 2012. A comprehensive Geography. New Delhi, India: Kalyani Publishers.

Moyra, S. K. and Mahavidyalaya, M. N. 2015. Study of agricultural regionalization status using GIS platform in Bilaspur District, Chhattisgarh, India. *International Journal for Scientific Research and Development,* 3(4).

Ogale, S. B. 2014. A study of crop combination region of Baramati Tehsil in Pune District. *International Journal of Innovation and Scientific Research,* 2(2), pp.329-334.

Statistical Hand book. 2016. Department of Economics and Statistics, Government of Tamil Nadu. Available at: www.tn.gov.in>deptst>stat.htm

Annexe- I: Doi's Deviation Analysis

An Abridged Part of Deviation Analysis Table (One-Sheet Table)

Cumulative percentage of higher ranking elements	Rank of Element												
	1	*2*	*3*	*4*	*5*	*6*	*7*	*8*	*9*	*10*	*11*	*12*	*13*
	Critical Value												
95											6.98	6.27	5.68
90								8.84	7.60	6.67	5.94	5.35	4.49
85					12.93	10.00	8.17	6.91	5.99	5.29	4.73	4.29	3.91
80				13.83	10.00	7.85	6.46	5.49	4.78	4.23	3.79	3.33	3.14
75			16.67	10.57	7.75	6.13	5.06	4.32	3.76	3.33	2.99	2.71	2.49
70		27.64	12.25	7.93	5.96	4.65	3.85	3.29	2.87	2.55	2.29	2.08	1.90
65		18.38	8.66	5.63	4.19	3.14	2.77	2.37	2.07	1.84	1.65	1.50	1.37
60		11.27	5.46	3.59	2.68	2.14	1.78	1.52	1.33	1.18	1.06	0.97	0.88
55		5.38	2.68	1.73	1.29	1.04	0.86	0.74	0.64	0.57	0.52	0.47	0.43
50		0.00	0.00	0.00	0.00	0.00	0.00	0.00	0.00	0.00	0.00	0.00	0.00

Source: Doi, Kikukazu, "The Industrial Sturcture of Japan Prefectures", Tokyo, *Proceedings of the International Geographical Union*, Regional Conference in Japan, 1957, pp. 310-316.

Cloud Publications
International Journal of Advanced Earth Science and Engineering
2017, Volume 6, Issue 1, pp. 567-576
ISSN: 2320–3609, Crossref: 10.23953/cloud.ijaese.304

Research Article

Seismic Hazard Assessment for Indira Sagar Dam

Rakesh Kumar Grover[1], Tripathi R. K.[2], Rajeev Chandak[1], Mishra H. K.[3]

[1]Department of Civil Engineering, Jabalpur Engineering College, Jabalpur, Madhya Pradesh, India
[2]Professor, Department of Civil Engineering, National Institute of Technology, Raipur, Chhattisgarh, India
[3]Principal, Indira Gandhi Engineering College, Sagar, Madhya Pradesh, India

Publication Date: 11 September 2017

DOI: https://doi.org/10.23953/cloud.ijaese.304

Abstract Indira Sagar Project is a multipurpose project in the state of Madhya Pradesh (India). In this study, seismic hazard has been assessed for Indira Sagar Dam site. The probabilistic Seismic Hazard analysis has been used. Effects of all the faults, who can produce earthquake equal to or more than 3.5 Magnitude and those within a radius of 300 Km from the centre of the Concrete Gravity Dam have been considered. The past history of earthquakes indicated that a total 66 earthquakes of magnitude 3.5 or more have been occurred in last 172 years. The maximum magnitude reported within the region of consideration is 6.2 in 1938 in Satpura range. Probabilistic approach used these data for hazard Analysis. Results are presented in the form of peak ground acceleration and seismic hazard curves.
Keywords *Ground motion; Indira Sagar Dam; Peak ground acceleration; PSHA; Seismic hazard*

1. Introduction

Large food grain requirements and shortage of electrical energy, forced India to go for different multipurpose schemes for water reservoirs so that sufficient water may be available for irrigation purpose and surplus water may be used for electrical energy generation. A large number of major dams (multipurpose) were constructed in the past. At that time, consideration for seismic activity was not that sensitive for designing and construction of these dams. In the present study the Indira Sagar Multipurpose Project (22°17'05"N, 76°28'15"E) popularly known as Indira Sagar Dam or Narmada Sagar Dam, site is considered for analysis. This dam is situated in the state of Madhya Pradesh (India) was constructed about 20 years ago. Occurrence of various earthquakes in recent past in the intra-plate region of peninsular India has clearly warned about the safety aspects of structures in the region.

Indira Sagar Dam has been constructed across the River Narmada, near village Punasa in Khandwa District. Indira Sagar Dam site is situated in Central Indian tectonic zone and come under seismic zone III (BIS-1893-2002, Part I). It is surrounded by number of faults; Son Narmada South Fault, Son Narmada North Fault and Tapti North Fault are some of them and many unnamed faults. Indira Sagar Dam is situated within the range of famous 1938 Satpura (epicentre, 21.13^0N, 75.75^0E) Earthquake of Magnitude 6.2. Also Jabalpur earthquake of magnitude 6.0 on 22 May 1997 (epicenter, 23.07^0N, 80.02^0E) centered about 300 km North-East side of the dam site; depth of focus is at 33 km. The Dam site is located in Peninsular India (PI), which has experienced the devastating

Koyna (1967, Mw = 6.3), Killari (1993, Mw = 6.1), Jabalpur (1997, Mw=6.0) and Bhuj (2001, Mw = 7.7) earthquakes. The hazard in this part of India is considered to be less severe than in the Himalayan plate boundary region. However, intra-plate earthquakes are rarer than plate boundary events but usually tend to be more harmful.

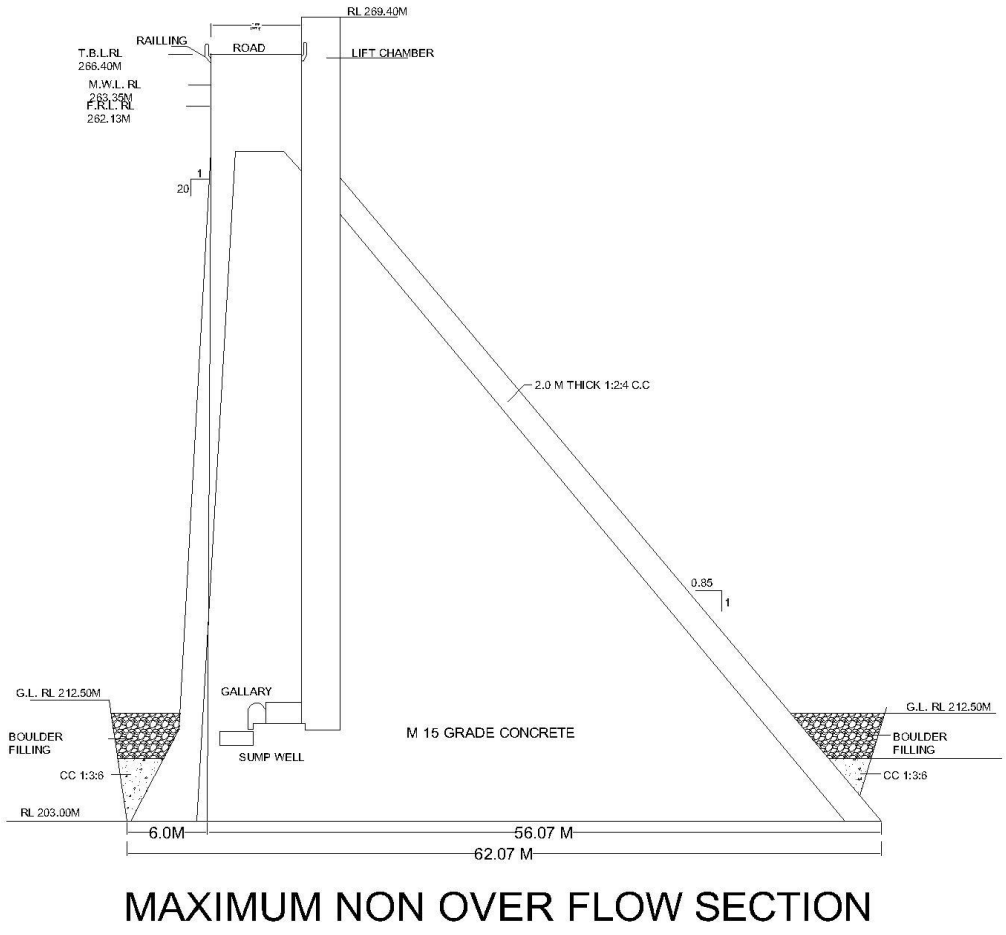

Figure 1: *Cross section of Indira Sagar Dam from DPR*

It is well established fact that past historical data plays very important role for any seismic hazard study. Age of earth is approximately 800 billion years. Seismic activities were there since very long period. As compared to this the available data for seismic activity is very small. Still earthquake engineers are trying to estimate the seismic hazard with these small numbers of recorded ground motion data. Ground motion introduces uncertainties into the nature of future and the dynamic forces to be considered in the design of dam structures. The response of any civil engineering structure depends primarily on the local ground motion at the foundation level. Accurate knowledge of such motion, due to all possible sources in the influence zone is the most sought information in engineering practice. The existing Indian code IS-1893 does not provide quantified seismic hazard, but lumps large parts of the India into unstructured regions of equal hazard of doubtful accuracy. There are other reasons also as to why probabilistic seismic hazard analysis (PSHA) should be adopted in India. The uncertain seismic scenario can be tailored to match the expected life of the structure. This way a normal building with a shorter life period of about 100 years may be designed for a shorter return period spectrum, whereas dam structure which has a longer social life could be designed for a longer return period scenario. In this work probabilistic seismic hazard has been estimated for Indira Sagar dam.

Indira Sagar dam is 654 meter long and 91.4 meter high (above deepest foundation level) concrete gravity dam with gross storage of 12200 MCM and a live storage of 9750 MCM corresponding to an FRL of +262.13 meter. There will also be a small saddle dam on the right side of reservoir. Central spillway, 495 meter long, to pass a design flood (SPF) of 83534 cumecs and PMF of 1.15Lakh cumecs through 20 numbers of radial crest gates of site 20x17 meter. A surface power house on the right bank to house 8 units of 125MW each, with conventional turbines installed. Cross section of Non Over flow section of Indira Sagar dam at deepest foundation level is shown in Figure 1 from Chief Engineer (1982), Detailed Project Report of Indira Sagar Dam.

2. Seismicity of the Region

Considered dam i.e. Indira Sagar Project (22°17'05"N, 76°28'15"E) is situated in Son Narmada Lineament Zone, which is ENE-WSW trending Lineament belongs to Central Indian tectonic zone(CITZ) extends roughly between 20^0N -24^0N latitude and 77^0E -83^0E longitudes (Consists of Son Narmada North Fault, Son Narmada South Fault, Govilgarh Fault, Tapti North Fault, Purna Fault, Kaddam Fault etc. and number of Unnamed Faults.) which is a part of Peninsular India. The major prominent rifts are the Narmada Son Lineament and the Tapti Lineament together called SONATA (Son-Narmada-Tapti Lineament) zone separating the northern and the southern blocks of the shield.

The most significant earthquakes have been Satpura-valley earthquake of 14 March, 1938, which had a magnitude of 6.2. This earthquake was located in Madhya Pradesh's Barwani District (21.13^0N, 75.75^0E) and was felt at many places of Madhya Bharat and Jabalpur Earthquake of magnitude 6.0 on 22 may 1997 (23.07^0N,80.02^0E), both were a deep-seated events, Rajendran et. al. (1998, 1999).

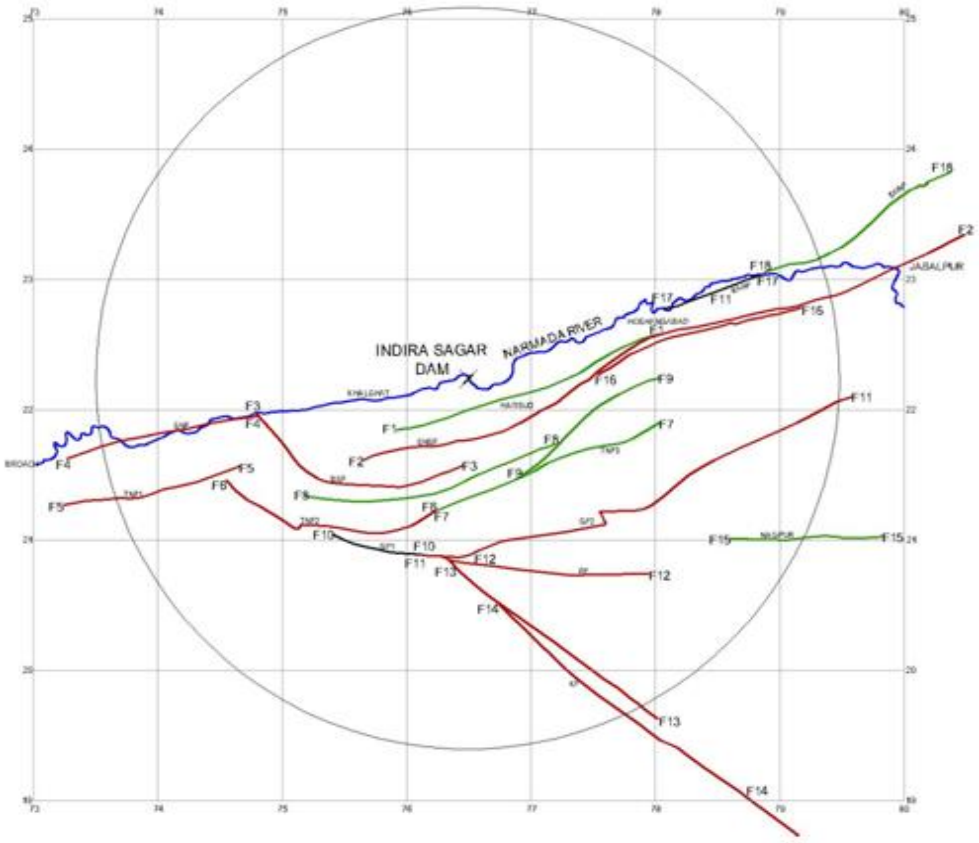

Figure 2: *Fault map for SHA prepared from Seismotectonic Atlas of India for Indira Sagar Dam*

According to Jain et al. (1995 CRUMSONATA) the western part of Son Narmada Tapti lineament (SONATA) zone, starting from Surat to east of Jabalpur, is covered mostly by Deccan basalt lava. The thickness of the lava pile varies in different parts. A huge thickness of 1450 m of basalts is preserved in the Western Ghats and in Satpura area while the Deccan basalts are very thin along the eastern margin of the main exposure. In Amarkantak (Origin of Narmada River), lava pile is about 150m thick. A series of N-S traverses were taken using deep seismic sounding (DSS) across the lineament zone to study the nature of Deccan volcanics, disposition pattern of the flows in the various physiographic segments, their correlation if any, it shows that Near Jabalpur, Narmada river the Lameta-Deeccan basalt is exposed at elevation of 410m msl while south wards lowest exposed flow occurs below 385m msl. This indicates reverse faulting at the Lameta contact.

The Deccan Basalts in the Narmada valleys and the Gondwana sediments in the area cut by numerous dykes trending NW-SE, ENE-WSW to NE-SW. The ENE-WSW trending dykes continuous further to the east of Seoni district (Dyke is a sheet of Rock that formed in a fracture in a pre-existing rock body) North of the Narmada valley, dyke are found only up to the foothills of the Malwa Plateau and its scrap. Here also it is in the area south of the Narmada river course that dykes are very predominant. The river bed is highly fractured and the fractures carry dykes in the vicinity of the Narmada river ENE-WSW trend is more prevalent.

According to Pimpricar S.D. (2009), the increase in the seismicity level during the recent years in the central Indian shield, this keeping in view that the lithospheric environment beneath this zone may be wet, thus accounting for higher rates of magmatic activity. Evidences indicate that CITZ has a major zone of differential crustal movement since Neo-archaean time. As per SEISAT (2000) a series seven number of very small faults on the western side (downstream side) of the Indira Sagar Dam.

There is lack of information on seismicity of PI, in so far as its application in engineering is concerned. For example, till some years back there was no region-specific attenuation relationship for PI that engineers could use as being rational enough, for future earthquake events, then Iyengar and Raghukant (2004) given an attenuation relationship for PI and Jaiswal and Sinha (2008) computed seismic Hazard parameters of PI. It may not be out of place to note here in 2002, the Code IS-1893 has eliminated the erstwhile low hazard region of PI (zone-I) and revised it to a higher hazard status as zone-II. The scientific basis for this revision, if any, remains obscure.

3. Fault Map

Identifications of different faults and their characteristics, around any site, are first and major step for any seismic hazard estimation. In the present study, Indira Sagar Dam has been selected as the target, a control region of radius 300 km around the Dam (22°17'05”N, 76°28'15”E) considered for further investigation. The fault map of this circular region prepared from the Seismo-tectonic Atlas of India (2000). Some researchers i.e. Raghukanth (2006) have taken 300 Km. Radius around the site and some researchers Sitharam (2012) mentioned the range 300 km to 400 km radius centered from site. Hence, 300 km. radius has been considered for this study. It is well established fact that earthquakes occurring at epicentral distances greater than 300 km do not generally cause structural damage. Hence, the faults lying within this radius from the site have been considered in estimating hazard. Fault map seismic hazard analysis is prepared from Seimotectonic atlas of India; GSI (2000) for Indira Sagar Dam is shown in Figure 2. A total of eighteen faults, influence seismic hazard at Indira Sagar Dam, can be identified from the above map. Details of considered faults are given in Table 1.

Table 1: *Details of faults considered*

Fault no.	Name of fault	M_{max} associated	Mu	Length of fault in Km	Shortage epicentral distance in Km	Average weightage factor
F1	-	4.0	4.5	188.6	19.4	0.0501
F2	SNSF	6.5	7.0	531.6	44.5	0.1136
F3	BSF	5.7	6.2	174.0	67.8	0.0578
F4	SNF	5.5	6.0	178.1	159.5	0.0545
F5	TNF-1	4.0	5.5	146.4	204.1	0.044
F6	TNF-2	4.0	4.5	165.5	107.7	0.0468
F7	TNF-3	4.8	5.3	261.4	86.6	0.0633
F8	-	4.0	4.5	138.8	71.8	0.0428
F9	-	4.5	5.0	139.4	86.0	0.0459
F10	GGF(SubS)	6.2	6.7	72.5	144.1	0.0461
F11	GGF	6.2	4.5	318.0	129.5	0.0813
F12	Purna F	4.0	4.5	112.0	146.7	0.0392
F13	-	4.0	6.7	170.6	206.0	0.0475
F14	Kaddam F	4.0	4.5	352.0	185.0	0.0486
F15	Nagpur	5.6	6.1	118.0	256.3	0.0492
F16	-	5.2	5.7	185.3	101.8	0.0565
F17	SNNF(sub)	4.0	4.5	85.8	174.8	0.0353
F18	SNNF	4.7	5.2	352.1	260.7	0.0776

4. Past Earthquake Records

Establishment of magnitude-frequency recurrence relation of individual fault is next step for seismic Hazard estimation. Fault recurrence estimate has been developed from regional recurrence relationship. Hence a catalogue of past earthquakes in the 300 km radial region has been developed. There have been several efforts made in the past to create an earthquake catalogue for India. A list of earthquakes of magnitude 3.5 and above is prepared using catalogue of Oldham, Raghukant (2004), Pimparikar (2009), CGS, USGS, IMD, GSI. Total 66 events from 172 years (1846-2016) are chosen for seismic hazard analysis, whenever the magnitude of an event was not available in the previous reports, the approximate empirical relation [$m = (2/3)\ I_0 + 1$] has been used to estimate it from the reported maximum MMI number. To avoid confusion associated with different magnitude scales, all magnitudes have been converted to moment magnitude Mw.

Some of the major earthquakes reported within 300 km radius of Indira Sagar Project are : 27th May 1846 (23.5^{O}N,79.5^{O}E) of Mw 6.5, near Fault F2, 31st March 1852 (22.1^{O}N,77.5^{O}E) of Magnitude 6, 31st December 1858 (21^{O}N,75^{O}E) of Magnitude 5.5, 18th November 1863 (21.8^{O}N,75.3^{O}E) of magnitude 5.7 Near Barwani Sukta fault, 14th March 1938 (21.13^{O}N,75.75^{O}E) of magnitude 6.2 and 25th August 1957 (22^{O}N,80^{O}E) of magnitude 5.6 Near Govil Garh fault.

Also recent earthquake events are 22nd May 1997 (23.07^{O}N, 80.02^{O}E) of magnitude 6.0 near Jabalpur SNS Fault F2, 18th October 2012 (23.5^{O}N, 79.5^{O}E) of magnitude 5.0 near Son Narmada south fault F2 and series of very small magnitude earthquakes in Khandwa District.

5. Regional Recurrence

In this work regional seismic activity has been characterized by the Gutenberg–Richter frequency–magnitude recurrence relationship $\log_{10}N = a - bM$, where N stands for the number of earthquakes

greater than or equal to a particular magnitude M. Parameters (a, b) characterize the seismicity of the region. The simplest way to obtain (a, b) is through least square regression as shown in Figure 3.

In the present study, the 172 (1846-2016) years sample of earthquake data around Indira Sagar Dam site was evaluated and obtained values of a is 1.884 and b value is 0.567 for the region around Indira Sagar Dam.

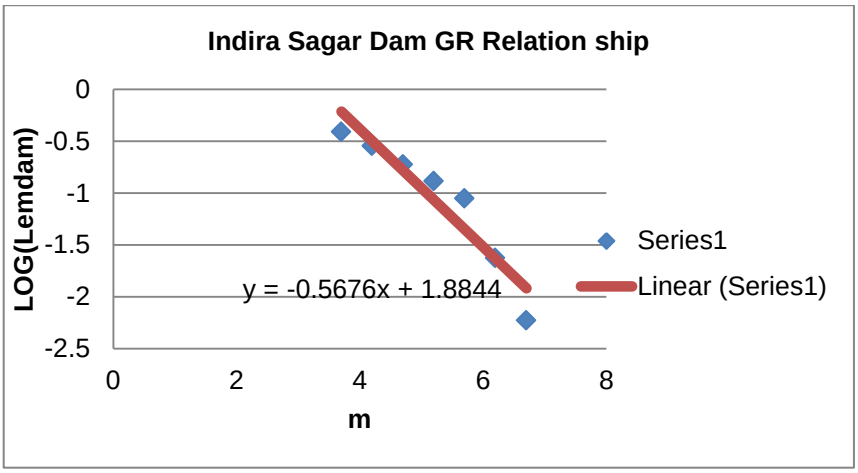

Figure 3: *Gutenberg Richter relationship*

6. Deaggregation

The fault level recurrence is required for differentiating the nearby sources or far off sources from the Indira Sagar Dam site. Fault level recurrence is rarely known due to meager amount of recorded earthquakes, because only recent data is available, old data are of lower magnitude earthquake are not available. The recurrence relation computed above for the 300 km radius region around Indira Sagar Dam is for whole region and is specific to any particular fault. Hence this problem can be tackled using the principle of conservation of seismic activity. According to this the region measured in terms of number of earthquakes per year with m $\geq m_o$, should be equal to the sum of such earthquakes occurring on individual faults. Considering that longer fault can produce more number of small events of magnitude m_o than a shorter fault. Hence, $Ni(m_0)$ may be taken as being proportional to the length of the fault, leading to a simple weight factor $p_i = L_i/\sum L_i$, Where L_i is length of individual ith fault in Kms. It is now well established fact that future activity will continue, at least in the short run, similar to past activity. Hence, seismic activity of a fault should be related to the number of past events associated with it in the catalogue. Hence, one can arrive at another weight factor q_i as the ratio of the past events associated with fault i to the total number of events in the region. Here, the average of pi and qi is taken as the final weight to get

$$N_i\,(m_0) = 0.5(p_i + q_i)\,N\,(m_0) \ldots (1)$$

The above weight factors are included in Table 1. Since the control region is in a seismically homogenous region, it would be appropriate to use the regional b-value for individual faults also. This give:

$$Ni(m) = Ni(m_0)\mathrm{v}\left[\frac{e^{-\beta(m-m_0)}-e^{-\beta(m_u-m_0)}}{1-e^{-\beta(m_u-m_0)}}\right]\ldots (2)$$

Where m_u is the maximum potential magnitude of the ith fault and β= 2.303b and v =$e^{\alpha-\beta mo}$. The above arguments provide a basis for decomposing the regional hazard into fault-level recurrence relations is shown in Figure 4 for Indira Sagar Dam.

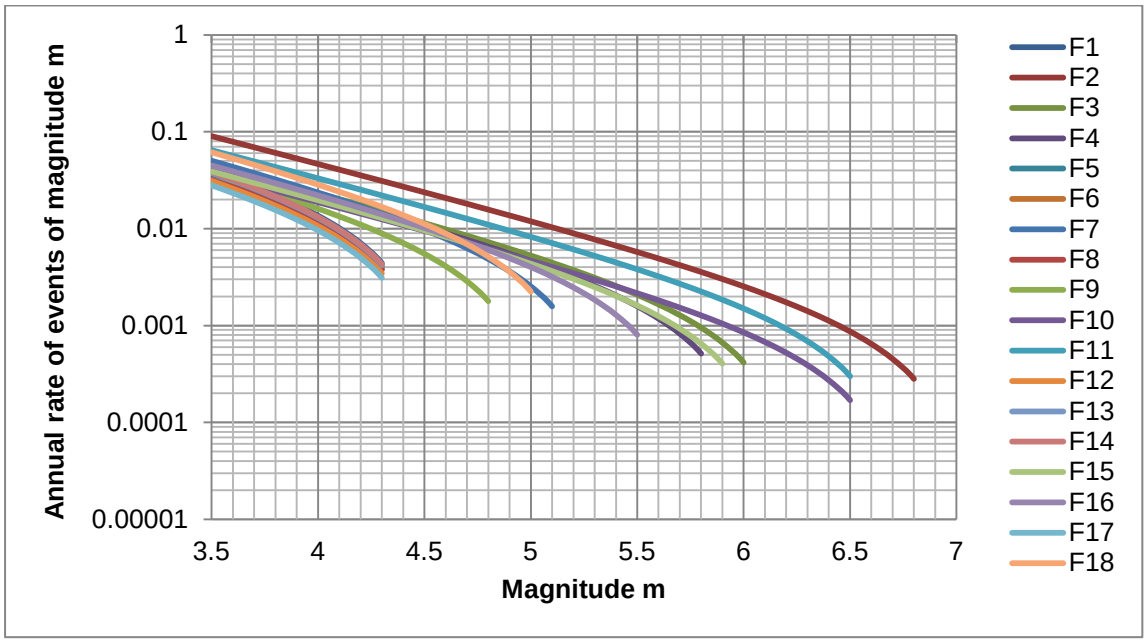

Figure 4: *Fault level recurrence relation*

7. Attenuation of Strong Motion

In engineering applications, the peak ground acceleration (PGA or zero period acceleration) and the response spectrum are needed at the site. These quantities depend primarily on the magnitude of the event and the distance of the site to the source. Thus, attenuation of spectral acceleration as a function of magnitude and hypo-central distance is a key element in further seismic hazard analysis. Attenuation relationship developed by Iyenger and Raghukanth (2004, 2007) considered for the analysis and PGA has been calculated. The form of the attenuation equation proposed for bedrock (*br*) condition is:

$$\ln(y_{br}) = C1 + C2(m-6) + C3(m-6)^2 - C4\,r - \ln r + ln\,\varepsilon_{br} \ldots \text{(3)}$$

In this equation, y_{br} stands for the spectral acceleration (S_a/g); m and r refers to moment magnitude and hypocentral distance respectively. The coefficients of the above equation taken from Raghukanth and Iyengar (2006). The average of the error term ln(ε_{br}) is zero, but the standard deviation is of importance in probabilistic hazard analysis. This relation is valid for bedrock sites with a shear wave velocity more than 1.5 km/s. The coefficients for zero period were used for the calculation which are C1=1.6858, C2=0.9241, C3=-0.0760, C4=0.0057 and standard deviation of ε_{br}=0.4648. The normal cumulative distribution function has a value which is most efficiently expressed in terms of the standard normal variables (z), which can be computed for any random variables using transformation as given below (Kramer, 1996):

$$z = \frac{lnPHA - lnPHA}{\sigma lnPHA} \ldots \text{(4)}$$

Where, PHA is the various targeted peak acceleration levels, which will be exceeded. ln PHA(bar) the value is calculated using attenuation relationship equation and ln PHA is the uncertainty in the attenuation relation expressed by the standard deviation.

8. Probabilistic Seismic Hazard Analysis

Probabilistic seismic hazard analysis (PSHA) estimates the probability of exceedance of spectral acceleration S_a at a site due to all possible future earthquakes. In reality, the seismic hazard at a site is influenced by all the earthquakes with different magnitudes and different distances. PSHA considers the contribution of all earthquakes in that region. PSHA also considers the uncertainties associated with time of occurrences of earthquakes and its location. The usefulness of PSHA in quantifying safety of man-made structures has been discussed extensively in the literature. PSHA has become a standard tool for estimating design basis ground motion. It also provides a framework where these uncertainties can be combined rationally to provide more complete picture of seismic hazard (Kramer, 1996). Following Raghukanth and Iyengar (2006), assuming that the number of earthquakes occurring on a fault follows a stationary Poisson process, the probability that the control variable *Y* exceeds level *y**, in a time window of *T* years is given by:

$$P(Y > y^* \text{ in } T \text{ years}) = 1 - \exp(-\mu_{y^*} T) \quad \ldots (5)$$

The rate of exceedance, μ_{y^*} is computed from the expression:

$$\mu_y^* = \sum_{j=1}^{Nm} \sum_{k=1}^{Nr} vi\, P(Y > y^* | mj, rk)\, P[M=mj]\, P[R=rk] \quad \ldots (6)$$

Here P[M=m] and P[R=r] are the probability density functions of the magnitude and hypocentral distance respectively. P(Y >y*|m, r) is the conditional probability of exceedance of the ground motion parameter Y. The reciprocal of the annual probability of exceedance gives the return period for the corresponding ground motion value.

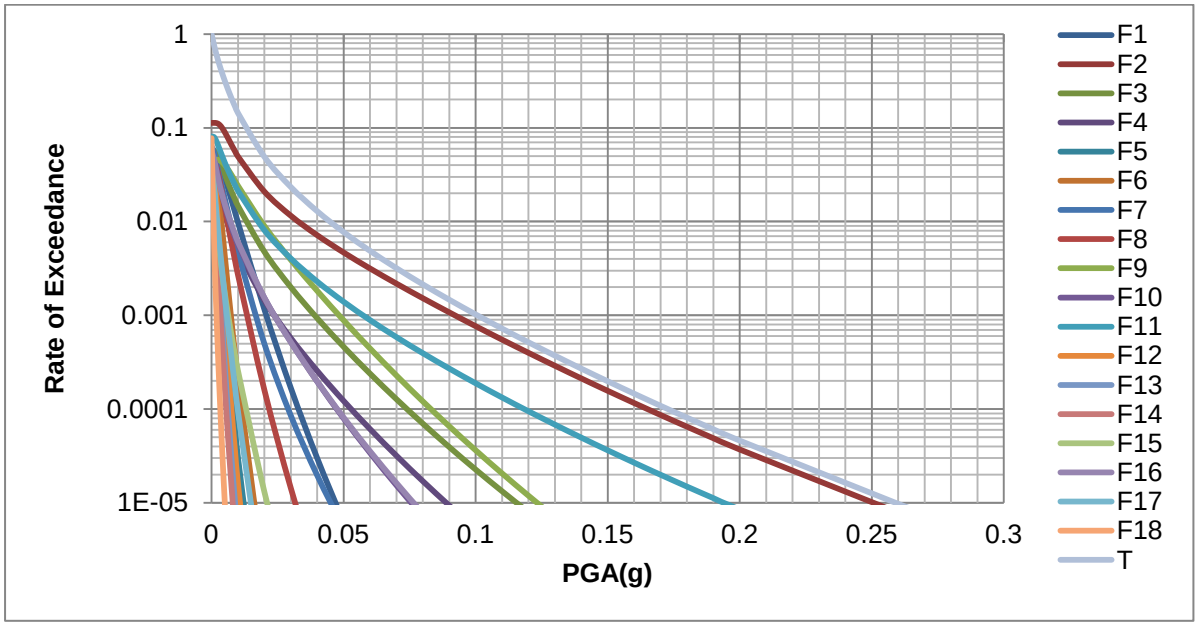

Figure 5: *Seismic hazard curves for Indira Sagar Dam site*

9. Seismic Hazard Curves

Seismic hazard curves can be obtained by computing the mean annual rate of exceedance μ_{y^*}, for different specified ground motion values y*. These curves are obtained individually for all the sixteen capable faults around Dam site and considering the individual effect of all eighteen faults and

combined them to estimate the aggregate hazard at the site. The seismic hazard curve for PGA at bed rock (foundation level of Dam) obtained by above procedure is shown in Figure 5 for Indira Sagar Dam Site. It is observed that seismic hazard at Indira Sagar dam is mainly influenced by Fault F2-Son Narmada South Fault, F11-Govilgarh Fault, F3-Barwani-Sukta Fault and F4-Son Narmad Fault.

10. Conclusions

The present article investigates seismic hazard of Indira Sagar Dam near Punasa village of Khandwa District of Madhya Pradesh state of India using state-of-the-art probabilistic analysis. Eighteen faults and Nine Lineaments Identified from Seismotectonic atlas of India and its environ, 2000, considered all the Eighteen Faults that can induce ground motion at Dam site have been identified from the seismo-tectonic map of the region and from old and recorded events of earthquake. Since slip rates of individual faults are not available, the recurrence relation of these faults has been estimated from the regional recurrence relation. The attenuation relations developed previously specifically for PI are used for computing spectral acceleration hazard curves. Probability that an acceleration of 0.1g would be exceeded in 50 years may be p[YT>y*] = 5.0%. The PGA that has a 10% Probability of exceedance in 50 year period (For return period of 475 years) is 0.12g and the PGA that has a 2% probability of exceedance in 50 year period (For return period of 2475 years) is 0.16g which is within limits of BIS-1893-2002, Part I coefficients for zone III.

The maximum regional magnitude for Indira Sagar Dam is also estimated. With the help of these data we can check the stability of Dam considering seismic activity in area.

References

Chief Engineer, 1982. Indira Sagar (Narmada Sagar) Detailed Project Report, Bhopal, Madhya Pradesh, India.

GSI. 2000. Seismo-tectonic atlas of India and its environs. *Geological Survey of India,* pp.1-87.

IS-1893 (Part-1). 2002. Indian standard criteria for earthquake resistant design of structures. Fifth Revision, *Bureau of Indian Standard,* New Delhi, India, pp.1-41.

Iyengar, R.N. and Raghu Kanth, S.T.G. 2004. Attenuation of strong ground motion in Peninsular India. *Seismological Research letters,* 75(4), pp.530-540.

Jaiswal, K. and Sinha, R. 2008. Spatial-temporal variability of seismic hazard in peninsular India. *Journal of Earth System Science,* 117, pp.707-718.

Kramer, S.L. 1996. Geotechnical earthquake engineering. NJ, USA: Prentice Hall, pp.1-653.

Pimprikar, S.D. 2009. Seismotectonics of deep crustal earthquakes in parts of Central Indian tectonic zone with special reference to Jabalpur and its surrounding environs, Ph.D. Thesis, Jabalpur, Madhya Pradesh, India. pp.1-70.

Rajendran, K. and Rajendran, C.P. 1998. Characteristics of the 1997 Jabalpur earthquake and their bearing on its mechanism. *Current Science,* 74(2), pp.168-174.

Rajendran, K. and Rajendran, C.P. 1999. Seismogenesis in the stable continental interiors: an appraisal based on two examples from India. *Tectono-physics,* 305, pp.355-370.

Raghukanth, S.T.G. 2004. Catalogue of earth quakes of moment magnitude ≥4 in and around India. pp.1-782.

Raghu Kanth, S.T.G. and Iyengar, R.N. 2006. Seismic hazard estimation for Mumbai City, *Current Science,* 91(11), pp.1486-1494.

Raghu Kanth, S.T.G. and Iyengar, R.N. 2007. Estimation of seismic spectral acceleration in Peninsular India. *Journal of Earth System Science,* 116(3), pp.199-214.

Cloud Publications
International Journal of Advanced Earth Science and Engineering
2017, Volume 6, Issue 1, pp. 587-595
ISSN: 2320–3609, Crossref: 10.23953/cloud.ijaese.316

Research Article

Environmental Impact Assessment (EIA) and Assessment of Soil Loss in Sandur Taluk due to Mining Activity in and Around Bellary District, South India

Suresh Kumar B.V., Sunil Kumar R.K., Kaliraj S.

Department of Studies in Earth Science, University of Mysore, Manasagangotri, Mysore, India-570006
Department of Geo-Technology, Manonmanian Sundarnar University, Tirunelveli, India - 627012

Publication Date: 14 October 2017

DOI: https://doi.org/10.23953/cloud.ijaese.316

Abstract The catchment boundary of Sandur Taluk covers an area about 1254.02 sq km. It is well known for repository of Iron and manganese ore mineralization, more than hundred mining companies were operated within the Sandur Taluk and majority of hillocks have undergone by mining activity. The Sandur Taluk is affected by excavation of Iron ore. An attempt is made to Environmental Impact Assessment (EIA) by attributing various parameters like Land Use Land cover, Soil, Geomorphology, and catchment boundary etc., The erosion is a natural geomorphic process occurring continually over the earth's surface and it largely depends on topography, vegetation, soil and climatic variables and, therefore, exhibits pronounced spatial variability due to catchments heterogeneity and climatic variation. This problem can be circumvented by discrediting the catchments into approximately homogeneous sub-areas using Geographic Information System (GIS). Soil erosion assessment modeling was carried out based on the Revised Universal Soil Loss Equation (RUSLE). A set of factors are involved in RUSLE equation are A = Average annual soil loss (mt/ha/year), R = Rainfall erosivity factor (mt/ha/year), k = Soil erodibility factor, LS = Slope length factor, C = Crop cover management factor, P = Supporting conservation practice factor. These factors extracted from different surface features by analysis and brought in to raster format. The output depicts the amount of sediment rate from a particular grid in spatial domain and the pixel value of the outlet grid indicates the sediment yield at the outlet of the watershed.
Keywords *GIS; revised universal soil loss equation; soil erodibility; slope length factor; spatial analyst*

1. Introduction

Karnataka has a great history of mining activity that dates back to prehistoric times. In 1991 annual production of Iron ore between 2.75 to 4.5 million tones manganese ore between 0.13 million tones to 0.3 million tones. Now it has reached up to 150 MTPA (million tons per annum) by means of mechanized method. However the Sandur schist belt mining industry is facing increasing environmental pressure and regulatory controls. Whole regions are affected and in some cases devastated by the results of mining activities, and also by the more recent industrialized phase of mine development. The natural ecosystem of Sandur schist belt environments is extremely sensitive to human interference. The soil loss results in the decrease of arable land and its quality by

depleting the top fertile soil and thereby affecting the land productivity as a whole (Pal and Samanta, 2011). Estimation of soil loss from a place is necessary to measure sediment deposition in any area (Bali and Karale, 1977). Linkage of GIS and erosion is made possible by the spatial format in which RUSLE factors are presented (Yitayew et al., 2007). The most common and effective method such as universal soil loss equation (USLE) by (Wischmeier and Smith, 1978) is investigated to construct soil erosion modeling in study area through spatial analysis tool in ArcGIS 9.2. The USLE algorithm widely accepted method to estimate soil loss at catchment scale (Jain et al., 2001). Erosion Models are helpful for evaluating the Impact of land use practices on soil losses, and are increasingly being used for establishing guidelines and standards for regulation purposes (Croke and Nethery, 2006). Coupling GIS and USLE/RUSLE has been shown in many cases to be an effective approach for estimating the magnitude of soil loss and Identification spatial locations vulnerable to soil erosion (Lim et al., 2005; Fu et al., 2006; Wachal, 2007). The USLE model actively involved in Raster grid in GIS environment to compute various parameters such as R factor, P factor, Ls factor and K factor, etc., The technology of remote sensing and GIS is gaining importance as a powerful tool in the management of information in agriculture, natural resources assessment, environmental protection and conservation.

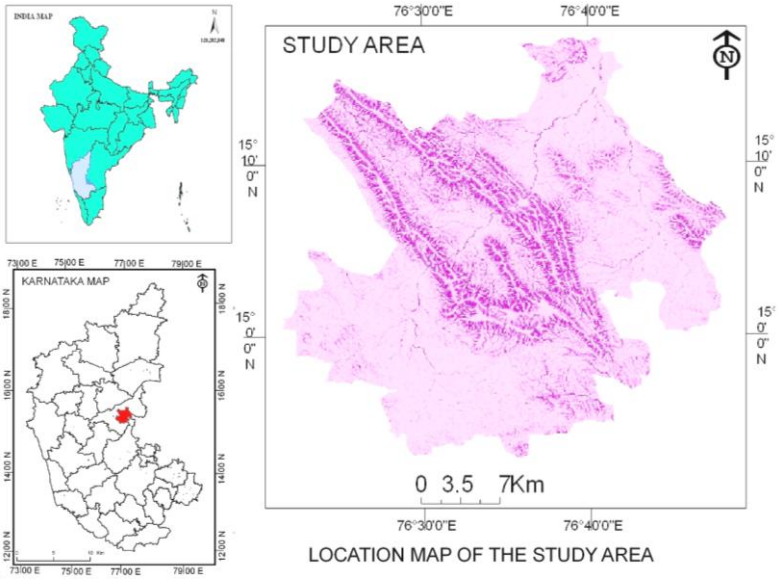

Figure 1: *Study area location*

1.1. Geographical Location

The area, study area falls under parts of Survey of India toposheets, 57 A/8, A/12, A/16 and 57 B/9, between the latitudes 15° 00′ N and 15° 15′ N and 76° 20′ E and 76° 55′ E. The study area is well known for its Iron occurrences and there are several operating open pit mines and abandoned Manganese open pits are located in the area. The lowest elevation is 625m above the MSL and the highest elevation 997m above the MSL. Covers an area of 1224.91 sq km, within the Dharwar craton (Figure 1).

Physiography and Drainage System

The study area lies in the Krishna Drainage system and the area exhibits dendritic drainage pattern (Figure 2). The Naarihalla stream flows along its north-eastern part of the Taluk. The Hire halla stream, later which joins the Kanigana halla, one of its right bank tributaries and a big stream itself, mark the eastern boundary of the Taluk. Both these major streams flow towards the north-east. The natural drainage of the Taluk is diverted in the opposite directions into these streams, the Naari halla

sharing about 75 percent of the water of the Taluk. The tributaries of the Hire halla and Kanigana halla flowing in the Sandur Taluk are Sige halla.

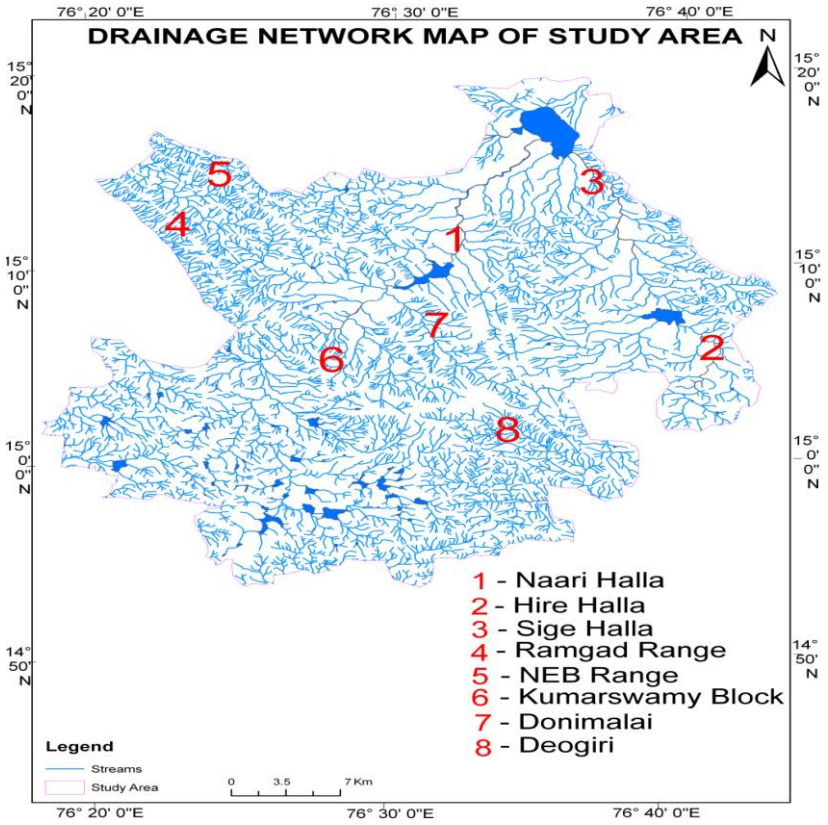

Figure 2: *Drainage system of study area*

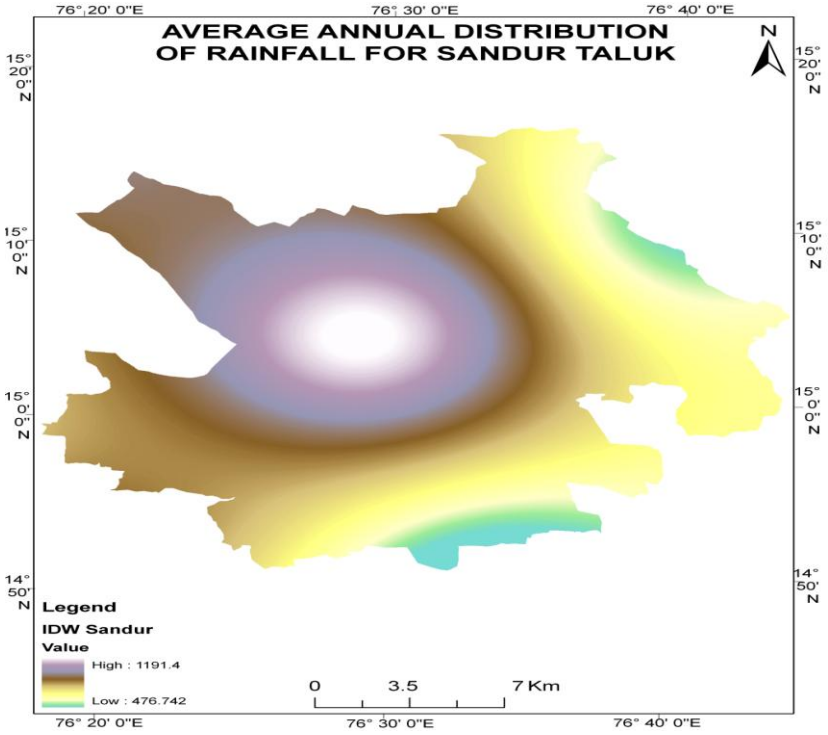

Figure 3: *Spatial distribution of rainfall*

Spatial Distribution of Rainfall

Spatially, Rainfall level is varies place to place. The average annual rainfall is 600 mm and the maximum and minimum rainfall level is varying from 400 mm to 600 mm in monsoon. A sub-tropical climatic condition is favorable in this region. The central part of the Taluk is structured by hillocks and mountain ranges covered by thick vegetation. Central part of the Taluk receives high rainfall when compared to other parts of the Taluk whereas South and South Eastern part of the Taluk receives low rainfall (Figure 3).

2. Methodology

Soil erosion assessment is done by using Geographical Information System (GIS) based on the Revised Universal Soil Loss Equation (RUSLE). A set of factors are involved in the RUSLE to assess the soil loss in watershed. The RUSLE can be done by following the equation, A = R x k x LS x C x P where, A = Average annual soil loss (mt/ha/year), R = Rainfall erosivity factor (in t / ha / year), k = Soil erodibility factor, LS = Slope length factor, C = Crop cover management factor, P = Supporting conservation practice factor. The equation groups the numerous interrelated physical and management parameters that influence the erosion rate under six major factors, of which site specific values can be expressed numerically (Singh et al., 1981).

2.1. Calculation of Rainfall Erosivity Factor (R factor)

The rainfall erosivity factor (R factor) represents the erosion potential caused by rainfall (Renard et al., 1997). The capacity of the rain to remove soil particles is one of the most important parameters in the RUSLE as this is a quantitative factor expressed in tone/hectare/year. The evaluation of R is given as, R factor = 79 + 0.363 * r, where r = Mean annual rainfall (mm). The mean annual rainfall data from three rain gauge station located at different place in study area which spatially interpolated using Kriging method of spatial analyst tool in ArcGIS 9.2 software. Here the value high represents intensity of rainfall within the Taluk.

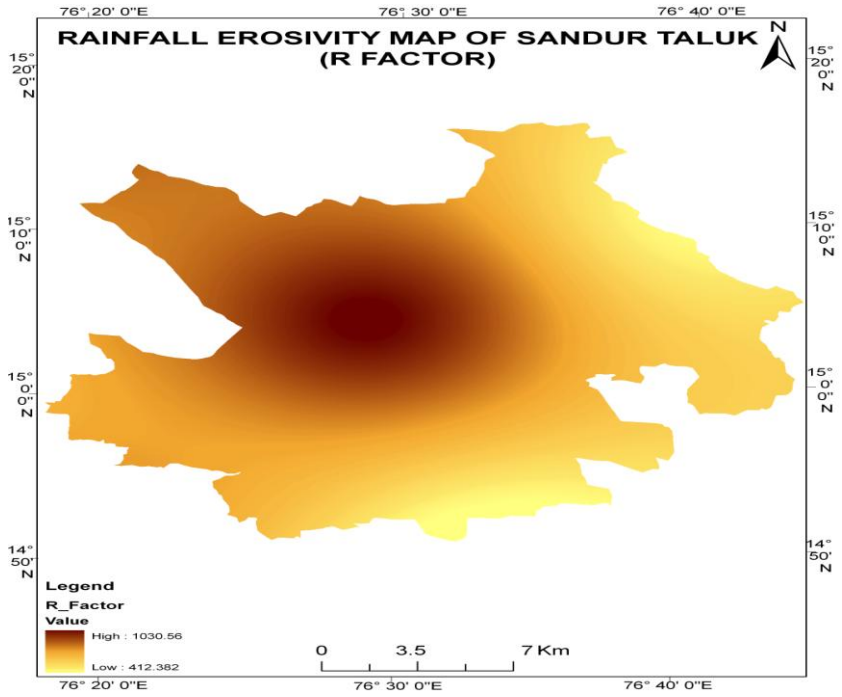

Figure 4: *R-Factor*

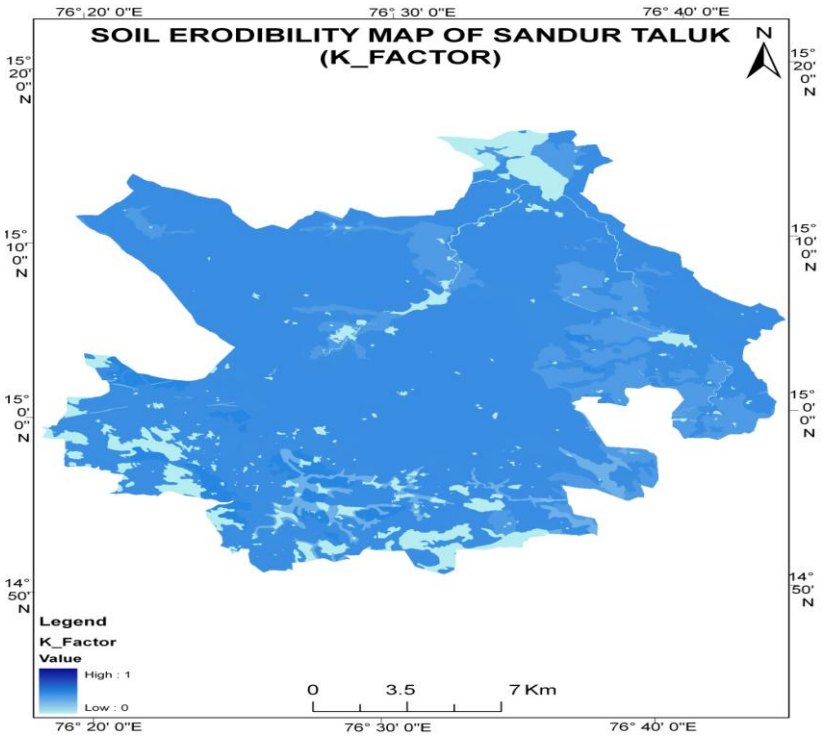

Figure 5: *K-Factor*

2.2. Calculation of Soil Erodibility Factor (K factor)

It is a measure of soil susceptibility to detachment and transport, by the erosion agents of the soil particles. The variation of K factor over the study area is shown in Figure 4. This is estimated by using the formula, K = 2.8 x 10-7 M-1.14 (12- a) + 4.3 x 10-3 (b-2) + 3.3 x 10-3 (c-3), where, K = Soil erodibility factor, M = Particle size parameter (% silt + % very fine sand) x (100 - % clay), a = % of organic matter, b = Soil structure code (very fine granular 1; fine granular 2; medium or coarse granular 3), c = Profile permeability class (rapid 1; moderate to rapid 2; moderate 3; slow to moderate 4; slow 5; very slow 6).

From the soil reports of the study area, the above parameters are computed for various types of soil in the study area and the K factor values calculated by inputting the above parameters and transformed in to Raster grid format by determining each pixel with K-Factor value. Lower values represent detached suspended soil sediment particles collected in surface water bodies.

2.3. Calculation of Slope Length Factor (LS factor)

Estimation of LS factor poses more problems than any other factors in RUSLE and it is a particular problem in applying to real landscape as part of a GIS. Data on aspect, land use and slope maps are overlaid to map the slope length. The LS factor of the study area is shown in (Figure 6) L and S are treated as combined factor to find the LS factor, LS = (n+1) x (As / 22.13) n x (sin β / 0.0896) m, where, LS = Slope length factor, n = 0.4 (a constant), β = Local slope angle, m = 1.3 (a constant), As = Contributing area.

It is known that the amount of runoff increases due to the continuous accumulation down the slope as the slope length (L factor) increases; the velocity of runoff increases as the slope steepness (S factor) increases (Kim, 2006). Here the map shows north-west and south-east part of the Study area represents high slope steepness, where the erosion rate will be more.

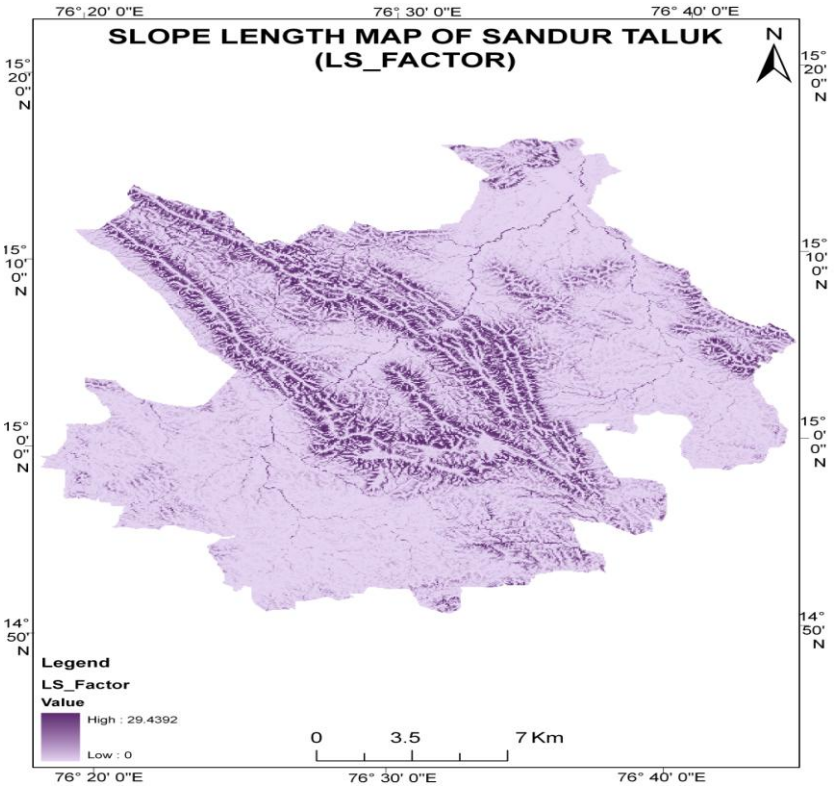

Figure 6: *LS-Factor*

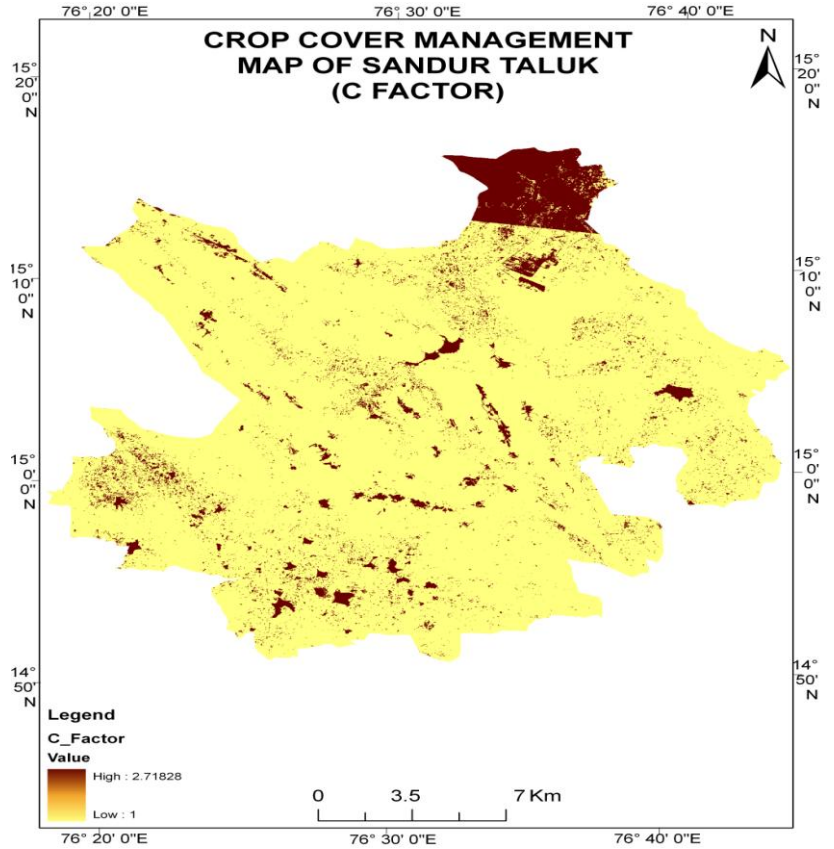

Figure 7: *C-Factor*

2.4. Calculation of Crop Management Factor (C factor)

This expresses the role of plants and of their management techniques on the water. The crop management factor includes the effects of crop cover, crop sequence and productivity level, length of growing season, tillage practices, residual management and expected temporal distribution of erosive rainstorms.

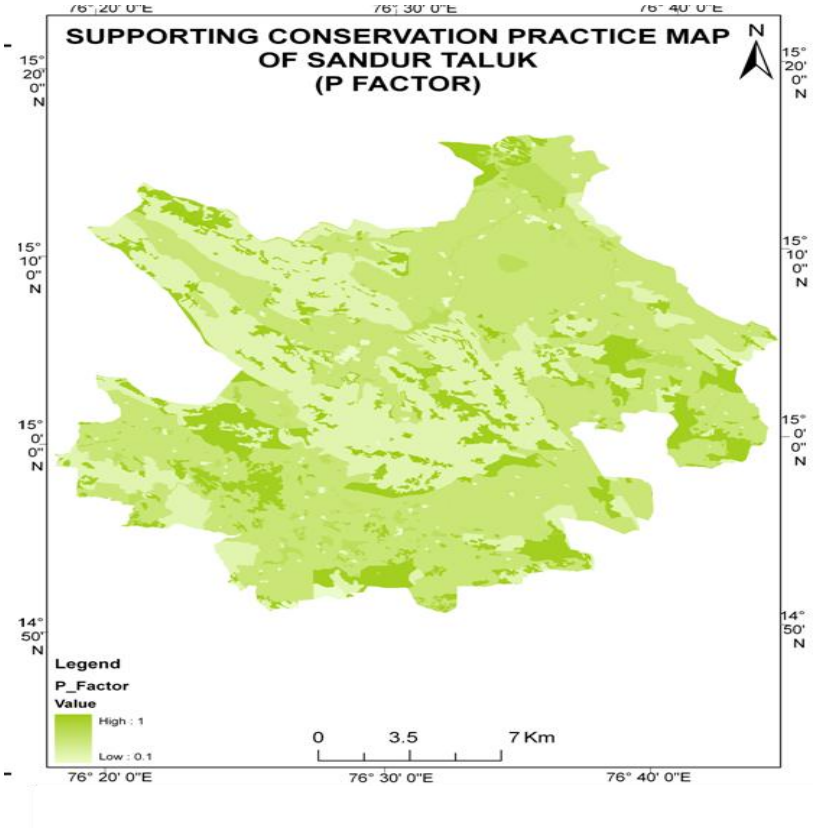

Figure 8: *P-Factor*

Table 1: *Mean of coefficient of P factor*

Land use	% Slope	P Factor
Agricultural land	0-5	0.11
	5-10	0.12
	10-15	0.14
	15-30	0.19
	>35	0.25
Waste land		1.00
Forest categories		0.8
Grassland		0.10
Built-up areas		0.00
Water bodies		0.00
Fallow land		1.00

2.5. Calculation of Conservation Practice Factor (P factor)

The effect of watershed management or conservation practices depends on the changes induced on manifold factors such as flow speed, surface roughness, infiltration etc., The standard values of particular soil estimated by calculating its means of co-efficient as in Table 1. According to the

values given in table, the map shows high erosion intensity and low erosion intensity in the study area. The bright colored are represents hillocks contributed to high erosion.

2.6. Estimation of Soil Loss using RUSLE Equation

The factors and parameters of soil loss estimation (RUSLE) equation have been analyzed in Spatial Analyst Tools of Arc GIS 9.2. The 3D Analyst Tool used to create the layers of R, K, L, S and P factors. As per the RUSLE algorithm, each raster grid of R, K, LS, C and P factors are multiplied to estimate the soil loss per hectare / year in the unit of Metric tons. The analysis spatially carried out to detect intensity of soil erosion in every parcel of grid. The output layer brought in to reclassification to categorize the area in to severe, moderate and less based on intensity of soil erosion.

3. Conclusion

In this study, the Geo-Statistical algorithm of RUSLE equation investigated to measurement of soil loss in the study area. This makes understanding on GIS capability in soil loss modeling. Estimation of soil loss is prim factor to compute sediment yield in watershed and catchment level studies. Spatially computed soil removal from most of the catchment area is estimated to 0.0052 MT/Ha/year to 0.43 MT/Ha/years. However, the range of sediment yield is depending upon the soil loss in and around the area. Deposition of sediment resulted at grids of the water bodies occurred with different level, the transportation of sediment depending on soil characteristics and slope condition. This is considerably primary study carried out to finding the changes of water resources in the study area, this may effective input for future study regarding to this analysis. The volume of each grid considers estimating the amount of soil loss in an area. As the result of soil loss estimation from the study area, there are following places were detected with severe soil erosion such names are Ramagad forest block, Devagiri hills, Northern parts of Donimali Village, North Eastern Block (NEB) hills and middle eastern parts of the Taluk including Tarangar village and Bommagatta village. The water tanks are highly affected in these areas due to deposition of sediment continuously.

References

Bali, Y.P. and Karale, K.L. 1977. A sediment yield index as a criterion for choosing priority basins. *Erosion and Solid Matter Transport in Inland Waters,* Paris, pp.180-188.

Croke, J. and Nethery, M. 2006. Modeling runoff and soil erosion in logged forests: scope and application of some existing models. *Cantena,* 67, pp.35-49.

Fu, G., Chen, S. and McCool, D.K. 2006. Modeling the impacts of no-till practice on soil erosion and sediment yield with RUSLE, SEDD, and Arcview GIS. *Soil and Tillage Research,* 85, pp.38-49.

Jain, S.K., Kumar, S. and Varghese, J. 2001. Estimation of soil erosion for a Himalayan watershed using GIS technique. *Water Resources Management,* 15, pp.41-54.

Kim, H. 2006. Soil Erosion Modeling using RUSLE and GIS on the IMHA Watershed, South Korea.

Lim, K.J., Sagong, M., Engel, B.A., Tang, Z., Choi, J. and Kim, K. 2005. GIS - based sediment assessment tool. *Catena,* 64, pp.61-80.

Pal, B. and Samanta, S. 2011. Estimation of soil loss using remote sensing and geographic information system techniques (Case study of Kaliaghai River basin, Purba & Paschim Medinipur District, West Bengal, India). *Indian Journal of Science and Technology,* 4(10), pp.1202-1207.

Renard, K.G., Foster, G.R., Weesies, G.A., McDool, D. and Yoder, D. 1997. Predicting soil erosion by water: a guide to conservation planning with the Revised Universal Soil Loss Equation (RUSLE). *Agricultural Handbook 703,* USDA-ARS.

Singh, G., Chandra, S. and Babu, R. 1981. Soil loss and prediction research in India. Central Soil and Water Conservation Research Training Institute, Bulletin No. T-12/D9.

Wachal, D.J. 2007. Integrating GIS and erosion modeling: a tool for watershed management. *ESRI - International User Conference,* Paper No. UC 1038.

Wischemier, W.H. and Smith, D.D. 1978. Predicting rainfall erosion losses-a-guide to conservation planning. *Agricultural Handbook No. 537,* Washington DC, USA.

Yitayew, M., Pokrzywka, S.J. and Reward, K.G. 2007. Using GIS for facilitating erosion estimation. *Journal of Applied Engineering in Agriculture,* 15(4), pp.295-301.

Cloud Publications
International Journal of Advanced Earth Science and Engineering
2017, Volume 6, Issue 1, pp. 577-586
ISSN: 2320–3609, Crossref: 10.23953/cloud.ijaese.314

Research Article

Iron Ore Mineralization of Ramagiri Greenstone Belt, Anantapur District, Andhra Pradesh, India

Lakshmidevamma B.[1], Venkatarami Reddy Y.[2], Gope Naik V.[3]

[1]Department of Geology, Government Arts College, Anantapur, Andhra Pradesh, India
[2, 3]Department of Geology, S. V. University, Tirupati, Andhra Pradesh, India

Publication Date: 10 October 2017

DOI: https://doi.org/10.23953/cloud.ijaese.314

Abstract Archaean provinces have rocks of 2500 Ma to 3000 Ma that contain, i. the granite – greenstone association, ii. The high-grade association and the cratonic basin association. Amongst the above said features, the granite - greenstone association is more in abundance and is characterized by the presence of mafic volcanic that has dominated the other units and is known as greenstone belts. These belts are surrounded by variant granitoids. These rocks are metamorphosed to greenschist to amphibolites facies and are hosts for mineralization of gold, copper, silver and iron etc. The main thrust in respect of mineralization is on the iron ore that is associated with the belt. It is mainly of “Algoma” type having alternate bands of magnetite and chert. The mineralization is in the Banded Iron formation of the Ilkal formation (Greenstone Group) and is very proximal to Ramagiri village. The thesis deals with all the details like distribution, possible origin and economic viability of the iron ore.
Keywords *Hypothesis for origin of early Proterozoic iron – formation; Mineralization of iron ore; Ramagiri Greenstone belt*

1. Introduction

Presence of Iron ore in the Greenstone belts is not uncommon, but the quality and intensity may not that much when compared with the association of Iron from the sedimentary rocks.

Iron also occurs in the Precambrian period, i.e., Archaean - Proterozoic. The Iron Formations of this period are divided into two types’ viz., Algoma and Superior types (Gross, 1965).

The Algoma Type is named after the place Algoma of Ontario. The associated rocks are of volcano - sedimentary sequence. This type of Iron formation is associated with gray or red jasper cherts, interbedded with magnetite and hematite rich layers. Further, siderite and pyrite are also common. The association with the volcanic rocks possibly indicates the volcanic nature of the iron formation. The iron formation runs into number of kilometers in length.

The Superior Type, named after the Lake Superior of the United States and Canada and also known to occur in Labrodar trough. The rocks are thinly bedded cherty rocks with granular and oolitic texture. Cherty magnetite and hematite and cherty iron silicates and carbonates rocks form into

different stratigraphic units. The associated rocks are quartzites, dolomites, black cherts, black ferruginous shale/slate and volcanic rocks. The beds are few hundred feet thick and extend for reasonably long distances.

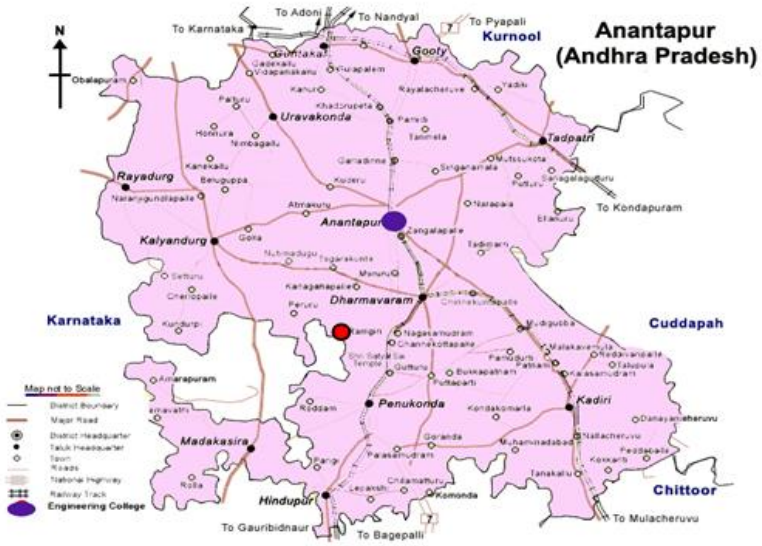

Figure 1: *The location map of Ramagiri (.) area*

1.1. Study Area

The village Ramagiri is located in the topographical map of 57/F11, of Survey of India. It is at the intersection of 14^0 26' 30" North latitude and 78^0 38' 20" East longitude. The villages of the Ramagiri Mandal area are located in both the topographical maps of 57 F/ 7 & 11(1:50,000), of Survey of India.

Ramagiri is accessible from Anantapur, the district headquarters. Anantapur can be reached either by South - Central Railway from Hyderabad, the state capital of Andhra Pradesh. The town Dharamavaram and Penukonda are the nearest locations and these can be approached by South - Central Railway. The said places can also be approached from Hyderabad by road. The Andhra Pradesh Road Transport Corporation runs number of buses from Anantapur, Dharamavaram and Penukonda to all the rural areas.

Ramagiri is the central place of the investigation and the adjacent villages are all well connected by all-weather roads from all the places.

2. Methodology

2.1. Iron Ores of Anantapur District

Iron ore occurs basically at two places, viz., one in the Oblapuram area of Rayadurg taluka and the other at Ramagiri of Ramagiri taluka. In both the cases the ore is with the greenstone belts. The ore at Oblapuram is with the Bellary greenstone belt i.e., the eastern arm of the Sandur-Bellary greenstone belt. The southern part of it extends into the Anantapur district. The Ramagiri iron ore is with the Ramagiri greenstone belt. This extends towards north into the Karnataka State. Both the greenstone belts run almost parallel to each other.

Similarities and Dissimilarities of Iron Oreat Obulapuram and Ramagiri

This can be studied under the following heads:

1. Geological setting
2. Nature of the ore
3. Chemistry/Grade of the ore

1. Geological Setting

The iron ore at Oblapuram is associated with the greenstone belt having amphibolites, meta-basalts with bands of phyllite and BIF. The BIF was earlier recognized as ferruginous quartzite. Chert is insignificant. The set up appears to be mainly sedimentary where the iron ore is seen. But higher up in the stratigraphy the above stated metamorphic are observed. This set up is intruded by younger granitoids.

The iron ore at Ramagiri is associated with the greenstone belt having amphibolites, meta-basalts with bands of phyllite and BIF. The BIF was earlier recognized as ferruginous quartzite. This set up is intruded by younger granitoids.

2. Nature of the Ore

The iron ore at Oblapuram though associated with the greenstone belt can be considered as 'Superior' type as it exhibits more sedimentary association. As stated earlier, the metamorphics of the greenstone are noticed at lower level in the stratigraphy. Evans (1993) describes similar set up and qualifies the ore as 'Superior' type. But the ore at Ramagiri is considered as 'Algoma' type as it is associated with the greenstone belts. The ore at Oblapuram is hematite and at Ramagiri it is magnetite. Chert percentage is more at Ramagiri compared to Oblapuram. The thickness at Oblapuram is much more than at Ramagiri. Extensive mining is being done at Oblapuram whereas no mining activity is seen at Ramagiri.

3. Chemistry/Grade of the Ore

The ore at Obulapuram has indicated the grade as 56.63% to 63.88% as Fe%. The ore at Ramagiri has 37.10% to 64.96% as Fe% in the western band and 23.24% to 34.72% as Fe% in the eastern band. As the ore at Ramagiri is mainly magnetite, pellitisation may be helpful in using the ore in different industries.

2.2. Ironstone and Iron Formation

Ironstone

Iron ore occurs in the form of Ironstones in the Phenerozoic Era. These ironstones are classified as Minette Type, named after the Minette beds of Jurassic age in the eastern France and the Clinton Type, called after the Clinton iron ores of Silurian age in the area south of Alabama, in the region of New York.

The Minette types of ironstones are main constituted by the chamosite and siderite. These are oolitic ores but oxides are less important.

The Clinton Type is deep red to purple, massive hematite - chamosite-siderite with oolitic textures. These ores contain 50% of iron. They also contain fairly high content of clastics including quartz.

Iron Formation

Iron formation has alternating layers of chert and iron. Hence it called Banded Iron Formation (BIF). It occurs in four different facies (Evans, 1992).

i. **Oxide Facies-** This is the most important facies and it can be divided into hematite and magnetite sub-facies. Carbonates may be present. Chert varies in percentage in sub-facies. The magnetite sub-facies show more of alternate banding of magnetite and chert.

ii. **Carbonate Facies-** This is interbanded with chert and siderite in equal proportions. If magnetite is also present in the bands it grades into oxide facies. If pyrite is present it may grade in to the sulphide facies.

iii. **Silicate Facies -**If the bands of magnetite-siderite chert are associated with iron silicate, it forms silicate facies. It is difficult to study this facies because of the complexity of the iron silicates. This has very low economic interest.

iv. **Sulphide Facies-** This will have pyritic carbonaceous argillites. It is thinly banded. The carbon content will be 7-8% and the pyrite will be 37%. This will be normally mined for its sulphur content.

The differences between Ironstone and Iron Formation (James, 1966) are documented as Table number 2 for better understanding.

Figure 2: *Algoma Type - Ramgiri Area (Anantapur District); the dark colored bands are magnetite and the light colored bands are that of chert*

The examples of Iron Formation from Andhra Pradesh are that the iron formation of the Ramagiri area is of Algoma type (Figure 2) and the one from Pendlimarri Mandal of the Kadapa district is of the Superior Type (Figure 3).

Figure 3: *Lake Superior Type – Gangannapalli -Pendlimarri Area (Kadapa District); the dark reddish colored material is iron, light brown is the dolomite and the rest is chert*

Figure 4: *The iron formation or BIF (western band) running and crowning the schistose hills of the Ramagiri West Reserved Forest*

2.3. The Ramagiri Iron Ore

Nature of Occurrence

Iron formation occurs in two independent blocks in the Ramagiri area. One is in the western limit of the greenstone belt in the Reserved Forest and the other in the eastern limit of the greenstone belt.

Ramagiri West Reserved Forest

The iron formation or BIF occurs as a thick band running for nearly 8km and crowning the schistose hills of the Ramagiri West Reserved Forest (Figure 4). It has alternating magnetite and chert bands (Figure 2).

Figure 5: *Reflection of the depth persistence and steep dip*

Figure 6: *Easterly dipping Iron ore along with chert*

Structure

The strike of the Banded Iron Formation is NW - SSE that is in conformity with the schistosity of the associated schists. It dips westerly and occasionally easterly at a steep angle of 80^0 to 85^0. The formation being a steep dipping, the width can be considered as thickness. In the present situation the thickness can be considered as 9 meters on average. The depth persistence of the Banded Iron Formation appears to be considerable. In one of the exposed section, it was found that the ore body was extending beyond 10 meters (Figure 5). It is assumed that it will extend beyond 20 meters depth.

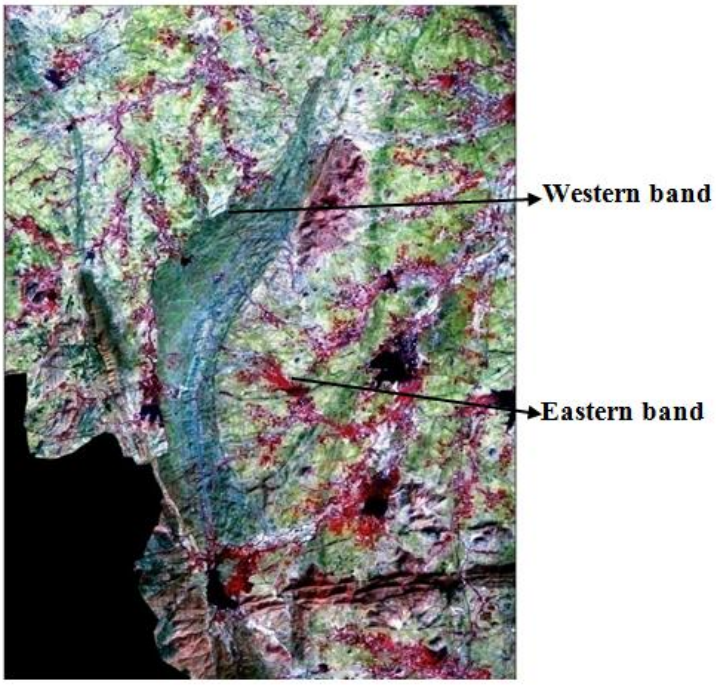

Figure 7: *Cherlopalle dome with the wextern and eastern iron bands*

Figure 8: *Minor warp in the iron formation in the eastern band*

The BIF dips easterly with 250 to 450. Sometimes the dip grades between 450 to 600 (Figure 6).

The iron formation extends north wards beyond the reserve forest area, occurring on top of a small mound. It runs for a distance of 2.75 km along the strike. The terrain from the reserve forest boundary up to a distance of 1 km is covered. A trench has been excavated in the covered and the continuity of the BIF is found.

In fact, the continuity of the iron formation can be established even without digging a trench, as the iron formation is steeply dipping, it will definitely continue in the strike direction unless affected by faulting.

On the Eastern Side

In the area around Cherlopaplle (57F/11), the iron ore occurs like a neck-lace around a gneissic elongated dome called Cherlopalle Dome (Figure 7). This makes the iron formation devisable into two, the western band and eastern band (Figure 7). Both the bands are similar in nature. The eastern band is more quartrzitic. It has two bands within it.

The western one runs for nearly 12 km and the eastern one extends for about 6.5 km. The iron ore formation reflects minor warps (Figure8), as observed in the eastern band.

Table 1 indicates that the western band has more Fe% than the eastern band. The scrutiny of literature suggests that there are number of hypothesis for the origin of Proterozoic iron formation. These are presented in the following Table 2.

Table 1: *Analysis of the iron ore*

Western band			Eastern band		
S. No	Iron as Fe_2O_3 %	Iron as Fe %	S. No	Iron as Fe_2O_3 %	Iron as Fe %
1	52.80	36.96	1	40.70	28.49
2	82.60	57.82	2	33.20	23.24
3	55.80	39.06	3	49.60	34.72
4	92.80	64.96	4	48.80	34.16
5	55.20	38.64	5	47.00	32.90
6	66.60	46.62	6	35.60	24.92
7	57.80	40.46	7	42.40	29.68
8	53.00	37.10	8	40.00	28.00

The exhalative origin of numerous Archaean iron – formations have been convincingly established, (Gross, 1980). But numbers of other theories have gained momentum. Hydrothermal model is supposed to be the modern one.

2.4. Origin of the Ramagiri Iron Ore

The origin of the Precambrian iron ore is highly debatable. The knowledge of the origin of the iron ore helps in planning mining and will also yield considerable useful information on the grade of the deposit.

The Ramagiri Iron ore is associated with the green schist grade of metamorphic rocks. The parentage for these schistose rocks is the basic volcanics. Hence, there is an opnion in respect of origin, is that, it (iron) is volcanic in origin. The differenciation of basic magma rich in magnesium starts with komatitic basalt and gradullay goes to iron rich tholeiites. If this is considered as a clue, then volcanic origin can be acceptable. In fact, there are volcanic cherts also. Hence, both the iron and chert of Ramagiri can be volcanic. However, these iron formations are banded giving a sedimentary look to the rock.

The Banded Iron Formation, (BIF), as it is popularly called, is an indicative of one cycle of magma eruption. In certain schist belts number of Banded Iron Formation are observed. This type of set up reflects that there are number of volcanic cycles in the schist belt. This can also be verified by calculating the Mg. No (beyond the scope of the present work) of the volcanics lying immediately above any BIF. If the Mg. No, crosses 60, it indicates that the magma is primary and a new volcanic cycle has started. This concept is valid and proved. However, in the present situation, there are two

locations of the bands of BIF. The extensive extension of the iron - formation of Ramagiri, indicates that it is possibly related to the volcanic activity.

Table 2: *Hypothesis for origin of early Proterozoic iron – formation*

Model	Suggested cause of IFM deposition	Reference
Lacustrine	Deposition in deep stratified or ephemeral Saline lakes	*Cowell, 1966 & Eugster & *Chou, 1973
Continental	Iron released during normal weathering	*Garells & others, 1973
Weathering	Under anoxic atmosphere precipitated in restricted marine basins	*Schidlowski, 1976
Evaporative	Iron and silica precipitated from sea water As a result of evaporative concentration	Trendall, 1973 *Button, 1976
Biological	Iron and silica precipitated from sea water As a by – product of metabolic activity	*Cloud, 1973 *LaBerg, 1973
Upwelling	Iron and silica precipitated from marine Bottom waters as a result upwelling	*Holland, 1073 *Drever, 1974
Hydrothermal	Sea water enriched in iron and silica by Sea floor hot spring to point of precipitation	*Gross, 1980 *Simonson, 1982a

IFM = Iron Formation
*Referenced by Cross references.

Use of the Mineral

The analysis when compared with the standards (Table 1), the ores of Ramagir, Nossannakota has the Fe range “between” 30% - 60% have higher percentage of silica. The fines can be used in the Sintering industry where the Fe required is 56% - minimum. Beneficiation sand pelletisation may increase the chance of its utility. Higher percentage of SiO2, i.e., up to 6% is used in the Durgapur Steel Plant.

3. Conclusion

Iron is associated with the greenstone belts. In Anantapur district iron is (part of Bellary greenstone belt) in Obulapuram - Rayadurg taluk and with the Ramagiri belt in the Ramagiri area. In the Ramagiri area, the ore occurs in two different styles. On the western side nearer to Ramagiri it is mainly “Algoma” type. The iron ore is magnetite occurring as bands alternating with chert bands reflecting sedimentary nature. In the opinion of the author, both the iron and chert are of igneous origins that have formed at the end of differentiation of the basic magma. This set up can be called as Iron Formation. On the eastern side of the belt iron occurs in the form of a necklace around Cherlopalle dome. Each arm of the necklace has two bands. These bands are like ironstones rather than iron formation. The differences between the iron formation and ironstone are documented clearly. The different concepts expressed on the origin of iron are also presented for reference. The chemistry and the use of the mineral are also given to understand its suitability in different industries.

References

Button, A. 1976. Transvaal and Hamersley basins: review of basin development and mineral deposits. *Minerals Science and Engineering*, 8, pp.262-293.

Cloud, P. 1973. Paleoecological significance of the banded iron – formation. *Economic Geology*, 68, pp.1135-1143.

Evans, A.M. 1992. Ore Geology and Industrial Minerals: An Introduction. Hoboken, New Jersey: Wiley-Blackwell Science, p.400.

Gross, C. A. 1965. The geology of iron deposits in Canada: 1. General geology and evolution of iron deposits. *Geol. Survey. Can., Econ. Geol. Rep*., 22, p.181.

Schidlowski. 1976. Isotropic fraction between organic carbon and carbonate carbon in Precambrian banded iron stone series from Brazil. *Neues Jahrbuch fuer Mineralogie, Monatshefte*, 8(20), pp.344-353.

Cloud Publications
International Journal of Advanced Earth Science and Engineering
2017, Volume 6, Issue 1, pp. 596-621
ISSN: 2320–3609, Crossref: 10.23953/cloud.ijaese.330

Research Article

Early Mesozoic Detrital and Evaporitic Syn-Rift Series of Mohammedia-Benslimane-ElGara-Berrechid Basin (Meseta, Morocco): Sedimentary and Palaeoenvironmental Evolution and Comparison with Neighboring Basins

Abdelkrim Afenzar, Rachid Essamoud

Dynamics of Sedimentary Basins and Geological Correlations Laboratory, Faculty of Sciences, Ben M'Sik, Hassan II University of Casablanca, B.P. 7955, Sidi Othmane, Casablanca, Morocco

Publication Date: 20 December 2017

DOI: https://doi.org/10.23953/cloud.ijaese.330

Abstract The Triassic basin of Mohammedia-Benslimane-ElGara-Berrechid contains a sedimentary series consisting of a sandy-conglomeratic formation (Formation A) at the base, surmounted by an argillaceous-saliferous formation (Formation B), the whole being capped by Late Triassic-Early Jurassic basalts. Formation (A) is formed by conglomeratic facies with alternations of sandstone in the middle and top of the formation. Formation (B) is subdivided into two members: (1) mudstone-siltstone member formed by alternations of mudstone and siltstone facies; and an argillaceous-saliferous member (2) composed by mudstone and evaporite facies. Sedimentary analysis carried out on more than ten outcrops and on four cores sample that have identified fifteen types of facies and seven architectural element and facies associations. It leads to the reconstruction of depositional environments during the Upper Triassic in the basin. Also, this work allowed a comparison of the sedimentary series of this basin with those of the other basins of the Moroccan Atlantic margin on one side and the North-east American margin on the other side.
Keywords *Architectural element; Comparison; Depositional environment; Evaporites; Facies; Triassic*

1. Introduction

The Mohammedia-Benslimane-ElGara-Berrechid (MBEB) basin is considered among the most important Triassic basins in Morocco and even in the world. This importance is reflected in its role in understanding the geodynamic and paleogeographic history of the Central Atlantic domain during the Triassic time.

Most of these Triassic basins belonging to the Central Atlantic domain show a similar sedimentological evolution. They are dominated by continental deposits (Withjack et al., 1998; Leleu and Hartley, 2010; Withjack et al., 2012; Leleu et al., 2016). The sedimentary filling of these basins is strongly diachronous, and the timing and duration of the deposition phase vary from one basin to another (Leleu et al., 2016).

In the studied basin, the sedimentary series show that, at the beginning of its opening, it was subject to coarse detrital deposits, and then it became more and more fine. At the end of the Upper Triassic, the detrital sedimentation was replaced by evaporitic sedimentation (Salvan, 1982, 1984; Peretsman-Clement and Holser, 1988; Lyazidi, 2004) interrupted by basaltic effusions at the Triassic-Jurassic boundary (Peretsman-Clement, 1985).

The description, classification and interpretation of deposits are based on several criteria: hierarchies of strata and their boundary surfaces, lithofacies, geometry of sedimentary bodies and architectural elements (Miall, 1985; Bridge, 1993; Miall, 2006). The main objective of this study is to reconstruct the paleoenvironment and the syn-rift sedimentological filling history of the basin. Then to deduce many points of similarity and difference between this basin and the other Triassic basins belonging to the Central Atlantic domain.

2. Regional Context

The MBEB basin, concerned by this study, is part of the Mesetian domain and precisely the north-western Meseta. It is located about twenty kilometers north-east of Casablanca and about thirty kilometers south of Benslimane. The structural studies present this basin as a vast shallow depression which seems to have originated from N-S to NE-SW half-graben structure (Fadli, 1990; El Wartiti et al., 1992; Medina, 1994; Lyazidi, 2004).

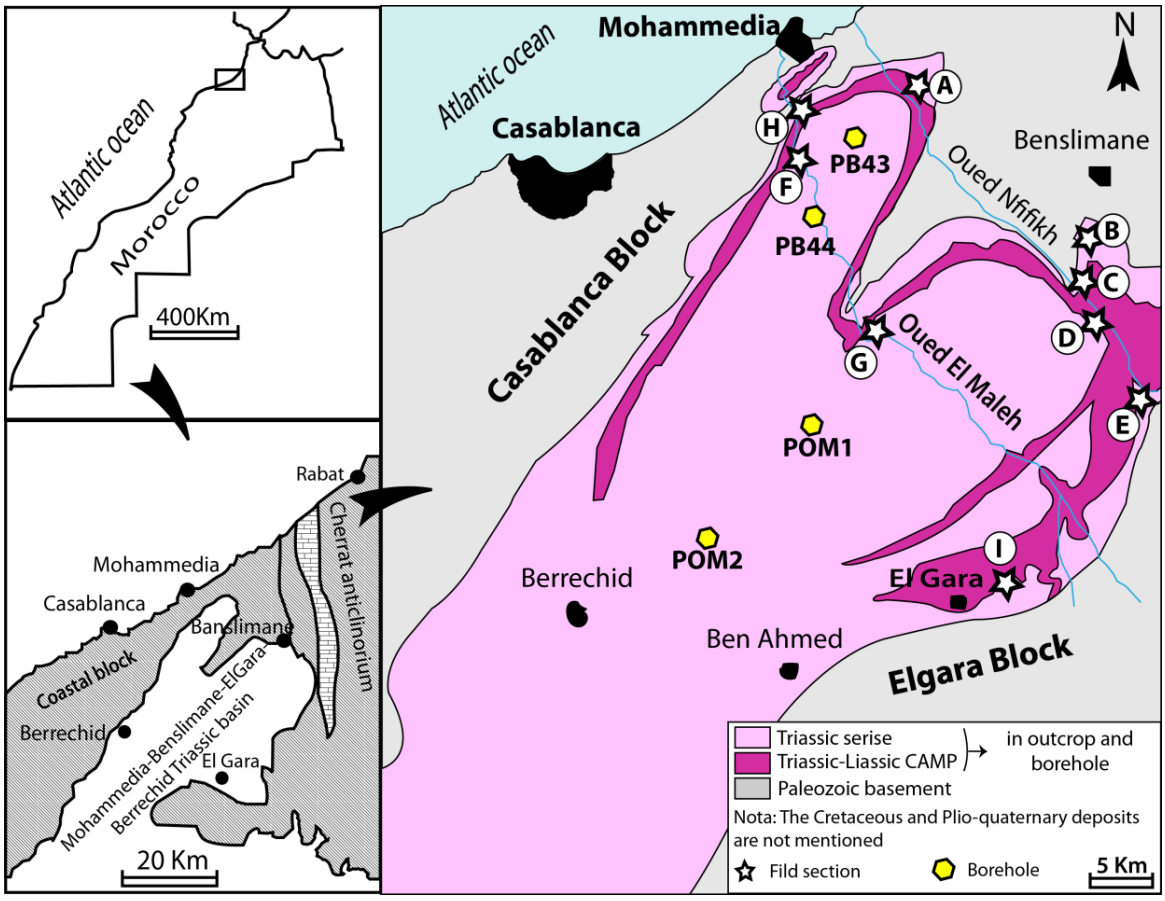

Figure 1: *General context of the studied basin (Lyazidi, 2004, modified), and location of the studied sections and boreholes*

This area is characterized by a Palaeozoic basement deformed during Hercynian orogeny. At the end of the Paleozoic and the early Mesozoic, a half-graben is developed and filled by an important

detrital and evaporitic syn-rift sedimentary series (at the Triassic-Liassic time); with a magmatic activity belonging to CAMP (Central Atlantic Magmatic Province). It is presented by basaltic flows produced by 1 to 5 eruptions, with flow composed of 5 units (Bensalah et al., 2011). This magmatic activity was triggered at the Triassic-Liassic boundary (Manspeizer et al., 1978, 1988a, 1988b; Peretsman-Clement, 1985) (Plate 1).

From a structural point of view, at the Carnian/Norian, this basin was subjected to a NW-SE extension with a slight deformation component (El Wartiti et al., 1992; Medina, 1994). According to these authors, this structure is controlled by a deep detachment, which is probably an ancient Hercynian weakness zone, and which plunges slightly towards the NNW (Medina et al., 1996). This is related to the opening of the proto-Atlantic domain flooded by the Tethys which probably crossed the fracture zone of Gibraltar (E-W or NE-SW: Ricou, 1994).

3. Methodology

This sedimentological study consists in a detailed analysis of the field sections and drill cores for a better view of the sedimentary bodies and their spatial arrangements. This allows to characterize the different facies and their associations as well as the architectural elements (Allen, 1983; Miall, 1985 and 2006) which allow us to reconstruct the depositional environments and their evolutions over time. In this step, we used the lithological and textural criteria, grain sizes and sedimentary structures observed at the outcrop. The nomenclature of facies in this study is compared with that established by Miall (1978, 2006).

The vertical and horizontal arrangement of these facies gives birth to the architectural elements characterized according to several criteria determined by Allen (1983) and Miall (1985, 2006), which are: the nature of the upper and lower bounding surfaces, the external geometry, the scale, and the internal structures. The last step is the determination of paleoenvironment which is based on the nature and types of lithofacies already characterized and also on types of architectural elements formed by these lithofacies.

4. Sedimentary Analysis Results

4.1. Lithofacies

4.1.1. Conglomeratic Lithofacies

4.1.1.1. *Description*

These conglomerates (Plate 3 and Table 1) are deposited in the basal part of the series (formation A). The conglomerate displays red to purple color, with matrix-supported fabric formed by sandstone and siltstone. The pebble-gravels are centimeter to decimeter-sized, showing angular to sub angular shapes. Sometimes horizontal stratification may be absent (debris flow), other times this stratification may be apparent and characterized by horizontal bedding imbrication or planar cross beds. The thicknesses of these conglomerates and micro conglomerates vary in places between 50cm and 6m.

Table 1: *Description and interpretation of the sedimentary facies identified in the basin and their correspondence with those of Miall (1978, 1985 & 2006)*

Lithofacies	Characteristics	Interpretation
Conglomeratic facies		
Fc1: Gms	Massive disorganized conglomerates, matrix-supported gravel, without sedimentary structures	Mass flows, debris flows deposits
Fc2a: Gm	Clast-supported stratified conglomerates,	Longitudinal bar

	horizontal bedding imbrication	
Fc2b: Gm	Organized conglomerate, Poor matrix	Sieve deposits, lag deposit
Fc3: Gp	Clast-supported planar cross-stratified conglomerate	Linguoid bar, transverse bar
Sandstone facies		
Fc4: Sm	Massive sandstone, fine to coarse-grain size	Rapid deposition, sediment gravity flow
Fc5: Sp	Planar cross-stratified sandstone, very fine to coarse	Linguoid, transverse bars, lower flow regime
Fc6: Sh	Horizontally stratified sandstone	Planar bed flow, upper flow regime
Fc7: Sl	Fine sandstone, low angle (<10°) crossbeds	Crevasse splays deposits
Siltstone and Mudstone facies		
Fc8: Fl	Laminated to massive siltstone	Overbank deposit
Fc9: Fm	Massive to laminated mudstone	Overbank or abandoned channel deposits

4.1.1.2. *Interpretation*

4.1.1.2.1. *Lithofaciès Fc1*

It is a massive conglomerate (2 to 8m thick) with angular, disorganized and poorly sorted gravels. The matrix is mainly formed by very fine sandstone. The absence of sedimentary structures and the existence of a mixture of fine and coarse materials suggest that this conglomerate is deposited by gravity flows: debris flow, (Miall, 1978, 2006; Poli, 1997; Opluštil et al., 2005). According to Sohn (2000), these debris flows have been interpreted by two models: the viscoplastic flow model (Johnson, 1984) and the grain interstitial flow model (Takahashi, 1978, 1981, 1991). These characteristics reveal a similarity between this facies (Fc1) and facies Gms of Miall (1978, 1985 and 2006) which have been deposited at proximal alluvial fans (Plate 2).

4.1.1.2.2. *Lithofaciès Fc2a*

These conglomeratic facies are distinguished by the presence of the subangular to sub-rounded pebbles and gravels. They are commonly interbedded and sometimes imbricated. The matrix (formed by sandstone and silt) is very sparse. These facies correspond to facies Gm of Miall (1978, 2006); it is deposited at longitudinal bars in the braided rivers system (Plate 2).

4.1.1.2.3. *Lithofaciès Fc2b*

The facies Fc2b resemble the facies Fc2a, the only difference between these two is that the Fc2b shows an abundance of the gravel and very poor matrix. These facies is probably deposited by sheet flood. These facies characteristics are similar to those determined by Miall (1978, 1985 and 2006) for the facies Gm which can correspond to sieve and/or lag deposits.

4.1.1.2.4. *Lithofaciès Fc3*

It is some conglomerate facies (1 to 2,5 m thick) with planar crossbeds structure. The matrix is formed mainly by clastic materials (clast-supported) which are very fine sandstones. Based on the planar crossbeds structure, we can say that the Fc3 corresponds to the Gp facies of Miall (1978, 2006). According to Boothroyd and Ashley (1975); Miall (1977, 1978 and 2006) and Eji Uba (2005) these facies was deposited in longitudinal bar in a braided rivers system with shallow channels (Plate 2).

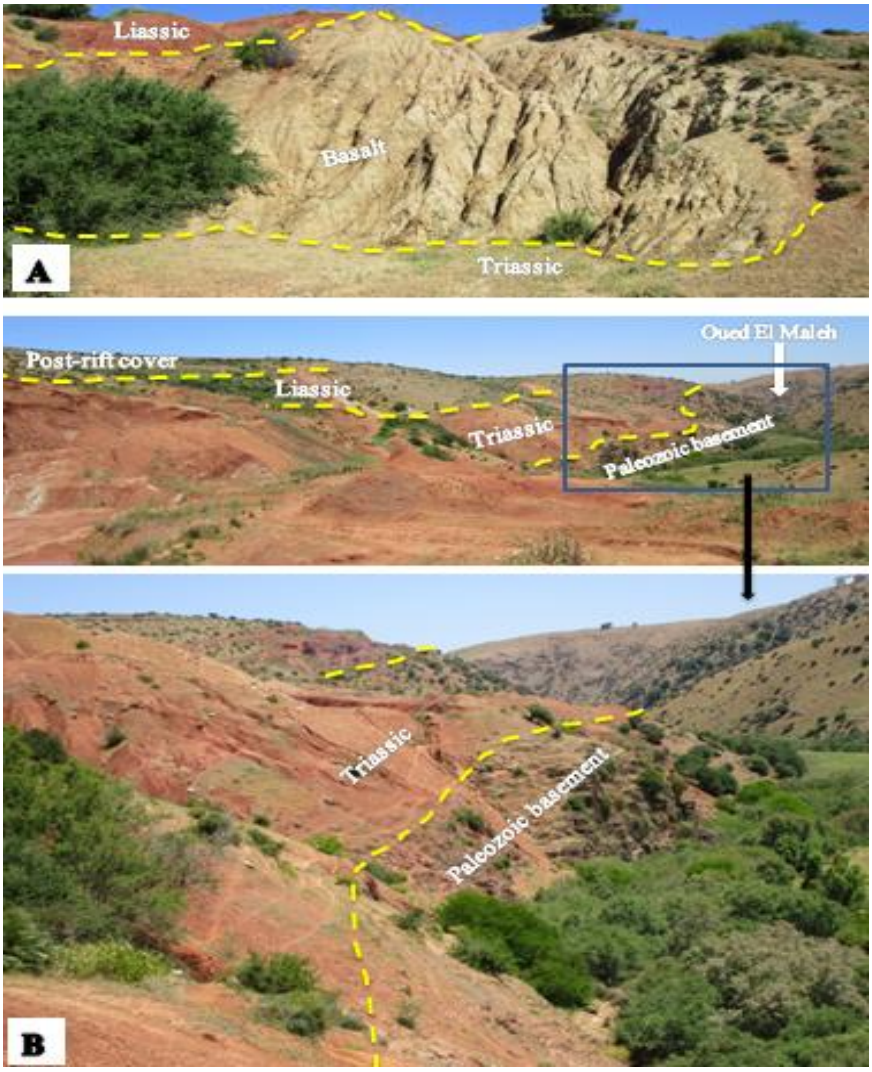

Plate 1: *Overview showing the lower and upper limits of the Triassic in the basin; (A): Basalts constituting the Triassic-Liassic boundary; (B): Contacts between the Triassic and the Hercynian basement*

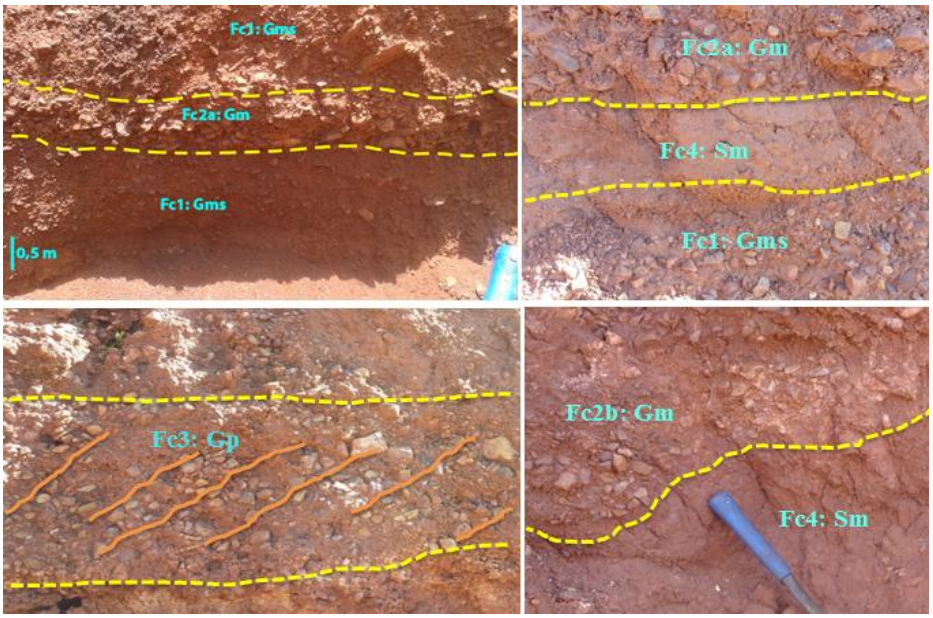

Plate 2: *Different conglomerate lithofacies identified in the basin*

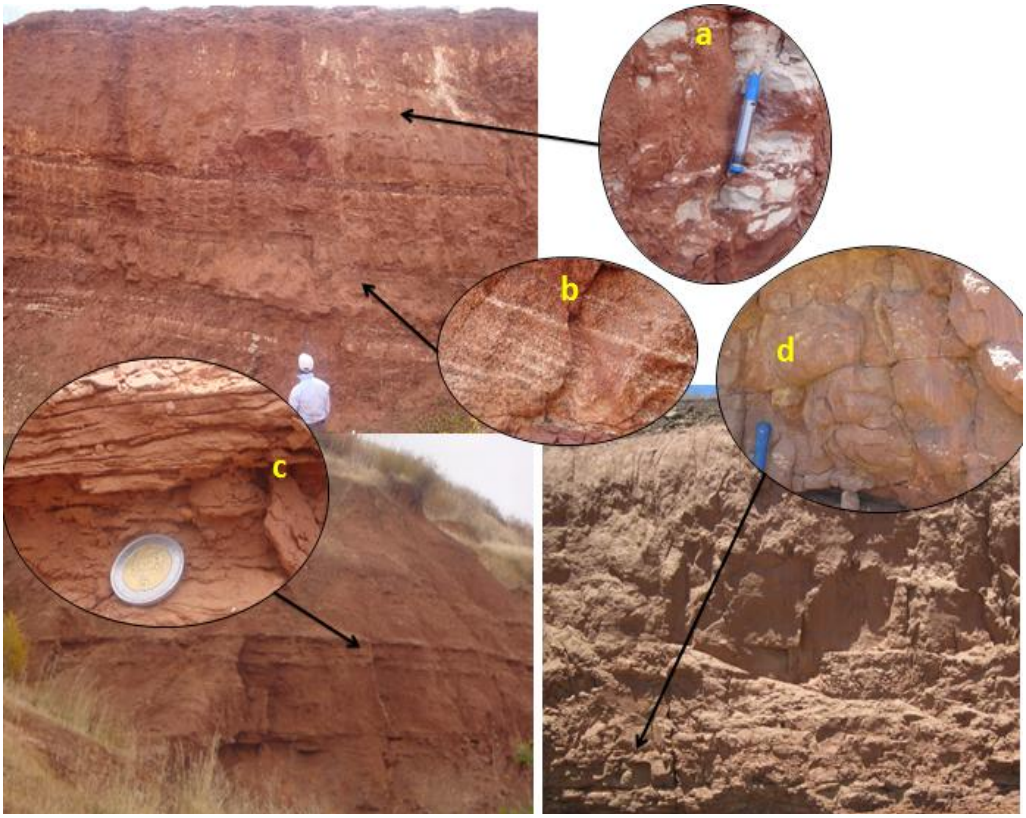

Plate 3: *Different sandstone lithofacies studied in the basin; a: massive sandstone (Fc4: Sm); b: planar crossbeds sandstone (Fc5: Sp); c: sandstone with horizontal lamination (Fc6: Sh); d: sandstone with low angle (< 10 °) crossbeds (Fc7: Sl)*

4.1.2. Sandstone Lithofacies

4.1.2.1. *Description*

The reddish to purplish sandstones are deposited at the base of the series alternating with conglomerates and especially micro conglomerates. At the end of the formation (A) and at the base of the formation (B), these sandstones alternate with the siltstone and mudstone (Member 1). These sandstones are sometimes characterized by centimeter to decimeter thicknesses with planar horizontally-bedding and/or planar crossbeds. In other cases, they are characterized by massive thicknesses (up to 8m). Regarding the grain-size, these sandstones are coarse at the base of the series and becoming fines at the middle (Plate 3 and Table 1).

4.1.2.2. *Interpretation*

4.1.2.2.1. *Lithofacies Fc4*

The Fc4 is massive coarse sandstone with two to three meter thick (picture a, Plate 3). The presence of isolated large fragments is probably related to their falling along the slope (Sohn et al., 1997), associated with the deposition mechanism itself or movement in a high load flow (Postma and Cruickshank, 1988). The characteristics of this facies show that corresponds to facies Sm. According to Miall (1985, 1996); Einsele (2000); Eji Uba et al., (2005) these facies corresponds to rapid deposits or gravity flow deposits.

4.1.2.2.2. *Lithofacies Fc5*

It is a medium to coarse sandstone, showing the planar crossbeds (picture b, Plate 3). These facies may be interpreted as a linguoid or transverse bars deposits (lower flow regime) (Miall 1977, 1978; Todd, 1996; Bridge, 2003; Miall, 2006). Fc5 corresponds to facies Sp of Miall (1977, 1978 and 2006).

4.1.2.2.3. *Lithofacies Fc6*

This sandstone facies (picture c, Plate 3) are characterized by horizontal laminations with parting or streaming lineation. This structure is generated by small longitudinal vortices affecting the entire turbulent boundary layer, and provides an excellent paleocurrent indicator. These facies show similarities with Sh facies of Miall (1978, 1985 and 2006). It can be interpreted as being upper flow regime deposits.

4.1.2.2.4. *Lithofacies Fc7*

This lithofacies (picture d, Plate 3) is characterized by low angle (<10°) planar cross beds. By this we can say that this facies (Fc7) corresponds to facies Sl of Miall (1978, 1985 and 2006). It is interpreted as a crevasse channel and/or crevasse splay deposit often formed in the floodplain at anastomosed fluvial system.

4.1.3. Siltstone and Mudstone Lithofacies

4.1.3.1. *Description*

The reddish siltstones and mudstones are predominating all other lithofacies of the Triassic series in the basin. They can be laminated or massive, up to 20 m thick. These facies are alternated with sandstones. In the all studied outcrops and boreholes these lithofacies show millimetric to centimetric levels of mottling.

4.1.3.2. *Interpretation*

4.1.3.2.1. *Lithofacies Fc8*

These facies (picture a, Plate 4) is represented by horizontally laminated siltstone. In other cases, these siltstones are massive with a 1 to 5 m in thickness. They have a reddish appearance with grey to greenish levels of mottling due to the transformation of iron in the sediment. These facies resemble to the Fl facies of Miall (1977, 1978 and 2006), which corresponds to vertical accretion deposit showing a laminar flow of very low energy. We can interpret this facies as a flood plain or overbank deposit according to the same author.

4.1.3.2.2. *Lithofacies Fc9*

It is a massive reddish mudstone showing mottling spots. It has been identified in all outcrops studied in the basin with a variation in thickness from one region to another (from 0.5 to 10 m). These facies correspond to facies Fm (picture a, Plate 4) interpreted as overbank deposit formed in flood plain or abandoned channels (Miall, 1985, 1996; Einsele, 2000; Eji Uba et al., 2005). According to Mader (1985), these mudstones can be deposited in (1) the alluvial plain of a braided system, (2) the floodplain and playas, and sometimes in (3) distal alluvial fans. According to Miall (2006), these mudstones are interpreted as lacustrine or overbank deposit.

4.1.4. Evaporitic Lithofacies

Table 2: *Description and interpretation of evaporite lithofacies identified in the Basin*

Lithofacies	Characteristics	Interpretation
	Evaporite facies	
Fc10	Gypsum bed	Mudflats/Lagoon deposits
Fc11	Fibrous gypsum	Diagenetic origin
Fc12	Milky Halite	Lagoon, playa and mudflats deposits
Fc13	Phenoblastic halite	Mudflats or diagenetic deposits
Fc14	Fibrous halite	Diagenetic origin

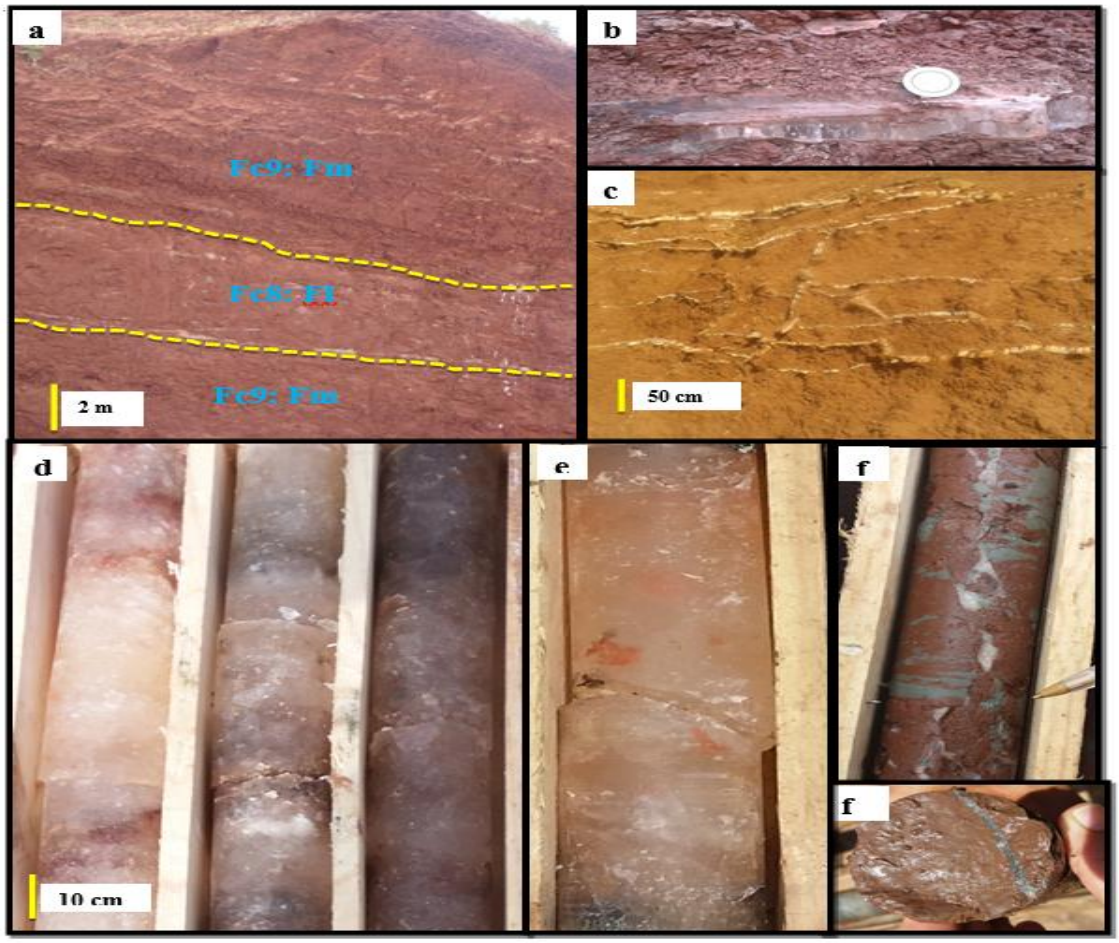

Plate 4: *Siltstone, mudstone and evaporite lithofacies, a: interbedding of Siltstone and mudstone; b: gypsum bed; c: fibrous gypsum, d: milky halite; e: phenoblastic halite; f and f ': fibrous halite*

4.1.4.1. *Description*

The evaporites observed in outcrop (pictures b, c, d, e and f in Plate 4) are in the form of centimeter banks of fibrous gypsum and Gypsum beds in the middle and top of the Triassic series. They also occur as sub-vertical fibrous veins and often alternate with reddish mudstone. In the boreholes, these evaporites are represented by large facies of salt whose total thickness can reach 200 m. These are sometimes pure halite facies and in other cases show a mixture with mudstone.

4.1.4.2. *Interpretation*

4.1.4.2.1. *Lithofacies Fc10*

It is a whitish (milky) gypsum facies with 10 to 20 cm thick. This gypsum facies is presented in the form of centimeter banks alternating with the siltstones (Fc8: Fl) and the mudstones (Fc9: Fm) facies. The Fc10 facies is formed in relatively arid environments by the precipitation of sulfated ions in supersaturated solutions (brine) subjected to intense evaporation (Warren, 1985, 2006 and 2010) (picture b Plate 4).

4.1.4.2.2. *Lithofacies Fc11*

This lithofacies appears as sub-vertical to inclined fibrous veins, filling pre-existing fractures in massive mudstone. The thickness of these veins does not exceed tens of centimeters. This fibrous gypsum is similar to that described by Gustavson et al. (1994) in the Amadens Basin in Australia, the Appalachian Basin, the Paradox Duroet Basin in the United States, the Cheshire Basin in England and the Elk Point Basin in Canada. According to Gustavson et al. (1994), this type of gypsum is the product of several concurrent processes that are duplicated in most basins containing halite and anhydrite. The formation of the fibrous gypsum veins requires the conjunction of several phenomena: (i) creation of extension fractures resulting from subsidence over areas of halite dissolution, (ii) hydration of anhydrite to gypsum by circulating groundwater and (iii) transport of excess calcium sulphate and precipitation of fibrous gypsum in fractures (picture c Plate 4; Table 2).

4.1.4.2.3. *Lithofacies Fc12*

It is a milky salt facies with fluid inclusions. It is a milky halite sometimes associated with variable portions of limpid halite. In all studied boreholes, we noticed two types of milky halite: (i) a dark halite controlled by the quantity and color of the clay inclusions (greyish, reddish or brownish tint), and (ii) another clean halite deposited as decimetric beds rarely associated with very fine anhydrite laminae. This type of halite, well known in many basins including ours, is considered to result from primary and rapid crystallization (Wardlaw and Schwerdtner, 1966; Shearman, 1970; Schreiber et al., 1976; Orti and Pueyo, 1977; Moretto, 1985; Et-Touhami, 1998; Schreiber and El Tabakh, 2000). The rhythmicity of this facies with the mudstone faces is probably due to the interventions of the slightly turbid continental waters which propagate on the surface of the brine (Sonnenfeld and Hodcc 1985, Et Touhami 1992, 1994 and 1998). The alternation of this halite with detrital and sulphate (gypsum) levels indicates that it is probably deposited in saline mudflats or in a shallow water (evaporite flat) (picture d Plate 4; Table 2).

4.1.4.2.4. *Lithofacies Fc13*

It is a phenoblastic halite with limpid crystals characterized by absence of fluid inclusions and by a slower growth than the previous one (facies Fc12) (Shearman, 1970; Smith, 1971; Moretto, 1985). The origin of this type of phenoblastic halite is diagenetic and/or primary. In the first case, Fc13 occurs either as filling of dissolution cavities or as continuous beds characterized by a large development of phenoblasts disturbing the primary organization of deposit (Et-Touhami, 1992, 1994 and 1998). These facies are related to the drying of water (Lowenstein and Hardie, 1985), but may also be the result of descending brine diffusion. This halite characterizes very shallow depositional environments that can be subjected to desiccation, such as saline mudflats (Lowenstein and Hardie, 1985, Et-Touhami, 1998). In the second case and after Chemin (1990), this type of halite is formed by evaporation of supersaturated brine within clayey sediment. Halite crystals are generally automorphic to subautomorphic of centimeter size or even in some cases forming aggregates of polycrystals of the xenomorphous limpid halite (Chemin, 1990) (picture e Plate 4; Table 2).

4.1.4.2.5. *Lithofacies Fc14*

It is millimeter to centimeter veins of the fibrous halite. These facies are formed in pre-existing fractures in the mudstones levels. It is presented as thin fibers elongated perpendicularly to the walls of mudstones. Probably, this type of halite is formed during diagenesis in the very fine sediments (mudstone) (Hovorka, 1983; Dumas, 1988; Moretto, 1985; Et Touhami, 1998) (picture f Plate 4).

4.2. Architectural Elements and Other Facies Associations

4.2.1. Architectural Elements

For the coding of these elements, we have used the abbreviation AE (Architectural Element). This analysis allowed us to characterize six architectural elements (AE1 ... AE6) and two facies associations.

4.2.1.1. *AE1*

This element forms the basis of the series with a thickness of 4 to 6 m. It is characterized in the northern and eastern borders of the basin. AE1 is formed mainly by facies association Fc1 (Gms) and Fc2a (Gm). This element is limited at the base by an unconformity with the hercynian basement, and at the top by the architectural element AE2. According to all the criteria, this element corresponds to the SG element (Sediment Gravity Flow) of Miall (1985, 2006), it is formed by gravity flow deposits, mainly pebbles and gravels poorly sorted, deposited in the proximal regions of alluvial fans.

4.2.1.2. *AE2*

The architectural element AE2 is formed by assembling the facies Fc2a, Fc2b (Gm), Fc4 (Sm), Fc5 (Sp), Fc6 (Sh) and Fc9 (Fm). This architectural element is characterized by basal bounding surfaces of fourth order and more (5th, 6th). These boundaries are sometimes erosive slightly planar and in other cases erosive and concave-up. Inside the architectural element, and between the lithofacies, small limits can be identified. From these characteristics, we deduce that the element AE2 resembles the architectural element CH (Channels) of Miall (1985, 2006). According to this author, the determination of this element differs according to the size and the type of channel, the minor channels can be more easily identifiable than the large ones because of outcrop constraints (Friend et al., 1979; Friend, 1983; Blakey et Gubitosa, 1984; Miall, 1985).

4.2.1.3. *AE3*

It is formed mainly by assemblages of coarse lithofacies containing imbricated pebbles and gravels, showing horizontal stratification, sometimes planar crossbeds: Fc2a, Fc2b (Gm) and Fc3 (Gp), sometimes minors lithofacies were identified between these major facies (facies Fc4 (Sm) and Fc6 (Sh)). Most facies of this element are organized as tabular bodies of five to six meters thick. Also it is formed from a 4% to 6% of fine to medium sandstones. AE3 corresponds to the architectural element GB (Gravel bars and bedforms) of Miall (1985, 2006). It is usually coarse deposits formed at gravels bars, these coarse deposits are sometimes intercalated with thin levels sandstones formed during lower flows (speed decrease) (Massari, 1983; Miall, 1985, 2006).

4.2.1.4. *AE4*

This architectural element is formed by medium to fines lithofacies assemblages: facies Fc5 (Sp), Fc6 (Sh) and Fc7 (Sl), the Fc6 and Fc7 facies are sometimes separated by very fines facies: Fc8

(Fl). Architectural element AE4 is characterized by internal boundaries of second to third order, while its outer boundaries are fourth order. For this, AE4 has many similarities with the architectural element SB (Sand Bedform) of Miall (1985, 2006). This architectural element characterizes in our case, crevasse channels and/or crevasse splays deposits.

4.2.1.5. *AE5*

This element is presented by sandstone sheets with horizontal laminations from 40 to 80 cm thick: facies Fc6 (Sh), intercalated with thin siltstones and mudstones laminae: facies Fc8 (Fl) and Fc9 (Fm). This architectural element resembles to architectural element LS (sand laminated sheets) of Miall (1985). Lithofacies forming this architectural element have been interpreted as the product of flash floods (Miall, 1977, 1984; Rust, 1978; Tunbridge, 1981, 1984; Sneh, 1983; Miall, 1985). The architectural characteristics of this element are well described by Tunbridge (1981) and Sneh (1983). The sand sheets (sandstone) are deposited on flat surfaces slightly eroded, with a lateral extension of hundreds of meters. The beds of this element probably represent the margins of the individual sheets flood (Miall, 1985, 2006).

4.2.1.6. *AE6*

The AE6 is formed by mudstone, siltstone and sandstone lithofacies associations: Fc8 (Fl), Fc9 (Fm) and Fc6 (Sh). This architectural element is considered as a major element in the basin, its thickness can reach forty meters. It is presented as large sheets (2 to 50 meters thick), formed by purplish or red brick siltstones and mottled mudstones, these siltstones and mudstones sometimes show a massive aspect with crude planar laminations indicating a quiet depositional setting. In other cases, they show horizontal laminations with very thin intercalations (5-15 cm) of fine sandstones.

By these characteristics we can say that AE6 corresponds to the architectural element OF (Overbank fines) of Miall (1985, 2006). According to this author, in most cases this element has a sheet geometrical form, reflecting its origin by vertical aggradation. In the vicinity of the active channels, these sheets are separated by crevasses splays. This architectural element may fill abandoned channels, provided it has concave-up basal contact and ribbon to lensoid geometry of the channel itself (Ethridge et al., 1981; Miall, 1985).

4.2.2. Other Facies Associations

In addition to these six architectural elements that correspond to those of Miall (1985, 1996 and 2006) and recognized in our basin, two other facies associations not described by Miall have been characterized here:

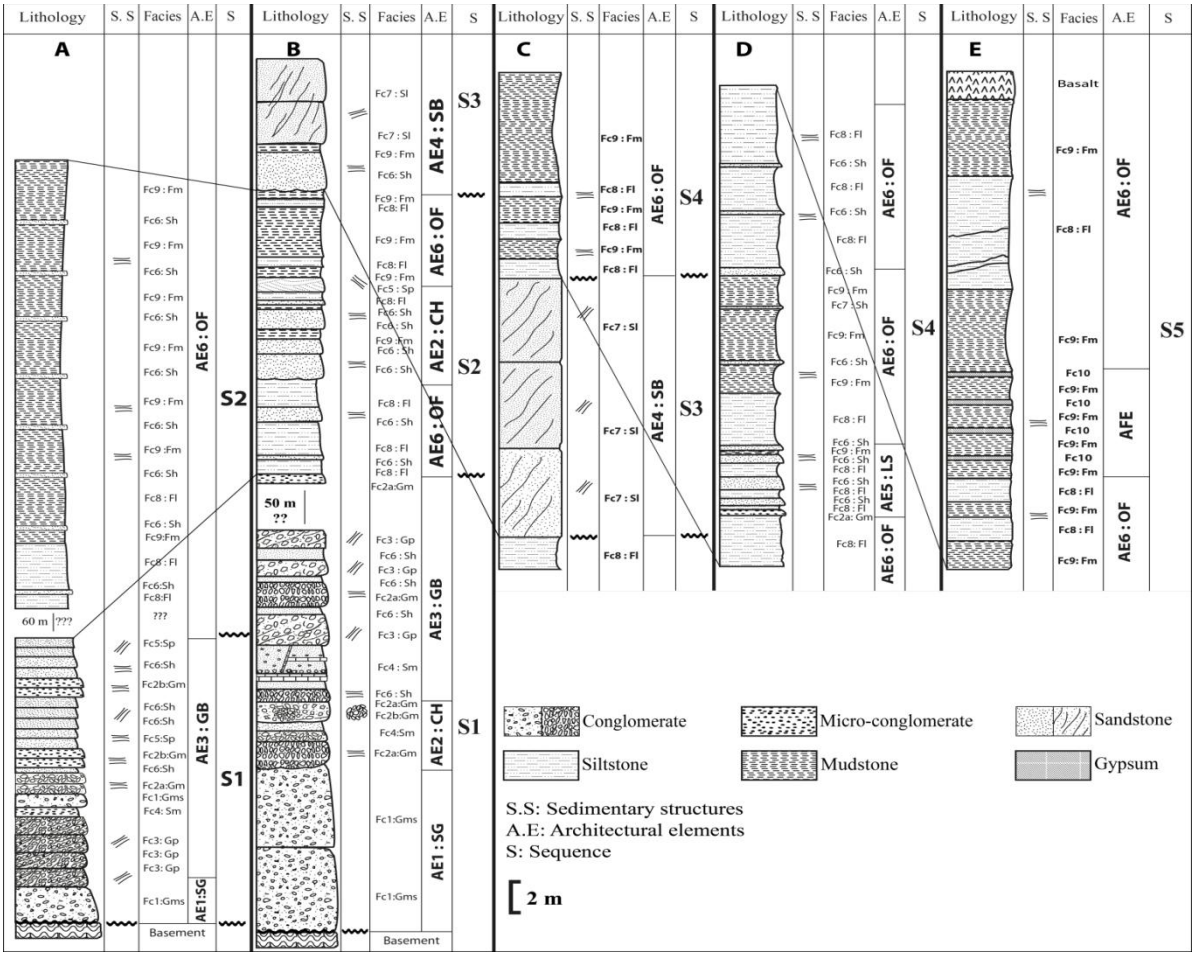

Figure 2: *Facies, architectural elements and sequences identified on the studied outcrops in the Oued Nfifikh area; A: Chaâbat Lhamra section; B: Chaâbat Lhmira section; C: Sidi Amor section; D: Assikriat section; E: section of Tlet Ziaida (Location in the Figure 1)*

4.2.2.1. *Facies Association of Playa (AFP)*

It is a lithofacies combination of 5 to 6 m thick. It is formed by alternations of fine silts and argillites of brick red color (lithofacies Fc8: Fl and Fc9: Fm) and fine sandstones sometimes showing horizontal flat beddings (lithofacies Fc6: Sh). The facies association (AFP) presents a cyclicity of the sandstone, siltstone and mudstone facies; which shows that it is deposited in Playa Lake. The presence of sandstone deposits also shows that these playa lakes are shallow (Liu and Wang, 2001) (Figure 2, 3 and 4).

4.2.2.2. *Evaporite Facies Association (AFE)*

It is an association of mudstone facies (Fc9: Fm) and evaporite facies (Fc10: beds gypsum, Fc11: fibrous gypsum, Fc12: milky halite, Fc13: phenoblastic halite, Fc14: fibrous halite). The thickness of the facies varies between 1 and 1.5 m for the siltites, between 10 and 20 cm for the gypsum and between 10 cm and 2 m for the halite. These evaporite facies have often primary and in other cases diagenetic origin. They are formed by the evaporation of saline waters in mudflats and lagoons in a hot and arid climate in relation to a ‘pellicular’ sea that covered the basin in the Upper Triassic (Figure 2, 3 and 4).

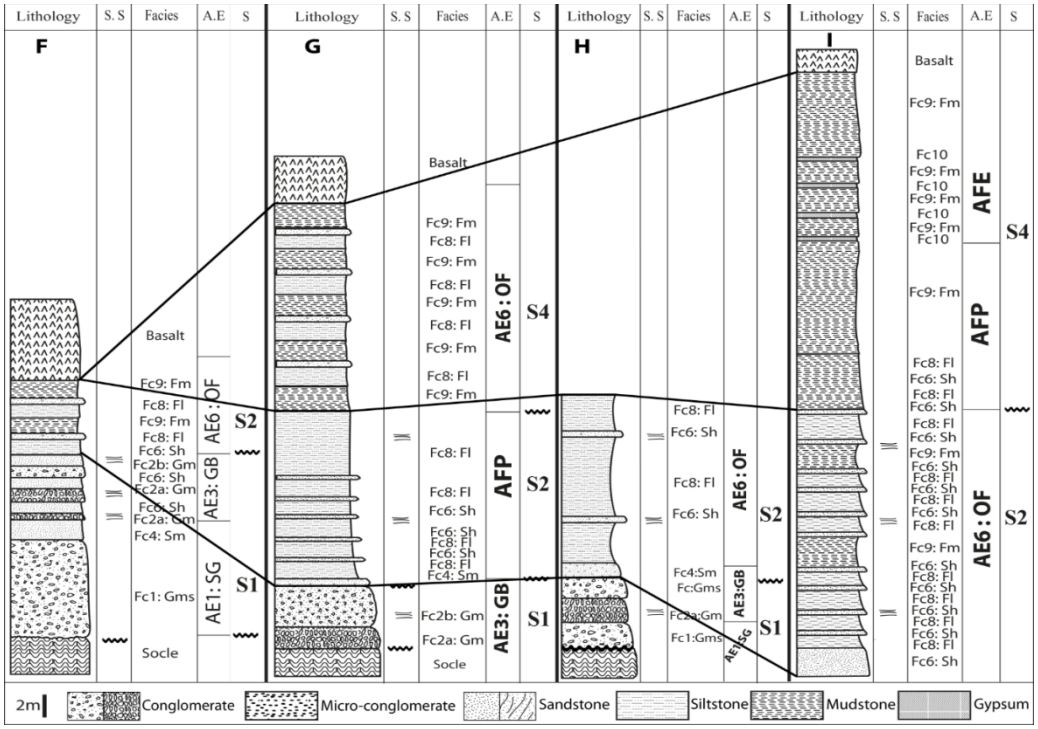

Figure 3: *Facies, architectural elements and sequences identified on the outcrops studied in the Oued El Maleh and ElGara areas, F: Sidi Bouchaibe section; G: Kachlat Al Arian section; H: Sidi Bou Amar section; I: Oulad Jhaych section in the ElGara region (Location in Figure 1)*

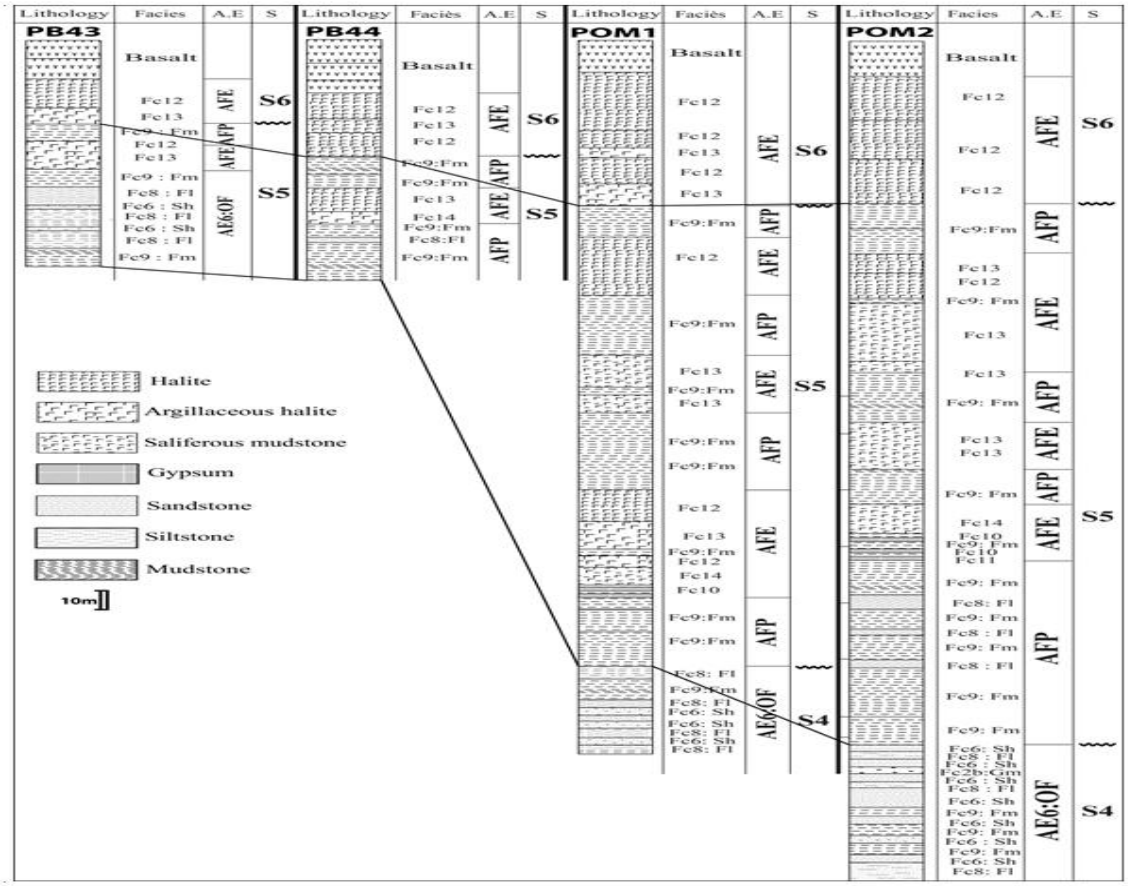

Figure 4: *Facies, architectural elements and sequences identified on the cores of the studied boreholes (PB43, PB44, POM1 and POM2, location in Figure 1)*

4.3. Paleo-Environmental Reconstruction

4.3.1. Alluvial Fans System with Gravity Flow Rivers

This proximal fluvial environment is well represented in the area of Chaâbat Lhamra (Figure 2, A), Chaâbat Lhmira (Figure 2, B), Sidi Bouchaibe (Figure 3, F) and Sidi Bou Amar (Figure 3, H). It corresponds to the deposition environment of the sandy-conglomerate formation (A).

In most outcrops, this fluvial model is characterized essentially by coarse deposits Fc1 (Gms), Fc2a (Gm), Fc2b (Gm), Fc3 (Gp) and medium deposit Fc4 (Sm) and Fc6 (Sh). These lithofacies are associated in three architectural elements: AE1 (Sediment gravity flow SG), AE2 (Channels CH) and AE3 (Gravel bars and bedforms GB). By these characteristics, we can deduce that this depositional environment is more similar to the models N°1 of Miall (1985, 2006). This model corresponds to alluvial fans with gravity flows of gravelly rivers and proximal braided rivers (Figure 5, A).

4.3.2. Braided Rivers System with Shallow Channels and Gravel Bars

This fluvial system is represented in the Chaâbat Lhamra area and at the base of Kachlat Al Arian outcrop (Figure 3, G). In the Chaâbat Lhamra area, this fluvial model is represented by conglomeratic (Fc2a: Gm, Fc2b: Gm and Fc3: Gp) and sandstone (Fc4: Sm, Fc5: Sp and Fc6: Sh) facies. The association of these facies forms the architectural element AE3 (GB). In the Kachlat Al Arian region, this depositional environment is characterized by coarse deposits (facies Fc2a: Gm, Fc2b: Gm) and by medium deposits (facies Fc3: Sm). This combination of facies forms the architectural element AE3 (GB).

By comparing the architectural elements of this fluvial style with the depositional models of Miall (1985 and 2006), we noticed that model N°2 is similar to our case. It is a braided rivers system with gravel bars (Figure 5, B).

4.3.3. Anastomosed Rivers with Floodplains and Crevasse Splays

The deposits of this fluvial model belong to the mudstone-siltstone member (1) in the middle of the Triassic series in the MBEB basin. This environment is preserved in more than 80% of studied outcrops and boreholes in this basin.

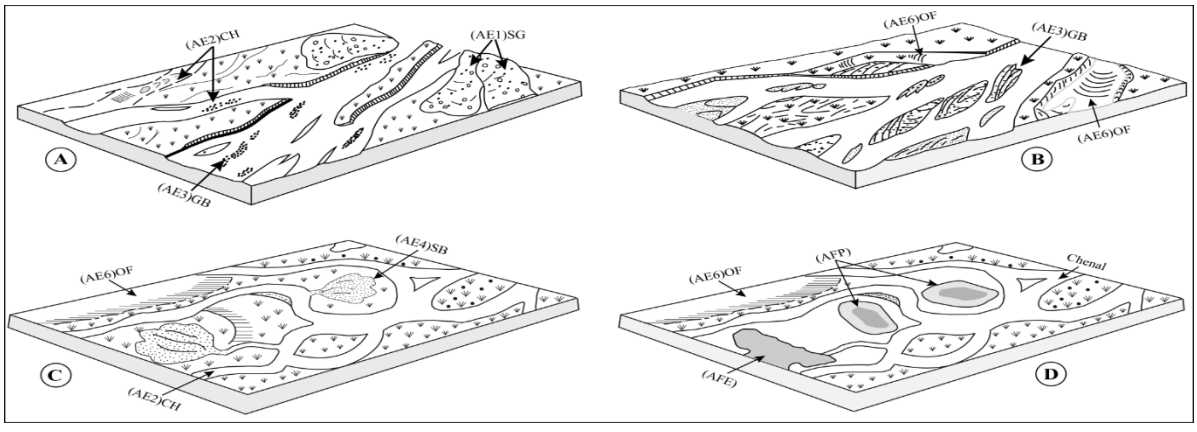

Figure 5: *Depositional environment models of the sedimentary series in the basin. (A): Depositional model corresponding to an alluvial fans system with Gravity Flow Rivers (Miall, 2006, modified); (B): Depositional model corresponding to gravelly braided rivers (Miall, 2006, modified); (C): Depositional model of anastomosed rivers with floodplains and crevasse splays; (D): deposition model corresponding to the coastal plains associated with playas, mudflats and lagoons*

This depositional environment is characterized by deposits with a large thickness (from ten to one hundred meters). It is characterized essentially by fine to very fine deposits. The facies characterizing this environment are: Fc6 (Sh), Fc6 (Sl), Fc8 (Fl) and Fc9 (Fm). They are alternations of horizontal bedded sandstones, low angle (<10°) crossbeds sandstones and laminated to massive siltstones and mudstones. These facies are associated and organized into two architectural elements: AE4 (SB: Sand Bedform) deposited in the crevasses splay and architectural element AE6 (OF: Overbank Fine) formed in flood plains and abandoned channels.

According to Farrell, (1987), Kraus (1987), Kraus and Bown (1988), Miall, (1985 and 2006), this type of depositional environment is much less studied and interpreted, unlike other types of depositional environment. However, it is linked to an anastomosed environment characterized by low-energy floods with crevasse channels and crevasse splays (Miall, 2006).

4.3.4. Coastal Plains Associated with Playas, Mudflats and Lagoons

These environments have been identified in the Tlet Ziaida, ElGara, Oued El Maleh areas and in all boreholes. This model is characterized by deposits recorded in the argillaceous-saliferous member (2) which belongs to the middle and top of the argillaceous-saliferous formation (B), and which is capped by Late Triassic-Early Jurassic basalts. This depositional environment is characterized by very fine sandy facies (Fc6: Sh), mudstone facies (Fc8: Fm), siltstone facies (Fc9: Fl) and evaporites facies (Fc10: beds Gypsum, Fc11: Fibrous gypsum, Fc12: Milky halite, Fc13: Phenoblastic halite and Fc14: Fibrous halite). Two facies associations are identified: facies association of Playa (interbedding of very fine sandstone and mudstone) and evaporite facies association (interbedding of mudstone, gypsum and halite).

This model (Figure 5, D) probably corresponds to the large coastal plain downstream characterized by the development of playas lakes, mudflats and lagoons where the evaporite facies are formed by the evaporation of marine waters under a hot and arid climate and in relation to a pellicular sea that covered the domain during the Upper Triassic time.

5. Discussion

5.1. Structural Evolution and Sedimentary Filling

5.1.1. Pre-Rift Phase

Hercynian tectonics in the North-Western Meseta evolved in three main phases (Michard, 1976) during the first phase, this part of the Meseta was mainly structured. The second phase is characterized by an episode of retromorphic metamorphism, followed by a late third phase that caused the replay of major faults (Fadli, 1990; Lyazidi, 2004).

The shear zone located in the Chaâbat El Hmira region represents the southern extension of the Bouznika fault (Piqué, 1979; Fadli, 1990; Lyazidi, 2004). This is a syntectonic fault located in a corridor characterized by high deformation and metamorphism; this zone presents the eastern boundary of the coastal block at the Hercynian time (Piqué, 1979; Zahraoui, 1991; Fadli, 1990; Lyazidi, 2004). According to Zahraoui (1991) the deformed Paleozoic terranes have a succession from the oldest to the less old in the west-east direction: Cambrian, Ordovician, Silurian, Lower Devonian, Strunian and Upper Visean.

5.1.2. Syn-Rift Phase

Detrital sedimentation in the Mohammedia-Benslimane-ElGara-Berrechid basin can be interpreted as resulting from the filling of a ditch in the form of half-graben (El Wartiti and Fadli, 1985; El Wartiti et al., 1992; Lyazidi, 2004), the rework of the Hercynian faults which caused the collapse of this ditch and the activation of erosion during the Central Atlantic rifting. At this time the detrital syn-rift series recorded a synsedimentary faults with a N50° dip (El Wartiti & Fadli, 1985; El Wartiti et al., 1992), showing the synchronization of sedimentary filling and basin extension. Other post-sedimentary normal faults affected all the Triassic and Jurassic series; which indicates the continuity of the NW-SE extension to the Jurassic (El Wartiti and Fadli, 1985; El Wartiti et al., 1992).

The works of El Wartiti et al. (1992) showed that during the lower Liassic the NW-SE extension is continued and is related to the formation of horsts and grabens followed by an erosion phase until the Cretaceous.

Sedimentological analysis showed that the MBEB basin experienced two large phases of sedimentary filling during the upper Triassic syn-rift stage. The first phase is purely continental. During this period, the first deposits arrived in the basin during opening (thus during the beginning of the rifting) are of proximal fluvial origin; they are conglomerates and sandstones formed mainly in proximal alluvial fans and in braided rivers systems. Subsequently, the decrease of palaeopente and base level rise caused a paleoenvironmental changes in the basin, and the deposition system tends to distal setting. Anastomosing fluvial system with large flood plains and playa where fine sandstone, mudstone and siltstone sediments have been deposited.

During the second phase, the syn-rift sedimentary series recorded a marine incursion at the terminal Triassic with salt sedimentation. This marine intervention is deduced from the presence of a thick saliferous series whose isotopic sulfur ratios and bromine contents (Peretsman-Clement & Holser, 1988) indicate their marine origin. These marine waters are probably of Tethyan origin and are also related to the opening of the Proto-Atlantic Ocean. This transgression was punctuated by a magmatic activity (CAMP (Central Atlantic Magmatic Province): dated 200 Ma in the MBEB basin by Peretsman, 1985) at the Triassic-Jurassic boundary, and then continued to the Liassic time.

5.2. Comparison with the Basins of the Moroccan Atlantic and North-east American Margin

5.2.1. Comparison with Moroccan Atlantic Margin Basins

In this comparison (Figure 6), we are based on the synthetic sedimentary series of five basins of the Moroccan Atlantic margin. For the Doukkala basin we made a synthetic section from field data published by Hminna et al. (2013) and boreholes data EBA1, OYB1, OBZ1 and PS4 published by Salvan (1984) and Echarfaoui et al. (2002a). For the Essaouira Basin, we used data from the MAC1 and DOT1 boreholes of Echarfaoui et al. (2002b) and seismic sections of Hafid (2000) and Hafid et al. (2006). For the Khémisset basin, we used the outcrop and borehole (PKB2) data published by Salvan (1984) and Et-Touhami (1994, 1996 and 1998). For the Boufekrane basin, we used the data of the BFP5 borehole studied by Salvan (1982) and Ouarhache et al. (2012).

This comparison led to the following conclusions:

- The thicknesses of the sedimentary series vary from one basin to another. This difference in thickness is probably due to the opening time of each basin, the tectonic factors and the rate of subsidence, the sediment supply and accommodation, and erosion, or the combination of all these factors.

- The proximal fluvial deposits (basal conglomerates and sandstones) are thicker in the Mohammedia-Benslimane-ElGara-Berrechid basin and in the Doukkala basin than in the other three basins. This is probably related to the relief's abundance and relief-rejuvenation in these two basins.
- The medium and fine facies (fine sandstone, siltstones and mudstones) formed in distal fluvial environments are almost of equal potency in all the basins compared.
- The thickness of the argillaceous halite increases from north to south of the Moroccan Atlantic margin. Pure halite is thicker in the Khémisset basin (north of the margin) than in the other basins. This is probably related to significant incursions of the marine waters of the Tethys and the Proto-Atlantic into the Khémisset Basin (Et-Touhami, 1994, 1996).
- The majority of the evaporitic facies in these basins are of marine origin except in the Essaouira basin whose origin of the evaporites is continental (Peretsman-Clement, 1988).
- Generally, the Triassic volcano-sedimentary series is structured in the same way in the five basins. It consists of a lower detrital formation deposited on the Hercynian basement: subdivided into a sandy-conglomeratic member and silty-mudstone member; and an argillaceous-saliferous formation: subdivided into a clay-halite member and pure halite member.

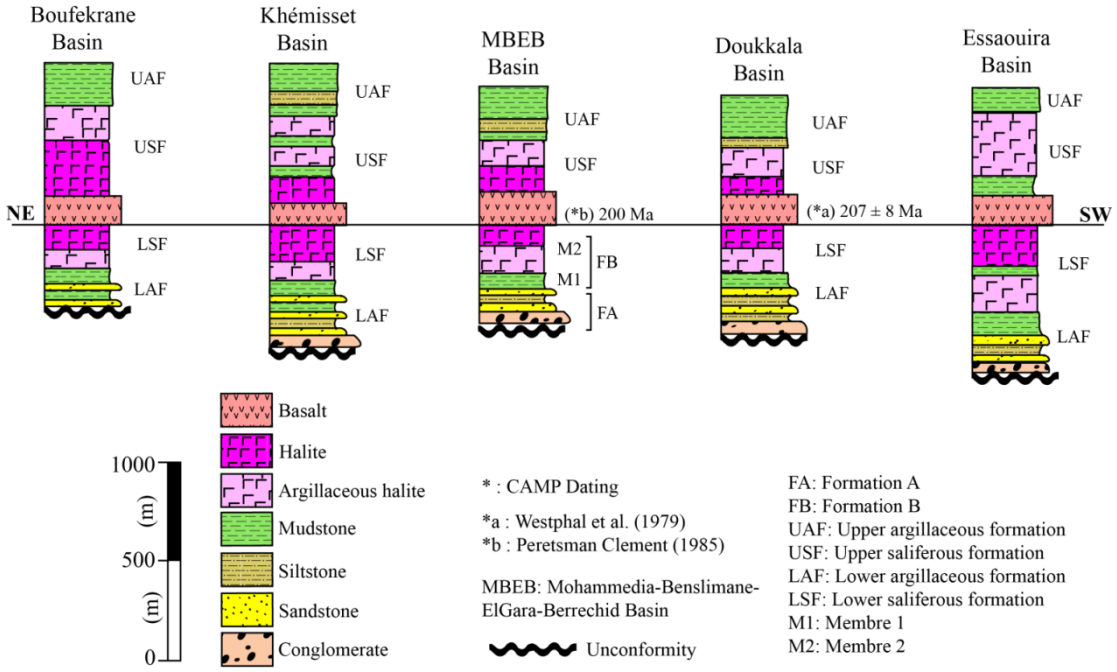

Figure 6: *Comparison of the studied basin with the other Triassic basins of the Moroccan Atlantic margin*

5.2.2. Comparison with the Basins of North-east American Margin

The opening of the basins of the North-east American margin and those of the North-West African margin (Moroccan margin) is synchronous with the Central Atlantic rifting (Withjack et al., 1998; Piqué et al., 1998; Piqué and Laville, 1995; Leleu et al., 2016). They are subject to almost the same tectonic regime at the Triassic time. These basins present a set of common points and other different:

- From a tectonic point of view, the Northeast American basins have undergone the same tectonic regime as the MBEB basin as well as the other Moroccan Triassic basins. It is an extension often NW-SE resulting from the reactivation of preexisting structures in the Paleozoic basement and inherited from the Hercynian/Alleghanian orogeny (Doré et al., 1997; Matte, 2001; Stampfli and Borel, 2002; Laville et al., 2004).

- This extension gave to the Northeastern American basins half-grabens geometry (Manspeizer and Cousminer, 1988; Olsen et al., 1989; Schlische, 1993; Withjack et al., 1998, 2012). It is almost the same geometry as a set of Moroccan basins, including the MBEB basin.
- Regarding to sedimentary filling history, the American basins belonging to the southern segment and the central segment (Newark basin, Deep-River basin, Culpeper basin, Fundy basin, Franklin basin, Connecticut Valley) (Keen et al., 1987; Welsink et al., 1989; Withjack and Callaway, 2000; Tanner and Brown, 2003; Withjack et al., 2012; Leleu et al., 2016) resemble to the Moroccan Atlasic basins as well as the basal detrital formation of the Mesetian and Moroccan Atlantic margin basins. These basins are characterized by continental sedimentation during the Upper Triassic. These are fluvial deposits interbedded with lacustrine and playa deposits.
- From the seismic sections of Keen et al. (1987); Welsink et al. (1989), Sinclair (1995); Withjack and Callaway (2000), Tanner and Brown (2003), Syamsir et al. (2010), Withjack et al. (2012) and Leleu et al. (2016), we conclude that only the basins of the North Atlantic segment (Orpheus basin, Flemish Pass basins and Jeanne Arc basin) which contain a significant evaporitic series, in contrast to the basins of the central and southern segment, which are dominated by the detrital series. These three basins thus have a similarity with our study basin and with the other basins of the Moroccan Atlantic margin concerning the presence of evaporites. However, the evaporites from Canadian basins have a moderate marine origin with large continental influences (Holser et al., 1988) while evaporites in the MBEB basin have mostly a marine origin (Holser et al., 1988; Peretsman-Clement and Holser, 1988).
- In the Orpheus basin, the age of magmatic activity (CAMP) is about 200 Ma (Syamsir et al., 2010, Figure 1C). This is the same CAMP age in the MBEB basin (Peretsman-Clement, 1985).

These conclusions are summarized in the Figure 7 by which we proposed a correlation between the MBEB basin and some Triassic basins of the Northeastern Atlantic margin.

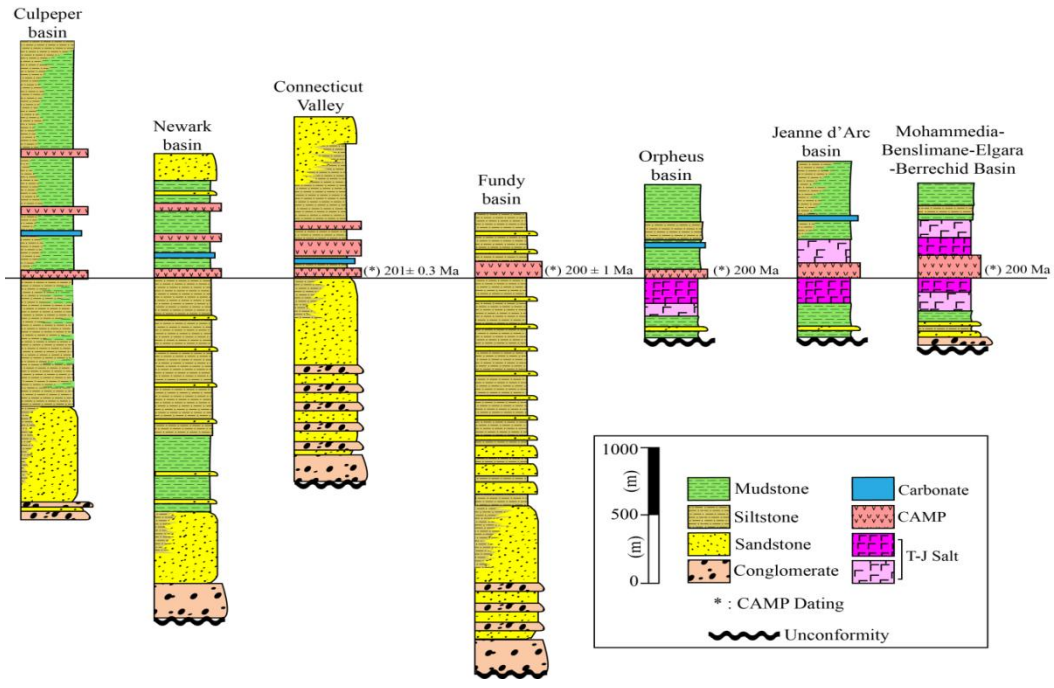

Figure 7: *Comparison of the sedimentary series of the MBEB basin with those of some Triassic basins of the Northeastern American margin. (Based on data published by: Keen et al. (1987); Welsink et al. (1989); Sinclair (1995); Withjack & Callaway (2000); Tanner & Brown (2003); Syamsir et al. (2010); Withjack et al. (2012) and Leleu et al. (2016)*

6. Conclusion

The results of this study show that the MBEB basin contains a syn-rift Triassic series with two sedimentary episodes. During the first episode, sedimentation is of a silisiclastic nature and is formed under purely continental conditions. The detrital materials come from the erosion of neighboring Paleozoic reliefs. During the second episode, the deposits consist of evaporites formed in a hot and arid climate, and controlled by a set of tectonic structures that led to the opening of the basin. This episode is the result of the marine transgression at the end of the Upper Triassic.

The depositional setting has evolved over time during these episodes. This evolution has been controlled by climate, tectonics, palaeopente and basic level variations. The deposition environments changed from a proximal alluvial fans system to a braided rivers style and then to an anastomosing system. These environments eventually evolve to an alluvial plain associated with a coastal plain where playa lakes, mudflats and lagoons had developed.

These vertical variations in sediment nature and size are due to variation in basal level and sediment supply during sedimentation in the basin. This variation is of tectonic and / or climatic origin (allocyclic), in relation with the Tethys and the Atlantic Ocean being opened. At the onset of sedimentation, the base level decreased and led to the formation of poorly organized conglomeratic facies in a proximal fluvial setting. Then, it began to rise which led to the formation of a fluvial sedimentary series followed by evaporitic facies before the magmatic activity (CAMP) at the Triassic-Jurassic boundary.

At the Moroccan Atlantic margin, the sedimentary series show a great similarity in all the basins of this margin. They are all composed of a detrital fluvio-lacustrine formation at the base surmounted by another saliferous formation covered by late Triassic-early Liassic basalt. The comparison with the basins of the Northeastern American margin revealed a similarity of our basin with the basins of the northern segment (Orpheus basin, Flemish Pass basins and Jeanne Arc basin); in these basins, the syn-rift sedimentary series consists of detrital deposits at the base with a salt series capped by basalts. It is almost the same case as the basins of the Moroccan margin.

References

Allen, J.R.L. 1983. Studies in fluviatile sedimentation: bars, bar-complexes and sandstone sheets (low-sinuosity braided streams) in the Brownstones (Devonian), Welsh Borders. *Sedimentary Geology*, pp.237-293.

Blakey, R.C. and Gubitosa, R. 1984. Controls of sandstone body geometry and architecture in the Chinle Formation (Upper Triassic), Colorado Plateau. *Sedimentary Geology*, 38, pp.51-86.

Bensalah, M.K., Youbi, N., Mahmoudi, A., Bertrand, H., Mata, J., El Hachimi, H., Madeira, J., Martins, L., Marzoli, A., Bellon, H., Medina, F., Karroum, M., Karroum, L.A. and Ben Abbou, M. 2011. The Central Atlantic Magmatic Province (CAMP) volcanic sequences of Berrechid and Doukkala basins (Western Meseta, Morocco): volcanology and geochemistry. *Comunicações Geológicas,* 98, pp.15-27.

Boothroyd, J.C. and Ashley, G.M. 1975. Process, bar morphology and sedimentary structures on braided outwash fans, northeastern Gulf of Alaska. In: Jopling, A.V. and McDonald, B.C. (eds.), *Glacio-fluvial and Glacio-lacustrine Sedimentation, Society of Economic Paleontologists and Mineralogists*, pp.193-222.

Bridge, J.S. 2003. *Rivers and floodplains: forms, processes, and sedimentary records*. Oxford: Blackwell, p.491.

Chemin, P. 1990. Etude du rôle des inclusions fluides dans les mécanismes de déformation des roches halitiques. Application aux formations salifères du bassin bressan, thèse, Géologie appliquée, Ecole Nationale des Ponts et Chaussées Français.

Doré, A.G., Lundin, E.R., Fichler, C. and Olesen, O. 1997. Patterns of basement structure and reactivation along the NE Atlantic margin. *Journal of the Geological Society of London*, 154, pp.85-92.

Dumas, D. 1988. Le Paléogène salifère du bassin de Valence (Sud-est de la France): géométrie et sédimentologie des dépôts, synthèse de bassin. Thèse, Doct., Univ. Claude Bernard, Lyon, p.293.

Echarfaoui, H., Hafid, M. and Aït Salem, A. 2002a. Structure sismique du socle paléozoïque du bassin des Doukkala, Môle côtier, Maroc occidental. *Indication en faveur de l'existence d'une phase éo-varisque*. 334, pp.13-20.

Echarfaoui, H., Hafid, M., Aït Salem, A. and Aït Fora, A. 2002b. Analyse sismo-stratigraphique du bassin d'Abda (Maroc occidental), exemple de structures inverses pendant le rifting atlantique. *Comptes Rendus Geoscience,* 334, pp.371-377.

Einsele, G. 2000. *Sedimentary Basins: Evolution, Facies, and Sediment Budget*. Berlin: Springer-Verlag, p.792.

Eji Uba, C., Heubeck, C. and Hulka C. 2005. Facies analysis and basin architecture of the Neogene Subandean synorogenic wedge, southern Bolivia. *Sedimentary* Geology, 180, pp.91-123.

El Wartiti, M. and Fadli, D. 1985. Relations socle-couverture au cours du Trias dans la zone de BenSlimane-ElGara (Maroc nord mesetien). *Bull. Sci. Ter., Rabat,* 1, pp.54-66.

El Wartiti, M., Medina, F. and Fadli, D. 1992. Effects of the Central Atlantic early rifting in the northern border of the Berrechid-ElGara basin (Morocco). *Gaia,* 4, pp.31-38.

Et-Touhami, M. 1992. Le Trias évaporitique du bassin de Khémisset (Maroc central). Géométrie du dépôt, évolution sédimentaire, Géochimie. Thèse Université Lyon, p.242.

Et-Touhami, M. 1994. Le Trias évaporitique du bassin de Khémisset (Maroc central). *Notes Mém. Serv. géol. Maroc, Rabat,* p.373, 211.

Et-Touhami, M. 1998. Le Trias salifère marocain: typologie des cristaux de l'halite et faciès halitiques. *Africa Geoscience Review,* 5, pp.107-115.

Fadli, D. 1990. Evolution sédimentaire et structurale des massifs de Mdakra et du Khatouat: deux segments hercyniens de la Meseta marocaine nord-occidentale. *Thèse ès Sciences, Univ. Mohammed V, Fac. Sci. Rabat,* p.294.

Farrell, K.M., 1987. Sedimentology and facies architecture of overbank deposits of the Mississippi River, False River region, Louisiana. In: Ethridge F.G., Flores R.M. and Harvey M.D. (eds.), Recent developments in fluvial sedimentology. *Soc Econ Paleontol Mineral Spec Publ*., 39, pp.111-120.

Friend, P.F., Slater, M.J. and Williams, R.C. 1979. Vertical and lateral building of river sandstone bodies, Ebro Basin, Spain. *Journal of the Geological Society of London,* 136, pp.39-46.

Friend, P.F. 1983. Towards the field classification of alluvial architecture or sequence. *In*: J.D, Collinson and J. Lewin (eds), Modern and Ancient Fluvial Systems. *Int. Assoc. Sediment. Spec. Publ.*, 6, pp.345-354.

Gustavson, T.C., Hovorka, S.D. and Dutton, A.R. 1994. Origin of satin spar veins in evaporite basins. *Journal of Sedimentary Research*, 64(1), pp.88-94.

Hafid, M. 2000. Triassic-early Liassic extensional systems and their Tertiary inversion, Essaouira Basin (Morocco). *Marine and Petroleum Geology*, 17, pp.409-429.

Hafid, M., Zizi, M., Bally, A.W. and Aït Salem, A. 2006. Structural styles of the western onshore and offshore termination of the High Atlas, Morocco, *Geoscience*, 338, pp.50-64.

Hminna, A., Voigt, S., Klein, H., Saber, H., Schneider, J.W. and Hmich, D. 2013. First occurrence of tetrapod footprints from the continental Triassic of the Sidi Said Maachou area (Western Meseta, Morocco). *Journal of African Earth Sciences*, 80, pp.1-7.

Holser, W.T., Clement, G.P., Jansa, L.F. and Wade, J.A. 1988. Evaporite deposits of the north Atlantic rift. In: Manspeizer, W. (ed.), *Triassic-Jurassic rifting: Continental breakup and the origin of the Atlantic Ocean and passive margins*. Elsevier, pp.525-556.

Hovorka, S.D. 1983. Sedimentary structures and diagenetic modifications in halite and anhydnte, Palo Duro Basin. In: Geology and geohydrology of the Palo Duro Basin, Texas Panhandle. *Bureau Economic Geology, Austin, Geological Circular*, 83-4, pp.49-57.

Johnson, S.Y. 1984. Cyclic fluvial sedimentation in a rapidly subsiding basin, North West Washington. *Sedimentary Geology*, 38, pp.361-392.

Keen, C.E., Boutilier, R., de Voogd, B., Mudford, B. and Enachescu, M.E. 1987. Crustal geometry and extensional models for the Grand Banks, eastern Canada: constraints from deep seismic reflection data. In: Beaumont, C., Tankard, A.J. (eds.): Sedimentary Basins and Basin-Forming Mechanisms. *Canadian Society of Petroleum Geologists, Memoir*, 12, pp.101-115.

Kraus, M.J. 1987. Integration of channel and floodplain suites, II. Vertical relations of alluvial paleosols. *Journal of Sedimentary Petrology*, 57, pp.602-612.

Kraus, M.J. and Bown, T.M. 1988. Pedofacies analysis; a new approach to reconstructing ancient fluvial sequences. *Geol Soc. Am. Spec. Paper*, 216, pp.143-152.

Laville, E. and Piqué, A. 1991. La distension crustale atlantique au Maroc au début du mésozoïque. Le rejet des structures hercyniennes. *Bull. Soc. Géol. Fr*., p.162.

Laville, E., Piqué, A., Amrhar, M. and Charroud, M. 2004. A restatement of the Mesozoic Atlasic Rifting (Morocco). *Journal of African Earth Sciences,* 38, pp.145–153.

Leleu, S. and Hartley, A.J. 2010. Controls on the stratigraphic development of the Triassic Fundy Basin, Nova Scotia: implications for the tectono-stratigraphic evolution of Triassic Atlantic rift basins. *Journal of the Geological Society of London*, 167, pp.437-454.

Leleu, S., Hartley, A.J., Oosterhout, C.V., Kennan, L., Ruckwied, K. and Gerdes, K. 2016. Structural, stratigraphic and sedimentological characterization of a wide rift system: The Triassic rift system of the Central Atlantic Domain. *Earth Science Reviews*, 158, pp.89-124.

Lister, G.S., Etheridge, M.A. and Symonds, P.A. 1991. Detachment models for the formation of passive continental margins. *Tectonics*, 10, pp.1038-1064.

Liu, Z. and Wang, C. 2001. Facies analysis and depositional systems of Cenozoic sediments in the Hoh Xil basin, northern Tibet. *Sedimentary Geology*, 140, pp.251-270.

Lowenstein, T.K. and Hardie, L.A. 1985. Criteria for the recognition of salt-pan evaporites. *Sedimentology*, 32, pp.627-644.

Lyazidi, A. 2004. Evolution géodynamique du bassin triasique de Berrechid-ElGara-Benslimane (Meseta Nord Occidentale, Maroc). Thesis, University of Mohammed V-Agdal Rabat, Morocco.

Manspeizer, W., Puffer, J.H. and Cousminer, H.L. 1978. Separation of Morocco and eastern North America: a Triassic-Liassic stratigraphic record. *Geological Society of America Bulletin*, pp.901-920.

Manspeizer, W. 1988a. Triassic-Jurassic rifting: continental breakup and the origin of the Atlantic Ocean and passive margins. *Elsevier Science Publishers B.V.*

Manspeizer, W. 1988b. A stratigraphic record from Morocco and North America of rifting, drifting and Tethyan transgressions of the Central proto-Atlantic. *Journal of African Earth Sciences*, 7, pp.369-373.

Manspeizer, W. and Cousminer, H.L. 1988. Late Triassic–Early Jurassic synrift basins of the U.S. Atlantic margin. In: Sheridan, R.E. and Grow, J.A. (eds.). *The Atlantic Continental Margin*, 2, pp.197-216.

Massari, F. 1983. Tabular cross-bedding in Messinian fluvial channel conglomerates, Southern Alps, Italy. *In*: J.D. Collinson and J. Lewin (eds), Modern and Ancient Fluvial Systems. *Int. Assoc. Sediment. Spec. Publ*., 6, pp.287-300.

Matte, P. 2001. The Variscan collage and orogeny (480–290 Ma) and the tectonic definition of the Armorica microplate: a review. *Terra Nova*, 13, pp.122-128.

Medina, F. 1994. Evolutions structurale du Haut Atlas occidental et des régions voisines du Trias à l'Actuel, dans le cadre de l'ouverture de l'Atlantique central et de la collision Afrique-Europe. State Thesis, University Mohammed, Rabat, Morocco.

Medina, F. 1995. Syn-and post-rift evolution of the ElJadida-Agadir basin (Morocco): constraints for the rifting models of the Central Atlantic. *Canadian Journal Earth Sciences*, 32, pp.1273-1291.

Medina, F. 1996. Le Trias du Maroc introduction. In: Medina, F. (ed.), Le Permien et le Trias du Maroc: état des connaissances. Pumag, Marrakech, pp.139-153.

Miall, A.D. 1977. A review of the braided river depositional environment. *Earth-Science Reviews*, 13, pp.1-62.

Miall, A.D. 1978. Lithofacies types and vertical profile models in braided river deposits: a summary. *Canadian Society of Petroleum Geologists Mem*, pp.597-604.

Miall, A.D. 1985. Architectural-element analysis: a new method of facies analysis applied to fluvial deposits. *Earth-Science Reviews*, 22, pp.261-308.

Miall, A.D. 1996. The geology of fluvial deposits, sedimentary facies, basin analysis and petroleum geology. Germany: Springer-Verlag.

Miall, A.D. 2006. The geology of fluvial deposits, sedimentary facies, basin analysis and petroleum geology. 4th ed., Germany: Springer-Verlag.

Moretto, R. 1985. Sédimentologie de la série salifère du Paléogène de la Bresse (France). *Bull. Soc. Géol. Fr. Sér*., 8, pp.849-855.

Olsen, P.E., Schlische, R.W. and Gore, P.J.W. 1989. Newark Basin, Pennsylvania and New Jersey: stratigraphy. *Am. Geophys. Union,* Washington, DC, pp.69-152.

Orti, F. and Pueyo, J.J. 1977. Asociacion halita bandeada anhidrita nodular del yacimiento de Remolinos, Zaragoza (sector central de la Cuenca del Ebro). *Nota petrogene Âtica. Rev. Inst. Inv. Geol. Diput.*, 32, pp.167-202.

Opluštil, S., Martínek, K. and Tasáryová, Z., 2005. Facies and architectural analysis of fluvial deposits of the Nýřany Member and the TýnecFormation (Westphalian D-Barruelian) in the Kladno-Rakovník and Pilsen basins. *Bulletin of Geosciences*, pp.45-66.

Ouarhache, D., Charrière, A., Chalot-Prat, F. and El Wartiti, M. 2012. Chronologie et modalités du rifting triasico-liasique à la marge sud-ouest de la Téthys alpine (Moyen Atlas et Haute Moulouya, Maroc); corrélations avec le rifting atlantique : simultanéité et diachronisme. *Bulletin de la Société géologique de France*, 183, pp.233-249.

Oujidi, M. and Et-Touhami, M. 2000. Stratigraphy of Permian and Triassic systems in Morocco: an overview. In: Oujich M. and Et-Touhami, M. (eds.), Le Permien et le Trias marocain: *Actes de la Première Réunion du Groupe Marocain du Permien et du Trias.* Oujda, pp.1-13.

Oujidi, M., Courel, L., Benaouiss, N., EL Mostaine, M., EL Youssi, M., Et Touhami, M., Ouarhache, D., Sabaoui, A. and Tourani, A. 2000. Triassic series of Morocco: stratigraphy, paleogeography and structuring of the southwestern peri Tethyan platform. An overview. *Mém. Mus. Natn. Hist. Nat.*, 182, pp.23-37.

Peretsman, C.G. 1985. A geochemical and petrographic analysis of early Mesozoic evaporites from Morocco: implications for the history of the North Atlantic. Ms. Thesis, University of Oregon, p.87.

Peretsman, C.G. and Holser, T.W. 1988. Geochemistry of Moroccan evaporites in the setting of the North Atlantic rift. *Journal of African Earth Sciences*, pp.375-383.

Piqué, A. 1994. Géologie du Maroc. In: Les domaines régionaux et leur évolution structurale. PUMAG, Rabat, p.284.

Piqué, A. and Laville, E. 1995. L'ouverture initiale de l'Atlantique central. *Bulletin Société Géologique de France*, 166, pp.725-738.

Piqué, A., Le Roy, P. and Amrhar, M. 1998. Transtensive synsedimentary tectonics associated with ocean opening: the Essaouira-Agadir segment of the Moroccan Atlantic margin. *Journal of the Geological Society*, 155, pp.913-928.

Poli, E. 1997. Stratigraphie séquentielle haute-résolution, modèles de dépôt et géométrie 2D-3D des séquences triasiques de la marge téthysienne ardéchoise. Thèse, Université de Bourgogne, Centre des Sciences de la Terre.

Postma, G. and Cruickshank, C. 1988. Sedimentology of a late Weichselian to Holocene terraced fan delta, Varangerfjord, northern Norway. In: Nemec, W. and Steel, R.J. (eds.), *Fan deltas: Sedimentology and tectonic settings*. London: Blackie, pp.144-158.

Reineck, H.E. and Singh, I.B. 1980. *Depositional sedimentary environments*. Springer-Verlag, Germany: Heidelberg.

Ricou, L.E. 1994. Tethys reconstructed: plates, continental fragments and their boundaries since 260 Ma from Central America to South-eastern Asia. *Geodinamica Acta*, pp.169-218.

Rust, B.R. 1978. Depositional models for braided alluvium. In: Miall, A.D. (ed.), Fluvial Sedimentology. *Canadian Society of Petroleum Geologists Mem.*, 5, pp.605-625.

Rust, B.R. 1981. Sedimentation in an arid-zone anastomosing fluvial system: Cooper's Creek, Central Australia. *Journal of Sedimentary Petrology*, 51(3), pp.745-755.

Salvan, H.M. 1982. Les évaporites triasiques du Maroc: Caractères généraux-répartition-interprétation. *Bulletin Fac. Sc. Marrakech*, p.73.

Salvan, H.M. 1984. Les formations évaporitiques du Trias marocain. Problèmes stratigraphiques, paléogéographiques et paléoclimatiques. *Rev. Géogr. Phys. Géol. Dyn.*, 25(3), pp.187-203.

Schreiber, B.C., Friedman, G.M., Decimas, A. and Schreiber, E. 1976. Depositional environments of Upper Miocene (Messinian) evaporite deposits of the Sicilian Basin. *Sedimentology*, 23, pp.729-760.

Schreiber, B.C. and EL Tabakh, M. 2000. Deposition and early alteration of evaporites. *Sedimentology*, 47(1), pp.215-238.

Schlische, R.W. 1993. Anatomy and evolution of the Triassic-Jurassic continental rift system, eastern North America. *Tectonics*, 12, pp.1026-1042.

Shearman, D.J. 1970. Recent halite rock, Baja California, Mexico. *Trans. Inst. Mining Metall.*, 79, pp.155-162.

Sinclair, I.K. 1995. Sequence stratigraphic response to Aptian-Albian rifting in conjugate margin basins: a comparison of the Jeanne d'Arc basin, offshore Newfoundland, and the Porcupine basin, offshore Ireland. In: Scrutton, R.A., Stoker, M.S., Shimmield, G.B. and Tudhope, A.W. (eds.), The Tectonics, Sedimentation and Paleoceanography of the North Atlantic Region. *Geological Society Special Publication*, 90, pp.29-49.

Smith, D.G. 1983. Anastomosed fluvial deposits; modern examples from Western Canada. In: Collinson, J.D. and Lewin, J. (eds.), *Modern and Ancient Fluvial Systems*. John Wiley & Sons, Inc.

Sneh, A. 1983. Desert stream sequences in the Sinai Peninsula. *Journal of Sedimentary Petrology*, pp.1271-1280.

Sohn, Y.K., Kim, S.B., Hwang, I.G., Bahk, J.J., Choe, M.Y. and Chough, S.K. 1997. Characteristics and depositional processes of large-scale gravelly Gilbert-type foresets in the Miocene Doumsan fan delta, Pohang Basin, SE Korea. *Journal of Sedimentary Research*, 67(1), pp.130-141.

Sohn, Y.K., 2000. Depositional process of submarine debris flows in the Miocene fan deltas, Pohang Basin, SE Korea with special reference to flow transformation. *Journal of Sedimentary Research*, 70, pp.491-503.

Sonnenfeld, P. and Hodec, P.P. 1985. Origin of clay films in rock salt. *Sedimentary Geology*, 44, pp.113-120.

Stampfli, G.M. and Borel, G.D. 2002. A plate tectonic model for the Palaeozoic and Mesozoic constrained by dynamic plate boundaries and restored synthetic oceanic isochrones. *Earth and Planetary Science Letters*, 196, pp.17-33.

Syamsir, Z., Withjack, M.O., Durcanin, M.A., Schlische, R.W. and Monteverde, D.H. 2010. The Mesozoic Orpheus rift basin, offshore Nova Scotia and Newfoundland, Canada: Synrift and early post rift evolution of a well imaged North Atlantic rift basin. Central and North Atlantic Conjugate Margins Conference, Lisbon, 5, pp.279-283.

Takahashi, T., 1981. Debris flow. *Annual Review of Fluid Mechanics. 13, pp.57-77.*

Takahashi, T. 1991. Debris flows. IAHR Monograph Series, Balkema, Rotterdam.

Tanner, L.H. and Brown, D.E. 2003. Tectonostratigraphy of the Orpheus graben, Scotian basin, offshore eastern Canada, and its relationship to the Fundy rift basin. In: Le Tourneau, P.M., Olsen, P.E. (eds.), *The Great Rift Valleys of Pangea in Eastern North America*. Sedimentology, Stratigraphy, and Paleontology. New York: Columbia University Press, 2, pp.59-68.

Todd, S.P. 1996. Process deduction from fluvial sedimentary structures. *In:* Carling, P.A., Dawson, M.R. (eds.), *Advances in Fluvial Dynamics and Stratigraphy*. Wiley, Chichester, pp. 299-350.

Tunbridge, I.P. 1981. Sandy high-energy flood sedimentation some criteria for recognition, with an example from the Devonian of S.W. England. *Sedimentary Geology*, 28, pp.79-96.

Tunbridge, I.P. 1984. Facies model for a sandy ephemeral stream and clay playa complex, the Middle Devonian Trentishoe Formation of North Devon, U.K. *Sedimentology*, 31(5), pp.697-715.

Warren, J.K. and Kendall, C.G.ST.C. 1985. Comparison of sequences formed in Marine Sabkha (Subaerial) and Salina (Subaqueous) settings, modern and ancient. *The American Association of Petroleum Geologists Bulletin*, 69(6), pp.1013-1023.

Warren, J.K. 2006. Evaporites: sediments, resources and hydrocarbons. Springer, p.1036.

Warren, J.K. 2010. Evaporites through time: tectonic, climatic and eustatic controls in marine and nonmarine deposits. *Earth-Science Reviews*, 98, pp.217-268.

Wardlaw, N. C. and Schwerdtner, W.M. 1966. Halite-anhydrite seasonal layers in the Middle Devonian Prairie Evaporite Formation, Saskatchewan, Canada. *Geological Society of America Bulletin*, 77, pp.331-342.

Welsink, H.J., Dwyer, J.D. and Knight, R.J. 1989. Tectono-stratigraphy of the passive margin off Nova Scotia. *In*: Tankard, A.J., Balkwill, H.R. (eds.), Extensional Tectonics and Stratigraphy of the North Atlantic Margins. *American Association of Petroleum Geologists Memoir*, 46, pp.215-231.

Westphal, M., Montigny, R., Thuizat, R., Bardon, C., Bosser, Hamze, R. and Rolle, J.P. 1979. Paléomagnétisme et datation du volcanisme permien, triasique et crétacé du Maroc. *Canadian Journal of Earth Sciences*, 16, pp.2150-2164.

Withjack, M.O., Schlische, R.W. and Olsen, P.E., 1998. Diachronous rifting, drifting, and inversion on the passive margin of central eastern North America: an analog for other passive margins. *American Association of Petroleum Geologists Bulletin*, 82, pp.817-835.

Withjack, M.O. and Callaway, S. 2000. Active normal faulting beneath a salt layer: an experimental study of deformation patterns in the cover sequence. *American Association of Petroleum Geologists*, 84, pp.627-651.

Withjack, M.O., Schlische, R.W. and Olsen, P.E. 2012. Development of the passive margin of Eastern North America: Mesozoic rifting, igneous activity, and breakup (Chapter 13). In: Roberts DG, Bally AW (eds.), *Regional geology and tectonics: phanerozoic rift systems and sedimentary basins.* Amsterdam: Elsevier, pp.301-335.

Zahraoui, M. 1991. La plate-forme carbonatée dévonienne du Maroc occidental et sa dislocation hercynienne. State Thesis, University of Brest, Belarus, p.261.

Cloud Publications
International Journal of Advanced Earth Science and Engineering
2018, Volume 7, Issue 1, pp. 649-664
ISSN: 2320–3609, Crossref: 10.23953/cloud.ijaese.384

Research Article

Susceptibility Zonation of the Soils of Mayo-Danay in East Part of the Sudano-Sahelian Cameroon, Central Africa

Tiki Denis[1], Shahina Tariq[2], Ibrahim Achille[1], Mamdem Lionelle[1], Leumbe Leumbe Olivier[3], Bitom Dieudonné[1,4]

[1]Department of Earth Sciences, Faculty of Science, University of Ngaoundere, P.O. Box 454 Ngaoundéré, Cameroon
[2]Department of Meteorology, COMSATS Institute of Information Technology, Islamabad, Pakistan
[3]National Institute of Cartography, P.O. Box 157 Yaoundé, Cameroon
[4]Faculty of Agronomy and Agricultural Sciences, P.O. Box 222 Dschang, Cameroon

Publication Date: 20 September 2018

DOI: https://doi.org/10.23953/cloud.ijaese.384

Abstract The study of soil resources of Mayo-Danay, located in the tropical zone of Cameroon, shows a diversity of soils characterized by specific properties. Indeed, this study area is generally a plain landscape whose average relative altitude (300 m). However, it indicates a vegetation of savanna type, very dominant. Hydrologically, Logone River, Maga Lake and tributary streams of the Mandara Mountains regularly flood the study area. The sharing of these parameters leads to soil's genesis, which have a sandy texture for floodplain soils and a very dominant clay texture for lacustrine soils. Otherwise, the geochemistry of these soils shows SiO_2 contents globally 70% in the different soils studied; Al_2O_3 contents are less than 10% in lacustrine soils and less than 5% in floodplain soils; while the major elements data of soils such as Fe_2O_3, CaO and MgO indicate relatively low contents ($\leqslant$2%) on soils studied. In addition, the mineralogy index of alteration expresses a moderate alteration of these soils. Thus, the distribution of these major elements of soil reveals its susceptibility to zonation, which is a consequence of intrinsic and extrinsic parameters to formation and differentiation of soils of the study area.
Keywords *Mayo-Danay division; Major elements Susceptibility zonation; Sudano-sahelian Cameroon*

1. Introduction

Due to its position on the globe, Sudano-Sahelian zone is located in Africa between 9° and 13° Northern latitude. It encloses Far-North Cameroon Region, located between 10° and 13° North Latitude and between 13° and 16° East Longitude. However, identified in eastern part of this region, these flood plains locally named "*yaéré*", extend over about 10.000 km^2 and actually start once crossed the Yagoua-Limani dune whose altitude are obviously less than 400 m; they consist essentially of alluviums of various types on which a variety of soils develop (Brabant and Gavaud, 1985; Garba, 2000). The soils of this sector dominated by sandy and clay texture, that are consequence of the direct contribution of the mountain zones located to above 800 m and piedmonts (between 400 and 800 m). Sandy-clayey or sandy-silty alluvial deposits of Logone River and Mayos

give little evolved soils, sometimes deep, with very variable drainage. They are punctuated by zones of hydromorphic spot of *"hardé"* which most often indicate paleo-stand sites (Brabant and Gavaud, 1985; Garba, 2000). The topography offers only lower slopes, most often at 1%. Soils are compact in the dry state and sticky when wet. The soils are deep on alluvia. The exchange capacity is always very high. On these fragile soils, the risks of gully erosion and flooding are obvious (Mamadou, 2000; Morin, 2000; Raunet, 2003; Sighomnou, 2003; Milleville and Serpantie, 1994; Seignobos and Moukouri, 2000).

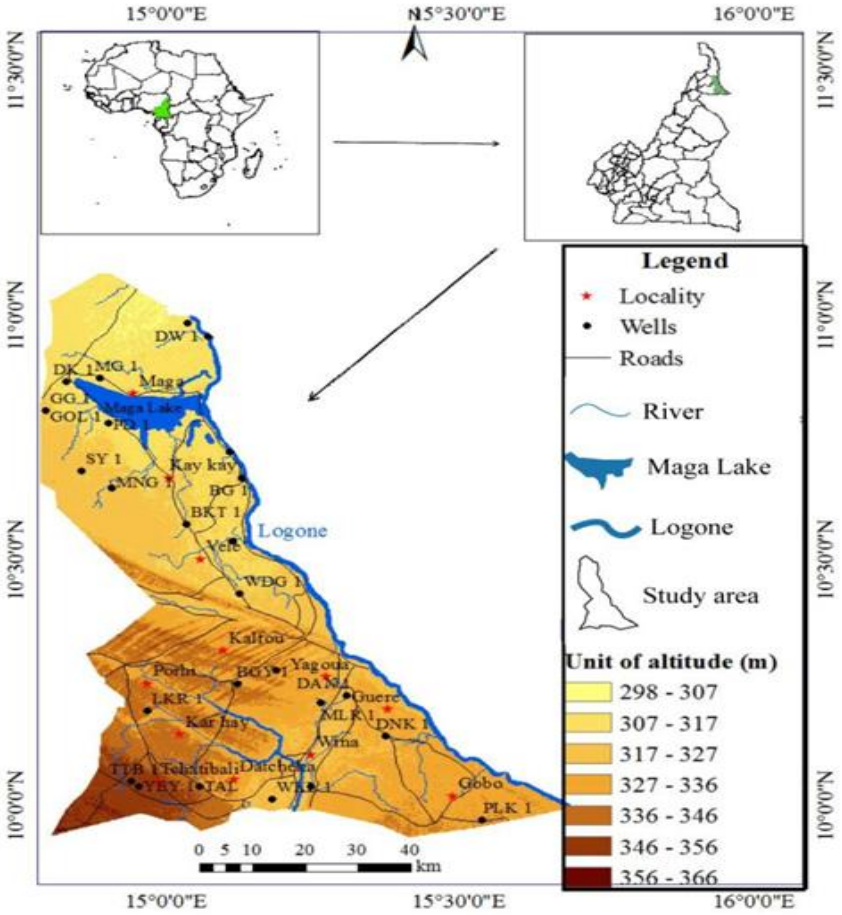

Figure 1: *Localization of study area*

As a natural element, soils constitute a three-dimensional dynamic complex occupying the superficial part of the earth's crust and thus supporting plants. As a result of interactions of varying duration between climate, living organisms (including human activity), parent materials and relief (including hydrography), have well-defined properties. Although it has been the subject of several studies, none of them has emphasized the susceptibility zonation of these soils. By their mode of formation and distribution in the landscape, the soils of the sector showed a specific zoning and characteristic of the plains zones. The aim of this research is to understand the susceptibility zonation of soil of Mayo-Danay Division, that is, the dynamic of soils in relation with their formation and distribution modes.

2. Study Area

The Mayo-Danay division is located between 10°00′ and 11°10′ north latitude and between 14°50′ and 15°40′ east longitude in Far-North Cameroon (Figure 1). It is triangular form and covers an area of about 6.300 km^2, oriented north-south. Delimiting part of the border with the Republic of Chad

through the Logone River, the head of Mayo-Danay division is Yagoua. It is limited to north by the Logone and Chari division, to south by the Republic of Chad (*Mayo-Kebbi*), to the west by Mayo-kani division and the Diamare division and to the east by the Republic of Chad (Logone/Bongor).

The climate of Sudano-Sahelian, characterized by a long dry season starts in early October and ends in late April to May and a short rainy season, from May to September. Rainfall density varies from 530 to 850 mm/year. The average temperature is 28°C; the hottest months are March, April and May with a maximum value of 35°C. The annual evapotranspiration is 1800 mm. The morphology is dominated by a floodplain and the lacustrine deposits as similar in Nigeria, Niger and Chad (Sighomnou, 2003). The floristic grouping consists of a shrubby savannah (low trees), herbaceous steppes with periodically flooded grasslands very marked in the lacustrine plains and sparse vegetation in degraded areas (Milleville and Serpantie, 1994). Geologically, recent and ancient alluvial deposits of various kinds occupy the study area (Barbery and Gavaud, 1980). Pedologically, we find poor soils, vertisols, and ferruginous tropical soils, hydromorphic soils and halomorphic soils (French soils classification) (Seignobos and Moukouri, 2000; Barbery and Gavaud, 1980; Tiki, 2014; Ibrahim, 2014; Leumbe et al., 2015; Temga, 2008). The human stands are composed of Massa, Toupouri, Musgum, Mousey, Peulhs, Kanuri, Kéra, etc. The main activities are agriculture, livestock farming and fishing (Seignobos and Moukouri, 2000).

3. Methods

3.1. Sampling and Analytical Techniques

3.1.1. Sampling

A field campaign was carried out by using topographic map of Yagoua at 1/20000 scale. It consisted of opening of the soil pits (average depths of 1.5 to 2.5 m with 1.5 x 1 m of opening). The latter made it possible to characterize soil samples morphologically, to collect them and to label them in polyethylene packaging and then to transport them to the laboratory for related analyzes.

3.1.2. Analytical Techniques

In the laboratory of Geological Survey of Pakistan (GSP), geochemical analysis carried out on following elements: SiO_2, Al_2O_3, Fe_2O_3, CaO, MgO, K_2O, Na_2O, P_2O_5, TiO_2 and MnO by pearl production and X-ray fluorescence (XRF). The preparation principle is to bring the sample and flux mixture (99.9% anhydrous di-lithium tetraborate tetra platinum) crucible in the muffle furnace at 1150° C for 5 minutes. The contents of the crucible at the outlet of the oven are poured into a cup for cooling, and a pearl is obtained. X-ray fluorescence spectrometry is a fast, non-destructive analytical technique. It consists of an irradiation of the sample to be analyzed by x-rays emitted by the spectrometer tube. The sample thus bombarded then emits x-rays (this is the fluorescence) characteristic of the composition of the sample; the energies of this secondary radiation are detected by the apparatus and the intensities measured are proportional to the concentration of the different elements composing the sample.

4. Results

4.1. Soil Morphology

4.1.1. Lacustrine Soil

The northern part of the study area, more specifically around Maga Lake, lacustrine soils are generally located on an altitude unit less than more or less to 310 m and develop particularly on floodplains with drying slots observed on the surface (1 m depth on average). In addition, the weeds

mainly consist of periodically flooded grasslands associated with savannah shrubs with trees. The lacustrine soils are mainly deposited on clayed to clayed-sandy alluviums. In order to characterize these soils horizon, MG1, BR1 and DW1; three (03) soil profiles were chosen in study area; these includes:

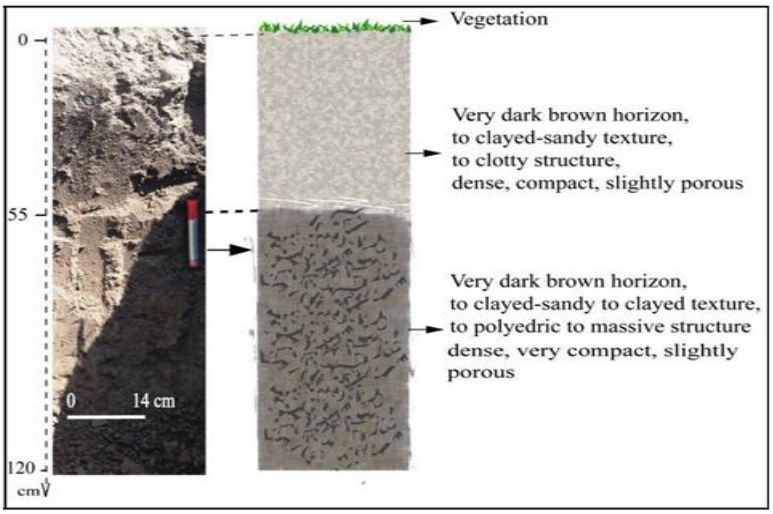

Figure 2: *Lacustrine soil of profile MG 1*

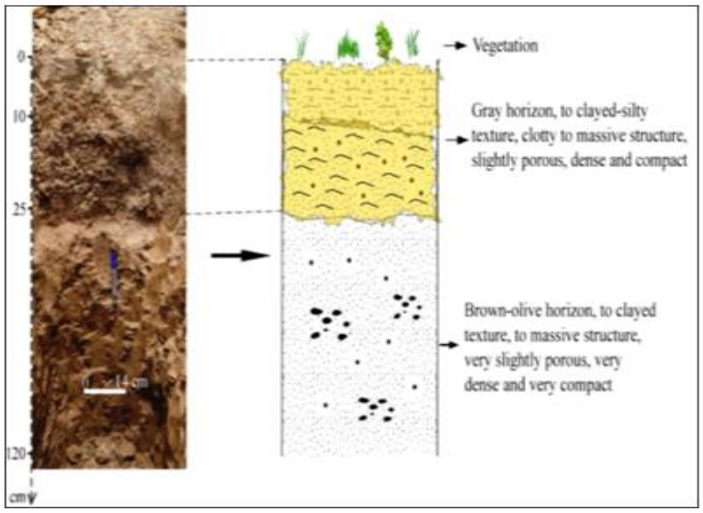

Figure 3: *Lacustrine soils of profile BR 1*

Profile MG 1

The profile MG 1 is located at 10° 52' 19" North latitude and 14° 53' 17" East longitude, at 310 m altitude and is approximately 120 cm deep. It is a differentiated well profile and presents two main horizons (Figure 2):

0 - 55 cm. Very dark brown horizon (10YR2/2), clay sandy to clay texture, clotty structure, dense, very slightly porous and compact. It is moist in depth and show hydromorphic spots, roots, rootlets with a gradual boundary to the underlying horizon of the same color;

55 - 120 cm. Very dark brown horizon (10YR2/2), clay-sandy to clay texture, polyedric to massive structure, very compact, dense and very slightly porous. It is not very moist, with deeper yellow spots and roots and rootlets.

Profile BR 1

The profile BR 1 is located at 10° 57' 22'' North latitude and 15° 04' 19'' East longitude and 310 m altitude. It is 120 cm deep and has two (02) specific horizons (Figure 3):

0-25 cm: Thin horizon, gray (2.5Y6/0), clay-silty to clay texture, clotty to massive structure, porous, slightly dense, plastic and very sticky to wet condition, desiccation slits ranging from 0.2 m to 1 m deep, friable and slightly brittle. It has rusty spots, light sub-rounded nodules of diameter between 0.3 and 0.6 cm, roots, rootlets and living organisms, gradual boundary to the underlying horizon;

25 to 120 cm: very thick horizon, brown olive (2.5Y4/4), clay texture, massive structure, very slightly porous, dense, plastic and very sticky, not friable and not fragile. It has rust spots and dark sub-rounded nodules of diameter between 0.3 and 0.6 cm, rock fragments (light gray) of diameter between 0.5 and 1.5 cm, many dark concretions and some roots and rootlets.

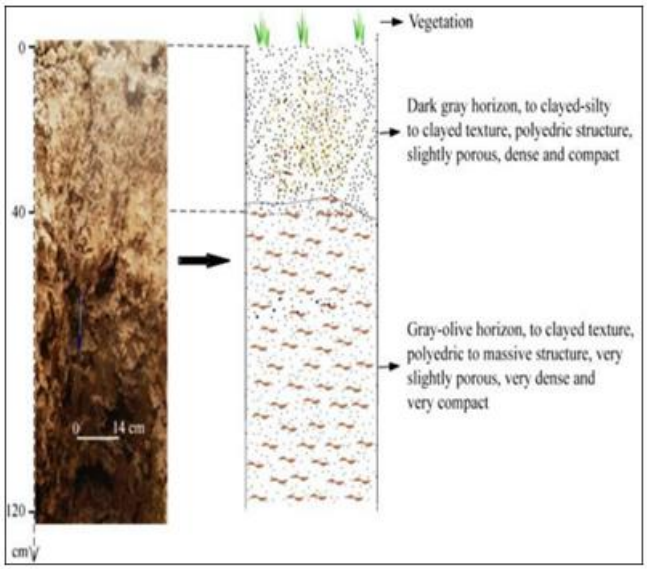

Figure 4: *Lacustrine soils of profile DW 1*

Profile DW 1

The profile DW 1 is located at 10° 58' 59'' North latitude and 15° 02' 13'' East longitude, a depth of 120 cm and an altitude of 310 m. It consists of two (02) horizons (Figure 4):

0 - 40 cm. Dark gray horizon (5Y4/1), clay-silty texture, polyedric structure, slightly porous, not very plastic, friable and not very brittle, show hydromorphic spots of 30 to 40%, characteristics of a constant humidity, an abundance of roots and rootlets, presence of living organisms and a sudden boundary to underlying horizon materialized by relatively light color;

40 - 120 cm. Gray olive horizon (5Y4/2), clay-silty texture, polyedric to massive structure, slightly porous, dense, sticky, presence of rust and hydromorphic spots of 20 to 25%, an abundance of roots and rootlets.

4.1.2. Floodplain Soil

They were mainly identified in the southern and central zone of study area on the sandy ergs of Kalfou, the sandy cord Yagoua-Limani and their surroundings. Primarily floodplain soils are formed at altitudes between 315 and 340 m. In contrast to lacustrine soils, floodplain soils are predominantly dominated by savannah shrubs with trees around which are also bare soils with sparse vegetation. The zone lithology essentially consists of very dominant sandy alluvial deposits, associated with sandy-clay alluvial deposits. Three (03) soil profiles were chosen in the study area to characterize morphostructural floodplain soils; these include DAN 1, TTB 1 and NDY 1.

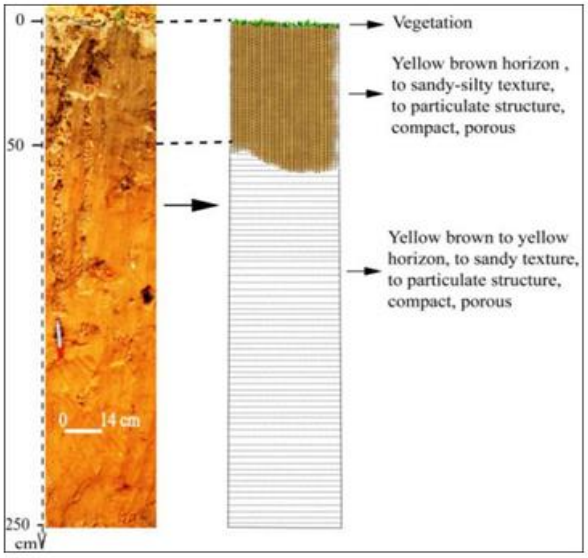

Figure 5: *Floodplain soil of profile DAN 1*

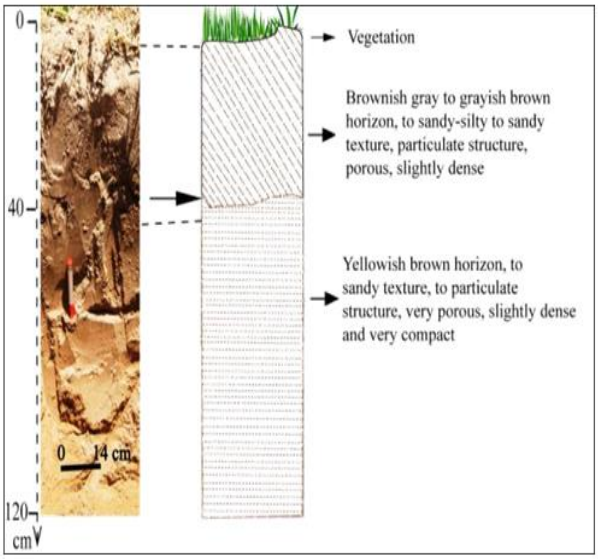

Figure 6: *Floodplain soils of profile NDN 1*

Profile DAN 1

The profile DAN (DAN 1) is located at 10° 13' 19" North latitude and 15° 18' 29" East longitude at 325 m altitude. It is very well developed, well differentiated and measures about 250 cm deep and has two (02) distinct horizons (Figure 5):

0 - 50 cm. Yellowish brown horizon (10YR5/4), sandy-silty to sandy texture, particulate structure, compact, porous and dense. It has roots, rootlets and a gradual boundary to brownish-yellow underlying horizon;

50 - 250 cm. Brownish yellow horizon (10YR7/8) to yellow (10YR7/8), sandy texture, particulate structure, compact, porous with the presence of roots and rootlets.

Profile NDN 1

The profile NDN 1 is located at 10°03'50" North latitude and 15°32'20" East longitude, at 329 m altitude. It is about 120 cm deep and shows two (02) horizons (Figure 6):

0 - 40 cm. Brownish gray horizon (10YR5/4), sandy-silty to sandy texture, particulate structure with hydromorphic spots. It is moist in depth and a gradual boundary to underlying horizon of yellowish brown color; 40 - 120 cm. Yellowish brown horizon (10YR5/4), sandy texture, particulate structure with few roots and rootlets. It is wetter at depth with hydromorphic spots of 30%.

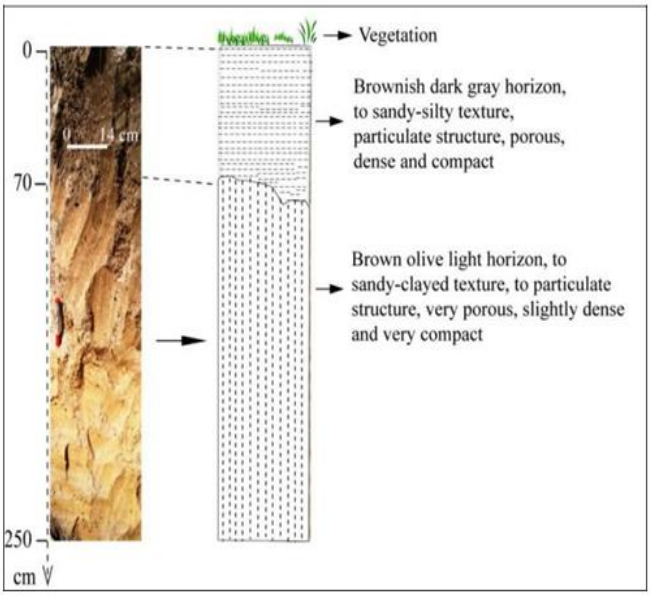

Figure 7: *Floodplain soils of profile TTB 1*

Profile of TTB 1

The profile TTB 1 is located at 10° 02' 48" North latitude and 14° 56' 30" East longitude at 350 m altitude. It measures approximately 250 cm and presents two (02) main horizons (Figure 7):

0 - 70 cm. Brownish dark gray horizon (2.5Y4/2) sandy-silty to sandy texture, particulate structure, compact, dense and porous. It is slightly moist with surface erosion figures, roots and rootlets and a gradual boundary of light olive-brown underlying horizon;

70 - 250 cm. Brown light olive horizon (2.5Y5/6), sandy texture, particulate structure, slightly compact and dense. It shows hydromorphy spots of 60% in depth, yellowish spots and black nodules. It is very humid in depth with some roots.

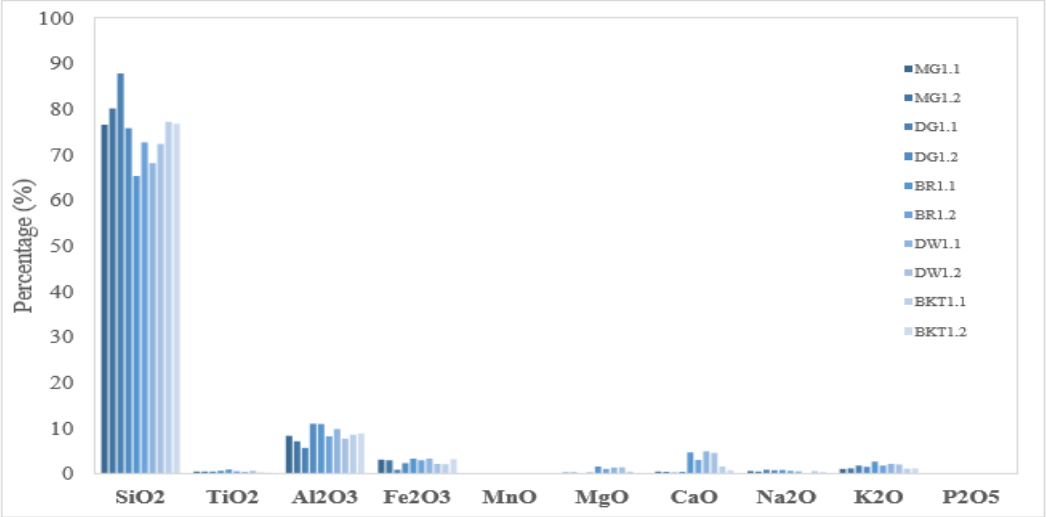

Figure 8: *Major elements oxides (in weight %) of lacustrine soils*

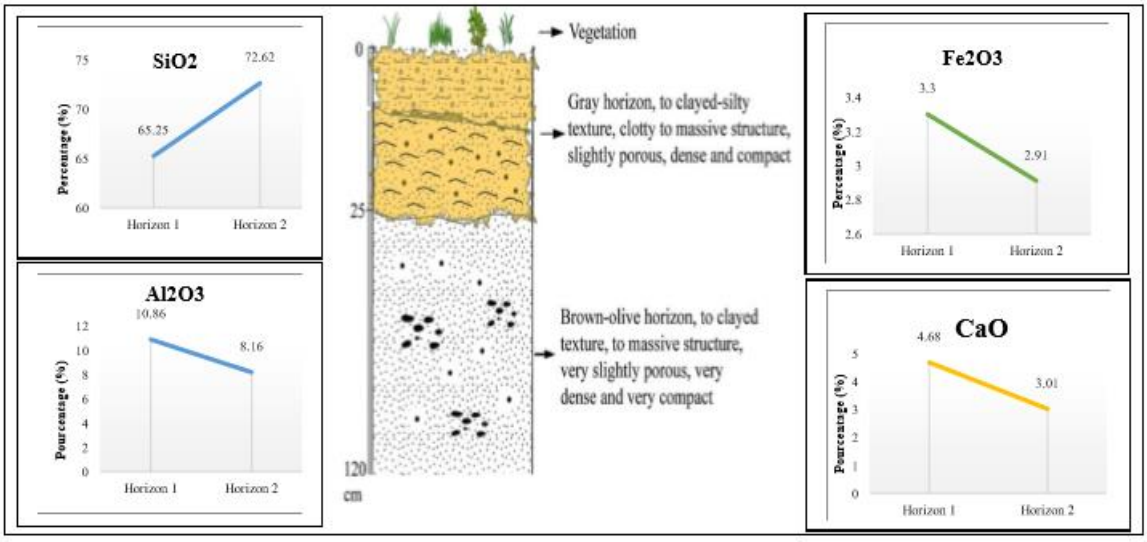

Figure 9: *Variation of some oxides (in weight %) of lacustrine soils profile*

5. Soils Geochemistry

Soil geochemical analysis focuses on major elements oxides. These elements make to understand origin of different soils associated with their alteration and evolution mode of distinct minerals.

MIA is the mineralogical index of alteration. It is calculated by applying the following formula:

$$MIA = 2\ ([Al_20_3 / (Al_20_3 + Ca0 + Na_20 + K_20)] \times 100) - 50)$$

It calculated the degree of transformation of primary minerals into secondary minerals. Voicu and Bardoux (2002) have established that for MIA <20% the alteration is insignificant; MIA between 20-40%, the alteration is weak; between 40-60%, the alteration is moderate and >60% the alteration is intense. When the values reached 100%, they correspond to a total alteration.

The Ruxton index is the SiO_2/Al_2O_3 ratio. It makes to evaluate the nature of secondary minerals along the profile. The secondary minerals are gibbsite when the SiO_2/Al_2O_3 ratio is less than 2,

kaolinites when SiO_2/Al_2O_3 is 2 and montmorillonites when SiO_2/Al_2O_3 is greater than 2 (Browelow, 1979; Ruxton, 1968; Chittleborough, 1991; Tardy, 1993).

5.1. Lacustrine Soil

Table 1: *Major elements oxides (in weight %) of lacustrine soil*

Profiles	MG1.1	MG1.2	DG1.1	DG1.2	BR1.1	BR1.2	DW1.1	DW1.2	BKT1.1	BKT1.2	Ave.
SiO_2	76.53	80.06	87.75	75.75	65.25	72.62	68.12	72.28	77.15	76.75	75.23
TiO_2	0.46	0.43	0.43	0.60	0.90	0.52	0.41	0.62	0.23	0.18	0.48
Al_2O_3	8.27	7.09	5.66	10.96	10.86	8.16	9.82	7.68	8.50	8.82	8.58
Fe_2O_3	3.06	2.91	0.85	2.32	3.30	2.91	3.30	2.10	2.09	3.17	2.60
MnO	0.03	0.11	0.02	0.02	0.04	0.02	0.03	0.03	0.03	0.02	0.04
MgO	0.24	0.20	0.02	0.22	1.53	1.02	1.30	1.37	0.45	0.12	0.65
CaO	0.45	0.40	0.22	0.39	4.68	3.01	4.88	4.52	1.55	0.71	2.08
Na_2O	0.56	0.47	0.87	0.76	0.80	0.62	0.53	0.13	0.57	0.32	0.56
K_2O	1.04	1.13	1.76	1.51	2.65	1.78	2.13	2.01	1.07	1.12	1.62
P_2O_5	0.00	0.00	0.00	0.00	0.01	0.02	0.01	0.01	0.00	0.00	0.01
Total	90.64	92.8	97.58	92.53	90.02	90.68	90.53	90.75	91.64	91.21	91.84
SiO_2/Al_2O_3	9.25	11.29	15.50	9.91	6.00	8.90	6.94	9.41	9.08	8.70	9.50
MIA	60.19	75.27	33.02	61.65	14.37	20.26	13.13	36.96	46.04	60.8	42.17

The geochemical data for lacustrine soils of study area are richer in SiO_2 (75%) in profiles characteristic (Table 1). This high content of SiO_2 is not limited to the surface horizons; rather it increased gradually in-depth horizons. However, it should be noted that, depending on the topographic positions, some samples showed horizons with higher levels of SiO_2 (87.75%) in sample DG1.1 and also relatively low values of 65.25% in BR1.1 sample. However, Al_2O_3 has relative low levels to SiO_2, which varies overall around 8.50% in all gray soils (sample BKT1.1). Specifically, it should be noted that its content gradually decreases with the depth going to 7.09% in sample MG1.2, while on the surface it increased to 10.96% (sample DG1.2). Similarly, Fe_2O_3, content is higher in some lower horizons up to 3.17% (sample BKT1.2). But it should be noted that the iron content varies around 2.60% over the entire profile. A little further, the CaO is very remarkable with maximum values of 4.88% in sample DWI.1, but decreasing with depth. It should be noted that the CaO content remains very low in some samples (0.22%), but the average content however around 2.08%. Similarly, K_2O gives an average of 1.62%, with a peak of 2.65% (Table 1). Finally, elements such as TiO2, MnO, Na_2O and P_2O_5 have very low levels and even zero (P_2O_5 in some wells). In addition, the Ruxton index, which is the SiO_2/Al_2O_3 ratio and which makes it possible to evaluate the nature of the secondary minerals along the profile, showed value greater than 2 (between 6.00 and 15.50). Its values grow according to the depth in some wells, while in others the opposite is true. However, it should be noted that the average value of the Ruxton index in lacustrine soils in general varies around 9.50. In the case of the MIA (Mineralogical Index of Alteration) which indicates the degree of primary minerals alteration in secondary minerals; it has values of the order of 60, except in wells where the CaO and K_2O contents are relatively high. It showed a net growth over the whole of the profiles of the surface (going even to 60.19%) towards the depth (going to 75.27%), but its average value varies of order 42.17% (Table 1, Figure 9).

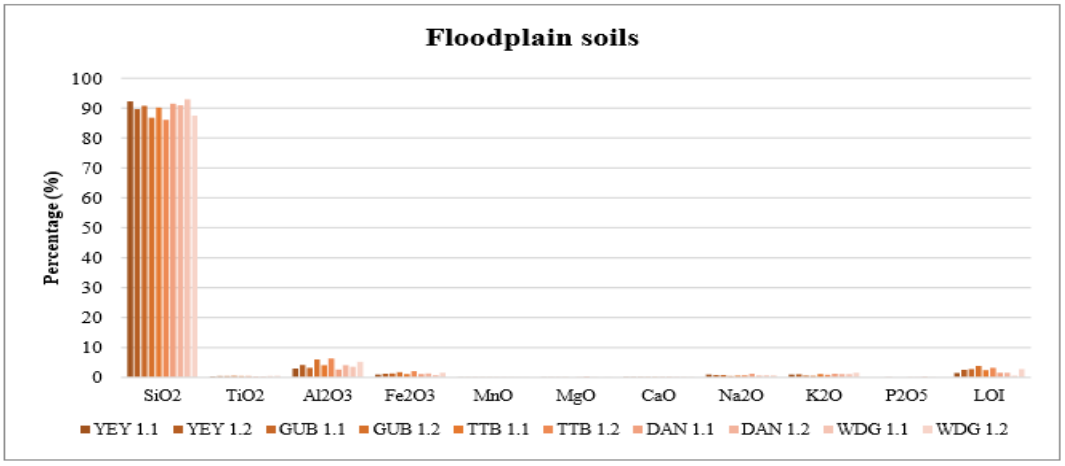

Figure 10: *Variation of major elements oxides (in weight %) of floodplain soils*

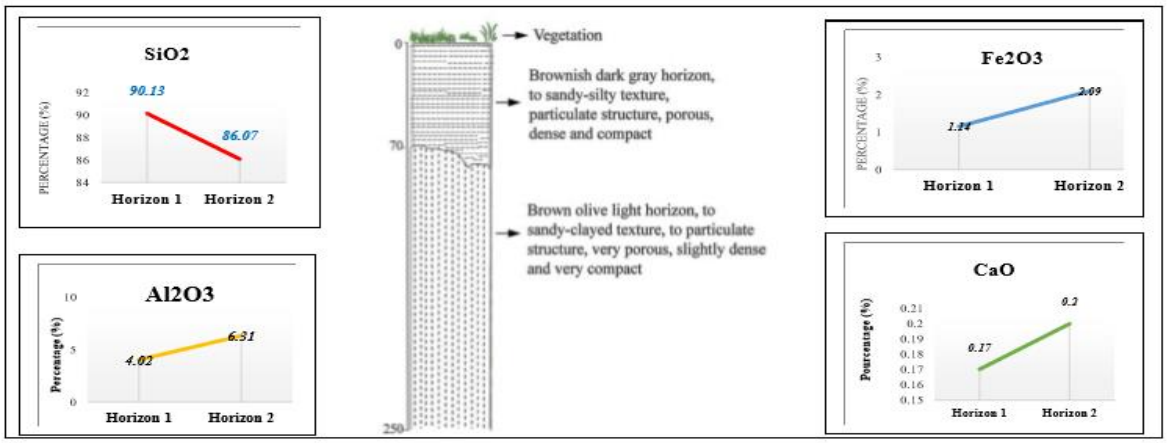

Figure 11: *Variation of some oxides (in weight %) of the floodplain soils profile*

5.2. Floodplain Soil

In its specificity, floodplains soils showed high level of SiO_2 around 90% with an irregular overall variation on the different horizons and whose lowest content is 86.07% (Table 2). Just below, despite its low representativeness, alumina gradually increased with depth (from 2.21% to 6.31%) with an average content estimated at 4.18%. Similarly, Fe_2O_3 increased with depth but with even lower levels (estimated at 1.29% across all profiles) (Table 2 & Figure 10). Elements such as TiO_2, MnO, CaO, Na_2O, K_2O are very low over profiles (with values less than 1%). The Ruxton index in floodplains soil is greater than 2 across all the different horizons and profiles (23.63). On the other hand, the MIA is of order of 42.25, but it grows with the depth going to more than 60 in certain horizons of soil (Figure 11).

Table 2: *Major elements oxides (in weight %) of floodplain soils*

Profile	GUB1.1	GUB1.2	TTB1.1	TTB1.2	DAN1.1	DAN1.2	WDG1.1	WDG1.2	DNW11	DNW12	SYL11	SYL12	Aver.
SiO_2	90.78	86.80	90.13	86.07	91.43	90.91	92.93	87.48	89.29	91.8	90.5	91.2	89.93
TiO_2	0.38	0.47	0.44	0.45	0.31	0.33	0.42	0.48	0.57	0.48	0.25	0.63	0.43
Al_2O_3	3.21	5.94	4.02	6.31	2.60	4.02	3.58	5.15	4.55	2.21	4.15	4.36	4.18
Fe_2O_3	1.27	1.71	1.14	2.09	1.15	1.32	0.77	1.57	1.25	0.97	1.41	0.80	1.29
MnO	0.02	0.02	0.03	0.01	0.03	0.02	0.02	0.05	0.01	0.02	0.03	0.02	0.02
MgO	0.07	0.07	/	0.10	0.32	0.05	/	0.03	0.23	0.05	/	0.02	0.12
CaO	0.17	0.15	0.17	0.20	0.23	0.13	0.12	0.15	0.15	0.17	0.15	0.12	0.16
Na_2O	0.73	0.45	0.62	0.68	1.18	0.56	0.68	0.72	0.89	0.73	0.02	0.55	0.65
K_2O	0.61	0.51	1.07	0.88	1.17	1.07	1.13	1.57	0.01	0.03	1.15	1.02	0.85
P_2O_5	0.01	0.00	0.00	0.01	0.03	0.33	0.01	0.00	0.01	0.01	0.00	0.01	0.04
Total	9.25	96.12	97.62	96.80	98.45	98.74	99.66	97.2	96.96	96.5	97.6	98.7	97.67
SiO_2/Al_2O_3	28.28	14.61	22.42	13.64	35.16	22.61	25.96	16.99	19.62	41.5	21.8	20.9	23.63
MIA	41.1	68.51	36.73	56.38	0.38	39.10	29.95	35.7	62.5	40.8	51.7	44.1	42.25

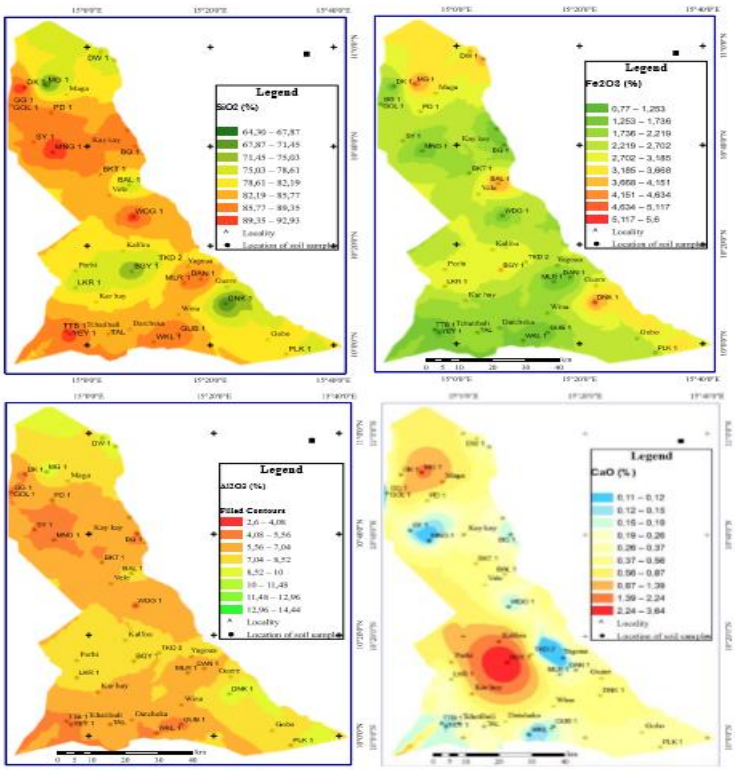

Figure 12: *Distribution map of SiO_2, Al_2O_3, Fe_2O_3 and CaO elements (in weight %)*

6. Comparative Geochemical Analysis

The comparative synthetic analysis of different types of soil (Figure 12) reveals more and less remarkable and appreciable variation of chemical elements and in particular of Ruxton index and Mineralogical Index of Alteration (MIA). Specifically, SiO_2 content remains above 70% on

characteristic soils of study area; however, it should be noted this element indicated an estimated 90% content in floodplain soils unlike lacustrine soils (75%). Although SiO_2, alumina indicated a low content in floodplain soils (4.18%); but it is still slightly higher in lacustrine soils at 8%. Similarly, Fe_2O_3 expressed at least very low values overall, but with appreciable levels in lacustrine soils (more than 2.50%); contrasting the floodplain soils where it showed very little of order of 1%. Distinctly from others elements, CaO showed a content of 2% in lacustrine soils; likewise, for K_2O, which remains more or less appreciable in these soils (more than 1.20%). Others elements (Na_2O, TiO_2, MnO, MgO and P_2O_5) are relatively very low on all soils characteristic of study area. In case of Ruxton index, it should be noted simply that its value is greater than 2 on the soils studied. And finally, the mineralogical alteration index (MIA) shows values greater than 60% in lacustrine soils; while in plain soils, this index is constant in order of 45%.

The comparative synthetic analysis of different types of soil reveals more and less remarkable and appreciable variation of chemical elements and in particular of Ruxton index and Mineralogical Index of Alteration (MIA). Specifically, SiO_2 content remains above 70% on characteristic soils of study area; however, it should be noted this element indicates an estimated 90% content in floodplain soils unlike lacustrine soils (75%). Unlike SiO_2, alumina indicates a low content in floodplain soils (4.18%); but it is still slightly higher in lacustrine soils at 8%. Similarly, Fe_2O_3 expresses at least very low values overall, but with appreciable levels in lacustrine soils (more than 2.50%); contrasting the floodplain soils where it expresses very little of order of 1%. Distinctly from others elements, CaO showed a content of 2% in lacustrine soils; likewise, for K_2O, which remains more or less appreciable in these soils (more than 1.20%). Others elements (Na_2O, TiO_2, MnO, MgO and P_2O_5) are relatively very low on all soils characteristic of study area. In case of Ruxton index, it should be noted simply that its value is greater than 2 on the soils studied. And finally, the mineralogical alteration index (MIA) shows values greater than 60% in lacustrine soils; while in plain soils, this index is constant in order of 45%.

7. Discussion

The lacustrine soils studied are generally located on a unit of altitude less than or equal to 310 m and are formed in particular around Maga Lake with drying slots observed on the surface (1 m deep on average). These drying slots indicated gilgai-type micro-reliefs that are regularly encountered in these soil types, as described by authors such as Barbery and Gavaud (1980), Sieffermann and Vallerie (1986), Garba (2000), Temga (2008) and Vizier (2010). This is due to their permanent contact with water and the dominant 2/1 clay minerals (smectites) in these soils. However, these soils are dominated by periodically flooded grasslands, shrub savannah and herbaceous steppes. On other hand, profile is characterized by a gray to dark gray color as described by CPCS (1967), Duchaufour (1977), Garba (2000) and Temga (2008). In agreement with Duchaufour (1977) and Temga (2008), it is accepted that organic matter plays a large role in pedogenetic processes. Their clay texture and clotty to polyedric to massive structure are result of their cultivation and high proportion of deep clay minerals and nature of lithologic materials.

Flooplain soils, unlike lacustrine soils, are located on floodplain zones, on a unit of altitude greater than or equal to 315 m, on plains rich in sandy-clay to sandy alluvial deposits. They develop a shrub savanna with trees, similar to those described by Baize et al. (2008). Their profile has in particular yellowish-brown to light brownish-gray to dark-gray horizons of variable thickness, sandy to sandy-clay-silty texture and particulate to massive structure. According to Barbery and Gavaud's work (1980), this seems to be explained by matter's movements and slow internal drainage (vertical leaching). In contrast to lacustrine soils showed dominant sandy texture and particulate structure; this is due to the nature of the lithology which consists essentially of sandy alluvium (Leumbe Leumbe et al., 2015). Soils geochemistry of study area highlights lateral and vertical variation of major elements that were the subject of this analysis.

Influence of Lithologic Materials

Lithologic nature of entire study area is essentially composed of alluvia. Thus, lithology of floodplain soils is mainly dominated by alluvia deposits of sandy nature associated with sandy-clay alluvium located upstream of the Limani-Yagoua dune. This explained why it has very high silica great quantity (90%) on all floodplain soils profiles. On other hand, lacustrine soils are exclusively formed on clay alluvia with slightly association of sandy-clay to sandy-clay alluvia; this nature contributed to its relative dominance in SiO_2 (75%) compared to floodplain soils. In addition, these lacustrine soils have been contributions of "Mayos" from Mandara Mountains located a little further in the western part (1400 m of altitude) of study area. It should be noted that these inputs have high levels of clays and silts (Tiki, 2014; Ibrahim, 2014; Leumbe Leumbe et al., 2015; CPCS, 1967; Duchaufour, 1977).

Influence of Topography

Study area has two distinct zones; the elevated zone located generally between 315 and 340 m of altitude on which floodplain soils are deposited; and the low zone which is organized around 290 and 315 m of altitude on which lacustrine soils are deposited. This difference in altitude would explain contents of different soil types. Bases indicated somewhat higher levels in lacustrine soils. The cases of CaO and K_2O showed a relative variation in content. The higher levels in lacustrine soils (2.68% for Ca_2O, 1.62% for K_2O and 0.65% for MgO) compared with higher levels in floodplain soils (0.16% for Ca_2O, 0.85% for K_2O and 0.12% for MgO). By their nature, bases are very mobile in soil and occupy low elevation areas by drainage processes. Ferruginous concretions up to 60% recognizable along lacustrine soils profiles confirm the relatively Fe_2O_3 content found in lacustrine compared to floodplain soils; they can be explained by the seasonal contrast characteristic of intertropical regions with a dry season of 4 to 5 months, a rainy season with annual rainfall of 400 to 1000 mm/year and high temperatures (28° C on average) as have shown it CPCS (1967), Baize et al., (2008), Vizier (2010), Tiki (2014), Basga (2015).

Comparison between alluvial plains soils of Mayo Danay (eastern part of Sudano-Sahelian zone of Cameroon) and Peshawar Basin of soils of Pakistan (Southern foothills of lesser Himalayas in the Khyber Pakhtunkhwa (KP).

Table 3: *Comparison between alluvial plain soils of Mayo-Danay and soils of Peshawar Basin (KP Pakistan)*

Soils	Alluvial plain soils of Mayo-Danay		Peshawar Basin Soils	
	Lacustrine	**Floodplain**	**Lacustrine**	**Floodplain**
Localization	10°00’ - 11°10’N, 14°50’ - 15°40’E		33°20’- 34°20'N, 71°25' – 72°40’E	
Climate	Subtropical hot		subtropical semi-arid hot	
Rainfall (mm/year)	650	800	400	
Temperature (°C)	27		23	
Lithology	clay and clay sand alluvia	sand and sand clay alluvia	clay and sand lake deposits	sand sediments with intercalation of clay
Topography (m)	290-315	315-340	350 m	

Soils of Peshawar Basin present geochemical data that shows significant difference in level of major elements in these soils relative to soils in study area. To better understand susceptibility to zonation of these soils, rigorous analyses of pedogenesis factors are highlighted; these include lithologic nature, climate and topography (Table 3). Thus, SiO_2 content is lower (about 50% in lacustrine and floodplain soils) than those of soils in study area (overall greater than 75%). This variation in SiO_2 content is due to nature of lithologic materials, which in case of soils of study area are mainly formed on dominant sandy alluvial soils (floodplain soils) associated with clay-sand to clay soils (lacustrine soils) resulting from the alteration of granitic and volcanic rocks (Ibrahim, 2014; Leumbe Leumbe et al., 2015; Segalen, 1964; Temga et al., 2015; Mohammad and Shahina, 2006). Silica, which is in

quartz form, represents a high proportion of sandy fractions (Vizier, 2010; Bear, 1975). Thus, sandy-clay texture of soil of study area may explain abundance in SiO_2 compared to Peshawar Basin soils. On the other hand, soils of Peshawar basin are formed in sedimentation zone where the soils show dominant clay-sand to clayey texture. In contrast to first element, alumina and iron indicate higher values in soils of Peshawar basin (5% Fe_2O_3 and 18% Al_2O_3); while in soils of sector, these values are lower (2% Fe_2O_3 and 8.5% Al_2O_3) (Table 3). Fe2O3 and Al_2O_3 contents are related to altered primary minerals present in the sandy-clay fraction. With regard to clay, to which iron is often associated, as well as phosphorus, which becomes more strongly bound to iron and alumina; the high soil levels in Peshawar Basin are mainly due to clay nature of these sediments from inputs from floods often very rich in clay and silt (Temga et al., 2015; Mohammad and Shahina, 2006). Similarly, alkaline (Na_2O and K_2O) and alkaline-earth elements contents remain higher in soils of Peshawar basin; this would be related to limestone deposits that are intimately related to sedimentary deposits (Temga et al., 2015; Mohammad and Shahina, 2006). However, it should be emphasized soils of Peshawar basin are mainly formed on sediments rich in limestones. These are flood products very frequently encountered in the area. This latitudinal difference observed on of major element variation content on lacustrine soils of these sectors would be essentially due to lithologic material nature. It should be emphasized that pedogenesis plays a very important role in this distribution, given the differences in the geochemical composition of soil classes studied (Vizier, 2010; Azinwi et al., 2011; Boukar, 2007) in the Peshawar Basin and the alluvial plains of Mayo Danay division (Table 3).

8. Conclusion

As part of Mayo Danay's alluvial plains are well developed morphologically with deep horizons in depth. They have a very dominant clay texture in case of lacustrine soils, while floodplain soils are sandy. Geochemically, they are very rich in SiO_2 and have relatively low levels of Fe_2O_3, Al_2O_3 and the group of alkaline and alkaline earth elements. This result is a direct consequence of lithologic nature, climate, relief and pedogenetic processes which play a very important role in formation, evolution of soils and their susceptibility zonation.

Acknowledgements

We express our sincere thanks to TWAS (The World Academy of Sciences) and all those who have contributed to success of this work, especially my supervisors.

References

Azinwi, P.T., Djoufac, W.E., Bitom, D. and Njopwouo, D. 2011. Petrological, physico-chemical and mechanical characterization of the topomorphic vertisols from the Sudano-sahelian region of Nord Cameroun. *Open Geol. J.*, 5, pp.33-55.

Baize, D., Girard, M.C., Herbland, A., Harache, Y., Citeau, L., Bispo, A., Bardy, M., King, D., Proteau, J.P., Schlumberger, O., Élie, P., Adam, G., Feunteun, E., Prouzet, P., Rigaud, C. 2008**.** Référentiel pédologique. AFES, p.435

Boukar, A. 2007. Morphologie, caractéristiques physico-chimiques et érodibilité des sols de Maga et environs (Extrême-Nord Cameroun). Mém. DEA, Univ. Ngaoundéré, p.56.

Brabant, P. and Gavaud M. 1985. Les sols et les ressources en terres du Nord-Cameroun (province du Nord et de l'Extrême-Nord). 46 cartes, ORSTOM-MESRES-IRA., Paris, 103, p.285.

Garba, M.A. 2000. Les grands types de sols du Niger. Quatorzième Réunion du Sous-Comité Ouest et Centre Africain de Corrélation des Sols - INRAN, pp.151-167.

Barbery. J. and Gavaud, M. 1980. Notice explicative de la Carte Pédologique du Cameroun feuille Bogo-Pouss à 1/100 000. ORSTOM-IRAF-ONAREST, Paris no. 88, p.58.

Basga, S.D. 2015. Etude des sols de Yagoua et de Mafa Tcheboa (Nord Cameroun): morphologie, mineralogie, geochimie, erodibilite et essai de fertilisation. Thèse de doctorat, University of Ngaoundere, p.183.

Bear, F.E. 1975. Soil Components, Washington. D.C., p.740.

Browelow, H. 1979. Geochemistry, Prentice-hall, Inc., New York.

Chittleborough, D.J. 1991. Indices of weathering for soils and paleosols formed on silice rocks. *Australian Journal of Earth Sciences*, 38, pp.115-120.

CPCS. 1967. Classification des sols. Commission de Pédologie et de Cartographie des Sols, AFES, p.96.

Duchaufour, P. 1977. Pédogenèse et classification des sols. Eds. Masson, Paris-New York-Barcelona-Milan, p.492.

Ibrahim, B.A. 2014. Etude morphologique, physico-chimique et cartographique des sols de Bogo (Extrême-Nord Cameroun). Mém. Master en Géosciences et Environnement. University of Ngaoundere, p.63.

Leumbe Leumbe, O., Bitom, D., Mamdem, L., Tiki, D., Ibrahim, B. 2015. Cartographie des zones à risques d'inondation en zone soudano-sahélienne: cas de Maga et ses environs dans la région de l'extrême-nord Cameroun. *Afrique Science*, 11(3), pp.45-61.

Mamadou, K. 2000. Les grands types de sols du Sénégal. Quatorzième réunion du Sous-Comité ouest et centre africain de corrélation des sols. ISRA-CNRA, Bambey, pp.77-94.

Morin. 2000. Géomorphologie: Atlas de la province de l'Extrême Nord-Cameroun. éd. Seignobos, C. and Iyebi-Mandjek, O., IRD-MINREST, Paris, pp.7-15.

Milleville, P. and Serpantie, G. 1994. Dynamiques agraires et problématique de l'intensification de l'agriculture en Afrique soudano-sahélienne. C.R. Fr, 80, n° 8, pp.149-152.

Mohammad, T.S. and Shahina, T. 2006. Environmental geochemistry of soils of Peshawar Basin, N.W.F.P., Pakistan, p.8.

Raunet, M. 2003. Quelques clés morphologiques pour le Nord Cameroun à l'usage des agronomes. Rapport projet ESA/SC., Cameroun, p.24.

Ruxton, B.P. 1968. Measure of the degree of chemical weathering of rocks. *Journal of Geology*, 76, pp.518-527.

Sighomnou, D. 2003. Gestion intégrée des eaux de crues - Cas de la plaine d'inondation du fleuve Logone. WMO-GWP, p.18.

Seignobos, C. and Moukouri, H.K. 2000. Potentialités des sols et terroirs agricoles: Atlas de la Province de l'Extrême-Nord Cameroun, pp.3.

Sieffermann, G. and Vallerie, M. 1963. Carte Pédologique du Cameroun - Feuille Yagoua à 1/100 000. ORSTOM, Paris.

Segalen, P. 1964. L'aluminium dans les sols. ORSTOM, Paris, p.152.

Tiki, D. 2014. Etude morphologique, physico-chimique et cartographique des sols de Maga (Extrême-Nord Cameroun). Mém. Master en Géosciences et Environment. University of Ngaoundere, p.71.

Temga, J.P. 2008. Etude des vertisols topomorphes sur alluvions de la zone soudano-sahélienne de l'Extrème-Nord Cameroun (Région de Moutourwa). Mém. DEA. Univ. Yaoundé I, p.61.

Temga, J.P., Nguetnkam, J.P., Balo, M.A., Basga, S.D. and Bitom, D.B. 2015. Morphological, physico chemical, mineralogical and geochemical properties of vertisols used in bricks production in the Logone Valley (Cameroon, Central Africa). *International Research Journal of Geology and Mining*, p.11.

Tardy, Y. 1993. Pétrologie des latérites et des sols tropicaux. Masson, Paris, p.459.

Vizier, J.F. 2010. Les phénomènes d'hydromorphie en régions tropicales à saisons contrastées - Application à une meilleure caractérisation des concepts de gley et de pseudogley. Association Française pour l'Etude du Sol, pp.225-238.